

**VISCOELASTIC INVERSE ANALYSIS OF FWD DATA USING GENETIC  
ALGORITHMS**

By

Sudhir Varma

A DISSERTATION

Submitted to  
Michigan State University  
in partial fulfillment of the requirements  
for the degree of

Civil Engineering–Doctor of Philosophy

2015

## ABSTRACT

### VISCOELASTIC INVERSE ANALYSIS OF FWD DATA USING GENETIC ALGORITHMS

By

Sudhir Varma

Dynamic modulus ( $|E^*|$ ) master curve is a fundamental material property for an asphalt pavement. It is also a key input to Pavement-ME, a pavement design and analysis software that can predict progression of distresses. Falling Weight Deflectometer (FWD) is a nondestructive test whose results are typically used for backcalculating layer properties of pavements in situ. Backcalculation of  $|E^*|$  master curve of an in-service pavement using FWD data can lead to more accurate estimation of its remaining service life. Flexible pavements are multilayered structures, with typically viscoelastic asphalt layer followed by unbound/bound layers. Conventionally, multilayered elastic analysis is performed to obtain response of flexible pavements for design and inverse analyses, however, assuming asphalt pavement as a linear elastic material is an oversimplification of its actual behavior. It is well known that the asphalt pavements' responses are both rate and temperature dependent. Appropriate characterization of individual layer properties is crucial for mechanistic analysis of flexible pavements. Hence, although elastic analysis is computationally efficient and well accepted in the engineering community, the theory cannot produce the viscoelastic properties of the asphalt concrete (AC) layer. Backcalculation of the entire  $|E^*|$  master curve, including the time-temperature superposition shift factor coefficients, requires more data than the surface deflection time-histories of FWD drops. In theory, it should be possible to obtain the  $|E^*|$  master curve, provided that the data contain time changing response at different temperature levels.

The specific objectives of the study were to (i) develop a layered viscoelastic pavement response model in the time domain, (ii) investigate whether the current FWD testing protocol generates data that is sufficient to backcalculate the  $|E^*|$  curve using such a model, (iii) if needed, recommend enhancements to the FWD testing protocol to be able to accurately backcalculate the  $|E^*|$  curve as well as the unbound material properties of in-service pavements. Two different approaches have been proposed to obtain comprehensive behavior of asphalt: (i) using series of FWD deflection time histories at different temperature levels and (ii) using uneven temperature profile information existing across the thickness of the asphaltic layer during a single or multiple FWD drops deflection histories. The models presented can consider the unbound granular material as both linear elastic as well as nonlinear-stress dependent material. Depending on the assumed unbound granular material property, and known temperature profile, several viscoelastic flexible pavement models were developed. The developed forward and backcalculation models for linear viscoelastic AC and elastic unbound layers have been referred to as LAVA and BACKLAVA, respectively. The developed forward and backcalculation models for linear viscoelastic AC and nonlinear elastic unbound layers have been termed as LAVAN and BACKLAVAN respectively in the study. LAVA and BACKLAVA algorithms assume a constant temperature along the depth of the AC layer. The algorithms were subsequently modified for temperature profile in the AC layer and have been referred to as LAVAP and BACKLAVAP. The major recommendations of the work are the estimated set of temperatures and number of deflection sensors where FWD tests should be conducted, in order to maximize the portion of the  $|E^*|$  curve that can be accurately backcalculated. The results indicate that there exists a range of temperatures at which the FWD response leads to better inverse solutions. A genetic algorithm based optimization scheme is offered to search for the pavement properties.

**Copyright by  
SUDHIR VARMA  
2015**

TO MY PARENTS

## ACKNOWLEDGEMENTS

I would like to dedicate my sincere gratitude to my adviser Dr. M. Emin Kutay for giving me his full support and encouragement throughout my study at Michigan State University. His enthusiasm and love towards research kept me motivated. Without his advice I would have not reached this point in my life. The valuable discussions with him gave me an insight into the field which will remain as a lifelong asset with me.

I would also like to thank Dr. Karim Chatti for his untiring efforts in making valuable suggestions and ideas. I would also like to thank my committee members, Dr. Neeraj Buch and Dr. Thomas Pence for their valuable time and comments.

Special thanks to Dr. Gilbert Baladi for his support and guidance. I would also like to thank Dr. Imen Zaabar for valuable discussions on dynamic backcalculation and parallel computing.

I would also like to thank my colleagues and friends for their support during my stay at Michigan State University.

Last but not the least I would like to thank my family for their support and encouragement.

This study was mainly funded by the Federal Highway Administration (FHWA) grant number DTFH61-11-C-00026. This support is greatly appreciated. I would like to express my gratitude towards Dr. Nadarajah Sivanesvaran from the FHWA for his valuable comments.

## TABLE OF CONTENTS

LIST OF TABLES .....	x
LIST OF FIGURES .....	xii
CHAPTER 1 .....	1
INTRODUCTION .....	1
1.1 Objectives .....	3
1.2 Outline.....	3
CHAPTER 2 .....	5
LITERATURE REVIEW AND BACKGROUND .....	5
2.1 FWD Data Collection, Analysis and Interpretation.....	5
2.2 Forward Analysis Methods to Calculate FWD Response.....	7
2.2.1 Boussinesq's Solution Method .....	7
2.2.2 Multilayer Elastic Theory .....	9
2.2.3 Finite Element Analysis.....	10
2.2.4 Forward Analysis Programs.....	11
2.3 Backcalculation Approaches.....	12
2.3.1 Traditional Optimization Techniques .....	13
2.3.2 Non-Traditional Optimization Methods .....	17
2.4 Modeling Issues in Backcalculation .....	22
2.5 Characterizing Linear Viscoelastic Properties of HMA in Laboratory .....	25
2.5.1 Interconversion of $E(t)$ to $ E^* $ .....	29
2.5.2 Interconversion $D(t)$ to $E(t)$ .....	31
2.6 Motivation and Scope .....	32
CHAPTER 3 .....	34
LAYERED VISCOELASTIC PAVEMENT MODEL .....	34
3.1 Introduction.....	34
3.2 Layered Viscoelastic (Forward) Algorithm (LAVA) .....	36
3.3 Implementation of Temperature Profile in LAVA .....	40
3.3.1 Layered Viscoelastic (Forward) Algorithm for Temperature Profile (LAVAP).....	40
3.3.2 Comparison of LAVAP with FEM Software ABAQUS .....	45
3.4 Layered Viscoelastic Nonlinear (LAVAN) Pavement Model .....	48
3.4.1 Nonlinear Multilayer Elastic Solutions.....	49
3.4.2 Proposed Constitutive Model for Multilayer Pavement Model under Uniaxial Loading: Combining Linear Viscoelastic AC and Nonlinear Base .....	52
3.4.3 Proposed Generalized Model for Multilayer Pavement Model: Combining Linear Viscoelastic AC and Nonlinear Base.....	55
3.4.3.1 Applicability of Existing Theories of Nonlinear Viscoelasticity.....	55
3.5 Proposed Model: LAVAN .....	59
3.5.1 Validation of the LAVAN .....	61
3.5.2 Comparison of LAVAN with FEM Software ABAQUS .....	62

3.6 Chapter Summary .....	67
CHAPTER 4 .....	68
BACKCALCULATION USING VISCOELASTICITY BASED ALGORITHM.....	68
4.1 Introduction.....	68
4.2 Backcalculation of Relaxation Modulus Master Curve Using Series of FWD Tests Run at Different Temperatures.....	74
4.2.1 Sensitivity of E(t) Backcalculation to the use of Data from Different FWD Sensors .....	76
4.2.2 Effect of Temperature Range of Different FWD Tests on Backcalculation.....	80
4.2.3 Normalization of Error Function (Objective Function) to Evaluate Range of Temperatures.....	85
4.2.4 Backcalculation of Viscoelastic Properties using Various Asphalt Mixtures .....	91
4.3 Backcalculation of Relaxation Modulus Master Curve using a Single FWD Test and Known Pavement Temperature Profile.....	94
4.3.1 Linear Viscoelastic Backcalculation using Single Stage Method.....	95
4.3.2 Backcalculation of the viscoelastic Properties of the LTPP Sections using a Single FWD Test with Known Temperature Profile.....	99
4.3.3 Backcalculation of Linear Viscoelastic Pavement Properties using Two-Stage Method .....	112
4.4 Layered Viscoelastic-Nonlinear Backcalculation (BACKLAVAN) Algorithm .....	117
4.4.1 Introduction.....	117
4.4.2 Verification of the Nonlinear Backcalculation Procedure.....	122
4.4.3 Validation of BACKLAVAN using Field FWD Data.....	129
4.5 Chapter Summary .....	133
CHAPTER 5 .....	135
EVOLUTION OF DYNAMIC MODULUS OVER TIME.....	135
5.1 Introduction.....	135
5.2 Aging Models.....	136
5.2.1 GAS Model .....	136
5.2.2 Mixture Conditioning of HMA: AASHTO R30 .....	138
5.3 Effect of Aging on Viscoelastic Properties of HMA .....	139
5.3.1 Effect of Variation of $c_1$ .....	140
5.3.2 Effect of Variation of $c_2$ .....	140
5.3.2 Effect of Variation of $c_3$ .....	141
5.3.2 Effect of Variation of $c_4$ .....	142
5.3.2 Effect of Variation of $a_1$ .....	142
5.3.2 Effect of Variation of $a_2$ .....	143
5.4 Proposed Solution .....	144
5.4.1 Results and Discussion of Age Hardening in LTPP Test Section .....	147
5.5 Summary .....	158
CHAPTER 6 .....	159
SENSITIVITY ANALYSIS FOR LAYER THICKNESS .....	159
6.1 Introduction.....	159



6.2 Sensitivity Analysis for Layer Thickness: 6 Inches AC Layer.....	163
6.2.1 Sensitivity Analysis for AC Layer Thickness.....	164
6.2.2 Sensitivity Analysis for Base Layer Thickness .....	167
6.2.3 Sensitivity Analysis for Total Pavement Thickness .....	171
6.2.4 Summary and Discussion.....	174
CHAPTER 7 .....	177
SUMMARY AND CONCLUSION .....	177
APPENDIX.....	182
BIBLIOGRAPHY .....	192

## LIST OF TABLES

Table 1: List of commonly used pavement response models .....	11
Table 2: List of commonly used backcalculation programs (Smith et. al 2010). .....	16
Table 3: LAVA computation times for different numbers of discrete time steps .....	39
Table 4: Pavement properties used in LAVAP validation with ABAQUS. ....	41
Table 5: Pavement section used in LAVAP validation .....	46
Table 6: Peak deflections at temperature profile {19-30}°C and at constant 30°C temperature using LAVA.....	47
Table 7: Comparison of ABAQUS and LAVAN: Peak surface deflections for different boundary conditions.....	64
Table 8: Comparison of ABAQUS and LAVAN: Percent error (PE <sub>peak</sub> ) calculated using the peaks of the deflections and average percent error (PE <sub>avg</sub> ) calculated using the entire time history. ....	66
Table 9: Upper and lower limit values in backcalculation .....	73
Table 10: Pavement Properties in viscoelastic backcalculation of optimal number of sensors....	76
Table 11: Backcalculation run time for ga-fminsearch seed Runs .....	82
Table 12: Details of the pavement properties used in single FWD test backcalculation at known temperature profile.....	96
Table 13: List of LTPP sections used in the analysis .....	101
Table 14: Structural properties of the LTPP sections used in the analysis.....	102
Table 15: Depths of stiff layer in each LTPP section estimated using Ullidtz’s method .....	103
Table 16: Elastic backcalculation results for LTPP unbound layers .....	103
Table 17: Viscoelastic backcalculation results for LTPP unbound layers.....	104
Table 18: Variables in two stage linear viscoelastic backcalculation analysis.....	113
Table 19: Pavement properties in two stage linear viscoelastic backcalculation analysis .....	113

Table 20: Pavement properties and test inputs in staged nonlinear viscoelastic backcalculation. ....	121
Table 21: Typical FWD test load levels .....	122
Table 22: Pavement geometric and material properties in two stage nonlinear viscoelastic backcalculation. ....	123
Table 23: FWD test data from LTPP section 01-0101 for years 2004-2005.....	130
Table 24: Nonlinear elastic backcalculation results for section 0101.....	130
Table 25: Comparison of viscoelastic nonlinear viscoelastic backcalculated results obtained at different stages.....	132
Table 26: Backcalculation performance in predicting aging of LTPP section. ....	154
Table 27: Pavement properties in sensitivity analysis .....	164
Table 28: Error in backcalculated relaxation modulus in structure-A.....	175
Table 29: Error in backcalculated relaxation modulus in structure-B .....	175
Table 30: Error in backcalculated base modulus in structure-A.....	176
Table 31: Error in backcalculated base modulus in structure-B.....	176

## LIST OF FIGURES

Figure 1: Half space notation for Boussinesq's solution .....	8
Figure 2: Typical steps in iterative backcalculation .....	14
Figure 3: Schematic figure of a neuron and ANN network .....	17
Figure 4: Typical steps in GA.....	20
Figure 5: Figure illustrating GA operations (a) Crossover and (b) Mutation.....	20
Figure 6: Figure illustrating steps in developing $ E^* $ master curve using laboratory measured $ E^* $ test data :(a) raw $ E^* $ data, (b) master curve development (c) time-temperature shift factors .....	29
Figure 7: Generalized Maxwell model .....	30
Figure 8: Typical flexible pavement geometry for analysis .....	37
Figure 9: Discretization of stress history in forward analysis.....	37
Figure 10: Discretization of the relaxation modulus master curve .....	38
Figure 11: Deflections calculated under unit stress for points at different distances from the centerline of the circular load at the surface. ....	39
Figure 12: Schematic diagram of temperature profile .....	40
Figure 13: Comparison of response calculated using LAVAP and original LAVA.....	42
Figure 14: Comparison of responses calculated using LAVAP at temperature profile {40-30-20} $^{\circ}$ C and original LAVA at constant 40 $^{\circ}$ C temperature. ....	43
Figure 15: Comparison of responses calculated using LAVAP at temperature profile {40-30-20} $^{\circ}$ C and original LAVA at constant 30 $^{\circ}$ C temperature. ....	43
Figure 16: Comparison of responses calculated using LAVAP at temperature profile {40-30-20} $^{\circ}$ C and original LAVA at constant 20 $^{\circ}$ C temperature. ....	44
Figure 17: Region of $E(t)$ master curve (at 19 $^{\circ}$ C reference temperature) used by LAVAP for calculating response at temperature profile {40-30-20} $^{\circ}$ C.....	44
Figure 18: Relaxation modulus and shift factor master curves at 19 $^{\circ}$ C reference temperature....	45
Figure 19: Comparison between LAVAP and ABAQUS at a temperature profile of {19-30} $^{\circ}$ C	

(Terpolymer).....	46
Figure 20: Comparison between LAVAP and ABAQUS at a temperature profile of {19-30}°C (SBS 64-40) .....	47
Figure 21: Cross section of multilayer viscoelastic nonlinear system used in uniaxial analysis..	52
Figure 22: Flexible pavement cross section.....	58
Figure 23: Variation of $g(\sigma)$ with stress and $E(t)$ of AC layer.....	58
Figure 24: Relaxation modulus master curve for LAVAN validation (at 19°C reference temperature).....	61
Figure 25: Surface deflection comparison of ABAQUS and LAVAN for the Control mix (*AS1= ABAQUS sensor 1; *LS1=LAVAN sensor 1). .....	66
Figure 26: Surface deflection comparison of ABAQUS and LAVAN for the CRTB mix (*AS1= ABAQUS sensor 1; *LS1=LAVAN sensor 1). .....	67
Figure 27: Figure illustrating steps in $E(t)$ master curve development.....	69
Figure 28: Backcalculation flow chart in BACKLAVA.....	73
Figure 29: Schematic of fitness evaluation in BACKLAVA.....	75
Figure 30: Error in unbound layer modulus in optimal number of sensor analysis.....	77
Figure 31: Backcalculation results using only sensor 1: (a) Backcalculated and actual $E(t)$ master curve at the reference temperature of 19°C (b) Variation of error, $\xi_{AC}(t_i)$ .....	79
Figure 32: Error in unbound layer modulus using FWD data only from farther sensors .....	80
Figure 33: Variation of error in backcalculated unbound layer moduli when FWD data run at different sets of pavement temperatures are used. ....	81
Figure 34: Error in backcalculated $E(t)$ curve in optimal backcalculation temperature set analysis minimizing percent error.....	82
Figure 35: Results for backcalculation at {10, 30}°C temperature set: (a) and (b) Only GA is used, (c) and (d): GA+fminsearch used. ....	83
Figure 36: Results for backcalculation at {30, 40}°C temperature set .....	84
Figure 37: Results for backcalculation at {30, 40, 50}°C temperature set .....	85

Figure 38: Search domain for unconstrained constrain .....	87
Figure 39: Search domain for constrained constrain .....	88
Figure 40: Backcalculated $ E^* $ master curve using FWD data at temperature set $\{10, 30\}^{\circ}\text{C}$ minimizing normalized error .....	88
Figure 41: Backcalculated $E(t)$ master curve using FWD data at temperature set $\{10, 20, 30\}^{\circ}\text{C}$ minimizing normalized error .....	89
Figure 42: Variation of $\xi_{AC}^{avg}$ at different FWD temperature sets using modified sigmoidal variables.....	90
Figure 43: Variation of $\xi_{unbound}$ at different FWD temperature sets using modified sigmoidal variable.....	90
Figure 44: Backcalculation results obtained using modified sigmoid variables.....	91
Figure 45: Viscoelastic properties of field mix in optimal temperature analysis: (a) Relaxation modulus at $19^{\circ}\text{C}$ , (b) Time-temperature shift factor.....	92
Figure 46: Variation of error, $\xi_{AC}(t_i)$ : (a) $t_i = 10^{-5}$ to $t_i = 1$ sec used in $\xi_{AC}(t_i)$ , (b) $t_i = 10^{-5}$ to $t_i = 10^{+2}$ sec used in $\xi_{AC}(t_i)$ and (c) $t_i = 10^{-5}$ to $t_i = 10^{+3}$ sec used in $\xi_{AC}(t_i)$ computation.....	93
Figure 47: Schematic of fitness evaluation in BACKLAVA.....	95
Figure 48: Comparison of actual and backcalculated values in backcalculation using temperature profile.....	98
Figure 49: Error in backcalculated $E(t)$ curve for a three-temperature profile .....	99
Figure 50: Time lag in LTPP section 06A805 (shifted based on constant displacement).....	101
Figure 51: LTPP section 01-0101 cross section and temperature profile in AC layer .....	106
Figure 52: Comparison of measured and forward calculated deflection histories for section 010101 (a) Viscoelastic backcalculation (b) Forward calculated using $E(t)$ obtained from LTPP measured $D(t)$ and elastic backcalculated modulus values.....	106
Figure 53: Comparison of measured and backcalculated $E(t)$ , $a_T(T)$ and $ E^* $ at section 010101.....	107
Figure 54: LTPP section 340802 cross section and temperature profile in AC layer.....	108
Figure 55: Comparison of measured and forward calculated deflection histories for section	

340802 (a) Viscoelastic backcalculation (b) Forward calculated using E(t) obtained from LTPP measured D(t) and elastic backcalculated modulus values.....	108
Figure 56: Comparison of measured and backcalculated E(t), $a_T(T)$ and $ E^* $ at section 340802.....	109
Figure 57: LTPP section 460804 cross section and temperature profile in AC layer.....	110
Figure 58: Comparison of measured and forward calculated deflection histories for section 460804 (a) Viscoelastic backcalculation (b) Forward calculated using E(t) obtained from LTPP measured D(t) and elastic backcalculated modulus values.....	111
Figure 59: Comparison of measured and backcalculated E(t), $a_T(T)$ and $ E^* $ at section 460804.....	111
Figure 60: Elastic backcalculation of two-step temperature profile FWD data, assuming AC as a single layer in two stage backcalculation.....	113
Figure 61: Elastic backcalculation of three-step temperature profile FWD data, assuming AC as a single layer in two stage backcalculation.....	114
Figure 62: Elastic backcalculation of two-step temperature profile FWD data, assuming two AC sublayers in two stage backcalculation.....	115
Figure 63: Elastic backcalculation of three-step temperature profile FWD data, assuming three AC sublayers in two stage backcalculation.....	115
Figure 64: Error in backcalculated E(t) curve from two-step temperature profile.....	116
Figure 65: Error in backcalculated E(t) curve from three-step temperature profile.....	117
Figure 66: Nonlinear elastic backcalculated AC modulus (in stage-1) for Control and CRTB Mixes, using FWD data at different test temperatures.....	124
Figure 67: Nonlinear elastic backcalculated unbound layer properties (in stage-1) for Control and CRTB Mixes, using FWD data at different test temperature.....	125
Figure 68: (a) Comparison of backcalculated and actual E(t) master curves (b) average percentage error, $\xi_{AC}^{avg}$ for the Control mixture and (c) time-temperature shift factor.....	127
Figure 69: (a) Comparison of backcalculated and actual E(t) master curves (b) average percentage error, $\xi_{AC}^{avg}$ for the CRTB mixture and (c) time-temperature shift factor.....	128
Figure 70: Backcalculated and measured FWD deflection time histories for LTPP section 0101: (a) test run in 2004 and (b) test run in 2005.....	131

Figure 71: Nonlinear viscoelastic backcalculation of section 0101 (a) Relaxation modulus (b) Shift factor at 19oC.....	132
Figure 72: Effect of variation in $c_1$ on $ E^* $ master curve.....	140
Figure 73: Effect of variation in $c_2$ on $ E^* $ master curve.....	141
Figure 74: Effect of variation in $c_3$ on $ E^* $ master curve.....	142
Figure 75: Effect of variation in $c_4$ on $ E^* $ master curve.....	143
Figure 76: Effect of variation in $a_1$ on $a_T(T)$ master curve .....	143
Figure 77: Effect of variation in $a_2$ on $a_T(T)$ master curve .....	144
Figure 78: Backcalculated $ E^* $ and $a_T(T)$ at section 01-0101 for year 1993, 1996 and 2000. ...	148
Figure 79: Backcalculated $ E^* $ and $a_T(T)$ at section 34-0802 for year 1993 and 1998. ....	148
Figure 80: Backcalculated $ E^* $ and $a_T(T)$ at section 46-0802 for year 1993, 1995, 1999, 2004 and 2011.....	149
Figure 81: Comparison of static and viscoelastic backcalculation ( $ E^* $ at 10 Hz) for section 01-0101.....	151
Figure 82: Comparison of static and viscoelastic backcalculation ( $ E^* $ at 10 Hz) for section 34-0802.....	152
Figure 83: Comparison of static and viscoelastic backcalculation ( $ E^* $ at 10 Hz) for section 46-0802.....	153
Figure 84: Normalized $ E^* $ and $a_T(T)$ coefficients with ageing time for section 01-0101 .....	155
Figure 85: Normalized $ E^* $ and $a_T(T)$ coefficients with aging time for section 34-0802.....	156
Figure 86: Normalized $ E^* $ and $a_T(T)$ coefficients with aging time for section 46-0802.....	157
Figure 87: Relaxation modulus master curves for the sensivity analysis .....	163
Figure 88: Error in backcalculated relaxation modulus from variation in 6 inch AC thickness. 165	
Figure 89: Error in backcalculated relaxation modulus from variation in 12 inch AC thickness. ....	165
Figure 90: Backcalculated relaxation modulus in 6 inch AC structure: Case-1 sensitivity analysis. ....	166



Figure 91: Backcalculated relaxation modulus in 12 inch AC structure: Case-1 sensitivity analysis.....	167
Figure 92: Error in backcalculated relaxation modulus from variation in base thickness for 6 inch AC structure.....	168
Figure 93: Error in backcalculated relaxation modulus from variation in base thickness for 12 inch AC structure.....	168
Figure 94: Backcalculated relaxation modulus in 6 inch AC structure, case-2 sensitivity analysis.....	169
Figure 95: Backcalculated relaxation modulus in 12 inch AC structure, case-2 sensitivity analysis.....	170
Figure 96: Error in backcalculated relaxation modulus in 6 inch AC structure, case-3 sensitivity analysis.....	172
Figure 97: Error in backcalculated relaxation modulus in 12 inch AC structure, case-3 sensitivity analysis.....	172
Figure 98: Backcalculated relaxation modulus in 6 inch AC structure, case-3 sensitivity analysis.....	173
Figure 99: Backcalculated relaxation modulus in 12 inch AC structure, case-3 sensitivity analysis.....	174
Figure 100: Backcalculated relaxation modulus for structure-A: Case-1 sensitivity analysis. ..	183
Figure 101: Backcalculated relaxation modulus for structure-B: Case-1 sensitivity analysis....	185
Figure 102: Backcalculated relaxation modulus for structure-A: case-2 sensitivity analysis. ....	186
Figure 103: Backcalculated relaxation modulus for structure-B: case-2 sensitivity analysis. ....	188
Figure 104: Backcalculated relaxation modulus for structure-A, case-3 sensitivity analysis. ....	189
Figure 105: Backcalculated relaxation modulus for structure-B, case-3 sensitivity analysis.....	191

# CHAPTER 1

## INTRODUCTION

Flexible pavements are multilayered structures with typically viscoelastic asphalt concrete (AC) as top layer, followed by unbound/bound granular layers. Combined response of linear viscoelastic and elastic materials that are in perfect bonding is linear viscoelastic. Assuming there is full bonding between the asphalt layer and the underlying base and subgrade layers, the overall response of the entire pavement system becomes viscoelastic. Recent developments in pavement design and rehabilitation drift the traditional empirical analysis of pavement to a more mechanistic framework. The MEPDG design guide (MEPDG, 2004) developed under National Cooperative Highway Research Program 1-37A, using mechanistic-empirical framework tries to address various shortcomings of previous empirical pavement design guides (AASHTO, 1993). MEPDG is based on the notion that actual material and loading condition along with locally calibrated mechanistic models would yield accurate response. Long Term Pavement Performance (LTPP) is aimed to develop such a database, which can be used to calibrate MEPDG models. MEPDG uses fundamental properties of pavement materials and acknowledge that the pavement distresses are the consequence of collective factors such as environmental, material and loading conditions. Out of the various contributing factors, temperature distribution in pavement has been given belligerent attention in MEPDG and is regarded as one of the most critical. One of the significant accomplishments of MEPDG is the recognition of AC layer as viscoelastic material. The viscoelastic properties vary with time (frequency) and temperature; and hence require both time and temperature functions to define it.

The characteristic mechanistic properties of an isotropic-thermorheologically simple viscoelastic system are the relaxation modulus  $E(t)$  and the creep compliance  $D(t)$ , which are function of time, the dynamic modulus  $|E^*|$ , which is a function of frequency, and the time-temperature shift factors ( $a_T(T)$ ), which is a function of temperature. These characteristic properties are often expressed at a specific reference temperature, in terms of a ‘master curve’.

It can be shown that if any of the three properties  $E(t)$ ,  $D(t)$  or  $|E^*|$  is known, the other two can be obtained through an inter-conversion method such as the Prony’s series approach (Park and Schapery 1999).  $|E^*|$  is used as the fundamental material property input in MEPDG to incorporate the viscoelastic properties of Hot Mixed Asphalt (HMA) mixes and for the temperature function, the time-temperature superposition principal is exploited. Being an important fundamental material property, knowledge of  $|E^*|$  master curve of an in-service pavement using falling weight deflectometer (FWD) data can lead to more accurate estimation of its remaining life and rehabilitation design. Hence, the viscoelastic properties proposed to be backcalculated from FWD data include two functions - a time function and a temperature function. In the present study, the time function refers to the relaxation modulus master curve  $E(t, T_R)$  in which  $t$  is physical time and  $T_R$  is the corresponding (constant) reference temperature. The temperature function refers to the time-temperature shift factor  $a_T(T)$ , which is a positive definite dimensionless scalar. Furthermore, AC has been assumed to be thermorheologically simple, which allows applying  $E(t, T_R)$  for any temperature level  $T$  (different than  $T_R$ ) by simply replacing physical time with a reduced time  $t_R$ ; therefore,  $a_T(T)$  is a function of both  $T$  and  $T_R$ , such that  $a_T(T) = 1$  if  $T = T_R$ .

## 1.1 Objectives

Appropriate characterization of individual layer properties is crucial for mechanical analysis of flexible pavements. For meaningful interpretation of FWD data it is important that all the factors that influence the test are considered in the analysis. The specific objectives of the study were:

- (i) Develop a layered viscoelastic flexible pavement response model in time domain which can consider variation in temperature with depth (temperature profile) in AC layer.
- (ii) Develop a layered viscoelastic flexible pavement model in time domain which can consider stress sensitive nonlinear unbound layers.
- (iii) Develop robust backcalculation algorithms based on GA which can calculate viscoelastic properties of AC layer and elastic properties of unbound layers.
- (iv) Investigate whether the current FWD testing protocol generates data that are sufficient to backcalculate the  $|E^*|$  master curve using such models.
- (v) If needed, recommend enhancement to the FWD testing protocol (testing temperature, number of sensors) to be able to accurately backcalculate the  $|E^*|$  master curve as well as the unbound material properties of in-service pavements.

## 1.2 Outline

This dissertation consists of seven chapters including the present one. Brief description of each chapter is provided below:

- The second chapter presents a literature review and an overview of the problem background.

- In the third chapter, several algorithms have been developed to implement multilayer viscoelastic forward solution. The models have been validated using Finite Element Method (FEM) based solutions.
- In chapter four, the forward models developed in chapter three were used to develop genetic algorithm (GA) based backcalculation schemes for determining  $E(t)$  or  $|E^*|$  master curve and time-temperature shift factors of AC layers and unbound material properties of in-service pavements. Further, the effect of FWD test temperatures and number of surface deflection sensors on backcalculation of  $|E^*|$  master curve were studied. Suitable FWD test data requirements have been discussed in the key findings from the study.
- In chapter five, the backcalculation algorithms developed in chapter four were used to develop a procedure to quantify evolution of  $|E^*|$  in in-service flexible pavements.
- Chapter six presents a sensitivity analysis on viscoelastic backcalculation.
- Summary and conclusions are presented in chapter seven.

## **CHAPTER 2**

### **LITERATURE REVIEW AND BACKGROUND**

#### **2.1 FWD Data Collection, Analysis and Interpretation**

The FWD test involves dropping a load and then measuring surface deflections through sensors placed at certain pre-designated distances. FWD field data collection usually involves collecting stress history, deflection history, sensor location and surface temperature. During the FWD testing, load is released from a given height onto a load plate, where the stress is recorded through a load cell. The stress and deflection histories are collected at a time step of 0.1-0.2 msec, with the deflection sensors placed at radial distance of 0, 8, 12, 18, 24, 36, 48, 60 and 72 inches. The primary issue with FWD data collection (stress and deflection history) is the error associated with data acquisition system. This issue is particularly relevant to time-based analysis of FWD. In time-based analysis, both the load and deflections are assumed to be coincident, which means any synchronization issue between load and deflection can seriously affect the results.

Most of the FWD devices are either trailer-mounted or vehicle-mounted. In a trailer-mounted system (such as KUAB, Dynatest 8000), the FWD device is fixed on a trailer which is mounted to a towing vehicle, whereas in a vehicle-mounted system, the FWD device is directly fixed into a van. These vehicles are loaded with infrared temperature gauge to collect pavement surface and air temperatures. The primary issue with the collected surface and air temperature is that they may not represent the actual temperature in the asphalt layer. Variation in temperature along the depth of AC layer may significantly influence flexible pavement response. To negate

the effect of temperature FWD deflections are often corrected for temperatures. Temperature correction in FWD analysis is generally done in two steps. In step one, temperature in AC is predicted and in step two, either the FWD deflections or backcalculated modulus values are corrected using the predicted temperature. These temperature prediction equations (Park et al., 2002; Park et al., 2001 and Lukanen et al., 2000) and modulus correction equations (Chen et al., 2000; Park et al., 2001 and Lukanen et al., 2000) are developed empirically using data collected from limited test regions. Further the models are calibrated to predict temperatures at specific depths (generally the mid depth) and reported to predict temperatures with accuracy of  $\pm 2^{\circ}\text{C}$  to  $5^{\circ}\text{C}$ . In order to predict any profile, temperatures at minimum two depths are needed. Further, temperature profile in field is typically small and (as discussed later in chapter 3 and chapter 4) this accuracy may not be sufficient for predicting actual property (i.e.  $|E^*|$ ) of AC layer. During LTPP FWD field tests, in addition to the surface temperature measurement, the temperature profile along the depth of AC layer is also collected. The temperature measurements are recorded at depths, 0mm, 25mm, 50mm, 100mm, 200mm, and 300mm (Schmalzer, 2006). In situ measurement of temperature profile eliminates the errors associated with temperature prediction and provides reliable data for mechanistic analysis.

FWD testing is commonly employed in project level analysis for assisting overlay designs. At network level, FWD testing is done to understand structural capacity of the network at large. Since the inception of FWD, several methods have been developed for the interpretation of FWD data. These methods are based on the understanding of pavement response theories, and techniques to interpret it in a backcalculation scheme. In general, the surface deflection at given radial offsets are calculated using a suitable response theory. The calculated deflections are then

compared with the measured deflections. Various pavement response theories and backcalculation process available in literature are discussed in the following section.

## 2.2 Forward Analysis Methods to Calculate FWD Response

In forward analysis, pavement surface deflections are calculated at specific radial distances. Some of the commonly used mechanistic pavement response theories are

- Boussinesq's solution method
- Multilayered elastic theory
- Finite element model

### 2.2.1 Boussinesq's Solution Method

Boussinesq developed closed form solutions to compute deflection, strain and stresses in a homogeneous, isotropic, linear elastic half-space. The solution was developed for an axisymmetric structure under a vertical point load. Vertical deflection at any point A in half-space can be calculated using equation:

$$d_z = \frac{(1+\nu)P}{2\pi ER} (2(1-\nu) + \cos^2 \theta) \quad (1)$$

where,  $d_z$  is vertical deflection at any point A, P is point load,  $\nu$  is Poisson's ratio, E is modulus of elasticity of the half space, and R and  $\theta$  are geometric distance and angle shown in the Figure 1. Equation 1 implies that surface deflection  $d_z$  at any radial distance  $r$  from the point load can be calculated substituting  $R = r$  and  $\theta = 90^\circ$

$$d_z = \frac{(1+\nu)P}{2\pi Er} (2(1-\nu)) \quad (2)$$



where,  $r$  is the radial distance between load and point of evaluation. Although the formulation given in Equation 2 is an easy to implement close-form solution, pavements in reality are not half spaced and are not subjected to point load. Pavements are multilayered structure with different material properties in each layer.

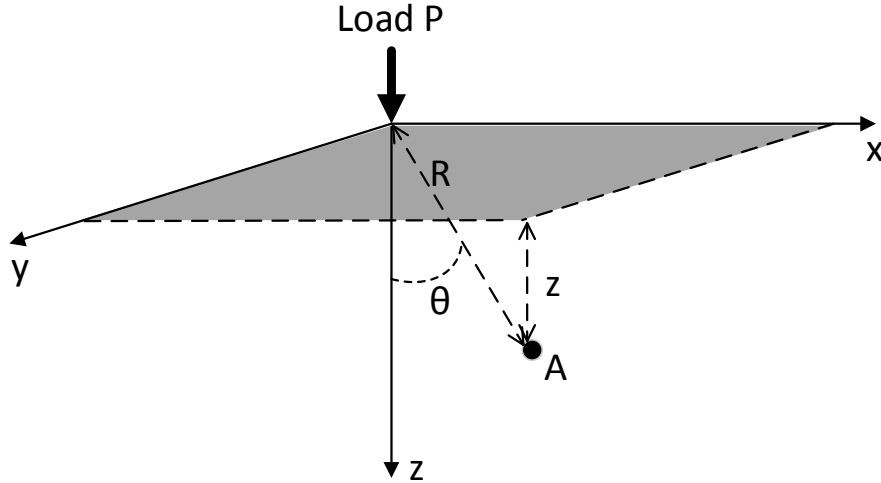


**Figure 1: Half space notation for Boussinesq's solution**

Odemark (Ullidtz, 1988) developed a method to transform multilayer system with different moduli into a single modulus system that makes Boussinesq's equations applicable. The method is based on the assumption that the stiffness of the transformed layers is equivalent to the stiffness of the original (untransformed) layers. Theoretically, the layer transformation can be applied to any number of layers using the transformation relationship:

$$h_e = C \sum_{i=1}^{n-1} h_i \left( \frac{E_i}{E_n} \right)^{\frac{1}{3}} \quad (3)$$

where,  $h_e$  is the equivalent thickness of first  $n-1$  layers,  $C$  is correction factor,  $h_i$  and  $E_i$  are the thickness and modulus of  $i$ th layer. The method is commonly known as method of equivalent thickness (MET). ELMOD3 and BOUSDEF are some of the programs that use MET as forward

solution in their backcalculation algorithms. The method is an approximation and requires appropriate correction factor for predicting pavement response.

### ***2.2.2 Multilayer Elastic Theory***

Multilayer elastic theories are much closer to the pavement system and are most commonly used in pavement analysis. Solution for 2-layer and 3-layer system was first developed by Burmister (1943, 1945). The theory has been extended to multilayer system by various researchers (Schiffman, 1962 and Michelow, 1963) and programmed in several multilayer analysis software.

The basic assumptions of the layered elastic solution are:

- The pavement system is axisymmetric multilayer structure.
- A circular uniformly distributed load is applied normally on the surface of the pavement.
- All the layers consist of homogeneous, isotropic and linearly elastic material and follow Hooke's law.
- All the layers are of homogeneous thickness and extend horizontally to infinity.
- The bottom layer is a semi-infinite half-space.

Basic equations in multilayer formulation are:

- Equilibrium equations
- Compatibility equations

A stress function  $\phi(r, z)$  that satisfies the governing differential equation  $\nabla^4\phi = 0$  can be assumed for each layer to derive stresses and displacement (Love, 1923). The vertical displacement in each layer in terms of stress function can be expressed as:

$$u = \frac{1+\nu}{E} \left[ 2(1-\nu)\nabla^2\phi - \frac{\partial^2\phi}{\partial z^2} \right] \quad (4)$$

where,  $u$  is vertical displacement,  $\phi(r, z)$  is Airy's stress function,  $\nu$  is Poisson's Ratio and  $E$  is modulus of elasticity. The main advantage of multilayer solution over the Boussinesq's solution is its ability to consider distributed surface loading and multiple layers with different properties. However, the solution cannot be used for nonlinear materials or viscoelastic materials. EVERCALC, MICHBACK, MODULUS and CHEVDEF are some of the programs that use linear layered elastic based forward solution in their backcalculation process.

### ***2.2.3 Finite Element Analysis***

Finite element analysis (FEA) offers much more flexibility in selecting material constitutive equations, loading condition and geometric variation. Some of the major advantages of FEA in pavement analysis are:

- Ability to consider nonlinearity in both vertical and horizontal direction
- Ability to consider the viscoelastic properties of HMA in analysis
- Ability to consider dynamics in analysis.

Researchers have mainly used FEA in pavement analysis using general purpose FEA software such as ABAQUS and ANSYS. General purpose software are not pavement-specific, as an example, stress nonlinearity in unbound pavement material are not predefined and need to be

defined as a user defined material (UMAT). Researchers have developed programs (MICHPAVE, CAPA-3D) that have inbuilt pavement-specific models to analyses unbound nonlinearity, dynamics and viscoelasticity. However, they are not designed for a backcalculation type analysis and usually slow.

#### **2.2.4 Forward Analysis Programs**

With the advancement of computing facilities, several pavement analysis softwares have been developed. Flexible pavements are multilayered structures, with typically viscoelastic asphalt layer followed by nonlinear unbound/bound layers. Conventionally, multilayered elastic analysis is performed to obtain response of flexible pavements for design and inverse analyses, however, assuming asphalt pavement as a linear elastic material is an oversimplification of its actual behavior. It is well known that the asphalt pavements' responses are both rate and temperature dependent. A list of common pavement analysis computer programs and their capability to account for nonlinear and viscoelastic behavior of pavement is presented in Table 1.

**Table 1: List of commonly used pavement response models**

Program Name	Developer	Response Model	Nonlinearity	Viscoelasticity
BISAR	Shell Oil Co.	Layered elastic analysis	No	No
CAPA-3D	Delf University of Technology	3D-FEM	Yes	Yes
CHEVRON	Chevron	Layered elastic analysis	No	No
ELSYMS	FHWA	Layered elastic analysis	No	No
Everstress	University of Washington	Layered elastic analysis	Yes	No
KENLAYER	Yang H. Huang	Layered elastic analysis	Yes	Yes
MICHPAVE	Michigan State University	Axi-symmetric FEM	Yes	No

Most of the softwares for pavement analysis are based on layered elastic theories and do not consider nonlinearity or viscoelasticity. The FEM based softwares CAPA-3D and MICHPAVE can consider nonlinearity. CAPA-3D is also capable of accounting for nonlinearity

as well as viscoelastic behavior. An approximate nonlinear analysis of pavements can also be performed using multilayered elastic based solution. Among the layered elastic analysis based softwares, Everstress and KENLAYER (Huang, 2004) account for nonlinearity through iteratively adjusting layer moduli. However, since the multilayer elastic theory assumes each individual layer to be vertically as well as horizontally homogeneous, it can be used to depict nonlinearity only through approximation. For incorporating variation in modulus with depth, Huang (Huang, 2004) suggested dividing the nonlinear layer into multiple sublayers. Furthermore, he suggested choosing a specific location in the nonlinear layers to evaluate modulus based on the stress state of the point. He showed that when the midpoint under the load is selected to calculate modulus values, the predicted response near the load is close to the actual response. However, the difference between actual and predicted response increased at points away from the loading.

### **2.3 Backcalculation Approaches**

Backcalculation analysis is essentially an inverse analysis, which involves determining the pavement layer properties using measured pavement surface deflections. The backcalculated results are sensitive to the backcalculation technique used in the analysis (Chou and Lytton, 1991; and Harichandran et al., 1993). Typically backcalculation programs adopt techniques such as nonlinear regression, iterative methods, close-form solutions and database search to predict pavement properties. Regression method and close form solution methods are simple and time efficient, but are mainly used to predict subgrade modulus (Newcomb, 1986; Horak, 1987; and AASHTO, 1993). Most of the backcalculation programs employ iterative methods to reach solution. Backcalculation using iterative methods are essentially optimization problem. The problem involves iteratively changing the unknowns till an objective function is minimized

under a pre-defined tolerance limit. For instance, in elastic backcalculation this objective function is generally root mean square error or percent difference between the measured and predicted deflection basin (peak deflection from each deflection sensor) and the unknowns are the elastic moduli of the layers. The optimization methods can be classified into two major categories. The first category is based on the traditional optimization techniques which repeatedly use a forward analysis method in a direct search or gradient based search technique. The second category is based on non-traditional optimization techniques which mimics mechanisms observed in nature.

### ***2.3.1 Traditional Optimization Techniques***

In traditional optimization direct search (such as simplex, Hooke-Jeeves) or gradient search (such as secant method, Newton Raphson, modified Levenberg-Marquardt algorithm, and modified Powell hybrid algorithm) based methods are used. Figure 2 illustrates the typical steps involved in a traditional optimization based backcalculation procedure.

An example of direct search method is MODULUS, which uses Hooke-Jeeves algorithm. The MODULUS program is a multilayer elastic based backcalculation program developed by Texas Transportation Institute. The program generates a database of deflection basin using linear elastic program WESLEA (Rohde and Scullion, 1990). The number of deflection basins generated is based on the number of layers and the expected moduli range. The generated deflection database is then searched. The program uses Hooke-Jeeves pattern search algorithm to minimize sum of square difference between the measured and calculated deflections. The program can also calculate depth to stiff layer and perform temperature correction. The program (MODULUS 6.0) can handle up to four layers and seven deflection sensors. COMDEF

(Anderson, 1989) is another example of backcalculation program which generates a database of deflection basin. It uses CHEVRON as the forward program to generate deflection database.

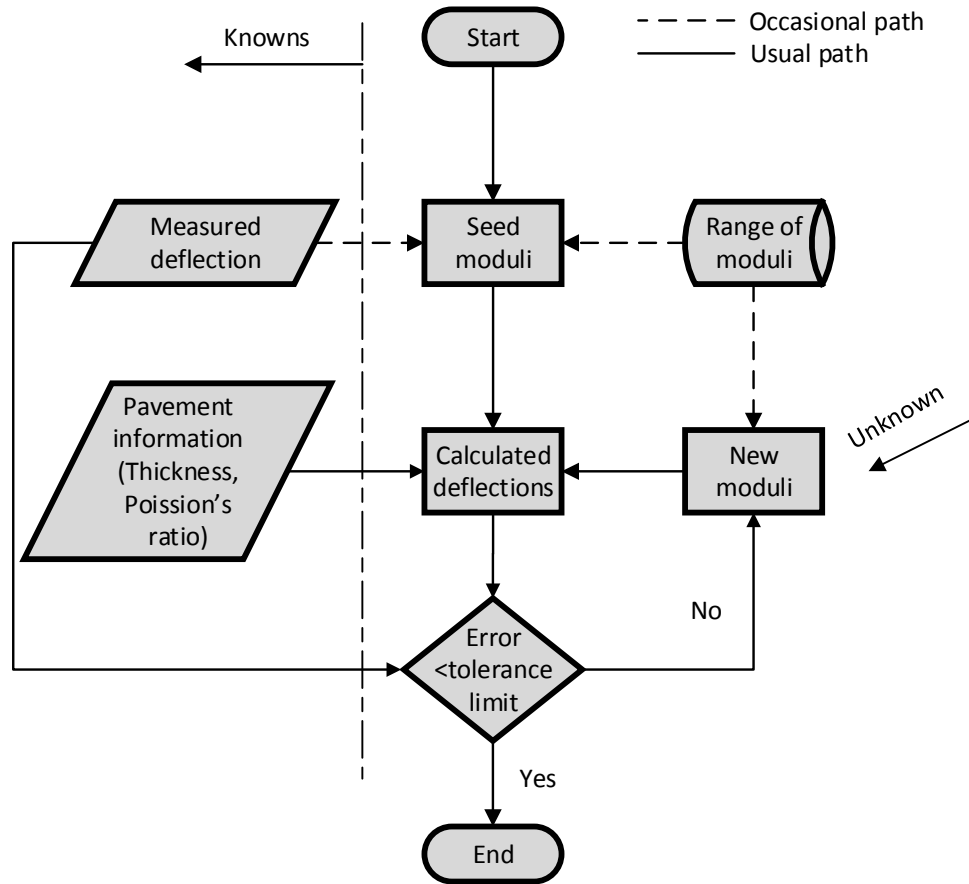


**Figure 2: Typical steps in iterative backcalculation**

MICHBACK, EVERCALC and CHEVDEF are some of the examples of gradient search method based backcalculation programs. EVERCALC iteratively varies elastic moduli and compute surface deflection using linear elastic forward program WESLEA. The calculated deflections are then compared with field measured deflections till one of the following termination criteria is reached: (a) Deflection tolerance: root mean square error between the calculated and measured deflection basin. (b) Moduli tolerance: percentage difference in the predicted moduli values between consecutive iterations. (c) Maximum number of iterations. The

software uses a Levenberg-Marquardt algorithm to minimize the error. Although the forward algorithm in EVERCALC is based on linear layer elastic solution, the software offers nonlinear characterization of unbound layers using linear regression. The software can also provide temperature correction and depth to stiff layer. MICHBACK is another layered elastic backcalculation program, developed by Michigan State University. It uses linear elastic layered solution program CHVERONX for forward calculation. The program uses modified Newton-Rapson method to minimize root mean square error between the measured and calculated deflection basin. The program can also predict depth to stiff layer in the analysis. A list of commonly used backcalculation programs is presented in Table 1. Backcalculation using traditional iterative methods are popular and most commonly used, but they have the following issues:

- All the conventional backcalculation procedures either require a seed value as an input or select a seed value within the software. These methods have the tendency to move towards the closest solution in the vicinity of the initial seed value. If the closest solution is not the global solution, then a local solution is approached.
- Convergence time may vary depending on the initial seed value chosen and the optimization technique used. Often if the selected seed value is not close to the optimum solution, the backcalculation would require longer time to reach the solution.

The disadvantages of classical methods listed above do not mean that they cannot be used in backcalculation procedure. In fact the classical methods can be hybridized along with non-traditional optimization techniques in developing more effective backcalculation procedures. Non-traditional techniques are much more capable of addressing these issues.



**Table 2: List of commonly used backcalculation programs (Smith et. al 2010).**

Program Name	Developer	Forward Calculation Method	Forward Calculation Sunroutine	Backcalculation Method	Non-Linear Analysis	Layer Interface Analysis	Maximum Number of Layers	Seed Moduli	Range of Acceptable Modulus	Ability to Fix Modulus	Convergence Scheme	Error Weighting Function
BISDEF	USACE-WES	Multi-Layer Elastic Theory	BISAR	Iterative	No	Variable	Number of deflections; best for 3 unknowns	Required	Required	Yes	Sum of squares of absolute error	Yes
BOUSDEF	Zhou et al. (Oregon State)	Method of Equivalent Thickness	MET	Iterative	Yes	Fixed (rough)	At least 4	Required	Required		Sum of percent errors	
CHEVDEF	USACE-WES	Multi-Layer Elastic Theory	CHEVRON	Iterative	No	Fixed (rough)	Number of deflections; best for 3 unknowns	Required	Required	Yes	Sum of squares of absolute error	Yes
COMDEF	USACE-WES	Multi-Layer Elastic Theory	BISAR	Database	No	Fixed (rough)	3	No	No		Various	No
DBCONPAS	Tia et al. (Univ. of Florida)	Finite Element	FEACONS III	Database	Yes?	Yes?		No	No			
ELMOD/ELCON	Ulidtz (Dynatest)	Method of Equivalent Thickness	MET	Iterative	Yes (subgrade only)	Fixed (rough)	4 (exclusive of rigid layer)	No	No	Yes	Relative error of 5 sensors	No
ELSDEF	Texas A&M, USACE-WES	Multi-Layer Elastic Theory	ELSYM5	Iterative	No	Fixed (rough)	Number of deflections; best for 3 unknowns	Required	Required	Yes	Sum of squares of absolute error	Yes
EMOD	PCS/Law	Multi-Layer Elastic Theory	CHEVRON	Iterative	Yes (subgrade only)	Fixed (rough)	3	Required	Required	Yes	Sum of relative squared error	No
EVERCALC	Mahoney et al.	Multi-Layer Elastic Theory	WESLEA	Iterative	Yes	Variable	5	Required (4 and more layers)	Required	Yes	Sum of absolute error	Yes
FPEDD1	Uddin	Multi-Layer Elastic Theory	BASINF?	Iterative	Yes	Fixed (rough)		Program Generated				No
ISSEM4	Ullidtz, Stubstad	Multi-Layer Elastic Theory	ELSYM5	Iterative	Yes (finite cylinder concept)	Fixed (rough)	4	Required	Required	Yes	Relative deflection error	No
MICHBACK	Harichandran et al.	Multi-Layer Elastic Theory	CHEVRON X	Newton method	No	Fixed (rough)	Number of deflections; best for 3 unknowns	Required	Required	Yes	Sum of relative squared error	
MODCOMP 5	Irwin, Szebenyl	Multi-Layer Elastic Theory	CHEVRON	Iterative	Yes	Fixed (rough)	2 to 15 layers; maximum of 5 unknown layers	Required	Required	Yes	Relative deflection error at sensors	No
MODULUS	Texas Transportation Institute	Multi-Layer Elastic Theory	WESLEA	Database	Yes?	Fixed?	4 unknown plus stiff layer	Required	Required	Yes	Sum of relative squared error	Yes
PADAL	Bown et al.	Multi-Layer Elastic Theory		Iterative	Yes (subgrade only)	Fixed?		Required			Sum of relative squared error	
RPEDD1	Uddin	Multi-Layer Elastic Theory	BASINR	Iterative	Yes	Fixed?		Program Generated				No
WESDEF	USACE-WES	Multi-Layer Elastic Theory	WESLEA	Iterative	No	Variable	5	Required	Required	Yes	Sum of squares of absolute error	Yes

### 2.3.2 Non-Traditional Optimization Methods

The difficulties and limitations of traditional techniques have contributed to the development of non-traditional methods in backcalculation. Limited literature exists on application of non-traditional methods in pavement backcalculation. Two methods that have been used by researchers in pavement backcalculation are genetic algorithm (GA) and artificial neural network (ANN). In ANN the biological neural networks in brain are mimicked by network of artificial neurons. Figure 3 shows a schematic figure of an artificial neuron and an artificial neural network.

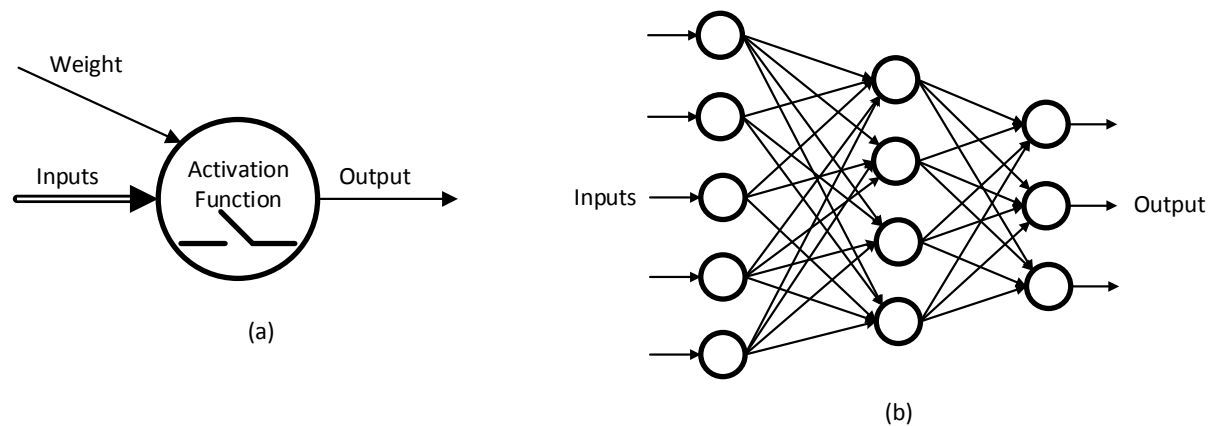


**Figure 3: Schematic figure of a neuron and ANN network**

Meier and Rix (1994) developed ANN network using synthetic deflection basin for three layer flexible pavement. They reported that the ANN performed three fold faster than the conventional gradient search method. The authors (Meier and Rix, (1995)) also developed an ANN for dynamic backcalculation of flexible pavement properties. Gopalakrishnan et al. (2006) trained an ANN for predicting nonlinear layer moduli of airfield pavements. The aim of the study was to develop networks which can perform backcalculation of airfield pavements subjected to heavy weight deflectometers. To train the ANN, synthetic deflections were generated using finite element (FE) based software ILLI-PAVE. Khazanovich and Roesler (1997) developed an ANN

based backcalculation program DIPLOBACK to backcalculate elastic properties of composite pavements. The developed ANN was verified using field FWD data. Similar trend was reported in the backcalculated results using ANN and the results obtained from WESDEF. One of the main advantages of ANN in backcalculation is its speed. However, ANN needs to be trained beforehand using synthetic or field data. Two main issues with ANN based backcalculation models are:

- (1) The quality of the backcalculated results depends on the quality of ANN trained.
- (2) Generally, to train ANN, synthetic database of deflections is generated by varying various parameters such as, number of pavement layer, layer thickness, layer moduli and depth to stiff layer. The developed ANN is expected to give reasonable results only for the problems which are within the bounds of the cases considered in the training of the ANN.

Genetic algorithm is another non-traditional method which mimics biological process in nature (Bremermann, 1958; Holland, 1975; and Goldberg, 1989). GA comes under the class of evolutionary algorithms in optimization. There are three major categories of evolutionary algorithm: genetic algorithm (GA), evolutionary strategies (ES) (Rechenberg, 1965) and evolutionary programming (EP) (Fogel, 1962; and Fogel et al., 1966). The differences between the three methods are very slim and mainly lie in the evolution process.

GA was first introduced by Bremermann in 1985. Holland (Holland, 1975) developed the much more formal mechanism of GA which was implementable in computers. He developed the mechanics of GA using schemata theory, which was based on the assumption that every candidate solution can be encoded as a series of binary numbers, so-called “chromosomes”.

Once the candidate solutions were transformed into chromosomes (parents), they were operated to reproduce new candidate solutions.

In general terms, GA performs the following operations: (a) initialization, (b) selection, (c) generation of offspring and (d) termination. Figure 4 illustrates the typical steps involved in a GA based optimization procedure.

In initialization, the GA generates a pool of solutions using a subset of the feasible search space, so-called 'population'. Each parameter in a solution is encoded as string which is attached to form a chromosome. It should be noted that the size of the population plays an important role in the success of the optimization. A large population size would unnecessarily lead to high computational time, whereas a small population size may lead to premature convergence at a local solution.

In selection process, each chromosome (solution) is evaluated using an objective function and the best fitted solutions are selected to create a mating pool. The parents from the mating pool are randomly selected to generate next generation population (offspring). This process mainly involves two operators: crossover and mutation.

In crossover, a new solution is formed by exchanging information between two parent solutions, which is done by swapping a portion of parent chromosomes (Figure 5a). In mutation, a new solution is formed by random bit-wise flipping a parent chromosome (Figure 5b). The newly generated population is evaluated using the objective function. This process is repeated until a termination criterion is reached. Through guided random search from one 'generation' to another, GA minimizes the desired objective function.

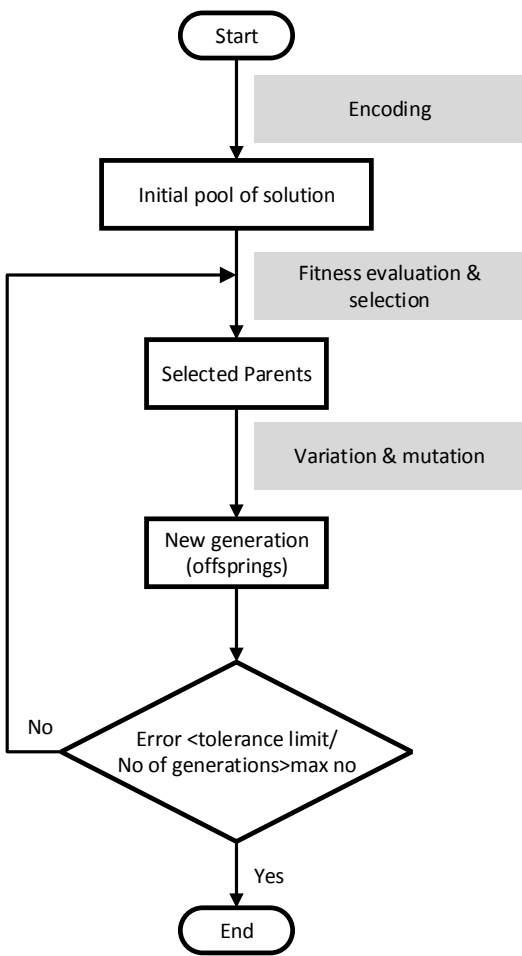


**Figure 4: Typical steps in GA**

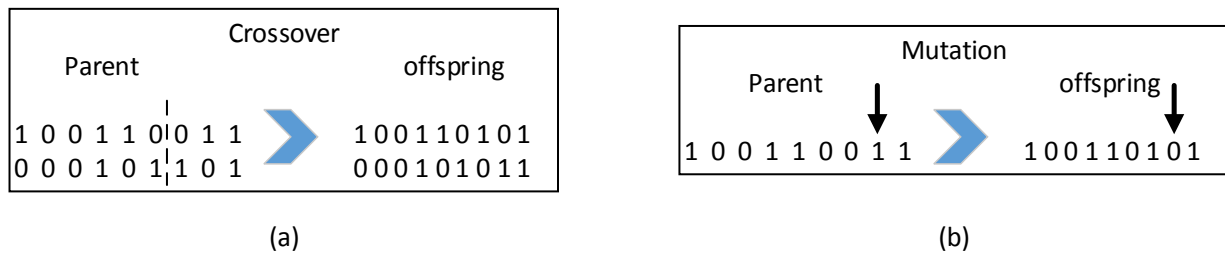


**Figure 5: Figure illustrating GA operations (a) Crossover and (b) Mutation**

GAs are much more suited for the following type of problems:

- Problems which do not have a close-form solution.
- Problems which have complex objective function and gradients are difficult to obtain.

- Problems with multiple constraints and limits on the variables.
- Problems involving multiple optimum solutions.
- When the search domain involved is very large.

Limited literature exists on application of GA in flexible pavement backcalculation (Fwa et al., 1997; Reddy et al., 2004; Tsai et al., 2004; Sangghaleh et al., 2013; and Alkasawneh, 2007). Fwa et al. (1997) developed a GA based backcalculation program NUS-GABACK. The program was compared with four other backcalculation programs, MICHBACK, MODULUS, EVERCALC and EVERCALC-Alt. For comparison, synthetic deflection basins were generated using 3 and 4 layer pavement structures. The population size and generation size used in the study were 60 and 150 respectively. The program was reported to produce more consistent and accurate backcalculation results compare to the other programs. Tsai et al. (2004) demonstrated the applicability of GA in flexible pavement backcalculation. Reddy et al. (2004) studied the effect of GA parameters on performance of GA in backcalculation. A population size of 60 and generation size of 60 was recommended for 3 and 4 layer pavement structures. Alkasawneh (2007) developed a GA-based backcalculation model BackGenetic3d, which can consider any number of layers in backcalculation. In elastic backcalculation, peak deflection measured at 7-8 sensors are used in backcalculation. This restricts the number of unknowns (preferably  $\leq 5$ ) in most of the traditional optimization based backcalculation programs. However, GA based optimization do not carry any indeterminacy with number of unknown. Although GA is an attractive optimization technique, if not used appropriately, it may lead to the following issues:

- If the objective function is computationally expensive or require large number of population and generations, then GA may take long time to reach the solution.

- The parameters in the algorithm (population size, number of generation, crossover and mutation probabilities) should be selected such that global solution is reached with minimum computational effort. Optimal parameters for running GA differ from problem to problem. Often for any problem a trial and error process is required to choose the best suited parameter values.
- Because of the inherent randomness in the optimization process, GAs produce results which are near-optimum solution.

## **2.4 Modeling Issues in Backcalculation**

Practical modeling of asphalt pavement systems has been traditionally carried out using layered elastic theory (Shell 1978, Shook et al. 1982, Monismith 2004); and the FWD data analyzed using elastic inverse analysis, which assumes pavement to be a multilayered elastic structure (Harichandran et al., 1993; Fwa et al., 1997; Irvin, 1994; and Bush, 1985). Such an analysis typically involves identifying layer moduli by matching measured peak displacements with computed displacements obtained at peak load. However, it is well known that the AC is linear viscoelastic at low strain levels (Kutay et al., 2011; and Levenberg, 2013). Like any viscoelastic material it shows properties dependent on time (or frequency) as well as temperature. In an attempt to provide the engineering community with a better mechanistic framework, there is a current movement towards treating the asphaltic layers, and hence the entire pavement system, as layered viscoelastic medium. Such a campaign naturally generates interest for obtaining viscoelastic pavement properties in situ, nondestructively, by way of inverse analysis (Kutay et al., 2011). For the asphaltic layers, assuming isotropy, constant Poisson's ratio, and thermo-rheological simplicity, the sought after viscoelastic properties

include the relaxation modulus  $E(t)$ , the dynamic modulus  $|E^*|$ , and the time-temperature shifting  $a_T(T)$ .

In fact, the impulse loading in the FWD test makes it a dynamic test (Uzan, 1994; Foinquinos et al., 1995; and Roesset et al., 1995). In dynamic backcalculation methods, typically, damped elastic or elasto-dynamic system is analyzed using finite layer or FE based forward computations (Uzan, 1994; Al-Khoury et al., 2001; Al-Khoury et al., 2002; and Losa, 2002), which can be performed either in the frequency domain or in the time domain (Uzan, 1994). In frequency domain backcalculation, the applied load and deflection response histories are transformed into the complex domain at various frequencies. This deflection response is then matched with the deflection obtained from optimized complex moduli of pavement layers. The aforementioned frequency domain based backcalculation procedure is known to be sensitive to deflection truncation (Chatti, 2004, Chatti et al., 2006), which is commonly applied about 60 milliseconds after the loading pulse. Recently Lee (2013) developed a time domain multilayer dynamic forward analysis program, ViscoWave. The solution used in the program is based on continuous Laplace and Hankel Transforms. Zaabar et al. 2014 implemented the ViscoWave solution in C++ and used parallel processing to develop a backcalculation program DYNABACK-VE. Although dynamic backcalculation can consider viscoelastic properties of the AC layer, it is computationally expensive and difficult to carry out by pavement engineers.

Contribution of dynamics in the FWD test depends mainly on the presence and depth of a stiff layer (Foinquinos et al., 1995; Roesset et al., 1995 and Uzan, 1994). Foinquinos et al. (1995) compared the static and dynamic response of pavements with various stiff layer depths. They showed that the difference between the two becomes smaller as the depth of the stiff layer increases. Lei (2011) showed that the dynamic effects in a multilayered viscoelastic structure are



negligible when the stiff layer is located at a depth of more than 5.5 m (18ft) from the pavement surface. Usually, backcalculation techniques are based on elasto-static analysis; expected to give solutions comparable to dynamic solutions when there is no stiff layer. Although elastic backcalculation is simple and computationally efficient, it lacks the inherent ability to reproduce the observed (time-temperature dependent) system behavior and infer the time and temperature dependent layer properties.

Kutay et al. (2011) developed a computationally efficient inverse technique based on layered viscoelastic forward analysis to backcalculate viscoelastic layer properties. Backcalculation of  $|E^*|$  from FWD field data needs both load and corresponding deflection time histories. The peak deflections alone may not be sufficient to provide enough information about the AC material property (Kutay et al., 2011). The method was used to backcalculate the relaxation modulus  $E(t)$  of an AC layer using FWD time history from a single drop under a single temperature level (temporally and spatially constant). In the study, a sigmoidal shape was a-priori assumed for  $E(t)$  and the backcalculated relaxation modulus was subsequently converted to provide the  $|E^*|$  master curve. A main limitation in the above backcalculation scheme is that it assumes the entire depth of the AC layer to be at a constant temperature. However, it is likely that a non-uniform temperature profile will exist in the field (MEPDG, 2004; and Alkasawneh, 2007a); a situation that should be taken into consideration because of the thermo-sensitivity of the AC layers, especially in comparison with base and subgrade materials (Alkasawneh, 2007a). The MEPDG accounts for the effects of non-uniform temperature profiles by subdividing the pavement layers into multiple sublayers and assigning a different modulus value to each on the basis of the prevailing temperature conditions. Similarly, Alkasawneh et al. (2007b) proposed to use sublayering to capture modulus variation in the AC layer through elastic layered analysis.

However, dividing the AC layer into multiple sublayers increases the number of variables in backcalculation and hence limits the information that can be obtained regarding the time-temperature properties of the AC layer.

## 2.5 Characterizing Linear Viscoelastic Properties of HMA in Laboratory

Linear viscoelastic materials possess both elastic as well as viscous characteristics. To ensure that the properties measured in laboratory are within the linear range, the applied strains are kept under 100-120  $\mu\epsilon$ . The theory of viscoelasticity states that if one of the following linear viscoelastic properties is known (i.e.  $|E^*|$ ,  $D(t)$  or  $E(t)$ ), the others can be calculated mathematically through numerical interconversion procedures (Park and Schapery, 1999; and Kim 2009). For ease in measurement, typically  $|E^*|$  is measured in laboratory through cyclic sinusoidal loading. As shown in equation below the measured strain lags the applied stress by an angle  $\delta$ .

$$\sigma = \sigma_o \cos(\omega t + \delta) \quad (5)$$

$$\epsilon = \epsilon_o \cos(\omega t) \quad (6)$$

where,  $\sigma_o$  is the stress amplitude,  $\epsilon_o$  is the strain amplitude,  $\omega = 2\pi f$  is applied angular frequency,  $t$  is time and  $\delta$  is phase angle. The  $|E^*|$  is calculated as the ratio of stress amplitude to strain amplitude as shown in the equation (Kim, 2009)

$$|E^*| = \frac{\sigma_o}{\epsilon_o} \quad (7)$$

A much convenient way to define the viscoelastic behavior is using complex form representation of stress and strain

$$\sigma^* = \sigma_o e^{i\omega t} \quad (8)$$

$$\varepsilon^* = \varepsilon_o e^{i(\omega t - \delta)} \quad (9)$$

The dynamic complex modulus  $E^*$  is defined through the stress strain relationship as shown in the equation.

$$E^* = \frac{\sigma^*}{\varepsilon^*} = \frac{\sigma_o}{\varepsilon_o} e^{i\delta} = E' + iE'' \quad (10)$$

where,

$$E' = \frac{\sigma_o}{\varepsilon_o} \cos(\delta) \text{ and}$$

$$E'' = \frac{\sigma_o}{\varepsilon_o} \sin(\delta)$$

$E'$  is the ratio of in-phase stress and strain and is called as the storage or elastic modulus.  $E''$  is the ratio of out-of-phase stress and strain and is called as the loss or viscoelastic modulus. For a perfectly elastic material  $E''$  is expected to be zero, whereas for a perfectly viscoelastic material  $E'$  is expected to be zero. In complex plain the dynamic modulus is defined as the norm of the  $E^*$  and phase angle is defined as the argument express as:

$$|E^*| = \sqrt{E'^2 + E''^2}$$

$$\delta = \tan^{-1}(E''/E') \quad (11)$$

MEPDG considers HMA as a viscoelastic material. It recognizes that  $|E^*|$  values of HMA vary with both, the test frequency and test temperature. To incorporate the effect of both the frequency and the temperature in a single curve, a master curve is generated at a chosen

reference temperature. Once a master curve is constructed,  $|E^*|$  values at temperatures different from the reference temperature are calculated using the time-temperature superposition principle. Level-1 analysis in MEPDG requires  $|E^*|$  values at minimum 3 temperatures and at minimum 4 frequencies directly measured from laboratory. While inputting  $|E^*|$  values in MEPDG, the following guidelines are outlined for selecting the temperatures and frequencies

- At least one data at temperature below 30°F.
- At least one data at temperature between 40F-100°F.
- At least one data at temperature higher than 125°F.
- At least one data at frequency less than 1 Hz.
- At least two data at frequency between 1-10 Hz.
- At least one data at frequency greater than 10 Hz.

Maximum of 8 temperature levels and a maximum of 6 frequency levels are allowed and inputs at 5 temperature and 4 frequency levels are recommended. The default temperatures and default frequencies used are: 14, 40, 70, 100 and 130°F and 0.1, 1, 10 and 25 Hz respectively.

The master curve and shift factor are obtained by fitting the raw  $|E^*|$  values measured at different temperatures to a single master curve. Typical steps followed in the development of  $|E^*|$  master curve from dynamic modulus test are:

- 1) Determine dynamic modulus at different temperatures (AASHTO T342 recommends -10, 4, 21, 37 and 54°C). At each temperature, test the specimen at a range of frequencies

(AASHTO T342 recommends 25, 10, 5, 1, 0.5, 0.1 Hz). Figure 6 shows an illustrative diagram of raw  $|E^*|$  data generated in lab.

- 2) Select a reference temperature,  $T_{ref}$  for the dynamic modulus master curve.
- 3) Using time-temperature superposition (TTS) principle, shift the measured raw  $|E^*|$  data to a single master curve. The master curve is usually defined as a sigmoid:

$$\log(|E^*|) = b_1 + \frac{b_2}{1 + \exp(-b_3 - b_4 \cdot \log(f_R))} \quad (12)$$

where,  $b_1$ ,  $b_2$ ,  $b_3$  and  $b_4$  are sigmoid coefficients and  $f_R$  is reduced frequency. Note that the shifted master curve is obtained for the reduce frequency  $f_R$  defined at the reference temperature  $T_{ref}$ . The equation used in the shift is:

$$f_R = f \cdot a_T(T) \quad (13)$$

where,  $f$  is the test frequency and  $a_T(T)$  is the shift factor for a given temperature  $T$ .

$$a_T(T) = 10^{a_1(T^2 - T_{ref}^2) + a_2(T - T_{ref})} \quad (14)$$

During the shifting process, the shift factor coefficients,  $a_1$  and  $a_2$  and sigmoid coefficients  $b_1$ ,  $b_2$ ,  $b_3$  and  $b_4$  are numerically optimized until a good sigmoid fit is obtained. Figure 6 shows an illustrative diagram of the shifting in the optimization process.

However, since the primary input of the layered viscoelastic algorithm utilized in this research is  $E(t)$ , it is backcalculated first, allowing then for  $|E^*|$  master curves to be derived via interconversion for comparison. In the next subsection, conversion predominantly used in the study,  $E(t)$  to  $|E^*|$  is explained.

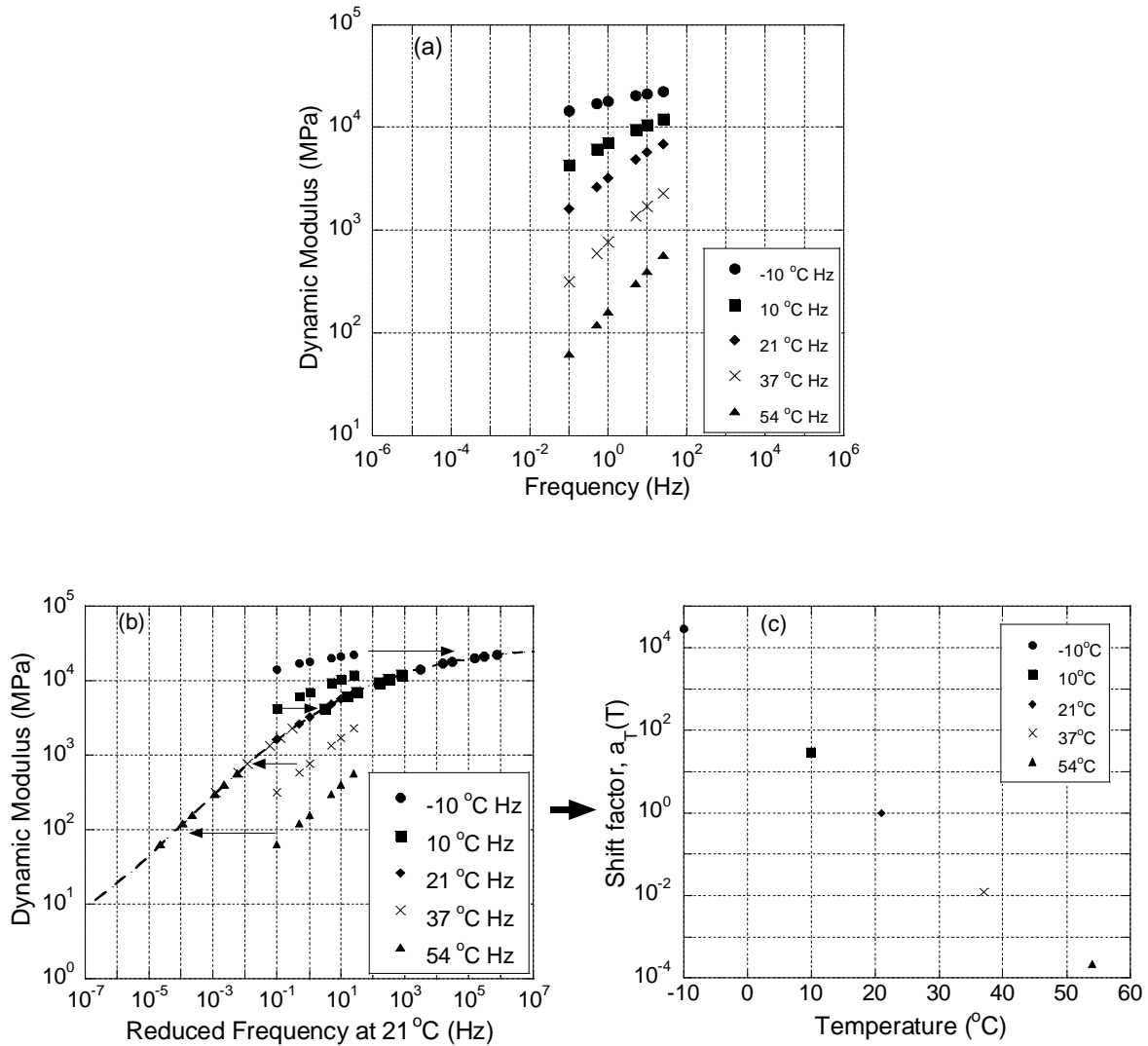


**Figure 6: Figure illustrating steps in developing  $|E^*|$  master curve using laboratory measured  $|E^*|$  test data : (a) raw  $|E^*|$  data, (b) master curve development (c) time-temperature shift factors**

### 2.5.1 Interconversion of $E(t)$ to $|E^*|$

Relaxation modulus is the ratio of stress response (with time) to a unit strain input. The relaxation behavior is typically fitted as Prony series (i.e., generalized Maxwell), which is a summation of sequence of exponentially decaying functions expressed as (Kim, 2009)

$$E(t) = E_{\infty} + \sum_{i=1}^N E_i e^{-t/\rho_i} \quad (15)$$

where,  $E_{\infty}$  = long term relaxation modulus,  $E_i$  = modulus of each maxwell spring,  $\rho_i = \eta_i/E_i$  is relaxation time, and  $\eta_i$  is the viscosity of each dashpot element in the generalized Maxwell model. A numerical optimization is performed to determine the Prony series coefficient  $E_{\infty}$  and  $E_i$  in equation. Typically, a series of relaxation time from a range of  $10^{-8}$  sec to  $10^{+8}$  seconds are selected.  $E_{\infty}$  and  $E_i$  values in Equation 15 are varied until a good fit to the  $E(t)$  is obtained. Behavior of viscoelastic materials are typically modeled using prudent combination of springs and dashpot. The mathematical expression in Equation 1 can be shown to have physical representation of springs and dashpot as shown in Figure 7, often referred to as Generalized Maxwell model.

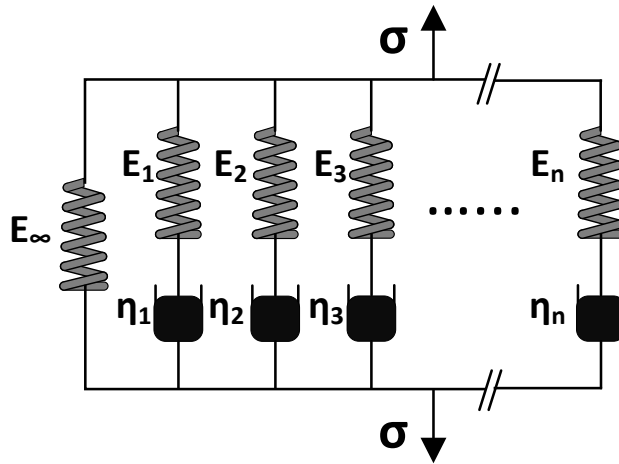


**Figure 7: Generalized Maxwell model**

Mathematically the complex modulus can be defined as a complex number as shown in Equation (10). The real part ( $E'(f)$  storage modulus) and the complex part ( $E''(f)$  loss modulus)

of complex modulus can be obtained for a Generalized Maxwell model (fitting Prony series to relaxation modulus) shown in Figure 7, using the following equations:

$$E'(f) = |E^*(f)| \cos(\delta) = E_\infty + \sum_{i=1}^N E_i \frac{(2\pi f \rho_i)^2}{1 + (2\pi f \rho_i)^2} \quad (16)$$

$$E''(f) = |E^*(f)| \sin(\delta) = \sum_{i=1}^N E_i \frac{2\pi f \rho_i}{1 + (2\pi f \rho_i)^2} \quad (17)$$

where  $\delta$  is the phase angle,  $|E^*|$  is the absolute value of the complex modulus  $E^*$  function,  $E_i =$  modulus of each Maxwell spring,  $\rho_i = \eta_i / E_i$  is relaxation time, and  $\eta_i$  is the viscosity of each dashpot element in the generalized Maxwell model. The dynamic modulus master curves were calculated from the storage modulus and the loss modulus using Equation (11).

### 2.5.2 Interconversion $D(t)$ to $E(t)$

Interconversion from  $D(t)$  to  $E(t)$  can be performed mathematically owing to the fact that the product of dynamic creep compliance  $D^*$  and dynamic modulus  $E^*$  in frequency domain is equal to one. An appropriate conversion using this method would require  $D(t)$  data over a large range of time ( $\sim 10^{-6}$  to  $10^{+6}$  seconds). However, due to testing constraints, creep data are available only over a smaller range of time and temperature, which is not sufficient for conversion using the method. Creep compliance data can be converted to  $E(t)$  assuming a classical power-law function for the creep compliance (see Equation (18)). The measured data at different temperatures can be fitted separately and the associated relaxation modulus is then obtained using the mathematically exact formula given in Equation (19) (Kim, 2009):



$$D(t) = D_1 t^n \quad (18)$$

$$E(t)D(t) = \frac{\sin n\pi}{n\pi} \quad (19)$$

where,  $D_1$  and  $n$  are the power function coefficients of  $D(t)$ . Once  $E(t)$  at each temperature are obtained,  $E(t)$  master curve can be generated using a similar procedure described for  $|E^*|$  (see Equation (12) and (13)).

## 2.6 Motivation and Scope

From the past studies it can be seen that most of the work on backcalculation have been carried out considering AC as elastic layer. Backcalculation programs which can consider viscoelastic properties of AC are computationally too expensive. Some of the issues related to the existing studies can be identified as follows:

- The existing backcalculation programs consider AC as elastic layer and cannot be used to predict viscoelastic properties of HMA in situ.
- In the existing backcalculation procedures the FWD temperature corrections are carried out using empirically developed equation. The correction procedure does not recognize the actual viscoelastic characteristics of the HMA.
- It is well known that FWD deflections and backcalculated properties are influenced by AC temperature. At present there are no guidelines for FWD testing temperature.
- Existing studies have shown that both the viscoelastic properties of AC and stress sensitivity of unbound layers can play a crucial role in pavement response. None of the

existing backcalculation programs consider both the effects simultaneously in backcalculation.

These shortcomings in the current practice have motivated the author to develop new forward and backcalculation models for FWD analysis. In the present work, a procedure was developed for backcalculating these properties from conventional Falling Weight Deflectometer (FWD) test data in combination with knowledge of the testing temperature profile in the asphalt layer. The present work has two main objectives: (1) Attempt to simulate more realistic FWD test conditions with respect to the existence of a non-uniform temperature profile across the depth of the AC layer, and (2) develop a procedure for viscoelastic backcalculation, taking into account the field measured temperatures. The models are based on Quasi Linear Viscoelasticity (QLV) theory developed by Schapery (Schapery, 1965). The current version of the algorithm is not able to consider the dynamics, i.e., the effects of wave propagation. In pavements where the bedrock is close to the surface and/or there is a shallow groundwater table, the FWD test deflection time history may exhibit significant wave propagation effects. In such cases, the current version of the algorithm should not be used.

## CHAPTER 3

### LAYERED VISCOELASTIC PAVEMENT MODEL

#### 3.1 Introduction

Traditionally, flexible pavements are analyzed using analytic multilayered elastic models (KENLAYER (Huang, 2004); BISAR (De Jong et al., 1973); CHEVRONX (Warren and Dieckmann, 1963)), which are based on Burmister's elastic solution of multilayered structures (Burmister, 1943; Burmister, 1945a,b,c). These models assume the material in each pavement layer to be linearly elastic.

In the proposed approach, the (asphalt) pavement system is modeled as a layered half-space, with top layer as a linear viscoelastic solid. All other layers (base, subbase, subgrade, bedrock) in the pavement are assumed either linear or nonlinear elastic. Assuming there is full-bonding between the asphalt layer and the underlying base and subgrade layers, the overall response of the entire pavement system becomes viscoelastic. Therefore, its response under arbitrary loading can be obtained using Boltzman's superposition principle (i.e., the convolution integral) (Kutay et al., 2011; and Levenberg, 2008):

$$R^{ve}(x, y, z, t) = \int_{\tau=0}^t R_H^{ve}(x, y, z, t-\tau) \frac{dI(\tau)}{d\tau} d\tau \quad (20)$$

where,  $R^{ve}(x, y, z, t)$  is linear viscoelastic response at coordinate (x,y,z) and time t,  $R_H^{ve}(x, y, z, t)$  is the (unit) viscoelastic response of the pavement system to a Heaviside step function input (H(t)) and  $dI(\tau)$  is the change in input at time  $\tau$ .

It is worth noting that for a uniaxial viscoelastic system (e.g., a cylindrical asphalt mixture), if response  $R^{ve} = \varepsilon(t) =$  strain, then  $R_H^{ve} = D(t) =$  creep compliance and  $I(t) = \sigma(t) =$  stress. Using Schapery's quasi-elastic theory, the viscoelastic response at time  $t$  to a unit input function, can be efficiently and accurately approximated by elastic response obtained using relaxation modulus at time  $t$  (Schapery, 1965; 1974) as follows:

$$R_H^{ve}(x, y, z, t) \cong R_H^e(x, y, z, E(t)) \quad (21)$$

where,  $R_H^e(x, y, z, E(t))$  is unit elastic response calculated using the elastic modulus equal to relaxed modulus (E(t)) at time=t. Flexible pavements are exposed to different temperatures over time, which in turn influence their response. For thermorheologically simple materials, this variation in response can be predicted by extending Equation (20) and Equation (21) as follows:

$$R^{ve}(x, y, z, t) = \int_{\tau=0}^{t_R} R_H^e(x, y, z, E(t_R - \tau)) \frac{dI(\tau)}{d\tau} d\tau \quad (22)$$

where,  $t_R = t/a_T(T)$ , where  $a_T(T)$  is shift factor at temperature  $T$  defined in Equation (11) and  $T_{ref}$  is reference temperature.

$$a_T(T) = a_1(T^2 - T_{ref}^2) + a_2(T - T_{ref}) \quad (23)$$

where,  $a_1$  and  $a_2$  are shift factor's polynomial coefficients. Using Equation (22), formulation for predicting vertical deflection of a linear viscoelastic asphalt pavement system subjected to an axisymmetric loading can be expressed as:

$$u_{vertical}^{ve}(r, z, t) = \int_{\tau=0}^{t_R} u_{H-vertical}^e(E(t_R - \tau), r, z) \frac{d\sigma(\tau)}{d\tau} d\tau \quad (24)$$

where,  $u_{vertical}^{ve}(r, z, t)$  is the viscoelastic response of viscoelastic multilayered structure at time  $t$  and coordinate  $(r, z)$ ,  $u_{H-vertical}^e(E(t_R - \tau), r, z)$  is the elastic unit response of the pavement system at reduced time  $t_R$  due to unit (Heaviside step) contact stress (i.e.,  $\sigma(t)=1$ ), and  $\sigma(\tau)$  is the applied stress at the pavement surface.

In this implementation, the vertical surface displacements, i.e.,  $u_H^{ve}(t) \cong u_H^e(t)$  values at the points of interest were computed using CHEVRONX which was later replaced by an in-house multilayer elastic analysis program called LayerE. Then, the convolution integral in Equation (12) is used to calculate the viscoelastic deflection  $u^{ve}(t)$ . Detailed stepwise description of the algorithm is given in the following section.

### 3.2 Layered Viscoelastic (Forward) Algorithm (LAVA)

As explained earlier, using TTS principle, flexible pavement response at any temperature and loading frequency can be obtained. An algorithm that numerically calculates the convolution integral described in Equation 24 has been developed and referred to as LAVA. Algorithm steps followed in LAVA are as follows (kutay et al. 2011):

1. Define the geometric (layer thicknesses, contact radius) and material ( $E(t)$ ,  $E_{\text{base}}$ ,  $E_{\text{subgrade}}$ , Poisson's Ratio) properties of a layered system as shown in Figure 8.
2. Discrete stress time history  $\sigma(t)$  into  $N_s$  intervals as shown in Figure 9.

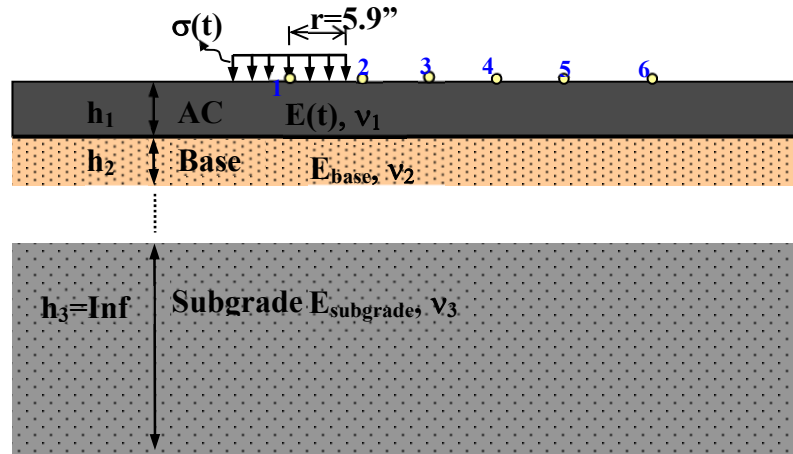


**Figure 8: Typical flexible pavement geometry for analysis**

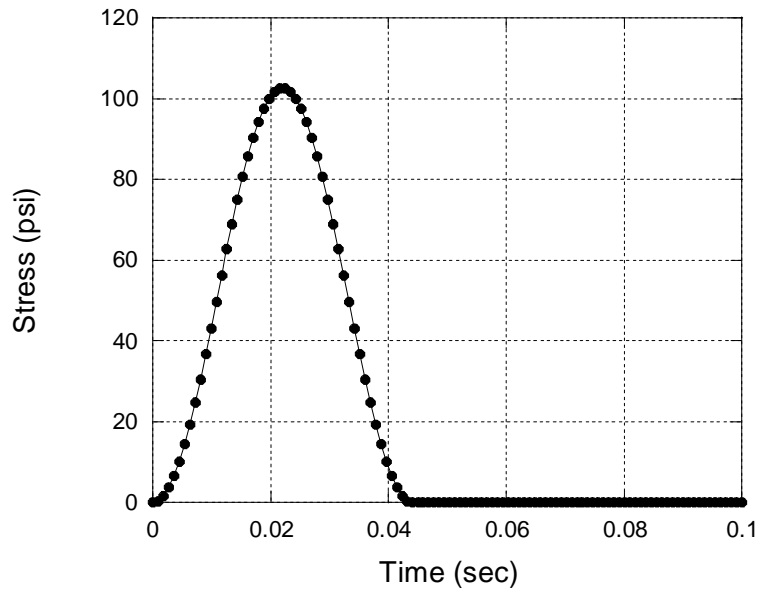


**Figure 9: Discretization of stress history in forward analysis**

3. As shown in Figure 10, divide the relaxation modulus master curve into  $N_E$  number of time steps in log scale. The relaxation modulus  $E(t)$  can be approximated with a sigmoid function as follows:

$$\log(E(t)) = c_1 + \frac{c_2}{1 + \exp(-c_3 - c_4 \log(t_R))} \quad (25)$$

where  $t_R$  is reduced time ( $t_R = t/a_T(T)$ ) and  $c_i$  are sigmoid coefficients. The shift factor coefficients are computed using the second order polynomial given in Equation (23).

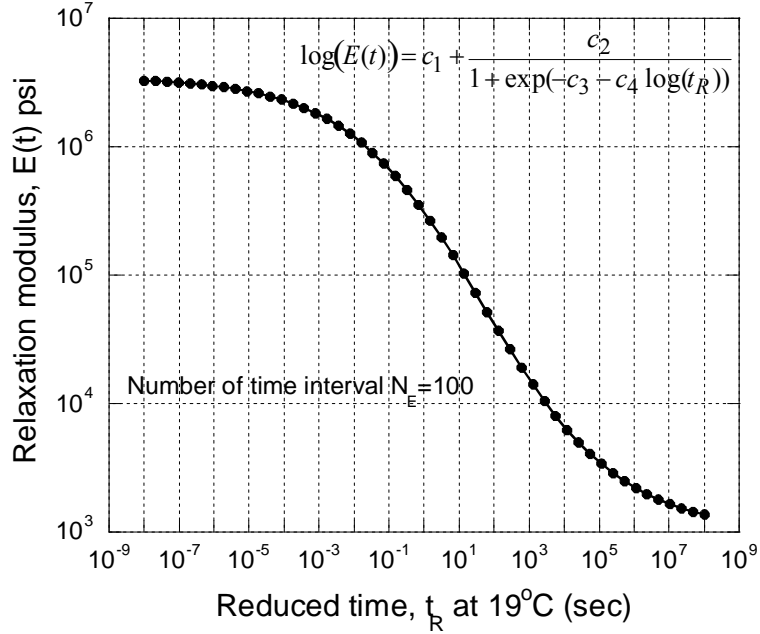


**Figure 10: Discretization of the relaxation modulus master curve**

4. For a unit stress load, calculate the elastic response at every discretized reduced time  $t_{R1}$ ,  $t_{R2}$ ,  $t_{R3}$  ...  $t_{RNE}$ , using the modulus values as  $E(t_{Ri})$  obtained from Figure 10 (Schapery 1965, 1974). Figure 11 shows the vertical surface deflection  $u_H^e$  values calculated using LayeredE at various radial distances similar to one shown Figure 8. Since, the computed  $u_H^e$  values are now the fundamental behavior of the viscoelastic multilayer system these curves are herein called “unit response master curves”.
5. Viscoelastic response is calculated numerically using the discrete form of Equation (24) given in Equation (26).

$$u^{ve}(t_i) = \sum_{j=0}^i u_H^e(t_i - \tau_j) d\sigma(\tau_j) \quad \text{where } i=1,2,\dots,N_s \quad (26)$$

One of the primary reasons for implementing Schapery's 'quasi-elastic' solution above is due its extreme computational efficiency. Table 3 shows the computation times using a Pentium 2.66 GHz computer with 3.25 GB ram for different number of discrete time steps in the 3 layered system shown in Figure 8.

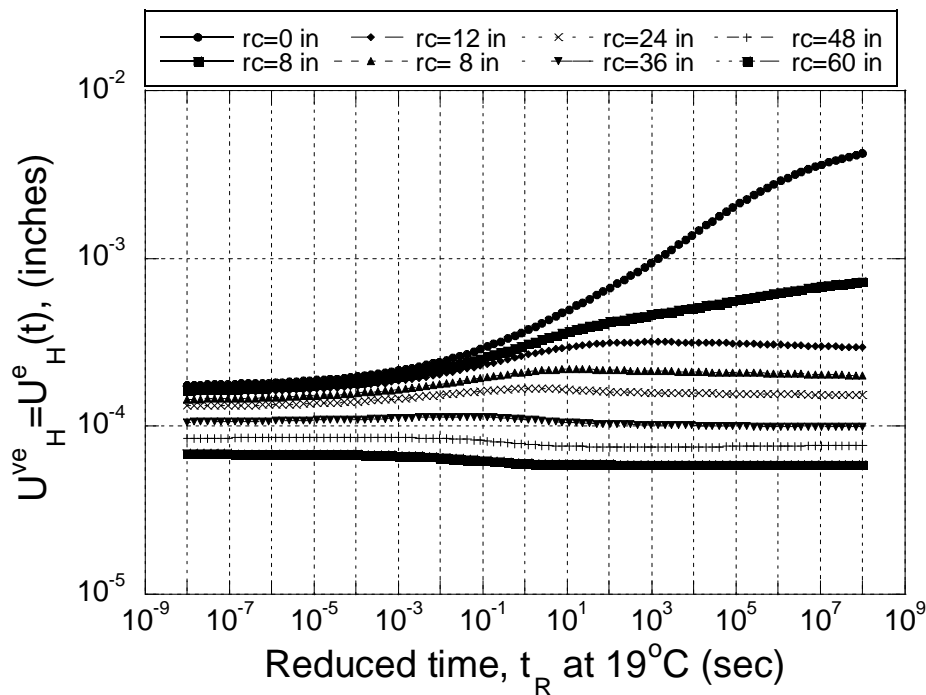


**Figure 11: Deflections calculated under unit stress for points at different distances from the centerline of the circular load at the surface.**

**Table 3: LAVA computation times for different numbers of discrete time steps**

$N_s$	$N_E$	Computation time (sec.)
50	50	1.96
24	100	2.88
50	100	3.03
100	100	3.05
100	200	5.01
200	200	5.13



### 3.3 Implementation of Temperature Profile in LAVA

Temperature in pavements typically varies with depth, which affects the response of the HMA to the applied load. As shown in Figure 12, the temperature may be increasing with depth (profile 1-linear, 2-piecewise, and 3-nonlinear) or decreasing with depth (profile 4-linear, 5-piecewise, and 6-nonlinear) depending on the time of the day. This variation in temperature with depth can be approximated with a piecewise continuous temperature profile function as shown in Figure 12 (profile 2 and 5). The advantage of using a piecewise function is that it may be used to approximate any arbitrary function.

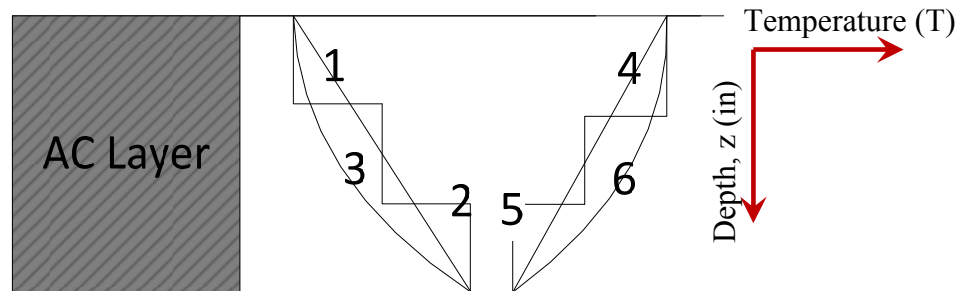


**Figure 12: Schematic diagram of temperature profile**

#### 3.3.1 Layered Viscoelastic (Forward) Algorithm for Temperature Profile (LAVAP)

An algorithm that considers HMA sublayers with different temperatures within the HMA layer has been developed, and referred to as “LAVAP” (LAVA profile). The steps involved in the algorithm were the same as for LAVA except that multiple viscoelastic sublayers exist in LAVAP. Algorithm steps followed in LAVAP are as follows (Chatti et al., 2014):

1. Define the geometric (layer thicknesses, contact radius) and material ( $E(t)$ ,  $a_T(T)$ ,  $E_{base}$ ,  $E_{subgrade}$ , Poisson's Ratio) properties of a layered system as shown in Figure 8.
2. Define number of sublayers in the AC layer  $N_{AC}$  and average temperature in each sublayer.

3. Discretize stress time history  $\sigma(t)$  into  $N_s$  intervals as shown in Figure 9.
4. As shown in Figure 10 divide the relaxation modulus master curve into  $N_E$  number of time steps in log scale. The relaxation modulus  $E(t)$  can be approximated with a sigmoid function given by Equation (25).
5. Calculate the shift factors  $a_T(T_j)$  for each sublayer  $j$ , computed using the second order polynomial given in the Equation (23).
6. For a unit stress load, calculate the elastic response at every discretized reduced time  $t_1, t_2, t_3 \dots t_{NE}$ , using the modulus values for  $j$ th AC sublayer as  $E(t_{Rij})$  obtained from Figure 10 (Schapery 1965, 1974), where  $t_{Rij} = t_i / a_T(T_j)$ .
7. Viscoelastic response is calculated numerically using the discretized Equation (26).

The algorithm has been compared with LAVA as well as ABAQUS. Comparison with LAVA was made for deflection response at all the sensors for constant temperature throughout all the sublayers. The pavement section and layer properties used in the forward analysis are shown in Table 4. Figure 13 shows the response obtained from the LAVAP algorithm at 0°C, 30°C and 50°C match very well with LAVA.

**Table 4: Pavement properties used in LAVAP validation with ABAQUS.**

Property		Constant temperature	Temperature profile
Thickness	AC sublayers	6 in	2in, 2in, 2in
	Granular layers	20, inf (in)	20, inf (in)
Poisson ratio {layer 1,2,3...}		0.35, 0.3, 0.45	0.35, 0.3, 0.45
$E_{unbound}$ {layer 2,3...}		11450, 15000 (psi)	11450, 15000 (psi)
Total number of sensors		8	
Sensor spacing from load (inches)		0, 7.99, 12.01, 17.99, 24.02, 35.98, 47.99, 60	
E(t) sigmoid coefficient {AC}		0.841, 3.54, 0.86, -0.515	
a(T) shift factor coefficients {AC}		4.42E-04, -1.32E-01	

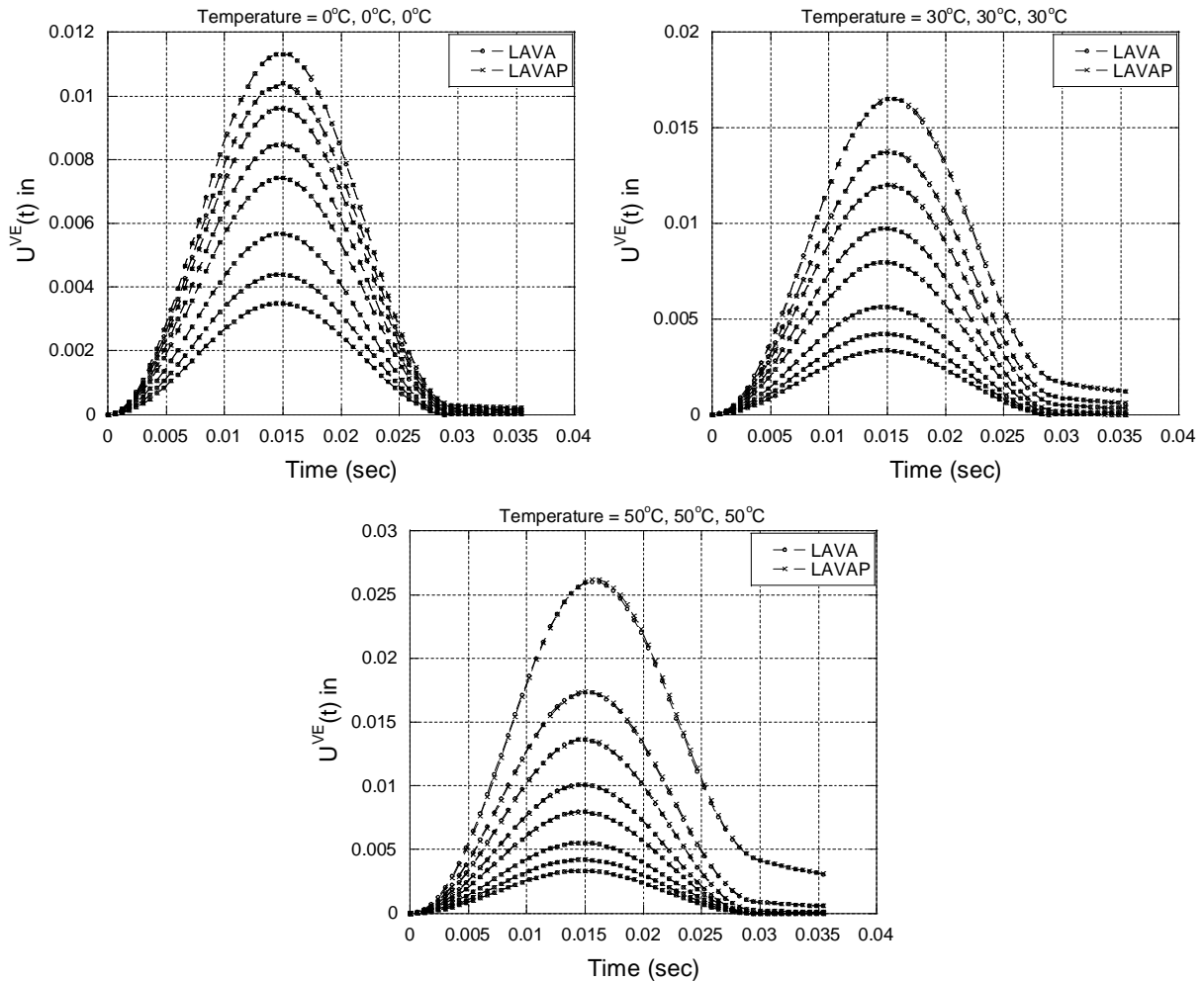


**Figure 13: Comparison of response calculated using LAVAP and original LAVA**

In order to qualitatively examine the response of flexible pavement predicted using LAVAP algorithm, the response obtained under temperature profile was compared with the response obtained under constant temperatures. As an example, a comparison of the response under a temperature profile of  $\{40-30-20\}^{\circ}\text{C}$  with that corresponding to a constant temperature of  $40^{\circ}\text{C}$ ,  $30^{\circ}\text{C}$  and  $20^{\circ}\text{C}$  for the entire depth is shown in Figure 14, Figure 15 and Figure 16, respectively. It can be seen from the figures that the effect of AC temperature is most prominent in sensors closer to the load center (sensors 1, 2, 3, and 4). For sensors away from the loading center (sensors 5, 6, 7 and 8), the deflection histories are not influenced by the AC temperature.

Figure 17 shows the region of  $E(t)$  master curve (at  $19^{\circ}\text{C}$  reference temperature) used by the LAVAP algorithm in calculating time histories.

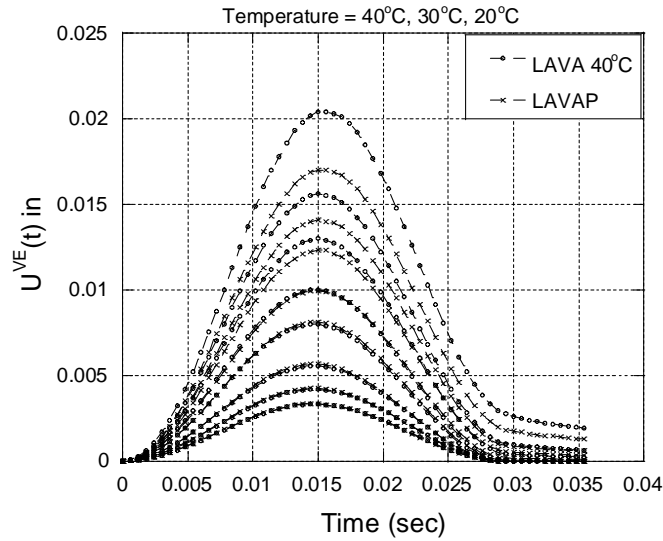


**Figure 14: Comparison of responses calculated using LAVAP at temperature profile {40-30-20} $^{\circ}\text{C}$  and original LAVA at constant  $40^{\circ}\text{C}$  temperature.**

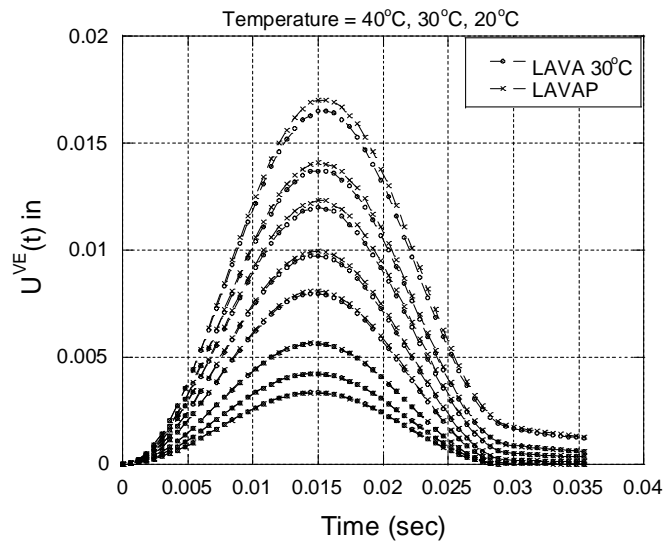


**Figure 15: Comparison of responses calculated using LAVAP at temperature profile {40-30-20} $^{\circ}\text{C}$  and original LAVA at constant  $30^{\circ}\text{C}$  temperature.**

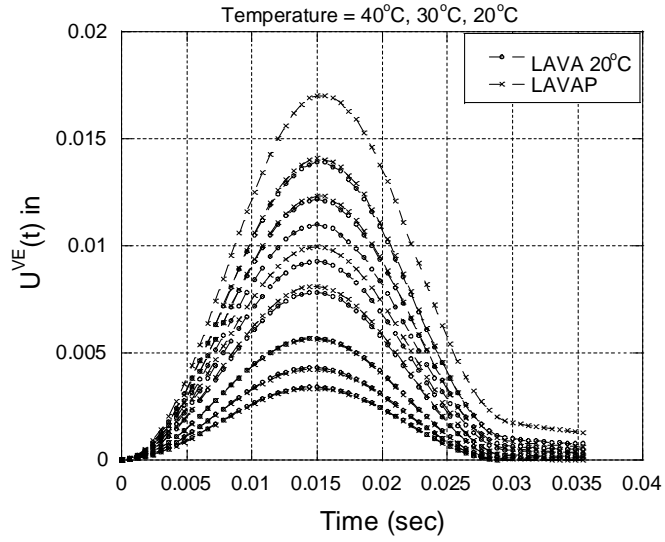


**Figure 16: Comparison of responses calculated using LAVAP at temperature profile {40-30-20}<sup>o</sup>C and original LAVA at constant 20<sup>o</sup>C temperature.**

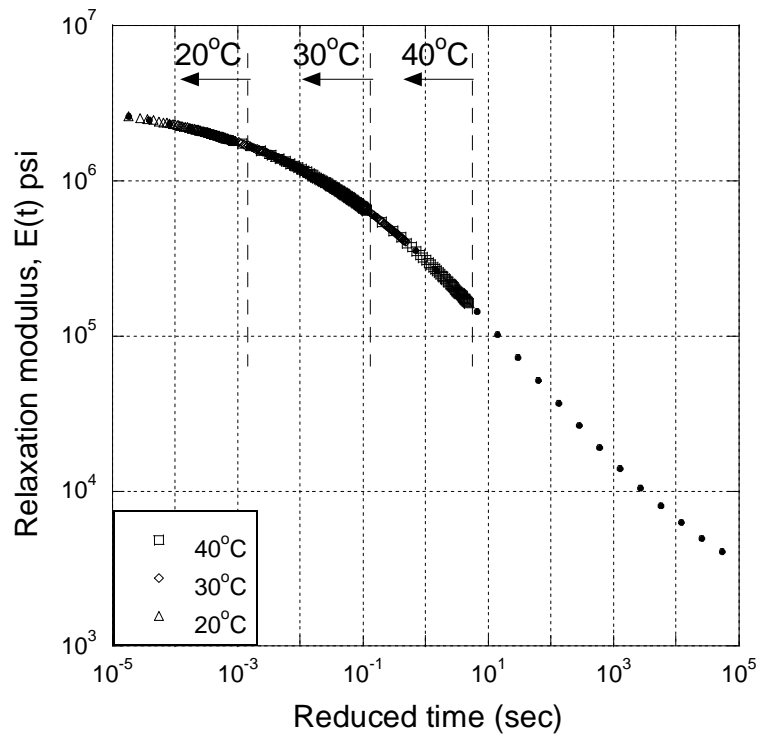


**Figure 17: Region of E(t) master curve (at 19<sup>o</sup>C reference temperature) used by LAVAP for calculating response at temperature profile {40-30-20}<sup>o</sup>C**

As expected, it can be seen that for a condition of higher temperature at the top and lower temperature at the bottom, the response with a higher constant temperature will always be greater than the response with a temperature profile. The response with a lower constant temperature will always be less than the response with a temperature profile. The response with a medium constant temperature may or may not be less than the profile response depending on the temperature profile and thickness of the sublayering.

### 3.3.2 Comparison of LAVAP with FEM Software ABAQUS

Next, the LAVA algorithm was validated against the well-known finite element software, ABAQUS, where temperature profile in AC layer was simulated as two-sublayers of AC with different temperatures. For this purpose, two different HMA types were considered, namely; Terpolymer and SBS 64-40. The viscoelastic properties of these two mixes are shown in Figure 18. As shown in Table 5, for both the mixes, the AC layer was divided into two sublayers, where temperature in the top and bottom sublayer were assumed to be 19°C and 30°C respectively.

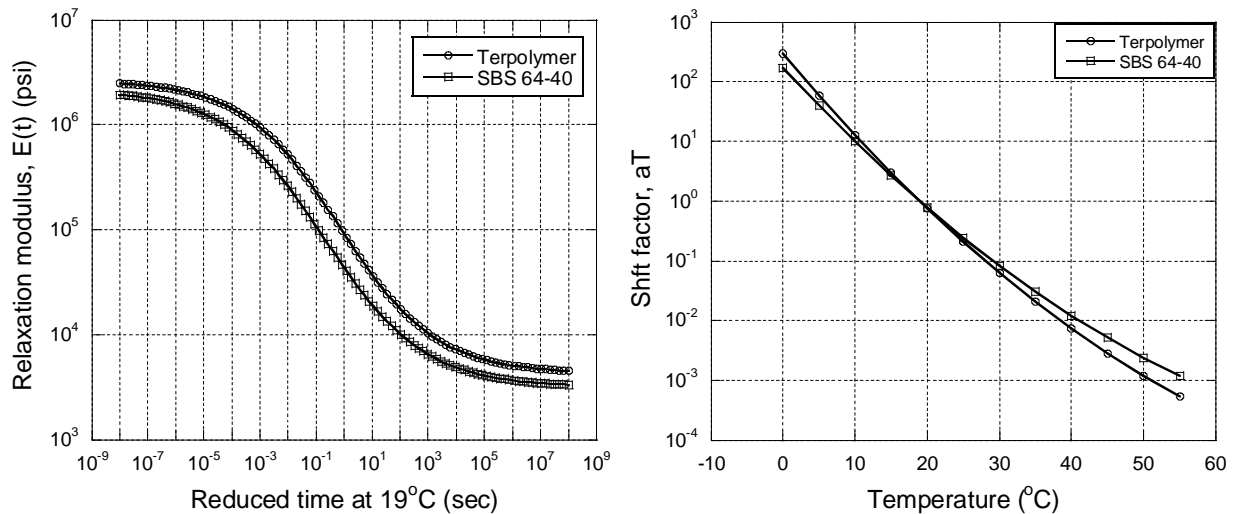


**Figure 18: Relaxation modulus and shift factor master curves at 19°C reference temperature**

**Table 5: Pavement section used in LAVAP validation**

Layer	Modulus (E(t) or E)	Thickness(in) (Temperature °C)	Poisson's Ratio
AC	Mix1: Terpolymer (E(t) = Figure 18); Mix 2: SBS 64-40 (E(t) = Figure 18)	Sublayer1 = 3.94" (19°C) Sublayer2 = 3.94" (30°C)	0.45
Base	15000 psi (linear elastic)	7.88"	0.35
Subgrade	10000 psi (linear elastic)	Infinity	0.45

Comparison of surface deflection time histories measured at radial distances 0, 8, 12, 18, 24, 36, 48, 60 inches for Mix 1 and 2 are shown in Figure 19 and Figure 20. From the figures it can be observed that the results obtained from LAVAP and ABAQUS match well.

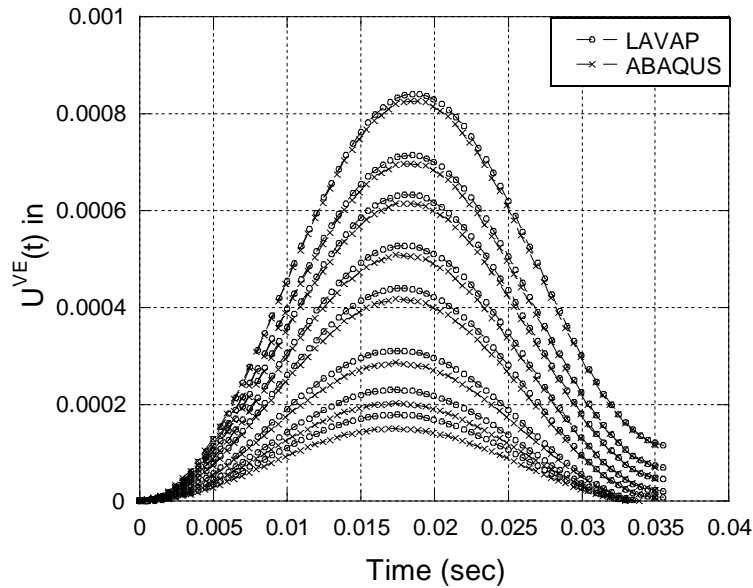


**Figure 19: Comparison between LAVAP and ABAQUS at a temperature profile of {19-30}°C (Terpolymer)**

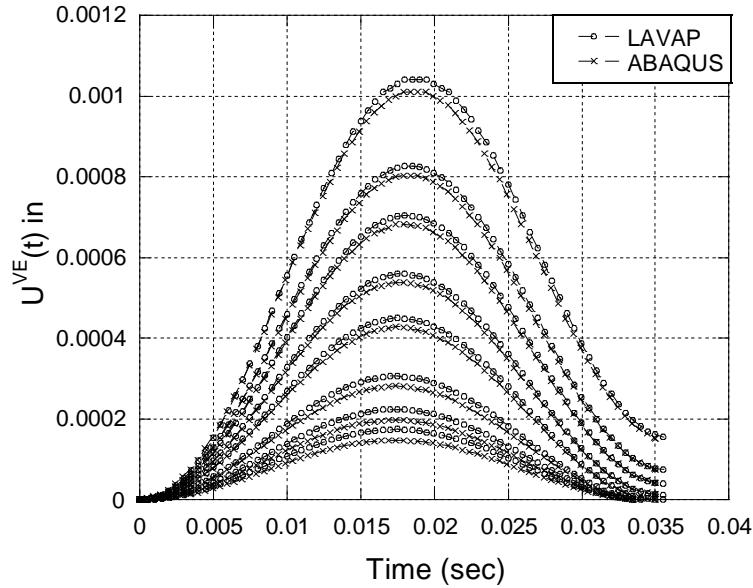


**Figure 20: Comparison between LAVAP and ABAQUS at a temperature profile of {19-30}°C (SBS 64-40)**

As expected, it can be seen from Table 6 that for both the mixes, surface deflection in the pavement section at two step AC temperature profile of {19-30}°C lies between the deflections obtained for constant AC temperatures of 19°C and 30°C.

**Table 6: Peak deflections at temperature profile {19-30}°C and at constant 30°C temperature using LAVA.**

Mix	Temp (°C)	Deflection (mx10 <sup>-4</sup> ) (Sensors)							
		1	2	3	4	5	6	7	8
Terpolymer	Constant: 19°C	7.14	6.27	5.72	4.95	4.26	3.14	2.36	1.84
	Profile: 19°C, 30°C	8.39	7.13	6.32	5.27	4.39	3.11	2.30	1.79
	Constant 30°C	9.76	7.84	6.81	5.54	4.52	3.10	2.27	1.76
SBS 64-40	Constant 19°C	8.94	7.40	6.53	5.41	4.47	3.13	2.30	1.78
	Profile: 19°C, 30°C	1.04	8.26	7.03	5.59	4.50	3.06	2.24	1.75
	Constant 30°C	1.21	8.92	7.42	5.76	4.55	3.04	2.22	1.73



### **3.4 Layered Viscoelastic Nonlinear (LAVAN) Pavement Model**

In this section, a computationally efficient layered viscoelastic nonlinear model, herein called LAVAN, is presented. The LAVAN can consider linear viscoelasticity of AC layers as well as stress-dependent modulus of granular layers. The formulation is inspired from Quasi-Linear-Viscoelastic (QLV) constitutive modeling (Leaderman, 1943; Schapery, 1969; Fung, 1996; Masad et al., 2008; Yong et al., 2010; and Nekouzadehn and Genin, 2013), which is often used in analyzing nonlinear viscoelastic materials. In literature, the various forms of the model are also named as Fung's model/ Schapery's nonlinearity model/ modified Boltzmann's superposition.

It is well known that the unbound granular materials exhibit nonlinearity, i.e. stress dependent modulus (Hicks and Monismith, 1971; Witczak and Uzan, 1988; and Ooi et al., 2004). Modeling response of flexible pavements with stress dependent granular layers requires iterative analysis, which makes the solution computationally intensive. In order to avoid this complexity, most of the standards (Shell, 1978; Asphalt Institute, 1999, Theyse et al., 1996; IRC, 2001; and Austroads, 2004) assume the granular layer to be elastic. Wang and Al-Qadi (2013) developed a FE based model for asphalt pavements in ABAQUS and considered both viscoelasticity of asphalt and nonlinearity of granular layers. They found that both the viscoelastic and nonlinear material properties need to be considered in order to accurately predict flexible pavement response. They also showed that the nonlinear response of the granular layer is influenced by the viscoelastic stress caused by the AC layer. Although FE-based modeling is very useful, they are computationally expensive and can be significantly affected by the boundary conditions. Furthermore, FE-based models are inefficient to be used as an inverse analysis tool, e.g., in

backcalculation algorithms. A computationally efficient semi-analytical model is inevitable in such algorithms.

In the present study, Quasi-Elastic theory is combined with generalized QLV theory, to develop an approximate model for predicting response of multilayered viscoelastic nonlinear flexible pavement structures. Before introducing the generalized QLV model, a brief overview of granular nonlinear pavement models is also presented. Development of a generalized QLV model for multilayered system is followed by numerical validation, in which response of flexible pavements under stationary transient loading has been analyzed. The model is implemented in general purpose FE-based software, ABAQUS, to validate the model.

### ***3.4.1 Nonlinear Multilayer Elastic Solutions***

Under constant cyclic loading, granular unbound materials exhibit plastic deformation during the initial cycles. As the number of load cycles increase, plastic deformation ceases to occur and the response becomes elastic in further load cycles (a phenomenon known as shakedown). Often this elastic response is defined by resilient modulus ( $M_R$ ) at that load level, which is expressed as:

$$M_R = \frac{\sigma_d}{\varepsilon_r} \quad (27)$$

where,  $\sigma_d = (\sigma_1 - \sigma_3)$ , is the deviatoric stress in a triaxial test and  $\varepsilon_r$  is recoverable strain. If the granular layer reaches this steady state condition under repeated vehicular loading, then the further response can be considered recoverable and Equation (27) can be used to characterize the material. However, the  $M_R$  value shown in Equation (27) is affected by the state of stress (or load level). Typically, unbound granular materials exhibit stress hardening (Yau and Von Quintus, 2002; and Taylor and Timm, 2009), i.e., the  $M_R$  increases with increasing stress. Hicks and

Monismith (1971) related hydrostatic stress and the resilient modulus obtained in Equation (27) to characterize the stress dependency of the material. The model suggested by Uzan (1985) and Witczak and Uzan (1988) use deviatory stress as well as octahedral stress to incorporate the distortional shear effect into the model. The model has been further modified by various researchers. Yau and Von Quintus (2002) analyzed LTPP  $M_R$  test data using generalized form of Uzan (1985) model expressed as:

$$M_R = k_1 p_a \left( \frac{\theta - 3k_6}{p_a} \right)^{k_2} \left( \frac{\tau_{oct}}{p_a} + k_7 \right)^{k_3} \quad (28)$$

where,  $\theta$  is hydrostatic stress,  $p_a$  is atmospheric pressure,  $\tau_{oct}$  is octahedral shear stress,  $k_1, k_2, k_3, k_6$  and  $k_7$  are regression coefficient. They found that parameter  $k_6$  in the equation regressed to zero for more than half of the tests, and hence the coefficient was set to zero for the subsequent analysis. The subsequently modified equation is shown in equation (29), which has been used in the present study to define resilient modulus of unbound granular layer:

$$M_R = k_1 p_a \left( \frac{\theta}{p_a} \right)^{k_2} \left( \frac{\tau_{oct}}{p_a} + 1 \right)^{k_3} \quad (29)$$

where,  $\theta = \sigma_1 + \sigma_2 + \sigma_3 + \gamma z(1 + 2K_o)$ ,  $\tau_{oct}$  is octahedral shear stress,  $k_1, k_2, k_3$  are regression constants,  $K_o$  is the coefficient of earth pressure at rest and  $p_a$  is atmospheric pressure.

Although the resilient modulus,  $M_R$ , is not the Young's Modulus (E) (Hjelmstad and Taciroglu, 2000), while formulating granular material constitutive equations, it is often used to replace E in the following equation:

$$\sigma_{ij} = \frac{vE}{(1+v)(1-2v)} \varepsilon_{kk} \delta_{ij} + \frac{E}{(1+v)} \varepsilon_{ij} \quad (30)$$

where,  $E$  is Young's Modulus,  $\nu$  is Poisson's Ratio,  $\sigma_{ij}$  is stress tensor,  $\varepsilon_{ij}$  is strain tensor,  $\varepsilon_{kk} = \varepsilon_{11} + \varepsilon_{22} + \varepsilon_{33}$ ,  $\delta_{ij}$  is Kroenecker delta. Nonlinear stress dependent  $M_R$  has been implemented in many FE-based models. These include GTPAVE (Tutumluer, 1995), ILLIPAVE (Raad and Figueroa, 1980), and MICHPAVE (Harichandran et al., 1989). Typically FE-based nonlinear pavement analysis is performed by defining a user defined material (UMAT) in FE-based softwares such as ABAQUS and ADINA (Hjelmstad and Taciroglu, 2000; Schwartz, 2002; and Kim et al., 2009). Although FE-based solutions are promising, apart from being computationally expensive, they may exhibit significant influence of boundary condition if the semi-infinite geometry of the problem is not implemented adequately in the model.

An approximate nonlinear analysis of pavement can also be performed using Burmister's multilayered elastic based solution (Burmister, 1945). For incorporating variation in modulus with depth, Huang (Huang 2004) suggested dividing the nonlinear layer into multiple sublayers. Furthermore, he suggested choosing a specific location in the nonlinear layers to evaluate modulus based on the stress state of the point. Zhou (2000) studied stress dependency of base layer modulus obtained from base layer mid depth stress state. They analyzed FWD testing at multiple load levels on two different pavement structures. The study showed that reasonable nonlinearity parameters can be obtained through regression of backcalculated modulus with stress state at mid-depth of the base layer.

In the present study, the elastic nonlinearity is solved iteratively assuming an initial set of elastic modulus. The evaluated stresses obtained using the initial values of modulus are used to evaluate new set of modulus using Equation (29). The iteration is continued until the computed modulus from the stresses predicted by the layered solution and input modulus used in the

layered solution converges. It is noted that the appropriate stress adjustments were made due to the fact that unbound granular material can't take tension. This means that in such a case either residual stress is generated such that stress state obeys a yield criterion or the tensile stresses are replaced with zero.

**3.4.2 Proposed Constitutive Model for Multilayer Pavement Model under Uniaxial Loading: Combining Linear Viscoelastic AC and Nonlinear Base**

Mechanical behavior of elastic and linear viscoelastic materials are well defined in literature using springs and dashpots. In the derivation presented, the standard mechanical responses using springs and dashpots is implied, and has not been stressed upon for brevity. As shown in Figure 21, for the uniaxial formulation, a two layer system comprising of linear viscoelastic layer that is in perfect bonding with the underlying nonlinear unbound layer is considered. A third layer of elastic material is avoided, because it can be easily lumped along the viscoelastic properties in the system. Under uniaxial loading, formulation for vertical surface response has been presented.

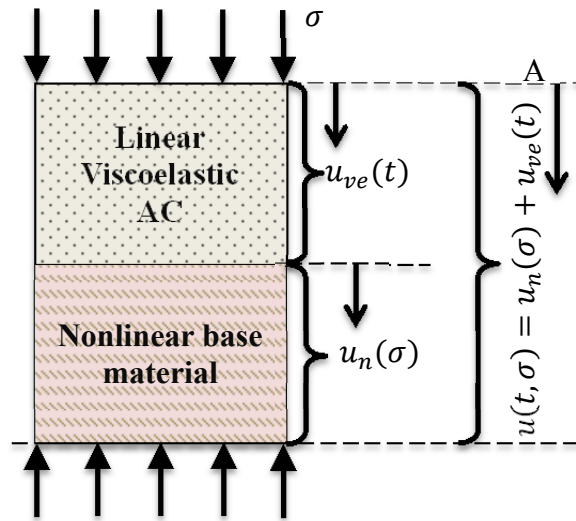


**Figure 21: Cross section of multilayer viscoelastic nonlinear system used in uniaxial analysis.**

The vertical deflection response of the two layer system can be obtained as an addition of responses of individual layers. That is, the vertical surface deflection at A in Figure 21 can be expressed as:

$$u_z(t, \sigma) = u_n(\sigma) + u_{ve}(t) \quad (31)$$

where,  $u_z(t)$  is the total vertical deflection at point A,  $u_n(\sigma)$  is the vertical deformation in nonlinear layer and  $u_{ve}(t)$  is the vertical deformation in the linear viscoelastic AC layer. Unlike a system comprising of only linear materials, a nonlinear system is expected to have different unit response functions at different loads. In this study, unit response function of the system at any load level has been defined as a secant property (like secant modulus), such that at any load level ( $\sigma^i$ ) the unit response function  $u_H(t, \sigma^i)$  can be defined similar to the definition used for linear viscoelastic materials. Equation (32) show expressions for unit response functions at different load levels,  $\sigma^i$  according to the definition explained. It is worth noting that in the uniaxial case, the loading stresses are same as the stress state for calculating the nonlinear modulus in the nonlinear layer.

$$u_{H-z}^i(t) = u_{H-z}(t, \sigma^i) = \frac{u_z^i(t)}{\sigma^i} = \frac{u_n^i + u_{ve}^i(t)}{\sigma^i} = \frac{u_n^i}{\sigma^i} + \frac{u_{ve}^i(t)}{\sigma^i} = \frac{1}{K_s(\sigma^i)} + u_{H-z}^{ve}(t) \quad (32)$$

where,  $u_{H-z}^i(t) = u_{H-z}(t, \sigma^i)$  is the nonlinear unit response of the system at stress equal to  $\sigma^i$ ,  $u_n^i$  is the deformation in the nonlinear layer at stress equal to  $\sigma^i$ ,  $u_{ve}^i(t)$  is the deformation in AC layer at stress equal to  $\sigma^i$ ,  $K_s(\sigma^i)$  is the secant stiffness of the nonlinear layer at stress equal to  $\sigma^i$ ,  $u_{H-z}^{ve}(t)$  is the unit response function of the linear viscoelastic AC material. It is clear from Equation (32) that, for a constant load a constant modulus exists for the nonlinear layer, which

can be used in estimating response of the combined viscoelastic-nonlinear system under any loading through Boltzmann superposition.

However, since the unit response functions are function of stress, the modified convolution is as shown below:

$$u_z(t) = \int_{\tau=0}^t u_{H-z}(t - \tau, \sigma) \frac{d\sigma(\tau)}{d\tau} d\tau \quad (33)$$

where,  $u_z(t)$  is the vertical deflection of the system at time,  $t$ ,  $u_{H-z}(t - \tau, \sigma)$  is unit nonlinear response function at stress equal to  $\sigma(\tau)$ ,  $\sigma(t)$  is arbitrary stress function used as succession of infinitesimal steps. The modified convolution has been further discussed in detail in the next section. Similar to the numerical discretization of convolution integral in linear viscoelasticity, the above equation can be numerically expressed as:

$$u_z(t) = u_{H-z}(t, \sigma^0) \Delta\sigma^0 + u_{H-z}(t, \sigma^1) \Delta\sigma^1 + u_{H-z}(t - \tau_1, \sigma^2) \Delta\sigma^2 + \dots + u_{H-z}(t - \tau_{k-1}, \sigma^k) \Delta\sigma^k \quad (34)$$

$$u_z(t) = \left( u_{H-z}^{ve}(t) + \frac{1}{K_s(\sigma^0)} \right) \Delta\sigma^0 + \left( u_{H-z}^{ve}(t - \tau_1) + \frac{1}{K_s(\sigma^1)} \right) \Delta\sigma^1 + \left( u_{H-z}^{ve}(t - \tau_2) + \frac{1}{K_s(\sigma^2)} \right) \Delta\sigma^2 + \dots + \left( u_{H-z}^{ve}(t - \tau_k) + \frac{1}{K_s(\sigma^k)} \right) \Delta\sigma^k \quad (35)$$

where,  $\Delta\sigma^i$  is infinitesimal stress increment at  $t = \tau_i$ . As shown in Equation (36) to Equation (38), Equation (35) can be further expressed as addition of independent response from linear viscoelastic and nonlinear elastic constituents of the system. The first summation in the equations represents the well-known convolution integration for linear viscoelastic materials, whereas the second term represents the secant response from the nonlinear constituent.

$$u_z(t) = \sum_{i=0}^k u_{H-z}^{ve}(t - \tau_i) \Delta\sigma^i + \sum_{i=0}^k \frac{1}{K_s(\sigma^i)} \Delta\sigma^i \quad (36)$$

$$u_z(t) = \sum_{i=1}^k u_{H-z}^{ve}(t - \tau_i) \Delta\sigma^i + \sum_{i=0}^k \Delta u_n^i \quad (37)$$

$$u_z(t) = \int_{\tau=0}^t u_{H-z}^{ve}(t - \tau) \frac{d\sigma}{d\tau} d\tau + \sum_{i=0}^k \Delta u_n^i \quad (38)$$

Although the uniaxial response derivation for multilayer viscoelastic nonlinear system reduces to a simpler form, it cannot be directly generalized for 2D or 3D (axisymmetric) conditions because of the following reasons: (1) loading is typically concentrated over specific loading area, and (2) due to the relaxation of the AC layer, stress state in the nonlinear layer can change with time. However, the impact of these issues can be minimal if the response of pavement to the variation in nonlinear modulus value in the radial direction is not significant, which has been shown by researchers to be an adequate assumption (Huang 2004) in multilayer nonlinear elastic analysis of flexible pavements. In the next section, this assumption has been used in deriving response for the viscoelastic nonlinear system, and subsequently, error in the analysis is discussed.

### ***3.4.3 Proposed Generalized Model for Multilayer Pavement Model: Combining Linear Viscoelastic AC and Nonlinear Base***

#### ***3.4.3.1 Applicability of Existing Theories of Nonlinear Viscoelasticity***

Mechanistic solutions for NLV (Nonlinear Viscoelastic) materials exhibit variation depending on the type of nonlinearity that is present. Typical NLV equations involve convolution integrals that are based on integration kernel which are function of stress or strain. Equation (39) and (40) show typical form of such expression:

$$\sigma(t) = \int_{\tau=0}^t E(t - \tau, \varepsilon) \frac{d\varepsilon(\tau)}{d\tau} d\tau \quad (39)$$



$$\varepsilon(t) = \int_{\tau=0}^t D(t - \tau, \sigma) \frac{d\sigma(\tau)}{d\tau} d\tau \quad (40)$$

where,  $\varepsilon$  is strain,  $\sigma$  is stress,  $E(t, \varepsilon)$  is strain dependent relaxation modulus and  $D(t, \sigma)$  is stress dependent creep compliance. Typically, in many nonlinear materials, the shape of relaxation modulus of the material is preserved, even though the material presents stress or strain dependency (Shames and Cozzarelli, 1997; and Nekouzadeh and Genin, 2013). Such NLV problems are solved by assuming that time dependence and stress (or strain) dependence can be decomposed into two functions as follows:

$$D(t, \sigma) = h(\sigma)D_t(t) \quad (41)$$

$$E(t, \varepsilon) = f(\varepsilon)E_t(t) \quad (42)$$

where  $h(\sigma)$  is a function of stress,  $D_t(t)$  is the (only) time dependent creep compliance,  $f(\varepsilon)$  is a function of strain,  $E_t(t)$  is the (only) time dependent relaxation modulus. This multiplicative decomposition facilitates an easy application of superposition principle. For such materials the following expression has been typically used in NLV formulations to develop the convolution integral (Nekouzadeh and Genin, 2013):

$$\sigma(t) = \int_{\tau=0}^{t_R} E_t(t_R - \tau) \frac{df(\varepsilon(\tau))}{d\varepsilon} \frac{d\varepsilon(\tau)}{d\tau} d\tau \quad (43)$$

where,  $E_t$  is a relaxation function that remains unchanged at any strain level, and  $f(\varepsilon(\tau))$  is a function of strain, such that  $df(\varepsilon(\tau))/d\varepsilon$  represents the elastic tangent stiffness at different strain levels. These models are designated as Fung's NLV material, which was first proposed by Leaderman in 1943 (Leaderman, 1943). A generalized form of this nonlinearity model was presented by Schapery (1969) using thermodynamic principals. Yong et al. (2010) used the

model to describe nonlinear viscoelastic-viscoplastic behavior of asphalt sand, whereas, Masad et al. (2008) used the model to describe nonlinear viscoelastic creep behavior of binders. The model suggests that nonlinear relaxation function can be expressed as a product of function of time  $E_t(t_R - \tau)$  and function of strain  $df(\varepsilon(\tau))/d\varepsilon$ . In Equation (43), nonlinearity is introduced by the elastic component,  $df(\varepsilon(\tau))/d\varepsilon$ , and the viscoelasticity comes from the  $E_t$ .

A direct extension of the concepts of QLV model to develop formulations for viscoelastic nonlinear multilayered system, where the unbound layer is nonlinear and the AC layer is linear viscoelastic lead to the following:

$$\sigma(t) = \int_{\tau=0}^{t_R} E_t(x, y, z, t_R - \tau) \frac{df(\varepsilon(\tau))}{d\varepsilon} \frac{d\varepsilon(\tau)}{d\tau} d\tau \quad (44)$$

where,  $E_t(x, y, z, t_R)$  is relaxation function at location  $(x, y, z)$ , and  $f(\varepsilon(\tau))$  is a function of strain  $\varepsilon(\tau)$ . Alternatively, to obtain vertical surface deflection in pavements, Equation (44) can be expressed in terms of vertical deflection response to Heaviside step loading as follows:

$$u_z^{ve}(t) = \int_{\tau=0}^{t_R} u_{H-t}^e(t_R - \tau, \sigma = 1) \frac{dg(\sigma)}{d\sigma} d\sigma(\tau) \quad (45)$$

where  $u_z^{ve}(t)$  is surface (NLV) displacement,  $u_{H-t}^e(t, \sigma = 1)$  is unit nonlinear elastic response due to a unit stress and  $g(\sigma)$  is a function of stress, which can be expressed as:

$$g(\sigma) = \frac{u_H^e(t_R, \sigma)}{u_{H-t}^e(t_R, \sigma=1)} \quad (46)$$

where,  $u_H^e(t_R, \sigma)$  is the nonlinear elastic unit displacement due to a given stress  $(\sigma)$ . For Fung's theory (i.e., Equations (44) through (46)) to hold,  $g(\sigma)$  must be purely a function of stress. In order to investigate this, the  $g(\sigma)$  values were computed using Equation (46) and plotted against

surface stress and relaxation modulus (i.e. time). The properties of pavement section and material properties are shown in Figure 22.

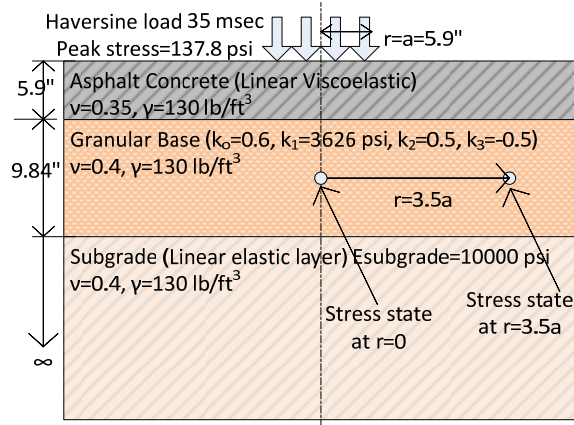


**Figure 22: Flexible pavement cross section.**

The LAVA algorithm was modified to implement an iterative nonlinear solution for the granular base, which was assumed to follow Equation (29). The  $u_H^e(t_R, \sigma)$  in Equation (36) was calculated at a range of stress values from 0.1 psi to 140 psi and using  $E(t)$  values (for AC) at a range of times, ranging from  $10^{-8}$  to  $10^8$  seconds. Then,  $u_{H-t}^e(t_R, \sigma = 1)$  was calculated for unit stress. Figure 23 shows the variation of  $g(\sigma)$ , where the  $g(\sigma)$  values decrease with increasing stress ( $\sigma$ ).

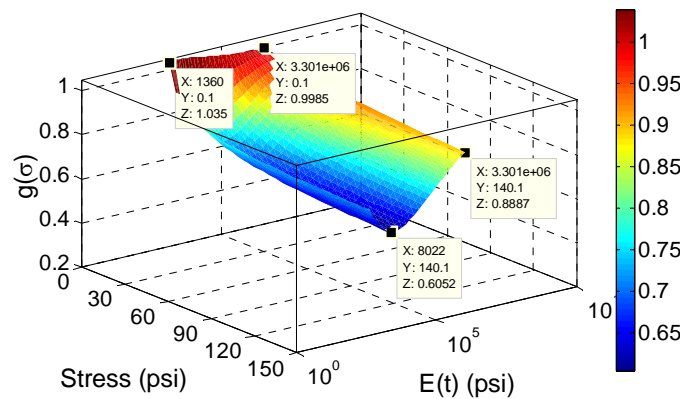


**Figure 23: Variation of  $g(\sigma)$  with stress and  $E(t)$  of AC layer.**

This is expected behavior for a nonlinear material since as the stress increases, the unbound layer moduli will increase. However, Figure 23 also illustrates that the  $g(\sigma)$  varies with change in  $E(t)$ . This means that  $g(\sigma)$  is not solely based on the stress, as a result, Fung's model cannot be used in a layered pavement structure. This is meaningful since the change in the stress distribution within the pavement layers due to viscoelastic effect (as  $E(t)$  varies) will impose changes in the behavior of stress dependent granular layer. Hence, even though the viscoelastic layer in a nonlinear multilayered system is linear, it cannot be formulated as a Fung's QLV model.

### 3.5 Proposed Model: LAVAN

QLV model can still be approximated as a convolution integral, provided the stress dependent relaxation function of the multilayered structure under all the load levels are known. Using modified superposition, such a generalized QLV model for a multilayered structure can be expressed as NLV equations involving the convolution integrals of unit response function of the structure, which is a function of stress or strain as follows:

$$R^{ve}(x, y, z, t) = \int_{\tau=0}^{t_R} R_H^e(x, y, z, I(\tau), t_R - \tau) \frac{dI(\tau)}{d\tau} d\tau \quad (47)$$

where,  $R^{ve}(x, y, z, t)$  is the NLV response of the layered pavement structure,  $R_H^e(x, y, z, I(\tau), t_R - \tau)$  is the unit response function that is both function of time and input,  $I(\tau)$ , which is equal to stress applied at the surface of the pavement. Note that in this formulation, unlike Fung's QLV model, time dependence and stress (or strain) dependence are not separated. Equation (47) can be rewritten in terms of vertical surface deflection under axisymmetric surface loading as follows:

$$u_z^{ve}(r, z, t) = \int_{\tau=0}^{t_R} u_{H-z}^e(r, z, \sigma(\tau), t_R - \tau) \frac{d\sigma(\tau)}{d\tau} d\tau \quad (48)$$

where,  $u_z^{ve}(r, z, t)$  is the vertical deflection at time  $t$  and location  $(r, z)$ ; and  $u_{H-z}^e(r, z, \sigma(\tau), t_R - \tau) = u_z^e(r, z, \sigma(\tau), t_R - \tau)/\sigma(\tau)$ , where  $u_z^e$  is the nonlinear response of the pavement at a loading stress level of  $\sigma$ . The model in Equation (48) can be expressed in discretized formulation as follows:

$$u_z^{ve}(r, z, t_i) = \sum_{j=1}^N u_{H-z}^e(r, z, \sigma(\tau_j), t_{R_i} - \tau_j) \Delta\sigma(\tau_j) \quad (49)$$

where  $\tau_1 = 0$ ,  $\tau_N = t$ . The  $u_{H-z}^e(\sigma(\tau_j), t_{R_i} - \tau_j)$  values are computed via interpolation using the 2D matrix pre-computed for  $u_{H-z}^e(\sigma, t)$  (which was computed at a range of stress values and  $E(t)$  values). The developed model has been referred to LAVAN as an abbreviation for LAVA-Nonlinear.

*Step by step procedure to numerically compute response is given below:*

1. Define a discrete set of surface stress values:  $\sigma_k = 0.1$  psi to 140 psi.
2. Calculate nonlinear elastic response  $u^e(\sigma_k, t_{R_i})$  at a range of  $t_{R_i}$  values, by using  $E_{AC} = E(t_{R_i})$  for each  $t_{R_i}$  value.
3. Recursively compute  $E_{base}$  until the stress in the middle of the base layer results in the same  $E_{base}$  as the one used in the layered elastic analysis. At this step, Equation 7 is used in the nonlinear formulation for the base.
4. Calculate the nonlinear unit elastic response,  $u_{H-z}^e(r, z, \sigma_k, t_i)$  as  $u_z^e(r, z, \sigma_k, t_i)/\sigma_k$ .
5. Perform convolution shown in Equation (49) to calculate the NLV response.

### 3.5.1 Validation of the LAVAN

In order to validate the LAVAN algorithm, a flexible pavement is modeled as a three layered structure, with viscoelastic AC top layer, followed by stress dependent (nonlinear) granular base layer on elastic half space (subgrade). Figure 22 shows the geometric properties of the pavement structure utilized in the validation, where  $h_{AC} = 5.9''$  and  $h_{base} = 9.84''$ . The viscoelastic properties of two HMA mixes, namely CRTB and Control (two materials from FHWA's ALF 2002 experiment – (Gibson et al., 2012)) were used for the AC layer in the analysis as case 1 and 2. The relaxation modulus master curves of the two mixes are shown in Figure 24.

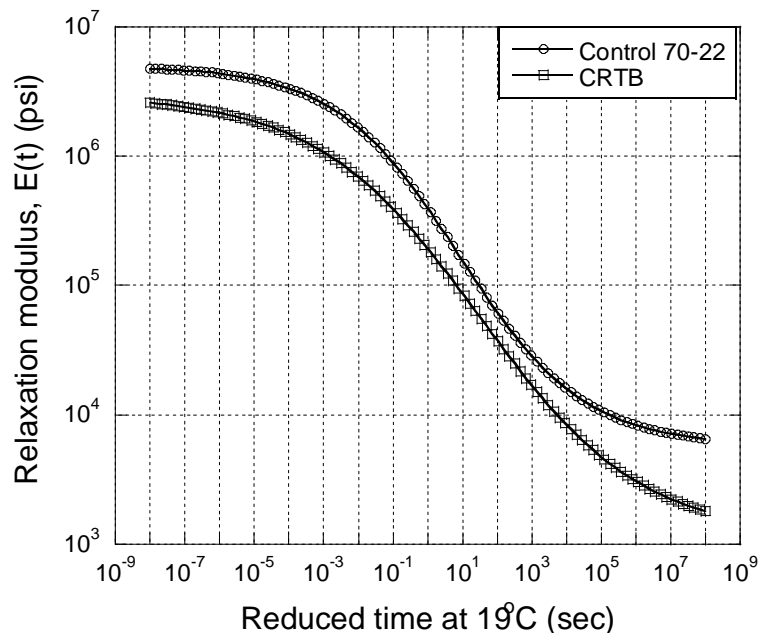


**Figure 24: Relaxation modulus master curve for LAVAN validation (at 19°C reference temperature).**

These curves were computed from their  $|E^*|$  master curves by following the Prony series-based interconversion procedure suggested by Park and Shapery (1999). From the theory of viscoelasticity, creep compliance, relaxation modulus and dynamic modulus are interconvertible. As a result, the developed viscoelastic nonlinear multilayered model can take any of three viscoelastic properties. The relaxation modulus  $E(t)$  can be approximated with a sigmoid

function given by Equation (25). Both the HMA mixes were analyzed with granular nonlinear model as shown in Equation (29).

### 3.5.2 Comparison of LAVAN with FEM Software ABAQUS

In ABAQUS, the viscoelastic properties of the HMAs were input in the form of normalized bulk modulus ( $K$ ) and normalized shear modulus ( $G$ ) (ABAQUS, 2011). For the unbound nonlinear layer, a user defined material UMAT was written. ABAQUS requires that any UMAT should have at least two main components; (i) updating the stiffness Jacobean Matrix, and (ii) stress increment. Equations (50) and (51) show the mathematical expressions for these two operations implemented in the UMAT.

$$J_{ijkl} = \frac{\partial \sigma_{ij}}{\partial \varepsilon_{kl}} \quad (50)$$

$$\sigma_{ij}^{n+1} = \sigma_{ij}^n + J_{ijkl} \partial \varepsilon_{kl}^{n+1} \quad (51)$$

where,  $J_{ijkl}$  is the Jacobian matrix,  $\sigma_{ij}^{n+1}$  is the updated stress. For nonlinear analysis using LAVAN, unbound modulus was calculated using stress state at the midpoint of unbound base layer (vertically). Since LAVAN cannot incorporate nonlinearity along horizontal direction, for comparison, modulus values were calculated using stress state at  $r = 3.5a$  (i.e.,  $r$  in Figure 22), where  $a$  is the radius of loading. Estimating base modulus using stress state along the centerline of the loading would result in stiffer base (Kim et al., 2009); hence it was expected to get closer results using stress state at some location radially away from the centerline.

In ABAQUS, solution is sensitive to the boundary condition used in the analysis. Kim et al. (2009) found that for multilayer nonlinear axisymmetric problem with the vertical boundaries supported using roller supports and the bottom fixed (finite boundaries), the domain size of  $140a$

in vertical direction and  $20a$  in the horizontal direction produce results comparable to analytic solution. Alternatively, researchers have used infinite elements as the boundary to imitate semi-infinite geometry. In the present study, both the boundary conditions were analyzed. It was observed that, when all the vertical boundaries were supported using roller supports and the bottom was fixed, the domain size of  $133a$  in vertical direction and  $53a$  in the horizontal direction was found to produce stable surface deflection (with less than 1% error at the center). The same domain size is later analyzed with all the vertical as well as the bottom boundaries supported using infinite elements. For the selected domain size, the FE mesh refinement of 10mm in the AC layer and 25mm in the base layer is used. The model response under transient loading is compared with results obtained from general purpose FE software ABAQUS. For this purpose, haversine loading in an axisymmetric setup is used. ABAQUS consumed approximately 17 minutes in analyzing a haversine loading of 138 psi and 35 ms, whereas LAVAN could generate the results in 3.6 minutes in the same desktop computer.

The surface deflection obtained using FE for the two boundary conditions, (a) finite boundaries: roller support on the vertical boundaries and fixed support on the bottom (b) infinite elements at boundaries are compared with LAVAN in Table 7. It should be noted that both the boundary conditions does not strictly represent the semi-infinite geometry of the problem. In ABAQUS the solution in the infinite element is considered to be linear, which is assumed to matches the material properties of the adjacent finite element. Hence the infinite elements provide stiffness to the boundary assuming the deflection at  $r = \infty$  to be zero. It can be seen from Table 7 that, for both the Control mix and CRTB mix, the surface deflection predicted by FE using finite boundaries were higher compared to results when infinite elements were used at



the boundaries. Further for both the mixes the surface deflections predicted by LAVAN were found to be lying between the FE results predicted by the two boundary conditions.

**Table 7: Comparison of ABAQUS and LAVAN: Peak surface deflections for different boundary conditions.**

Sensor radial distance	Control mix ( $\mu\text{m}$ )			CRTB mix ( $\mu\text{m}$ )		
	Finite boundary	LAVAN	Infinite boundary	Finite boundary	LAVAN	Infinite boundary
0"	810.9	794.7	747.3	1068.9	1079.5	1005.1
8"	757.4	734.6	693.6	966.3	955.0	902.2
12"	712.1	685.0	648.4	883.9	859.1	819.8
18"	639.5	605.5	575.7	758.6	715.5	694.5
24"	565.9	526.9	501.9	639.4	585.0	575.3
36"	433.9	388.4	369.6	445.5	384.3	381.3
48"	329.1	284.0	264.4	311.6	257.7	246.9
60"	252.5	210.4	187.0	227.2	183.4	161.9

Since, satisfactory performance of the model would require predicting a comparable time response by the model. The surface deflection history computed by LAVAN and ABAQUS (analysis with finite boundaries) for the Control mix and CRTB mix are plotted in Figure 25 and Figure 26 respectively. A comparable response is visible in the figures, which has been further quantified using Equation (52) and Equation (53). As expected, under the same geometric and loading conditions the stiffer Control mix generated lower deflections compare to softer CRTB mix. Figure 25a shows the results when stress at  $r = 0$  is used in LAVAN for nonlinearity computation, and provided for comparison purpose Figure 25b shows the results when stress at  $r = 3.5a$  is used in LAVAN. It is noted that S1, S2, S3, S4, S5, S6, S7, S8 in the figures corresponds to surface deflection at Sensor-1 through Sensor-8 spaced at, 0", 8", 12", 18", 24", 36", 48" and 60" away from the centerline of the load. In general a better match for the deflection basin between the FE and LAVAN results can be found when stress state at  $r = 3.5a$  is used while incorporating nonlinearity. It is worth noting that, for the structure in Figure 22,

Huang's (2004) procedure for the location of stress used in the nonlinear elastic analysis leads to  $r = 2.8a$ , when trapezoidal stress distribution with 0.5 horizontal slope, 1 vertical slope is assumed.

The difference between the FE results and LAVAN was quantified using the following two variables:

$$PE_{peak} = \frac{|u_{ABAQUS}^{peak} - u_{LAVAN}^{peak}|}{u_{ABAQUS}^{peak}} 100 \quad (52)$$

$$PE_{avg} = \frac{1}{N} \sum_{i=1}^N \frac{|u_{ABAQUS}(t_i)/u_{ABAQUS}^{peak} - u_{LAVAN}(t_i)/u_{LAVAN}^{peak}|}{u_{ABAQUS}(t_i)/u_{ABAQUS}^{peak}} 100 \quad (53)$$

where  $PE_{peak}$  is the percent error in the peaks,  $u_{ABAQUS}^{peak}$  is peak deflection predicted by ABAQUS,  $u_{LAVAN}^{peak}$  is peak deflection predicted by LAVAN,  $PE_{avg}$  is average percent error,  $u_{ABAQUS}(t_i)$  is deflection predicted by ABAQUS at time ( $t_i$ ),  $u_{LAVAN}(t_i)$  is deflection predicted by LAVAN at time ( $t_i$ ),  $N$  is total number of time intervals in the deflection time history. Since the model integrates both viscoelastic and nonlinear material properties, both peak deflection as well as relaxation of deflection time history should be predicted with accuracy. Therefore, normalized average error along the entire deflection history  $PE_{avg}$  was used to examine the model performance in creeping. As shown in Table 8, the  $PE_{peak}$  and  $PE_{avg}$  values for Control mix showed a slight improvement in the results when  $r = 3.5a$  is used. However, it can be seen from the table that, error for CRTB mix increased at sensor 1, 2 and 3. As expected, due to the limitations of LAVAN in incorporating horizontal nonlinearity, both the mixes showed increasing difference as compared to the FE solutions at sensors away from the loading. In both

the cases, however, errors in the first 4-5 sensors were within 6%, indicating good accuracy of LAVAN.

**Table 8: Comparison of ABAQUS and LAVAN: Percent error (PE<sub>peak</sub>) calculated using the peaks of the deflections and average percent error (PE<sub>avg</sub>) calculated using the entire time history.**

Sensor radial distance (inches)	Peak deflection error (%) PE <sub>peak</sub>				Average deflection history error (%) PE <sub>avg</sub>			
	Control mix		CRTB mix		Control mix		CRTB mix	
	r=0	r=3.5 a	r=0	r=3.5 a	r=0	r=3.5 a	r=0	r=3.5 a
0"	0.81	1.02	2.93	6.26	1.61	2.09	1.45	2.06
8"	1.83	0.07	0.77	4.26	1.47	1.86	1.29	1.75
12"	2.64	0.69	0.89	2.71	1.39	1.67	1.30	1.52
18"	4.18	2.17	3.83	0.18	1.31	1.48	1.56	1.30
24"	5.80	3.76	6.78	3.15	1.45	1.35	1.99	1.43
36"	9.52	7.53	12.43	9.32	1.82	1.53	2.58	2.04
48"	12.98	11.25	16.46	14.18	2.20	1.87	2.46	2.25
60"	16.19	14.81	18.96	17.74	2.27	2.10	1.42	1.77

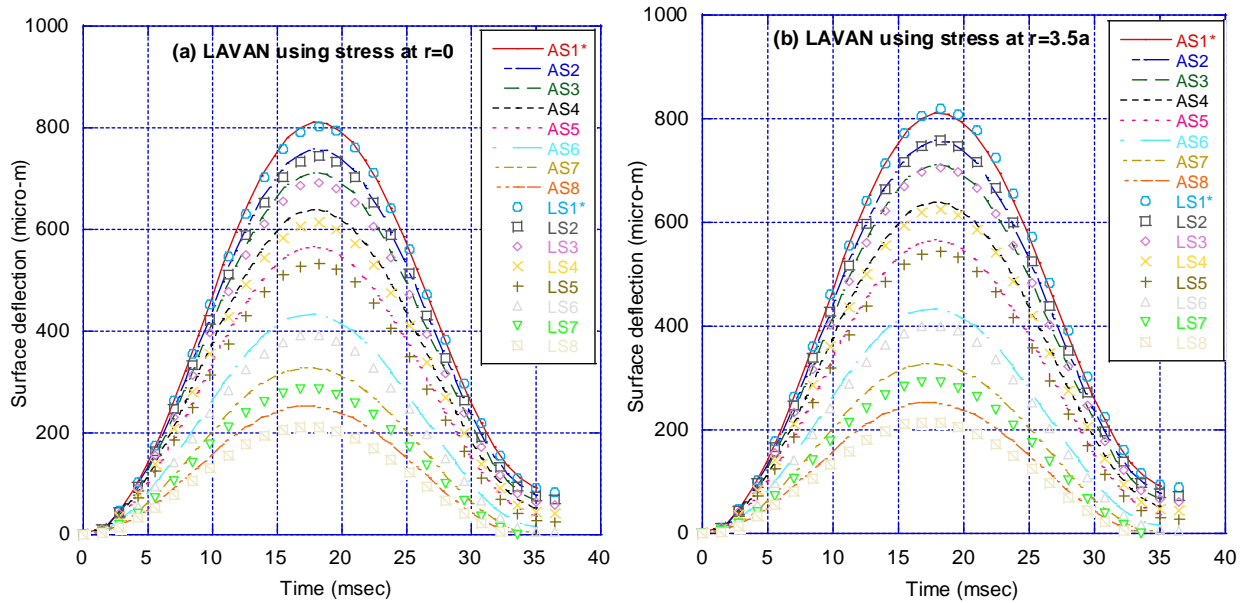


**Figure 25: Surface deflection comparison of ABAQUS and LAVAN for the Control mix (\*AS1= ABAQUS sensor 1; \*LS1=LAVAN sensor 1).**

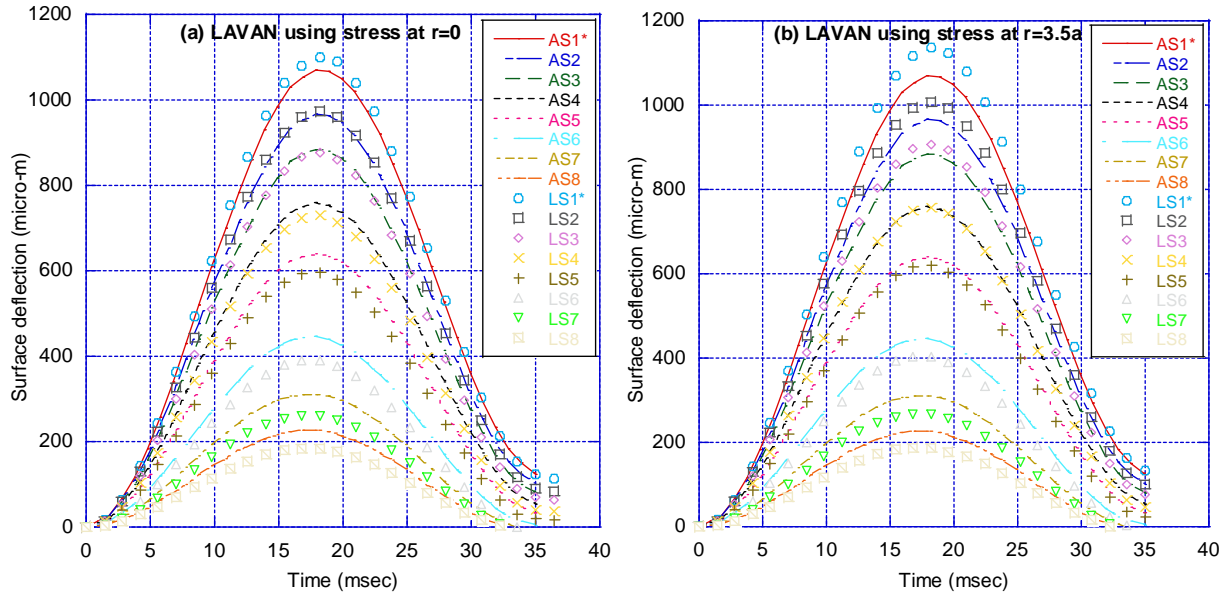


**Figure 26: Surface deflection comparison of ABAQUS and LAVAN for the CRTB mix (\*AS1= ABAQUS sensor 1; \*LS1=LAVAN sensor 1).**

### 3.6 Chapter Summary

Algorithms have been developed to model multilayer viscoelastic forward solution. The models presented can consider the unbound granular material as both linear elastic as well as nonlinear-stress dependent material. Depending on the assumed unbound granular material property, two generalized viscoelastic flexible pavement models were developed. The developed forward model for linear viscoelastic AC and elastic unbound layers has been referred to as LAVA. The developed forward model for linear viscoelastic AC and nonlinear elastic unbound layers have been termed as LAVAN. LAVA assumes a constant temperature along the depth of the AC layer. The algorithm was subsequently modified for temperature profile in the AC layer and has been referred to as LAVAP. The models have been validated using FE based solutions.

## CHAPTER 4

# BACKCALCULATION USING VISCOELASTICITY BASED ALGORITHM

### 4.1 Introduction

Typically, a load-displacement history of 60 milliseconds is recorded in an FWD test (which constitutes of 25-35 msec of applied load pulse). This can give only a limited information about the time varying  $E(t)$  behavior of the AC layer. However, in theory, it should be possible to obtain the two sought after functions (i.e.,  $E(t)$  and  $a_T(T)$ ). Two different approaches have been discussed to obtain comprehensive behavior of asphalt: (i) using series of FWD deflection time histories at different temperature levels (Varma et al., 2013b) and (ii) using uneven temperature profile information existing across the thickness of the asphaltic layer during a single or multiple FWD drops deflection histories (Varma et al., 2013a). Backcalculation of pavement properties using FWD data involves developing an optimization scheme. The analysis is based on formulating an objective function, which is minimized by varying the pavement properties. Response obtained from the forward analysis is compared with response obtained from the FWD test and the 'difference' is minimized by adjusting the layer properties of the system until a best match is achieved. Typically the existing backcalculation methods either use Root Mean Square (RMS) or percentage error of peak deflections as the objective function. However, since the viscoelastic properties are time dependent, the entire deflection history needs to be used. Hence, the primary component of the proposed backcalculation procedure is a layered viscoelastic forward solution. Such solution should provide accurate and rapid displacement response

histories due to a time-varying (stationary) surface loading. Herein, for linear viscoelastic pavement model, we used the computationally efficient layered viscoelastic algorithm LAVA/LAVAP (refer Chapter 3) to support the backcalculation algorithm called BACKLAVA/BACKLAVAP. Whereas, for viscoelastic nonlinear pavement model, we used the computationally efficient layered viscoelastic algorithm LAVAN (refer chapter 3) to support the backcalculation algorithm called BACKLAVAN.

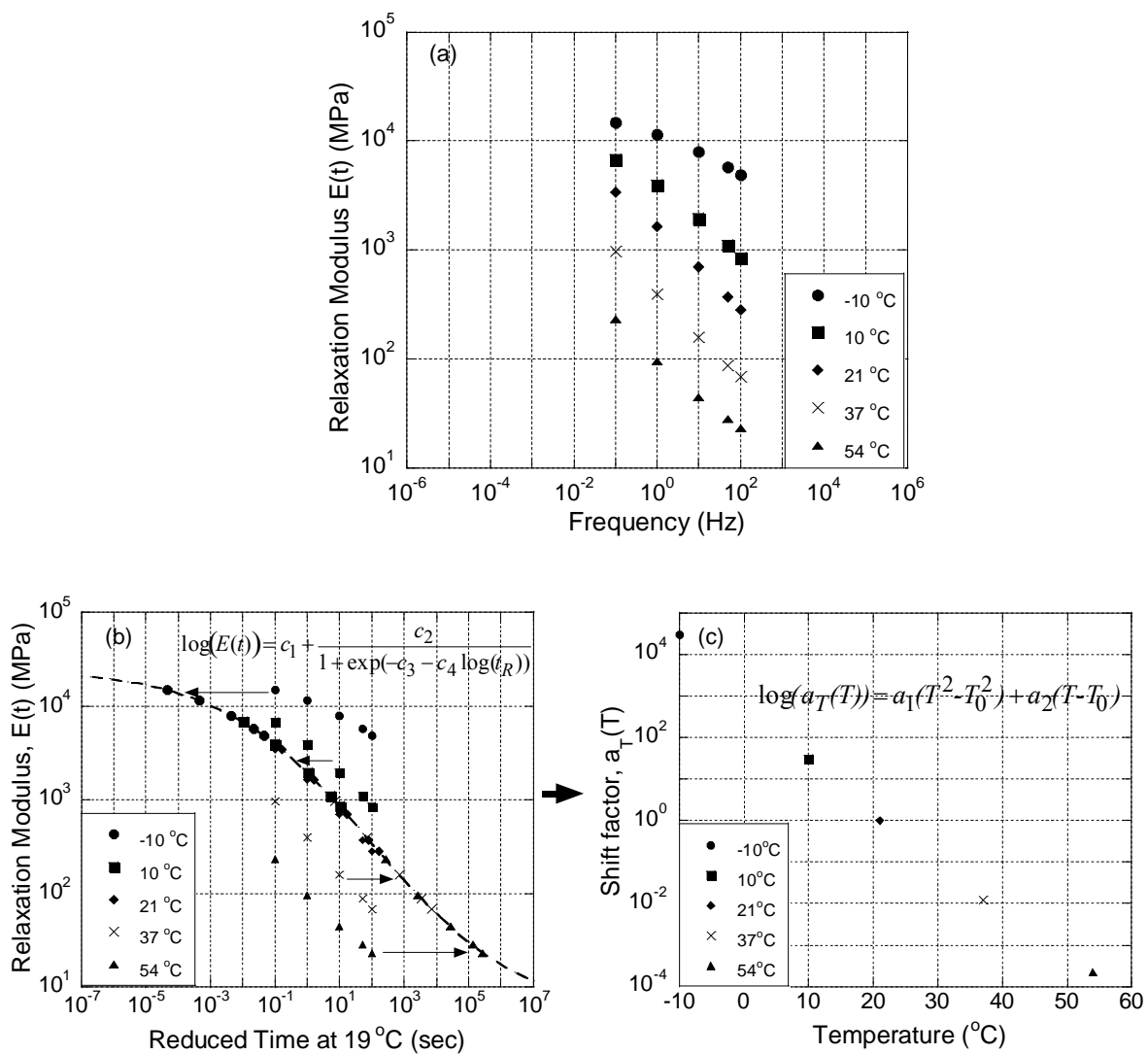


Figure 27: Figure illustrating steps in  $E(t)$  master curve development.

Whenever mechanical properties are derived by way of inverse analysis, it is desirable to minimize the number of undetermined parameters by using an economical scheme. Such approach is both advantageous from a computational speed perspective and it also addresses the non-uniqueness issue, as test data may not be detailed, accurate, or precise enough to allow calibration of a complicated model. Moreover, it is beneficial to have some inherent ‘protection’ within the formulation, forcing the analysis to a meaningful convergence - fully compliant with the physics of the problem. Therefore, as discussed before, the  $E(t)$  master curve (Figure 27) is initially assumed to follow a sigmoid shape with the Equation (25). Where, as discussed before,  $a_T(T)$  is the shift factor coefficient, which is a second order polynomial function of temperature ( $T$ ) and  $t$  is time (Equation (23)). Similar to the process used in generating  $|E^*|$  master curve,  $E(t)$  master curve can be generated using the concept of TTS. As shown by the relaxation modulus and shift factor equations, total six coefficients are needed to develop the  $E(t)$  master curve, including the temperature dependency (i.e., the shift factor coefficients). In theory, it should be possible to obtain these six coefficients in two ways: (i) using two or more FWD time history data at different temperature levels and (ii) using uneven temperature profile information existing across the thickness of the asphaltic layer during a single FWD drop containing time changing response data.

The objective function, which is based on deflection differences in the current work, is a multi-dimensional surface that can include many local minima. In elastic backcalculation methods, the modulus of the AC layer is defined using a single value. However, in the present problem the AC properties are represented by a sigmoid containing four parameters for  $E(t)$  and by a polynomial containing 2 parameters for  $a_T(T)$ . Hence, it is naturally expected that the probability of number of local minimums will increase. In traditional methods, due to the

presence of multiple local minima, selection of different initial solution may lead to different solutions. Reliability and accuracy of the backcalculated results depend on the optimization technique used. In the present work several optimization techniques were tried to formulate a procedure to backcalculate these six viscoelastic properties along with unbound material properties. These optimization techniques can be broadly classified as traditional methods and non-traditional methods. Traditional optimization methods could be computationally less expensive and can have better control over solution accuracy. However, typically traditional optimization methods (such as the “fminsearch” in MATLAB©) have the following issues:

1. Solution (local or global) may depend on initial seed values
2. Convergence time may vary depending on the initial seed values.

To extract benefits from both traditional and non-traditional methods, in this study they have been hybridized to develop a more effective backcalculation procedure. Simplex-based traditional optimization method was performed using MATLAB function “fminsearch”, whereas, genetic algorithm-based evolutionary optimization method was performed using MATLAB function “ga”. It is important to develop a backcalculation process such that FWD data obtained at relatively small range of pavement temperatures can be sufficient to derive the viscoelastic properties of AC. Among various optimization techniques, Genetic Algorithm (GA) was chosen because of its capability to converge to a unique global minimum solution, irrespective of the presence of local solutions (Fwa et al., 1997; Alksawneh, 2007; and Park et al., 2009). Through guided random search from one ‘generation’ to another, GA minimizes the desired objective function. The detailed discussion on genetic algorithm in FWD backcalculation is presented in chapter 2 and will not be repeated here for brevity.



Formulation of the optimization model using GA is:

Objective:

$$Er = \sum_{k=1}^m 100 \sum_{i,o=1}^n \frac{|(a_i^k - d_o^k)|}{d_i^k} \quad (54)$$

Subject to the following constraints:

$$c_1^l \leq c_1 \leq c_1^u, c_2^l \leq c_2 \leq c_2^u,$$

$$c_3^l \leq c_3 \leq c_3^u, c_4^l \leq c_4 \leq c_4^u$$

$$a_1^l \leq a_1 \leq a_1^u, a_2^l \leq a_2 \leq a_2^u,$$

$$E_b^l \leq E_b \leq E_b^u, E_s^l \leq E_s \leq E_s^u$$

where,  $m$  is the number of sensors,  $d_i$  is the input deflection information obtained from field at sensor  $k$ ,  $d_o^k$  is the output deflection information obtained from forward analysis at sensor  $k$ ,  $n$  is the total number of deflection data points recorded by a sensor,  $c_i$  are the sigmoid coefficients,  $E_b$  and  $E_s$  are base and subgrade modulus and  $a_i$  are the shift factor polynomial coefficients. The superscript  $l$  represents lower limit and  $u$  represents upper limit.

In order to obtain the lower and upper limits of  $c_i$  and  $a_i$ , values of sigmoid and shift factor coefficients of numerous HMA mixtures were calculated. Table 9 shows these limits which were used in the GA constraints shown in Equation (54). Limits to the elastic modulus were arbitrarily selected (based on typical values presented in the literature). It should be noted that sigmoid obtained by using the lower limits or the upper limits of the coefficients give larger range as compared to the actual range of  $E(t)$ . This can potentially slow down the

backcalculation process. Therefore, as described later in the report, additional constraints were defined to narrow down the search window. Figure 28 shows the steps in the GA based backcalculation programs.

**Table 9: Upper and lower limit values in backcalculation**

Limit	c <sub>1</sub>	c <sub>2</sub>	c <sub>3</sub>	c <sub>4</sub>	a <sub>1</sub>	a <sub>2</sub>	E <sub>1</sub>	E <sub>2</sub>
Lower	0.045	1.80	-0.523	-0.845	-5.380E-04	-1.598E-01	10000	22000
Upper	2.155	4.40	1.025	-0.380	1.136E-03	-0.770E-01	13000	28000

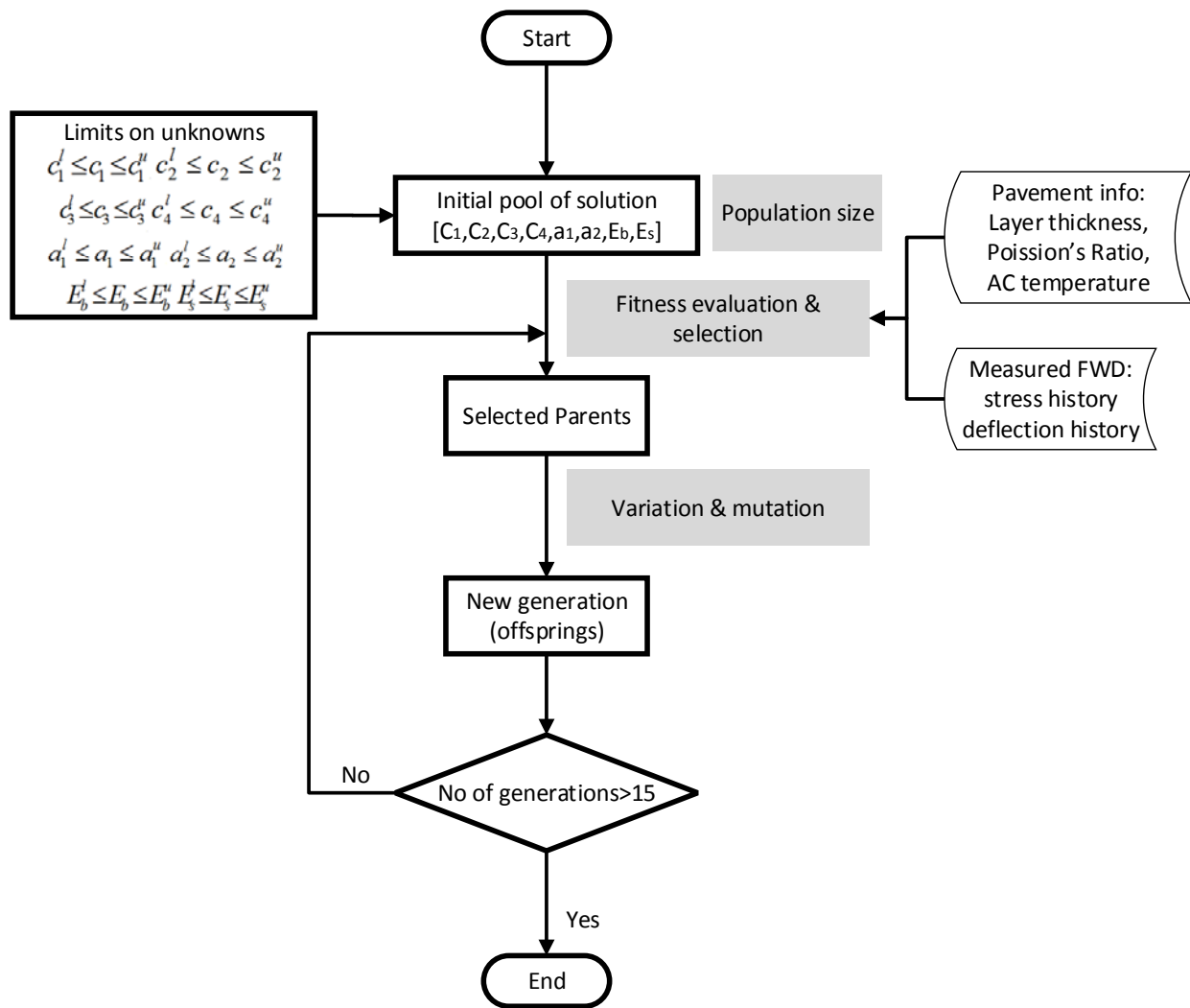


**Figure 28: Backcalculation flow chart in BACKLAVA**

## 4.2 Backcalculation of Relaxation Modulus Master Curve Using Series of FWD Tests Run at Different Temperatures

The duration of a single pulse of an FWD test is very short, which limits the portion of the  $E(t)$  curve used in the forward calculation using LAVA. As a result, it is not possible to backcalculate the entire  $E(t)$  curve accurately using the deflection data of such short duration. The longer the duration of the pulse, the larger portion of the  $E(t)$  curve is used in LAVA in the forward calculation process. Therefore, one may conclude that FWD tests need to produce long-duration deflection-time history. However, owing to the thermorheologically simple behavior of AC, time-temperature superposition principle can be used to obtain longer duration data by simply running the FWD tests at different temperatures and using the concept of reduced time. This process has been further illustrated in Figure 29. The figure shows a schematic example of the steps involved in the evaluation of a Candidate parent solution (refer to step two “Fitness evaluation and selection” in Figure 28). The figure shows simulation of two different FWD runs at temperatures  $T_1$  and  $T_2$  such that  $T_2 > T_1$ . Since the two tests are at different temperatures, they correspond to different reduced time in the master curve. For  $T_2 > T_1$ , FWD test at  $T_2$  would use  $E(t)$  from higher reduced time compare to FWD test at  $T_1$ . Before getting into the details of the required number of FWD test temperatures and magnitudes, first, an analysis on the effects of different FWD deflection sensor data on the backcalculated  $E(t)$  master curve is presented in the following section.

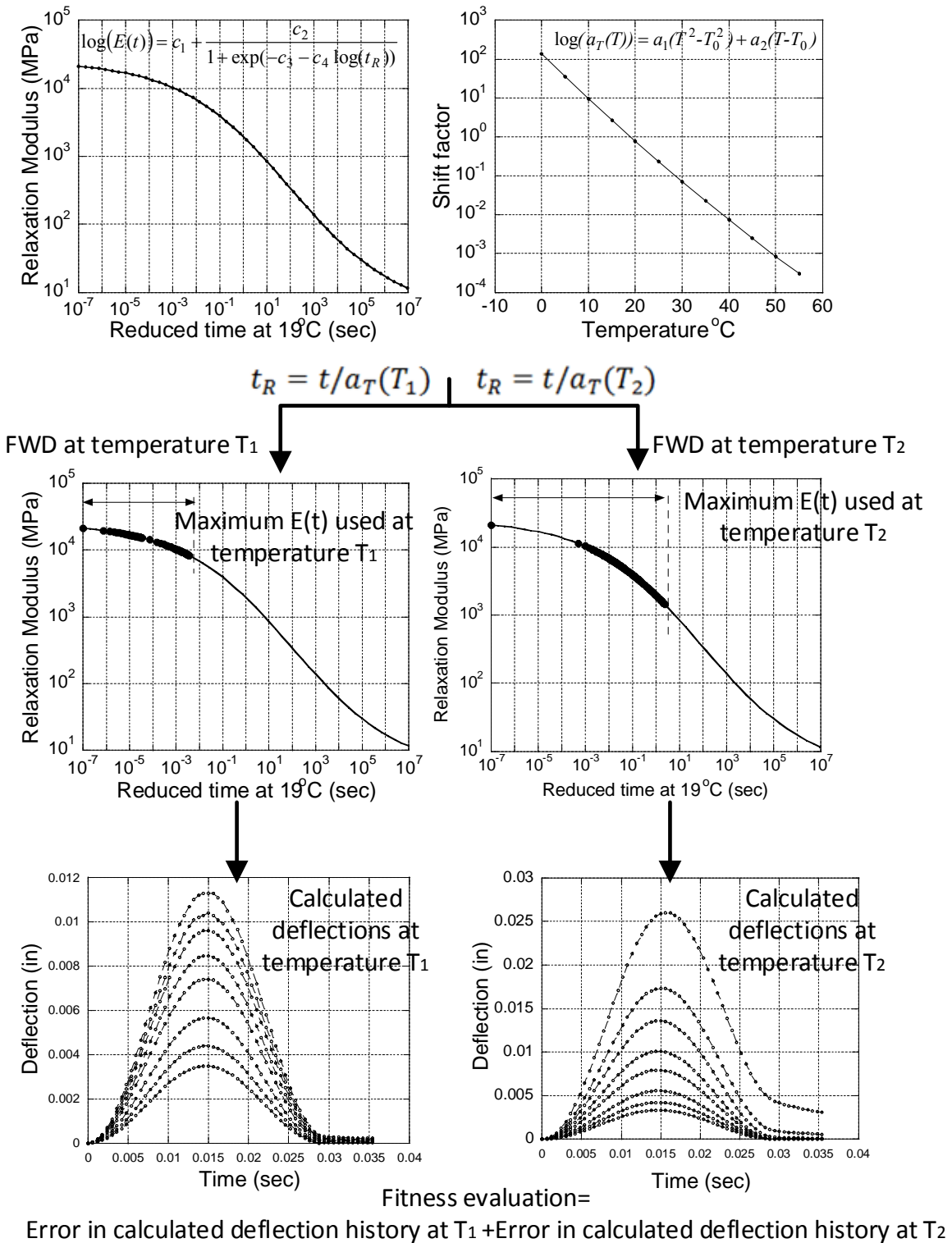


**Figure 29: Schematic of fitness evaluation in BACKLAVA**

#### 4.2.1 Sensitivity of E(t) Backcalculation to the use of Data from Different FWD Sensors

This section presents an analysis of contribution of individual and group of sensors on the backcalculation of E(t) master curve. The backcalculation process was run using a population-generation of 70 and 15 respectively (selected after trying various combinations), using FWD time histories obtained at a temperature set of {0, 10, 20, 30, 40, 50, 60, 70 and 80}°C. The pavement properties used (Table 10) have been kept same throughout the study.

**Table 10: Pavement Properties in viscoelastic backcalculation of optimal number of sensors**

Property	Case 1
Thickness (AC followed by granular layers)	10, 20 (in)
Poisson ratio {layer 1,2,3...}	0.35, 0.3, 0.45
E <sub>unbound</sub> {layer 2,3...}	11450, 15000 (psi)
E(t) sigmoid coefficient {layer 1}	0.841, 3.54, 0.86, -0.515
a <sub>T</sub> (T) shift factor polynomial coefficients {layer 1}	4.42E-04, -1.32E-01
Sensor spacing from the center of load (inches)	0, 8, 12,18,24, 36,48, 60

Convergence was evaluated based on the backcalculated modulus of base and subgrade layers as well as the E(t) curve of the AC layer. Average error in the modulus of base and subgrade are defined as follows:

$$\xi_{unbound} = \left| \left( \frac{E_{act} - E_{bc}}{E_{act}} \right) \right| \times 100 \quad (55)$$

where  $\xi_{unbound}$  is the absolute value of the error in the backcalculated unbound layer modulus,  $E_{act}$  and  $E_{bc}$  are the actual and backcalculated modulus (of the unbound layer), respectively. The variation of error in the backcalculated E(t) at different reduced times is defined as follows:

$$\xi_{AC}(t_i) = \frac{E_{act}(t_i) - E_{bc}(t_i)}{E_{act}(t_i)} \times 100 \quad (56)$$

where  $\xi_{AC}(t_i)$  is the  $E(t)$  error at reduced time  $t_i$ , where  $i$  ranges from 1 to  $n$  such that  $t_1 = 10^{-8}$  and  $t_n = 10^8$  sec,  $n$  is the total number of discrete points on  $E(t)$  curve,  $E_{act}(t_i)$  is the actual  $E(t)$  value at point  $i$ , and  $E_{bc}(t_i)$  is the backcalculated  $E(t)$  value at  $i$ . Finally, average error in  $E(t)$  is defined as follows:

$$\xi_{AC}^{avg} = \frac{1}{n} \left( \sum_{i=1}^n |\xi_{AC}(t_i)| \right) \quad (57)$$

where  $\xi_{AC}^{avg}$  is the average error in the  $E(t)$  of the AC layer. Figure 30 shows the variation of  $\xi_{unbound}$  when data from different FWD sensors are used. As shown, the error decreases as data from farther sensors are incorporated in the backcalculation. This may be because at farther sensors the deflections are primarily, if not solely, due to deformation in the lower layers.

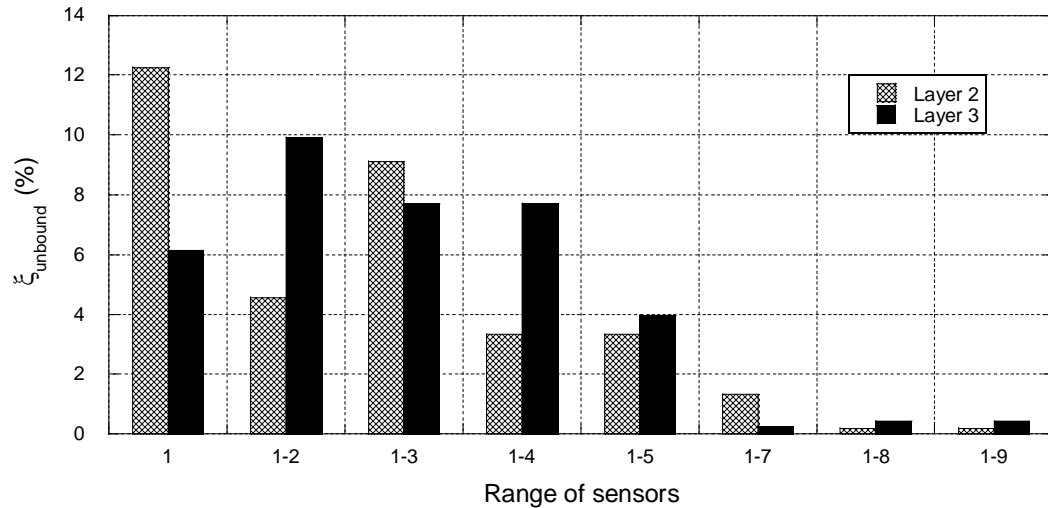


**Figure 30: Error in unbound layer modulus in optimal number of sensor analysis**

Figure 31a shows the actual and backcalculated  $E(t)$  curve, which is only based on deflection history obtained from sensor 1 (at the center of load plate). As shown, there is a very good match between the backcalculated and actual curves. Figure 31b shows the variation of

percentage error in  $E(t)$  with time, calculated using Equation (57). The magnitude of percent error ranges from about -9% to 23% and increases with reduced time. This is expected since the  $E(t)$  in longer durations ( $>10^{-6}$  sec) are not used in the forward computations. It is noted that the result is shown over a time range from  $10^{-8}$  to  $10^8$  sec. However, the forward calculations were actually made using temperatures ranging from 0 to  $80^{\circ}\text{C}$ , which corresponds to a reduced time range of approximately from  $10^{-6}$  to  $10^6$  sec.

In order to investigate if using just the farther sensors improves the backcalculated  $E_{unbound}$  values, backcalculations were performed using data from different combinations of farther sensors. Figure 32 shows the error in backcalculation of modulus of base (Layer 2) and subgrade (Layer 3), when data from only further sensors are used. As shown, for Layer 3, error ranges between 0.27 to 1.43%, with no specific trend. The error in the modulus of base (Layer 2) is higher, ranging from 1 to 8.96%. However, a clear trend was not observed. Compared to Figure 30, one can conclude that using all the sensors produces the least error in  $E_{unbound}$ .

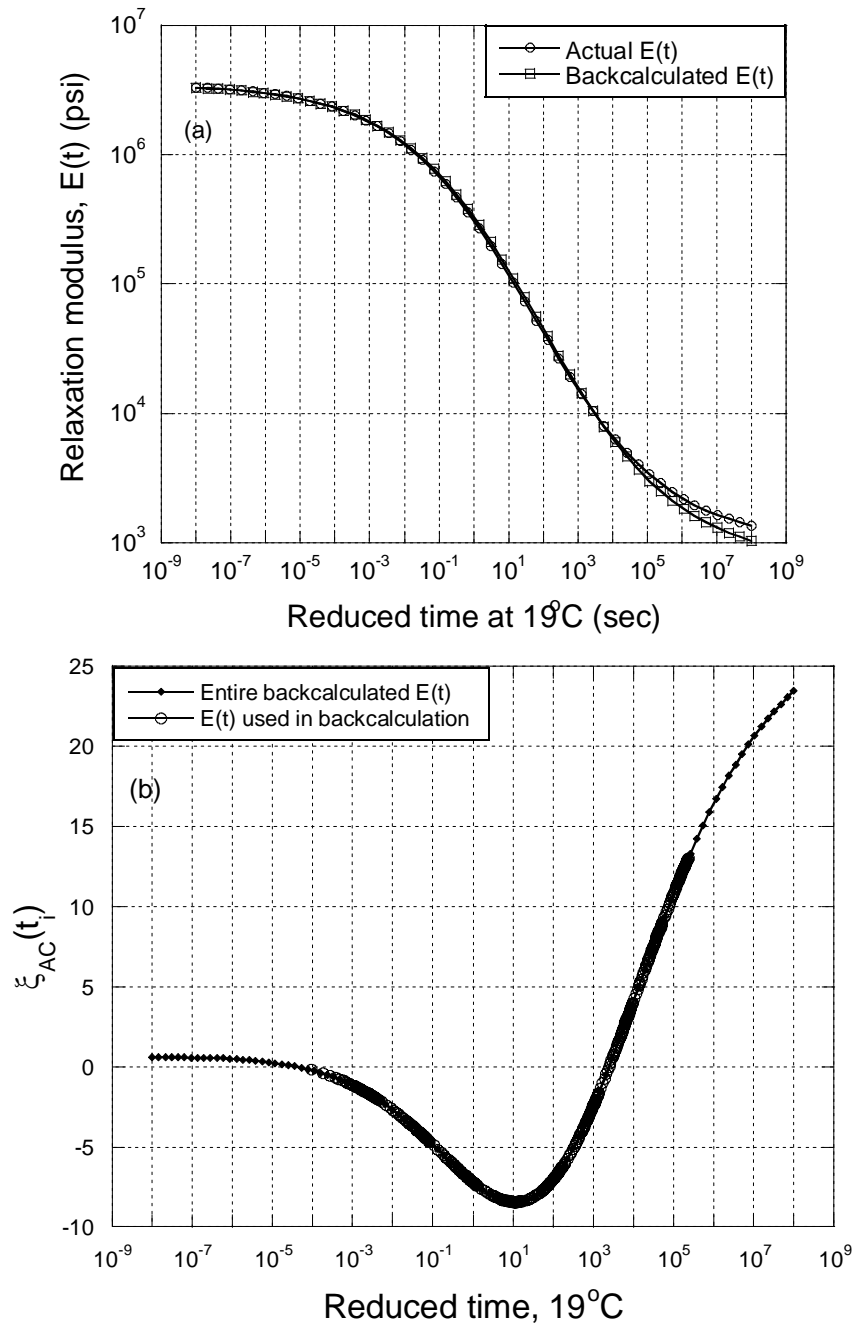


**Figure 31: Backcalculation results using only sensor 1: (a) Backcalculated and actual  $E(t)$  master curve at the reference temperature of  $19^\circ\text{C}$  (b) Variation of error,  $\xi_{AC}(t_i)$ .**



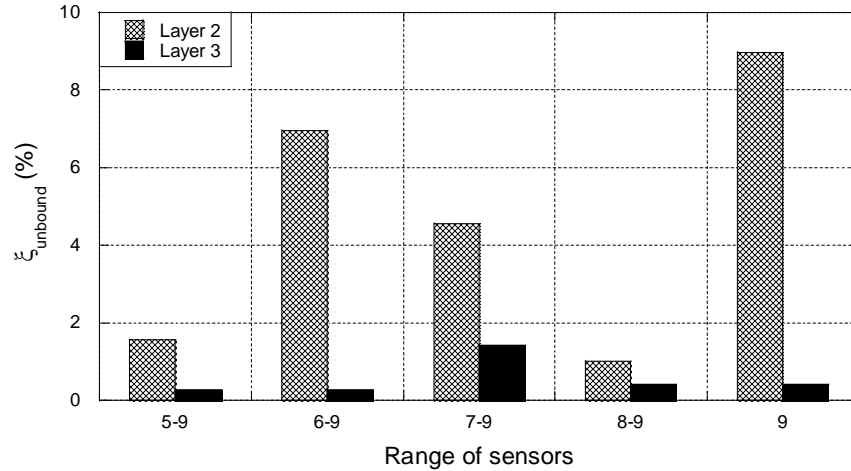


**Figure 32: Error in unbound layer modulus using FWD data only from farther sensors**

#### ***4.2.2 Effect of Temperature Range of Different FWD Tests on Backcalculation***

It is typically not feasible to run the FWD test over a wide range of temperatures (e.g., from 0°C to 80°C). Depending on the region and the month of the year, the variation of temperature in a day can be anywhere between 10°C and 30°C during the Fall, Summer and Spring when most data collection is done. This means that the performance of the backcalculation algorithm needs to be checked for various narrow temperature ranges. The purpose of the study explained in this section was to determine the effect of different temperature ranges on the backcalculated  $E(t)$  values. Further it was realized that the results obtained from GA may not be exact but only an approximation of the global solution. Hence a local search method was carried out through “fminsearch” using the results obtained from GA as seed. Figure 33 shows the error in the backcalculated elastic modulus values of base and subgrade when different pairs of temperatures are used. As shown, in most cases, the error was less than 0.1 %. It is noted that the errors shown in Figure 33 are less than the ones shown in Figure 30 (when all sensors are used). This is because in Figure 30, only GA was used, whereas in Figure 33, “fminsearch” is used after the GA, which improved the results.

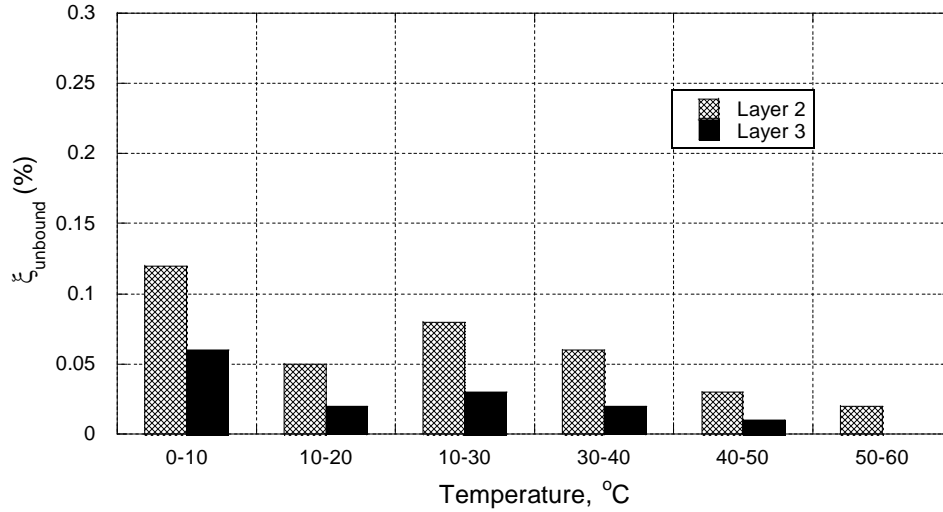


**Figure 33: Variation of error in backcalculated unbound layer moduli when FWD data run at different sets of pavement temperatures are used.**

Figure 34 shows the average error in  $E(t)$  (i.e.,  $\xi_{AC}^{avg}$  given in Equation (57)), where a pattern was observed. The error was the least when intermediate temperatures (i.e.,  $\{10-30\}$ ,  $\{10-20-30\}$ ,  $\{20-30-40\}$ ,  $\{30-40\}$ ,  $\{30-40-50\}$  °C) were used. At low temperatures, it seems the error increase. This is meaningful because at low temperatures, a small portion (upper left in Figure 31) is utilized in BACKLAVA. Therefore, the chance of mismatch at the later portions of the curve (lower right in Figure 31) is high. At high temperatures, error also seems to increase. Theoretically, the higher the temperature, the larger portion of the  $E(t)$  curve is used because of the nature of the convolution integral, which starts from zero. However, if, only the high temperatures are used, discrete nature of load and deflection time history leads to a big ‘jump’ from zero to the next time  $t_i$ , during evaluation of the convolution integral. This is because when the physical time at high temperatures is converted to reduced time, actual magnitudes become large and, in a sense, a large portion at the upper left side of the  $E(t)$  curve is skipped during the convolution integral. At intermediate temperatures, however, a more ‘balanced’ use of  $E(t)$  curve in BACKLAVA improves the results.

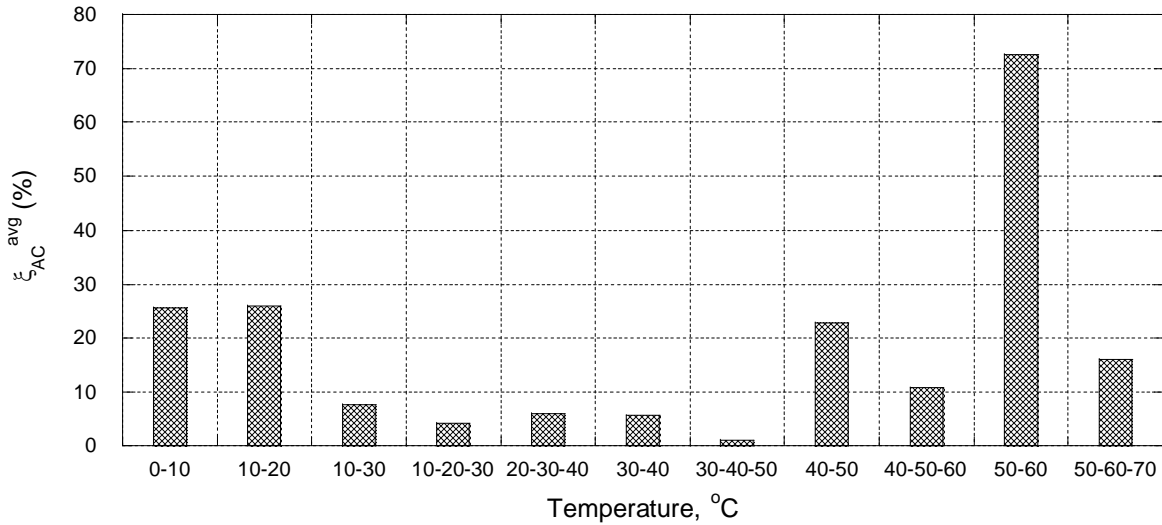
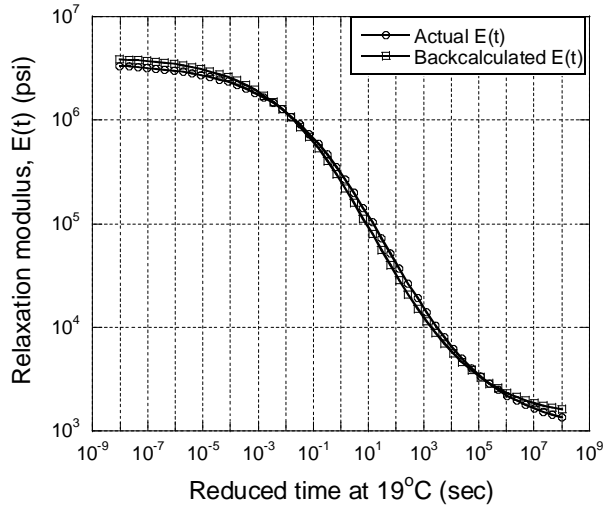


**Figure 34: Error in backcalculated E(t) curve in optimal backcalculation temperature set analysis minimizing percent error**

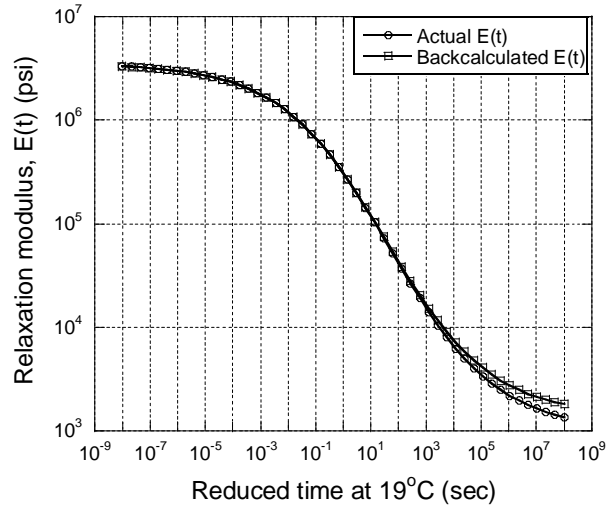
When results from GA were used as seed values in fminsearch, it was observed that in general error in E(t) was reduced. Figure 35, Figure 36 and Figure 37 show backcalculated E(t) master curve using GA and corresponding backcalculated E(t) master curves obtained using GA + “fminsearch”. As shown, combined use of GA and “fminsearch” results in improved backcalculation. Table 11 shows the time it takes to run the genetic algorithm for population-generation size of 70-15, followed by “fminsearch”. The results are shown for a computer that has Intel Core 2, 2.40 GHz, 1.98GB RAM.

**Table 11: Backcalculation run time for ga-fminsearch seed Runs**

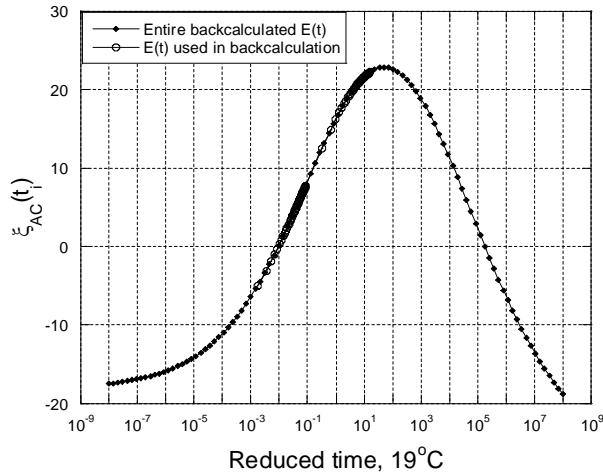
Number of Temperature data	Two (e.g. {10, 30}°C)	Three (e.g. {10, 20, 30}°C)	Seed Run (“fminsearch”)
Backcalculation time	30 min	40 min	15-20 min



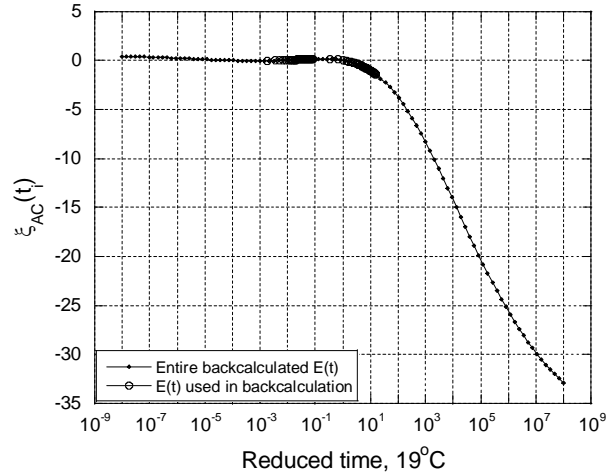
a. Backcalculated E(t) curve using GA only



c. Backcalculated E(t) curve using GA + fminsearch

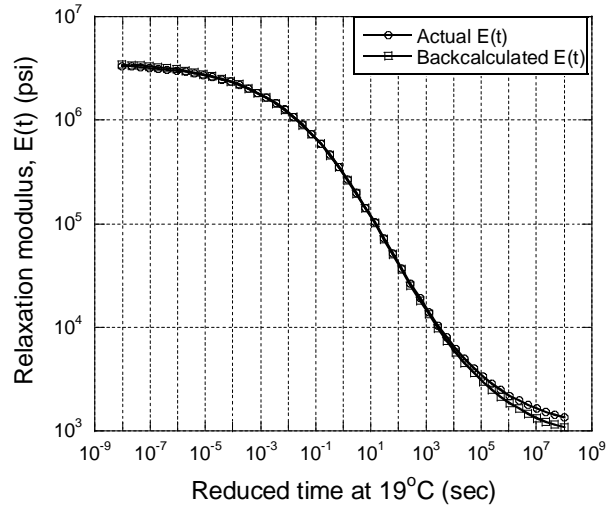
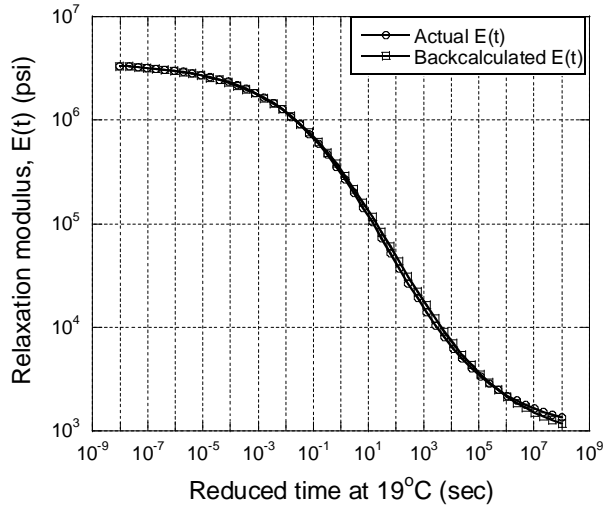


b. Variation of error,  $\xi_{AC}(t_i)$ : GA only.



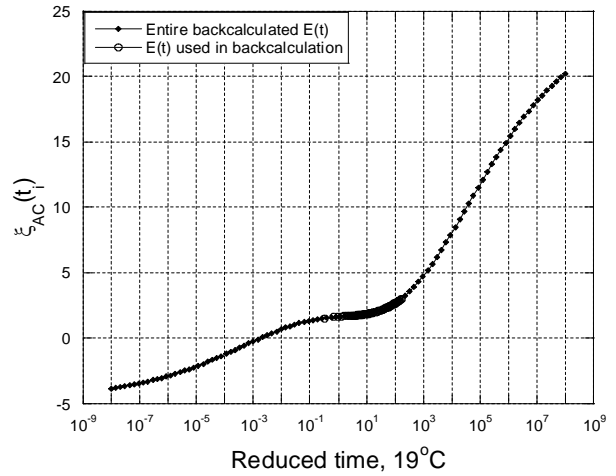
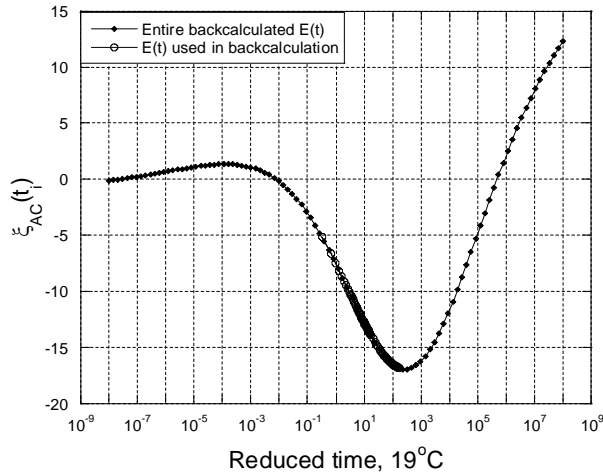
d. Variation of error,  $\xi_{AC}(t_i)$ : GA+fminsearch

**Figure 35: Results for backcalculation at {10, 30}°C temperature set: (a) and (b) Only GA is used, (c) and (d): GA+fminsearch used.**



a. Backcalculated E(t) curve using GA only

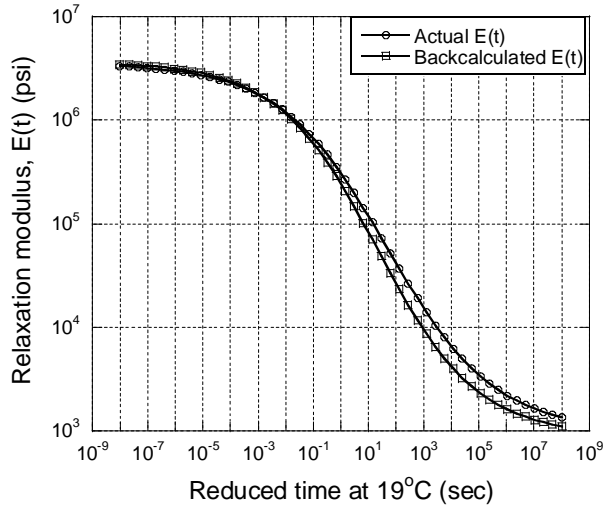
c. Backcalculated E(t) curve using GA+fminsearch



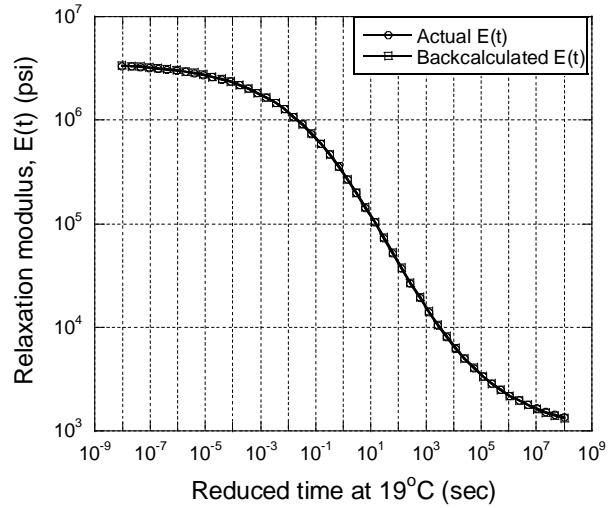
b. Variation of error,  $\xi_{AC}(t_i)$ : GA only

d. Variation of error,  $\xi_{AC}(t_i)$ : GA+fminsearch

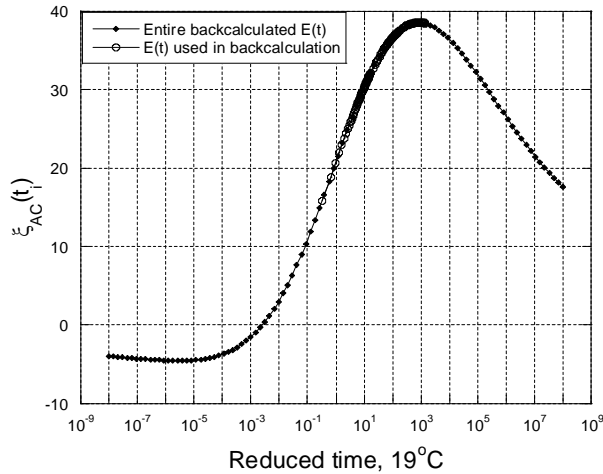
**Figure 36: Results for backcalculation at {30, 40}°C temperature set**



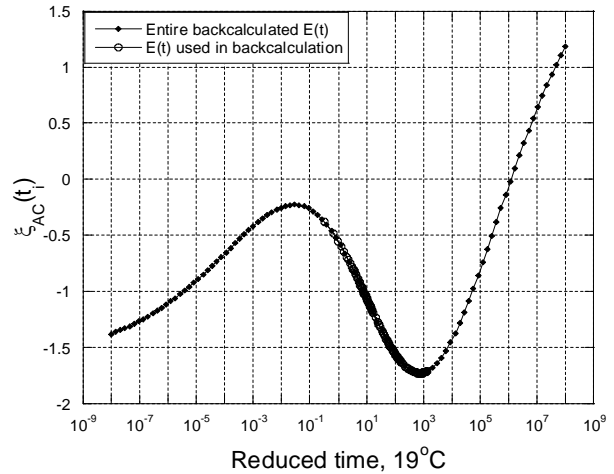
a: Backcalculated E(t) curve using GA only



c: Backcalculated E(t) curve using GA + fminsearch



b: Variation of error,  $\xi_{AC}(t_i)$ : GA only



d: Variation of error,  $\xi_{AC}(t_i)$ : GA+ fminsearch

**Figure 37: Results for backcalculation at {30, 40, 50}°C temperature set**

#### 4.2.3 Normalization of Error Function (Objective Function) to Evaluate Range of Temperatures

In the analysis presented in the previous sections, percentage error between the computed and measured displacement was used as the minimizing error. But deflection curve obtained from the field often includes noise, especially after the end of load pulse. If percentage error is used as the minimizing objective, this may lead to over emphasis of lower magnitudes of deflections at the later portion of the time history, which typically includes noise and integration

errors. Hence another fit function was proposed in which, the percentage error was calculated with respect to the peak of deflection at each sensor. This penalizes the tail data by normalizing it with respect to the peak.

$$Er = \sum_{k=1}^m 100 \sum_{i,o=1}^n \frac{|(d_i^k - d_o^k)|}{\{d^k\}_{\max}} \quad (58)$$

where,  $\{d^k\}_{\max}$  is the peak response at sensor  $k$ ,  $m$  is the number of sensors,  $d_i^k$  is the measured deflection at sensor  $k$ ,  $d_o^k$  is the output (calculated) deflection from forward analysis at sensor  $k$ ,  $n$  is the total number of deflection data points recorded by a sensor. The limits considered for E(t) so far were the limits on the individual parameters of the sigmoid curve (Table 9). The E(t) curves obtained by considering the upper and lower limits of the parameters represent curves well beyond the actual data base domain. To curtail this problem, constraints were introduced putting limit on sum of the sigmoid coefficients  $c_1$  and  $c_2$  as  $c_1 + c_2 \leq s_1$  and  $c_1 + c_2 \geq s_2$ , where  $s_1$  and  $s_2$  are arbitrary constants, which physically represents the maximum and minimum instantaneous modulus value of any HMA mix respectively. The arbitrary constants  $s_1$  and  $s_2$  were obtained by calculating maximum and minimum values of the sum of sigmoid coefficients  $c_1$  and  $c_2$  from numerous HMA mixes. Alternatively the problem was reframed by incorporating the constraints in limit form by redefining the variables as

$$\text{Variable 1} = c_1; c_1^l \leq c_1 \leq c_1^u$$

$$\text{Variable 2} = x; (c_1 + c_2)^l \leq x \leq (c_1 + c_2)^u$$

$$\text{Variable 3} = c_3; c_3^l \leq c_3 \leq c_3^u$$

$$\text{Variable 4} = c_4; c_4^l \leq c_4 \leq c_4^u \quad (59)$$

The problem was then resolved after replacing the inequality constraint with limits on the variables. Figure 38 and Figure 39 show the search domains in unconstrained and constrained optimization models. The unconstrained search zone comprise of many unrealistic solutions, which means the GA would require larger population and generations to search the entire domain, leading to high computation time. It can be seen from the figures that the search domain significantly reduces when the constraint is added to the model. The new function gave good results at temperature sets of  $\{10, 30\}^{\circ}\text{C}$ ,  $\{30, 40\}^{\circ}\text{C}$ ,  $\{10, 20, 30\}^{\circ}\text{C}$ ,  $\{20, 30, 40\}^{\circ}\text{C}$  and  $\{30, 40, 50\}^{\circ}\text{C}$ . The backcalculated  $E(t)$  curves were then converted to  $|E^*|$  using the interconversion relationship given in Equation (11) and (12). Backcalculated  $E(t)$  and  $|E^*|$  master curves are compared with the actual curves for temperature sets  $\{10, 30\}^{\circ}\text{C}$  and  $\{10, 20, 30\}^{\circ}\text{C}$  in Figure 40 and Figure 41 respectively.

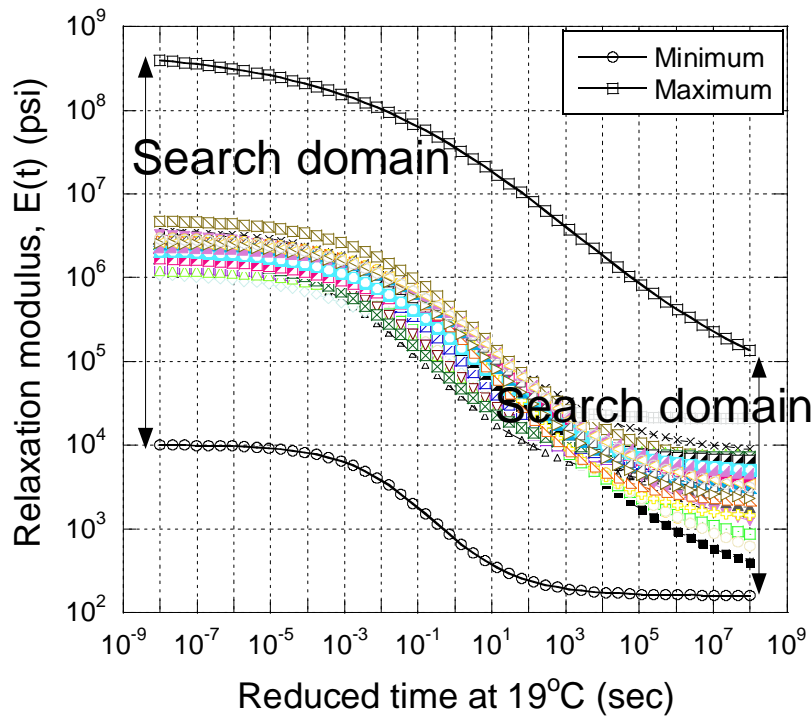


**Figure 38: Search domain for unconstrained constrain**



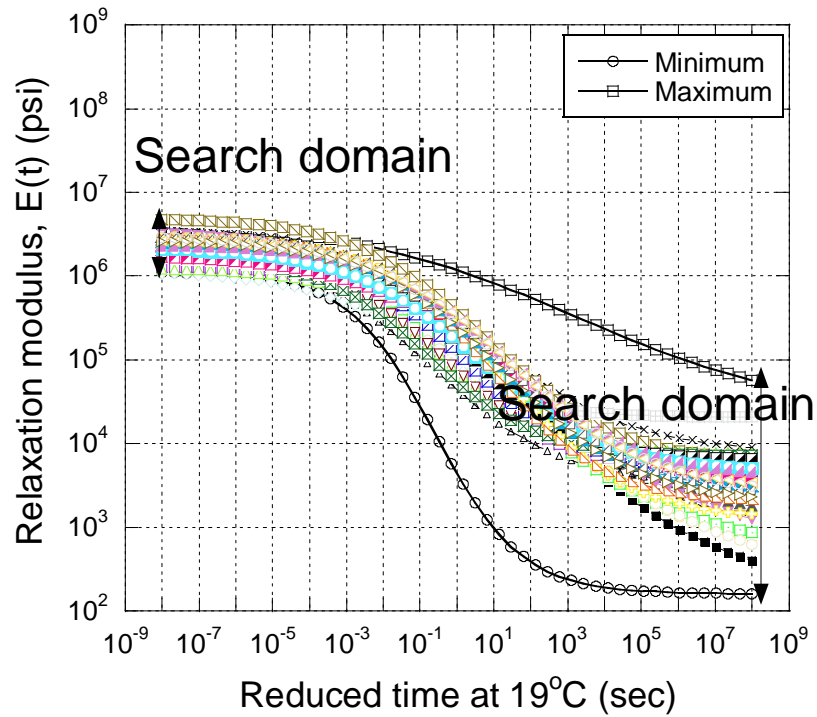


Figure 39: Search domain for constrained constrain

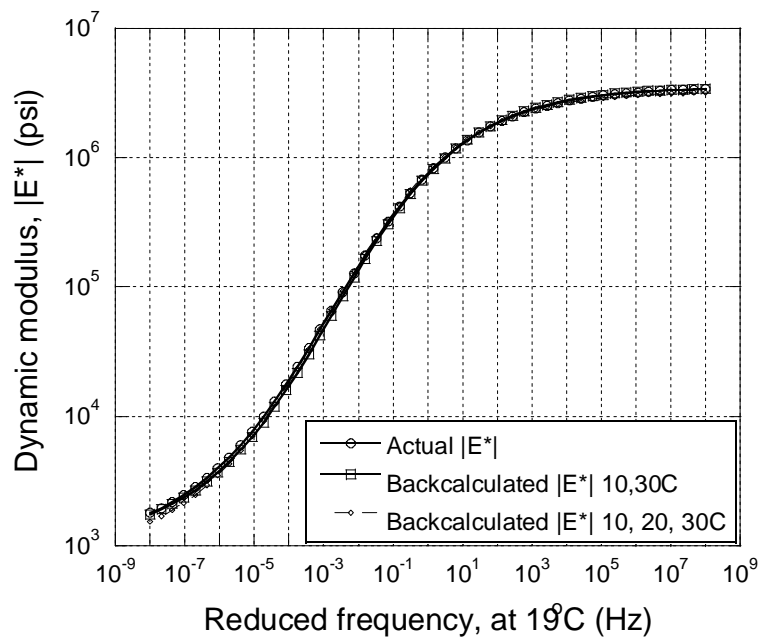
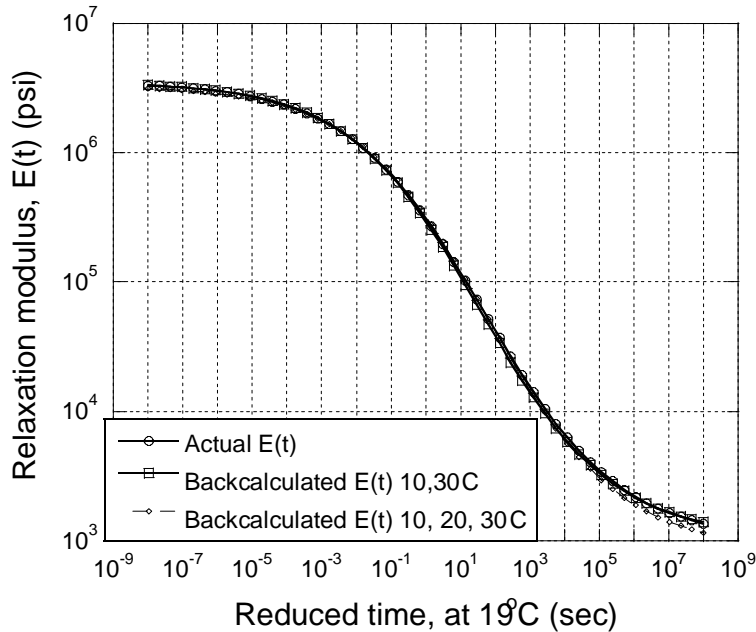
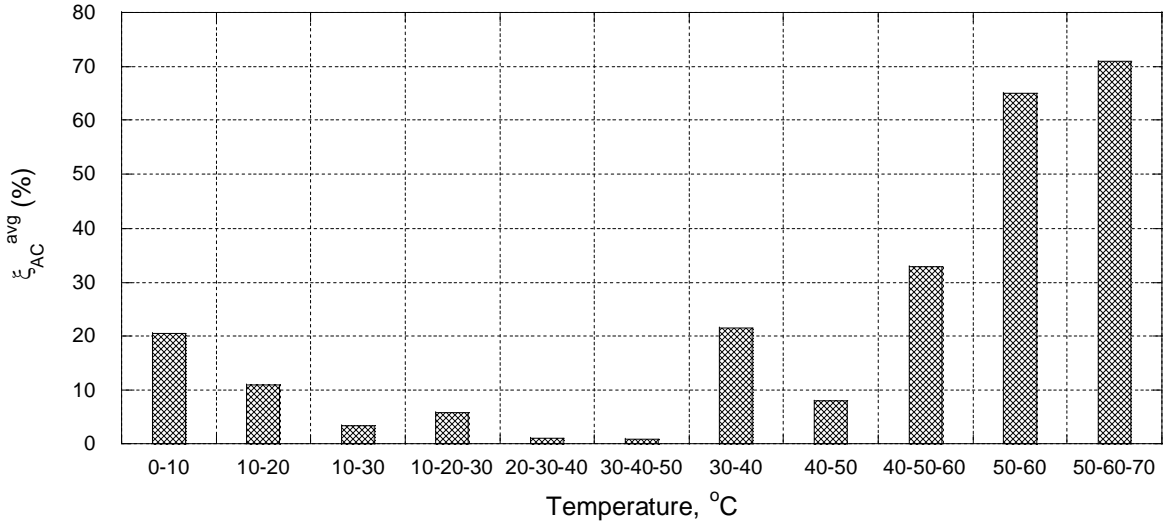


Figure 40: Backcalculated  $|E^*|$  master curve using FWD data at temperature set  $\{10, 30\}^\circ\text{C}$  minimizing normalized error



**Figure 41: Backcalculated E(t) master curve using FWD data at temperature set {10, 20, 30}°C minimizing normalized error**

It can be seen from Figure 42 that the results obtained for E(t) errors over temperature sets distinctly showed a pattern. The E(t) and  $E_{unbound}$  errors with respect to temperature sets showed trend similar to what was observed in case of percentage error (see Figure 33 and Figure 34). The error was observed to be high at sets of low {0-10}°C and high {50-60}°C, {40-50-60}°C, {50-60-70}°C temperatures. This is because the backcalculated E(t) at lower temperatures represents the left portion of the sigmoidal E(t) curve and higher temperatures represents the right. As explained earlier both the regions are fairly flat and hence represent constant values of E(t), which may not optimize to the actual E(t) curve. Better results were obtained for the temperature range of {10, 20}°C to {30, 40, 50}°C (Figure 42). The backcalculated E(t) master curves and corresponding error obtained at {10, 30}°C and {20, 30, 40}°C for the proposed backcalculation model are shown in Figure 44.



**Figure 42: Variation of  $\xi_{AC}^{avg}$  at different FWD temperature sets using modified sigmoidal variables.**

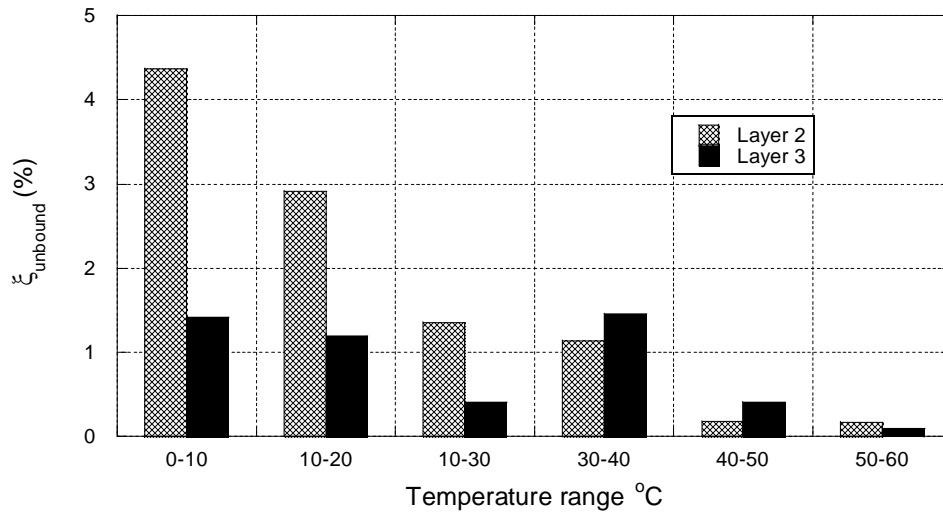
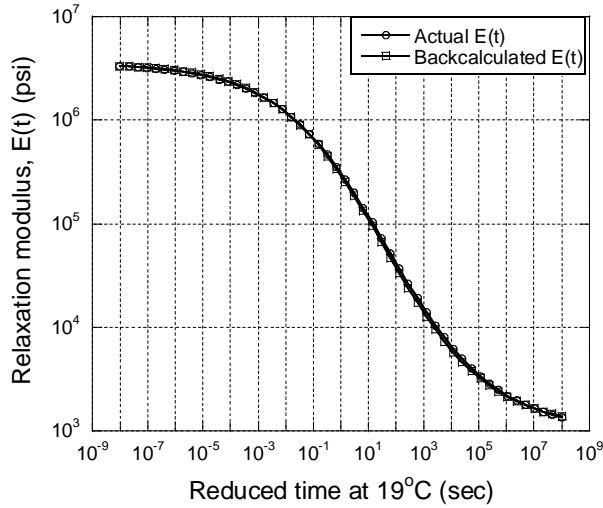
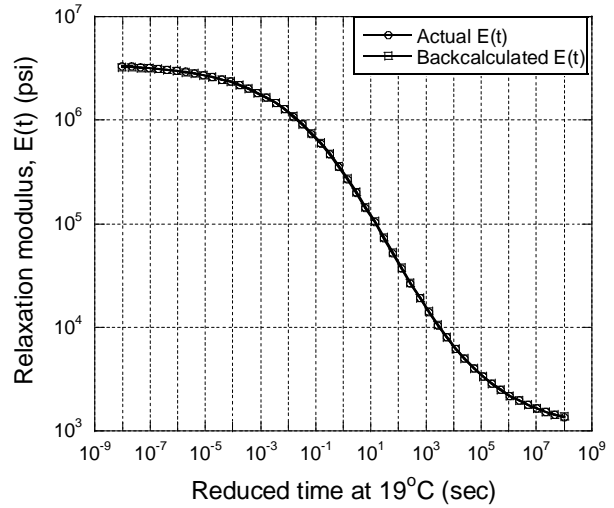


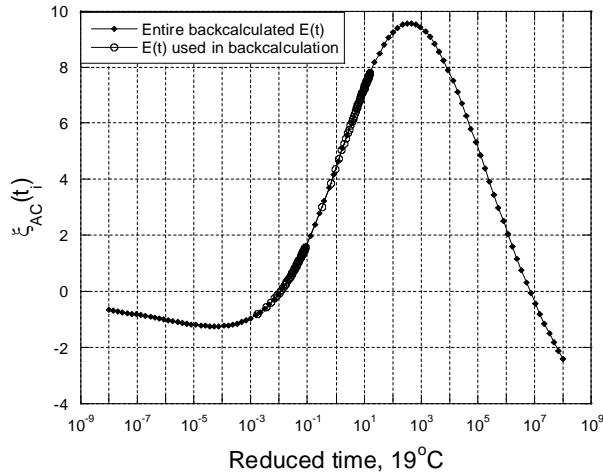
**Figure 43: Variation of  $\xi_{unbound}$  at different FWD temperature sets using modified sigmoidal variable.**



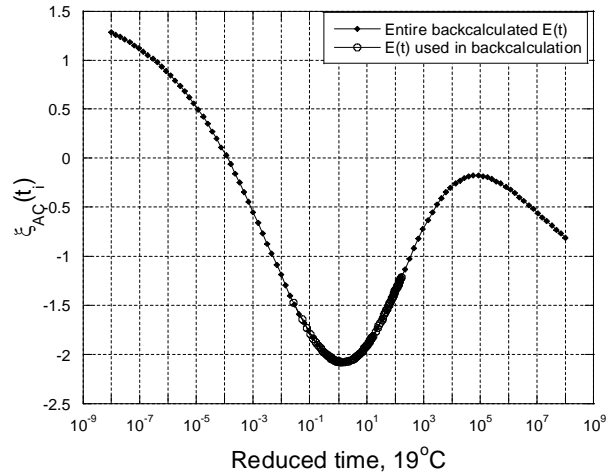
a. Backcalculated E(t) curve using GA (at temperature {10, 30}°C)



c. Backcalculated E(t) curve using GA (at temperature {20, 30, 40}°C)



b. Variation of error,  $\xi_{AC}(t_i)$ : (result at temperature {10, 30}°C)



d. Variation of error,  $\xi_{AC}(t_i)$ : (result at temperature {20, 30, 40}°C)

**Figure 44: Backcalculation results obtained using modified sigmoid variables**

#### 4.2.4 Backcalculation of Viscoelastic Properties using Various Asphalt Mixtures

In the previous sections, analyses were performed using only a single mix. In order to verify the conclusions made in the previous sections regarding the optimum range of temperatures of FWD testing, backcalculations have been performed on 9 typical mixtures. Actual viscoelastic properties: relaxation modulus and shift factors of the selected mixtures are shown in Figure 45. Comparison of average error in the backcalculated relaxation modulus

function calculated over four time ranges: (a)  $10^{-5}$  to 1 sec (b)  $10^{-5}$  to  $10^2$  sec and (c)  $10^{-5}$  to  $10^3$  sec are shown in Figure 46. It can be seen from the figure that, for all the mixes, relaxation modulus curve can be predicted close to less than 15% over a range of relaxation time less than  $10^{+3}$  seconds. Furthermore, it can be seen that, as suggested, the backcalculated relaxation modulus prediction provides a good match over an approximate temperature range of  $10^{\circ}\text{C}$  to  $30^{\circ}\text{C}$ .

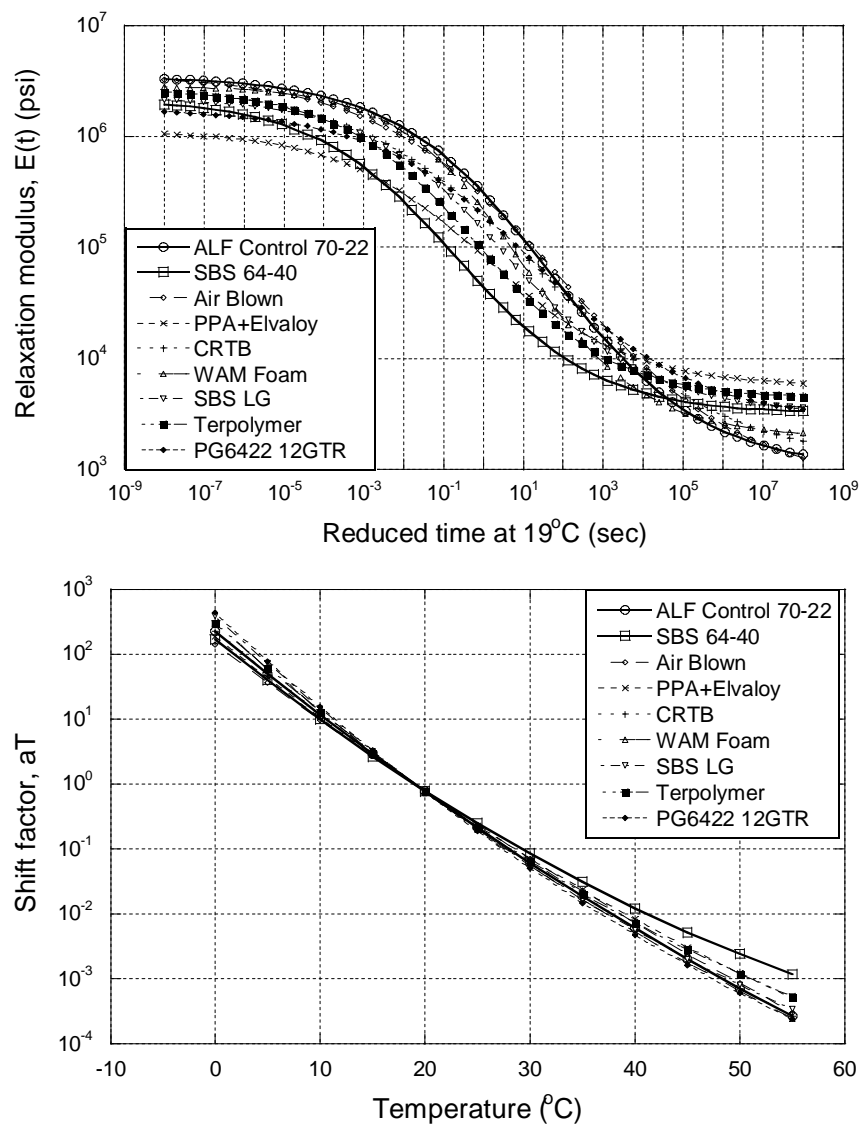


**Figure 45: Viscoelastic properties of field mix in optimal temperature analysis: (a) Relaxation modulus at 19°C, (b) Time-temperature shift factor.**

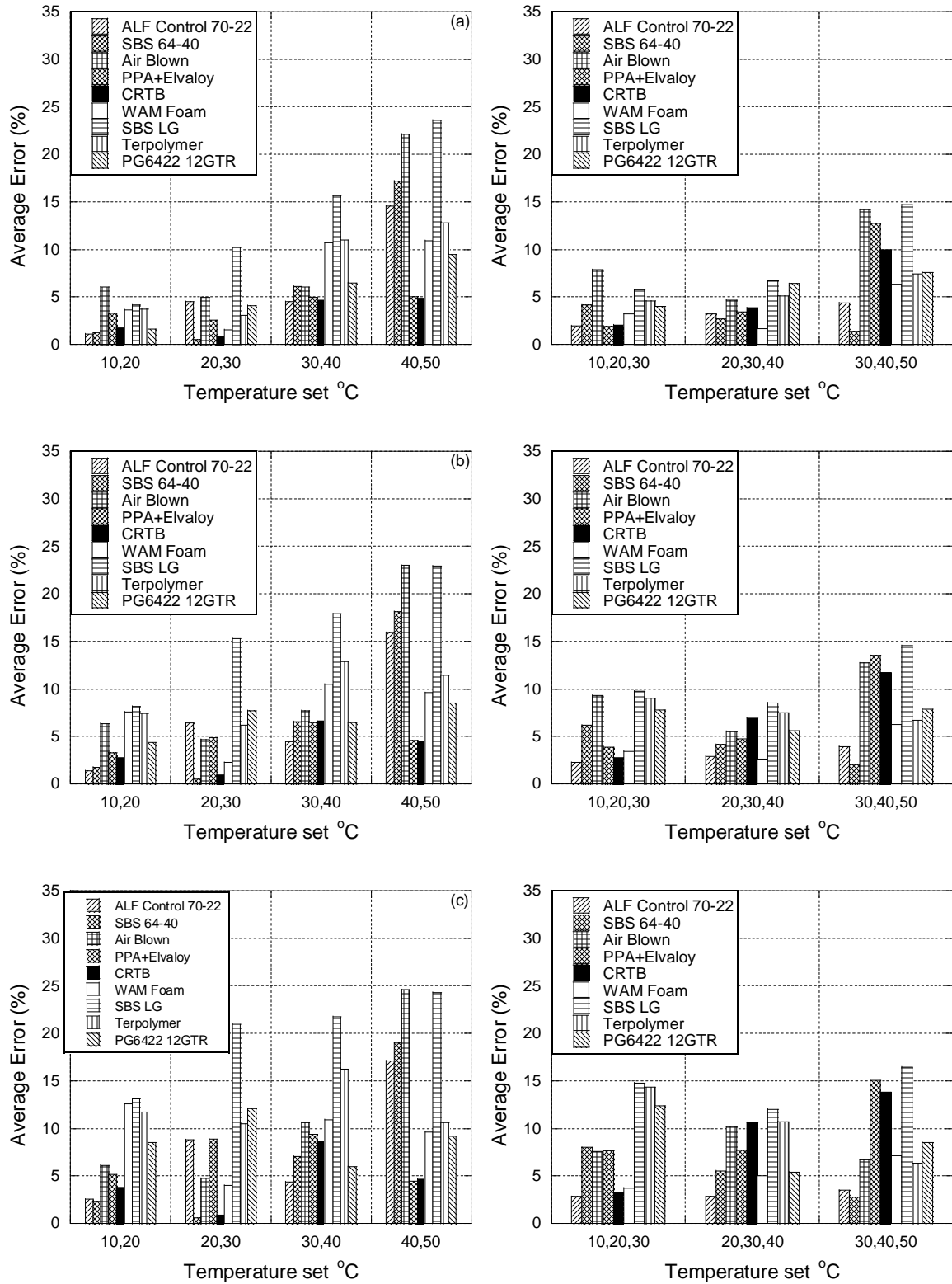


**Figure 46: Variation of error,  $\xi_{AC}(t_i)$ : (a)  $t_i = 10^{-5}$  to  $t_i = 1$  sec used in  $\xi_{AC}(t_i)$ , (b)  $t_i = 10^{-5}$  to  $t_i = 10^{+2}$  sec used in  $\xi_{AC}(t_i)$  and (c)  $t_i = 10^{-5}$  to  $t_i = 10^{+3}$  sec used in  $\xi_{AC}(t_i)$  computation.**

### **4.3 Backcalculation of Relaxation Modulus Master Curve using a Single FWD Test and Known Pavement Temperature Profile**

The uneven temperature profile existing across the thickness of the asphaltic layer during a single FWD drop can theoretically be used to backcalculate the  $E(t)$  master curve and the shift factor coefficients ( $a_T(T)$ ). The AC layer may be divided into several sublayers of same viscoelastic properties, with different temperature levels. This process has been further illustrated in Figure 47. The figure shows a schematic example of steps involved in the evaluation of a candid parent solution (refer to step two “Fitness evaluation and selection” in Figure 28). The figure shows simulation of a single FWD ran under a temperature profile  $\{T_1, T_2 \text{ and } T_3\}$  such that  $T_3 > T_2 > T_1$ . The response is expected to be a resultant of AC behavior from all the three temperatures (which would corresponds to three different reduce time in the master curve). Two different approaches of backcalculation have been discussed in the present section. In the first approach all the unknown variables (sigmoid coefficients, shift factor coefficients and unbound modulus) in the forward algorithm were varied during backcalculation. Whereas in the second approach, a two-staged backcalculation procedure was adopted. The two-stage method involved elastic backcalculation in the first stage (unbound modulus assuming elastic AC layer) followed by viscoelastic backcalculation in the second (sigmoid and shift factor coefficients). Both the approaches were explored in the present study.

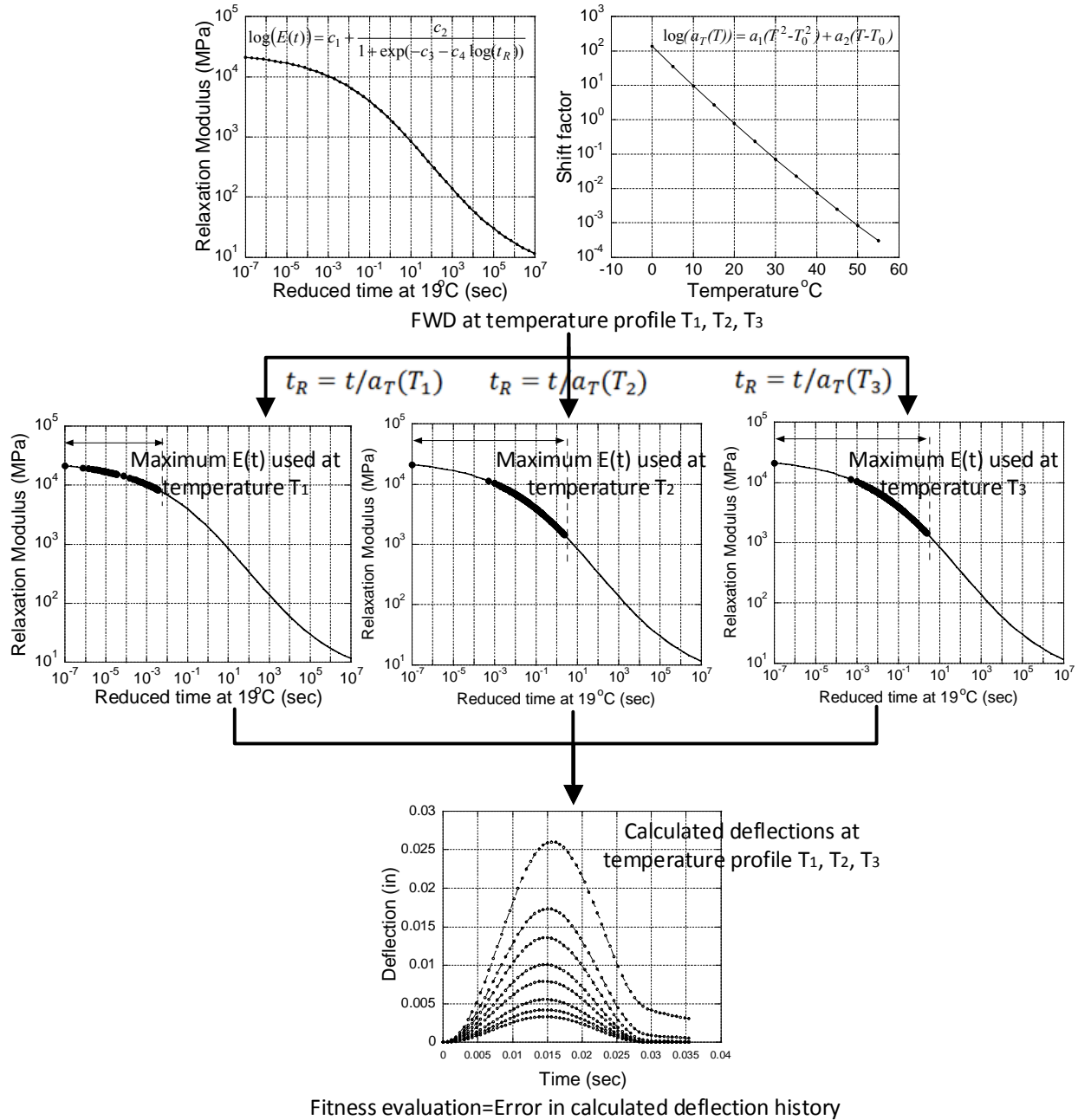


**Figure 47: Schematic of fitness evaluation in BACKLAVA**

#### 4.3.1 Linear Viscoelastic Backcalculation using Single Stage Method

As discussed earlier, total six coefficients are needed to represent the relaxation properties of the AC layer, including the temperature dependency. The backcalculation procedure used was same as used in the previous section (BACKLAVA), except the forward



analysis was replaced by LAVAP, which can consider varying temperature along the depth of the AC layer. Subsequently the backcalculation algorithm was referred as BACKLAVAP. For executing the GA, lower and upper limits of  $c_i$  and  $a_i$ , (sigmoid and shift factor coefficients) and other specifications were retained the same.

As a first step, the backcalculation algorithm was validated with a synthetic FWD deflection history, under two different temperature profiles. The data were generated using LAVAP, and then used in BACKLAVAP for backcalculation of  $E(t)$ . The AC layer was divided into three equal sublayers with three different temperatures. Pavement section, properties and temperature used in the forward analysis were as shown in Table 12.

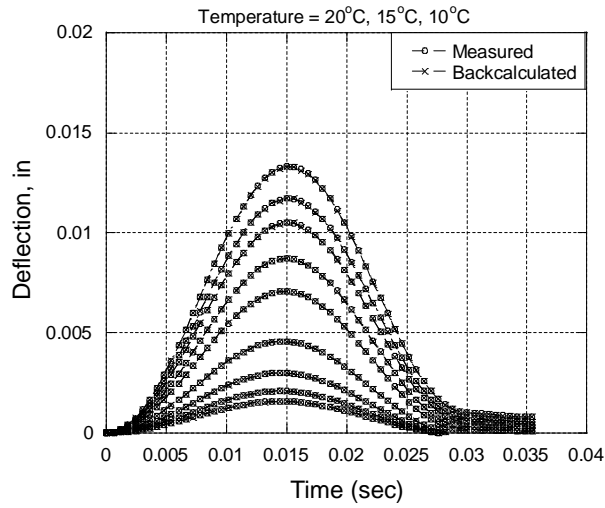
**Table 12: Details of the pavement properties used in single FWD test backcalculation at known temperature profile**

Property		Asphalt Concrete Layer			Granular Base	Subgrade
		Sublayer 1	Sublayer 2	Sublayer 3		
Thickness		51 mm	51 mm	51 mm	508 mm	Semi-inf
Temperature	Case 1	20 °C	15 °C	10 °C	N/A	N/A
	Case 2	30 °C	25 °C	20 °C	N/A	N/A
Poisson's Ratio		0.35			0.4	0.45
Relaxation Modulus		E(t) Coefficients ( $c_1, c_2, c_3, c_4$ ) <i>Backcalculated</i>			<i>Backcalculated</i>	<i>Backcalculated</i>
Time-Temperature Shifting Coefficients		$(a_1, a_2)$ <i>Backcalculated</i>			N/A	N/A
Sensor spacing from the center of load (inches): 0, 8, 12, 18, 24, 36, 48, 60						

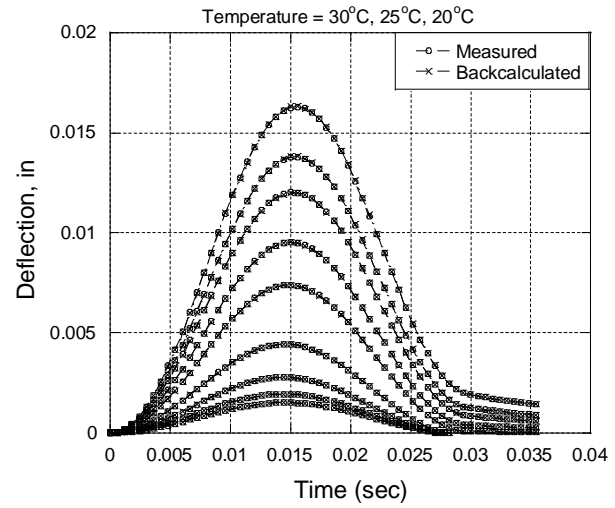
For the case of backcalculation using temperature profile, the GA parameters, namely population size and generation numbers were again selected after several trials of combinations. It was observed that at population size of 300, improvement in the best solution was marginal after 12 to 15 generations, and the population converged to the best solution at around 45 generations. Similarly for population size of 400, improvement in the best solution was marginal after 10 to 15 generations. Figure 48 shows the backcalculation results at the temperature sets

given in Table 12, where a good match is visible. Error in the backcalculated  $E(t)$  was quantified relative to the actual  $E(t)$  using  $\xi_{AC}(t_i)$  given in Equation (56). The  $\xi_{AC}(t_i)$  calculation was performed over a reduced time interval from  $10^{-8}$  to  $10^{+8}$  seconds. Then, the average error ( $\xi_{AC}^{avg}$ ) was computed using Equation (57). The average error level for the first temperature profile was found to be 5.2% and for the second: 4.4%.

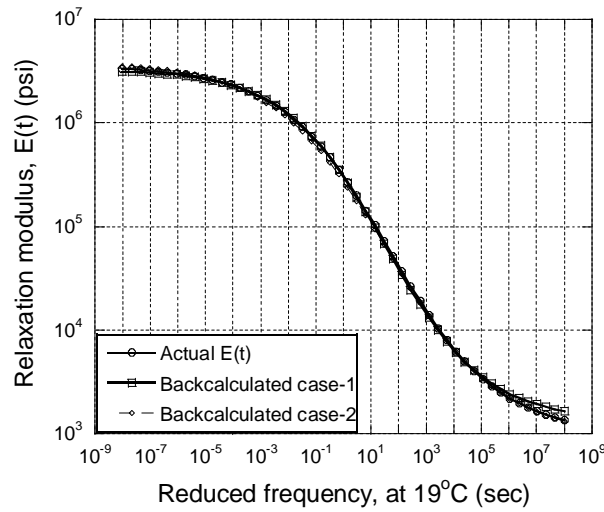
In order to further investigate the effect of magnitude of the pavement temperature profile on backcalculation of  $E(t)$  master curve, synthetic FWD deflection histories were generated. The synthetic data was then used in backcalculation. The structure was divided into three layers with different temperatures, and  $E(t)$  was backcalculated using these data. The pavement section properties used in the study were same as shown in Table 12. Backcalculation was performed assuming the temperature of the top, middle and bottom sublayers of the asphalt layer as  $\{20, 15, 10\}^{\circ}\text{C}$ ,  $\{30, 25, 20\}^{\circ}\text{C}$ ,  $\{40, 35, 30\}^{\circ}\text{C}$  and  $\{50, 45, 40\}^{\circ}\text{C}$ . It was again observed that the problem converged well with 300 GA populations at 45 GA generations. Backcalculated  $E(t)$  and deflection histories for temperature profile  $\{20, 15, 10\}^{\circ}\text{C}$  and  $\{30, 25, 20\}^{\circ}\text{C}$  are shown in Figure 48. The results shown in Figure 49 did exhibit some trend, suggesting that there is a good potential for backcalculation of  $E(t)$  using a single FWD response for the lower temperature ranges, assuming that the temperature profile of the pavement is known.



(a) Case 1 deflection history



(b) Case 2 deflection history



(c) Relaxation modulus

**Figure 48: Comparison of actual and backcalculated values in backcalculation using temperature profile.**

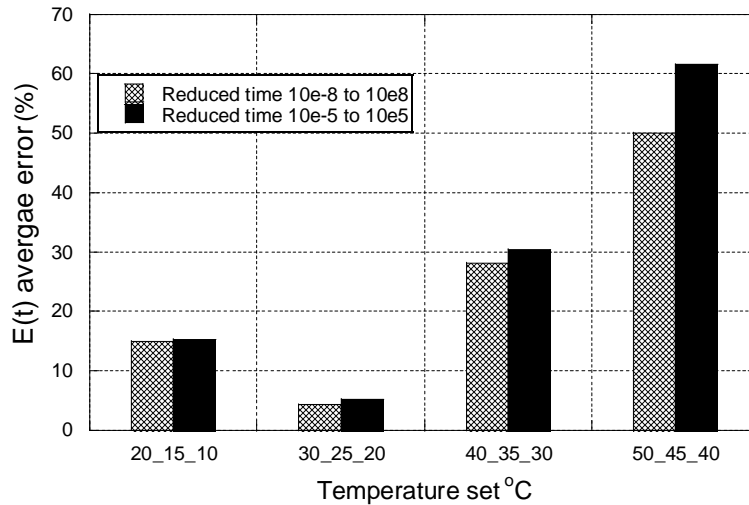


**Figure 49: Error in backcalculated E(t) curve for a three-temperature profile**

#### ***4.3.2 Backcalculation of the viscoelastic Properties of the LTPP Sections using a Single FWD Test with Known Temperature Profile***

The BACKLAVAP algorithm was next used with field data to backcalculate the viscoelastic properties of three LTPP sections. The selection of the sites was done based on the following rules: (a) Section comprising of three layers with only one AC layer, (b) total number of constructions of the section to be one, (c) SPS section type (experiment number 1 or 8), (d) flexible pavement and (e) presence of dynamics.

It was observed that the displacement readings obtained from the LTPP sections at all the sensors (including the sensor under the load), showed time delay with respect to loading. For an ideal multilayer elastic pavement, displacement peaks in all the sensors will be perfectly aligned with load peak. Whereas for a viscoelastic multilayer pavement system, displacement peaks are expected to be slightly misaligned due to viscoelasticity. However, in the measured FWD data the displacement peaks are completely staggered. In the absence of measurement error, this misaligned displacement peak is mainly due to dynamics. Typically this delay in displacement peaks increases with increase in the sensor location distance. It was assumed that the lag in

displacement can be removed by shifting of displacement curves assuming first non-zero value as the initial starting point of the displacement curves. The sections were checked for presence of time delay using the following procedure:

- 1) Perform elastic backcalculation to obtain an approximate estimate of unbound layers modulus values.
- 2) Perform forward calculation using creep converted  $E(t)$  and unbound modulus values obtained in step 1.
- 3) Shift the measured and calculated deflection histories assuming first non-zero value as the initial starting point.
- 4) If the peaks of the shifted curves do not reach at the same time then eliminate the section from the analysis.

Figure 50 shows misaligned displacement peaks after shifting the displacement curves in LTPP section 06A805. This misalignment after the shifting could be because of the following reasons:

- Measurement error.
- Error in  $D(t)$  measured values.
- Presence of significant dynamics.
- Erroneous temperature measurement in field.

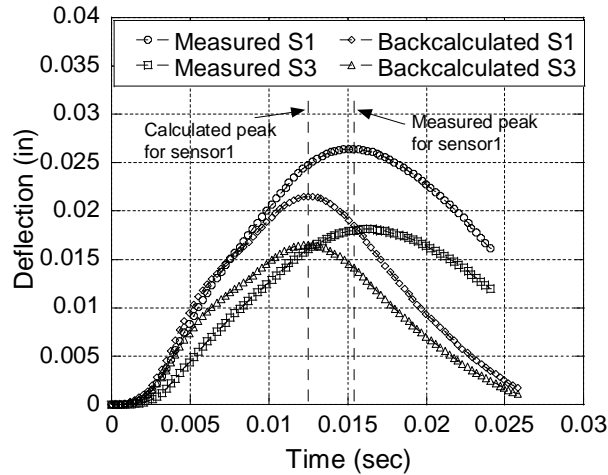


**Figure 50: Time lag in LTPP section 06A805 (shifted based on constant displacement)**

Table 13 and Table 14 contain general and structural information of the selected LTPP site. As shown in Table 14, section 010101 has total four layers which include two AC layers. However, since the  $D(t)$  of the two AC layers reported in the LTPP database are very close, the section was included in the list, assuming the two layers as a single AC layer in the analysis. However, it is not clear from the LTPP database whether the  $D(t)$  was measured before or after the constructions were done.

**Table 13: List of LTPP sections used in the analysis**

State	Section	Year of construction	Total no. of constructions	Test date	Section type	Experiment no.
1	0101	4/30/1991	1	03/11/1993	SPS	1
34	0802	1/1/1993	1	02/05/1997	SPS	8
46	0804	1/1/1992	1	06/18/1993	SPS	8

In the LTPP program, each section is tested according to a specific FWD testing plan, which consists of one or more test passes. Both SPS 1 and SPS 8 are tested along two test passes (test pass 1 and test pass 3) using test plan 4 in LTPP. Test pass 1 data includes FWD testing performed along the midlane (ML) whereas test pass 2 data includes FWD testing performed along outer wheel (OW) path. Since testing along the midlane test pass represent the

axisymmetric assumption better, it was used here in the analysis. In LTPP testing protocol, temperature gradient measurements are taken every 30 min, plus or minus 10 minutes. The necessary temperature profile data was obtained by interpolating the temperature measured during the FWD testing. The AC layer was divided into three equal sublayers and a constant temperature for each sublayer has been estimated.

**Table 14: Structural properties of the LTPP sections used in the analysis**

State	Section	Total no. of layers	No. of AC layers	AC layer thickness	Base layer thickness
1	0101	4	2	AC1=1.2, AC2=6.2	7.9
34	0802	3	1	6.7	11.6
46	0804	3	1	6.9	12

The FWD deflection data in the selected LTPP sections showed no or minimal waviness at the end of the load pulse, which indicated that there was no shallow stiff layer. The presence of a stiff layer was further evaluated using a graphical method suggested by Ullidtz (1988). The method involves plotting peak deflections obtained from FWD testing versus the reciprocal of the corresponding sensor location (measured from the center of loading) (Appea, 2003). Depths of stiff layer in each LTPP section estimated using Ullidtz’s method is shown in Table 15. It should be noted that negative depth to stiff layer is interpreted as absence of stiff layer in the method. The results indicate that stiff layers are generally deeper than 18 ft. It was suggested by Lei (2011) that if the stiff layer is below 18ft, effect of dynamics is not observed on the surface deflections.

Section properties used for elastic and viscoelastic backcalculations were the same (see Table 13) except that the modulus of the AC layer in the elastic backcalculation was assumed constant (modulus unknown). For elastic backcalculation, an in-house genetic algorithm was

developed. The Poisson's ratio for AC, granular base and subgrade layers were assumed to be 0.3, 0.4 and 0.45, respectively.

**Table 15: Depths of stiff layer in each LTPP section estimated using Ullidtz's method**

State	Section	Depths of stiff layer from surface (ft)
1	0101	25.13 ft
34	0802	185.61
46	0804	78.58

As noted above, the results obtained from elastic backcalculation were used to define bounds for base and subgrade modulus in BACKLAVAP. The elastic backcalculation results are presented in Table 16. The static backcalculated base modulus values varied between 16157 psi and 47202 psi, and the subgrade modulus values varied between 15789 psi and 36473 psi. Next, the viscoelastic backcalculation was performed. The backcalculated unbound layer moduli for the sections obtained from viscoelastic backcalculation are presented in Table 17. For the viscoelastic backcalculation, the GA algorithm in BACKLAVAP utilized 300 populations in each of the 15 generations.

**Table 16: Elastic backcalculation results for LTPP unbound layers**

State	Section	Test Date	Elastic modulus (psi)	
			E <sub>base</sub>	E <sub>subgrade</sub>
1	0101	3/11/1993	16157	35127
34	0802	09/08/1993	47202	36473
46	0804	6/18/1993	20877	17547

As shown in Table 17, the viscoelastic backcalculated base modulus values varied between 12117 psi and 39292, and the subgrade modulus values varied between 15299 psi and 34795 psi.



**Table 17: Viscoelastic backcalculation results for LTPP unbound layers**

State	Section	Test Date	Elastic modulus (psi)	
			E <sub>base</sub>	E <sub>subgrade</sub>
1	0101	3/11/1993	12808	34362
34	0802	09/08/1993	39292	34795
46	0804	6/18/1993	15283	16876

In order to validate the backcalculated results, creep compliance data available in the LTPP database were converted into relaxation modulus  $E(t)$ . Creep data were available in tabulated form at three temperatures:  $-10^{\circ}\text{C}$ ,  $5^{\circ}\text{C}$ , and  $25^{\circ}\text{C}$ , and seven different times: 1s, 2s, 5s, 10s, 20s, 50s and 100s. Assuming classical power law function for the creep compliance (Equation (18)), the available data was fitted separately to each temperature. The associated relaxation modulus was then obtained using the mathematically exact formula given in Equation (19) (Kim, 2009). Finally, for comparison, dynamic modulus master curve was calculated from the relaxation modulus via interconversion (Kutay et al., 2011). For further verification, estimated dynamic modulus obtained from Artificial Neural Network (ANN) based model ANNACAP is also compared. The ANNACAP predictive model developed under FHWA long term pavement program research (Kim et al., 2011) uses artificial neural network based five different models to predict dynamic modulus and time-temperature shift factor. Based on the inputs used each model is a separately trained neural network. In the present study the estimated dynamic modulus master curve and time-temperature shift factors obtained from ANNACAP are based on MR model in ANNACAP. From the results it was found that the dynamic modulus curves estimated using ANNACAP model, especially at higher frequencies, agree well with the dynamic modulus curves obtained through interconverted creep data. However, although the dynamic modulus master curve predicted by ANNACAP matched well at the higher frequencies, it typically predicted higher values at reduced frequencies less than  $10^{-2}$  Hz.

The section property and interpolated temperature profile for LTPP section 010101 is shown in Figure 51. The section was first evaluated to assess presence of any time delay. For this the  $E(t)$  obtained from  $D(t)$  and the unbound modulus values obtained from elastic backcalculation (Table 16) were used to calculate deflections. The forward calculated deflection curves were then shifted assuming first non-zero value as the initial starting point. Assuming that the  $E(t)$  obtained from  $D(t)$  and the elastic backcalculated modulus values approximately represent the AC and the unbound layer properties, the peaks of the measured and the calculated curves are expected to reach at the same time. The measured and calculated deflection histories are shown in Figure 52. The curves were found to reach peak at the same time and hence the section was chosen for further backcalculation analysis. Further it also indicates that the  $E(t)$  obtained from  $D(t)$  approximates the viscoelastic properties of the AC layer. As shown in Figure 53a, for section 010101, the backcalculated relaxation modulus master curve and the creep converted relaxation modulus matched well till  $10^2$  seconds. However, the curves showed disagreement for time greater than  $10^2$  seconds. The backcalculated time-temperature shift factors were compared with creep and ANNACAP computed results in Figure 53b. It can be seen from the figure that the backcalculated time-temperature shift factor functions showed a good match over the entire temperature range of  $0^\circ\text{C}$  to  $50^\circ\text{C}$ .

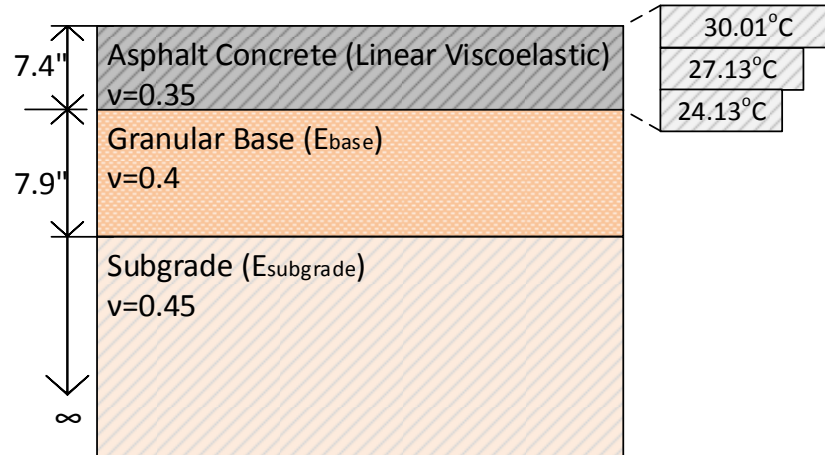


**Figure 51: LTPP section 01-0101 cross section and temperature profile in AC layer**

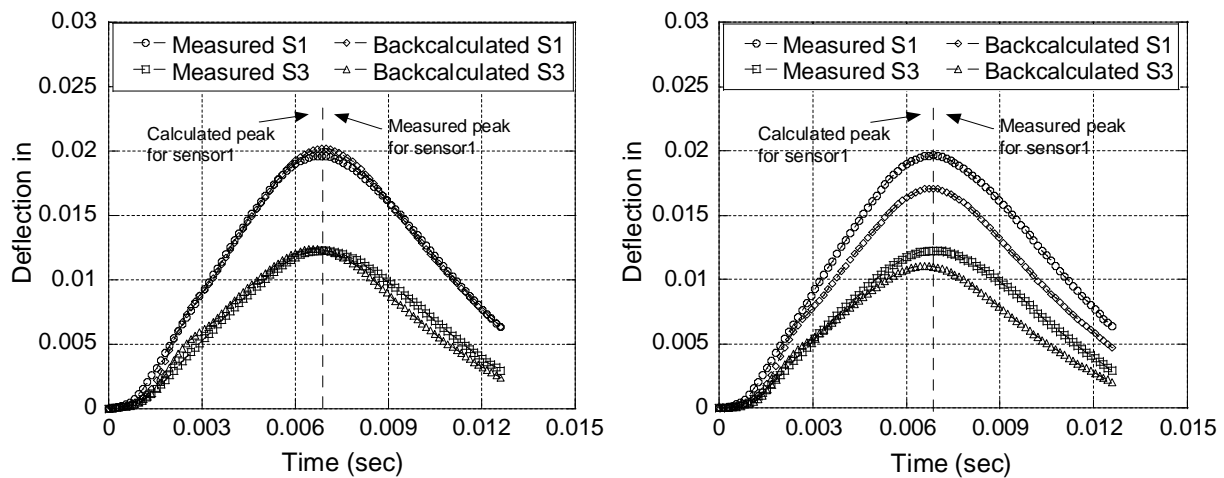
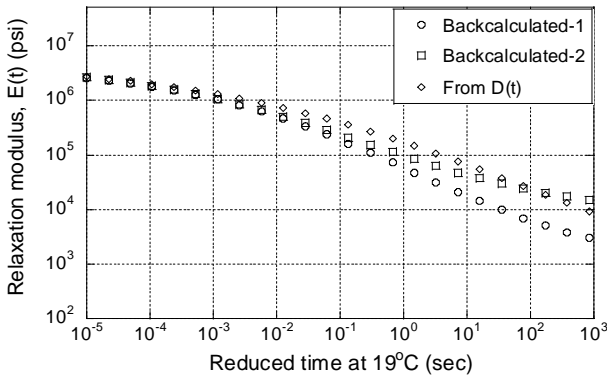
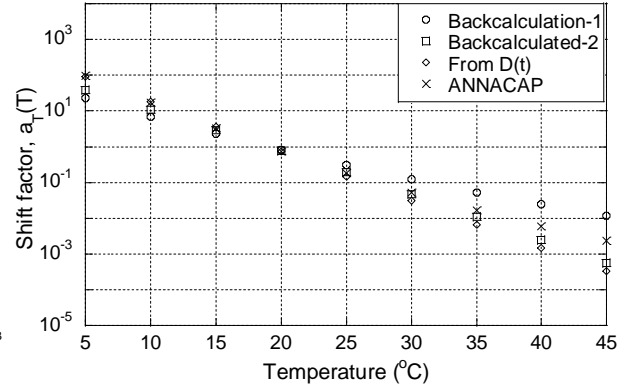


**Figure 52: Comparison of measured and forward calculated deflection histories for section 010101 (a) Viscoelastic backcalculation (b) Forward calculated using  $E(t)$  obtained from LTPP measured  $D(t)$  and elastic backcalculated modulus values.**

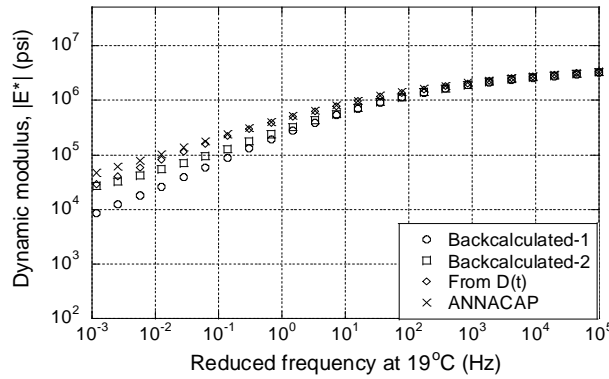
As shown in Figure 53c, backcalculated, creep converted and ANNACAP dynamic modulus curves matched well over frequencies greater than  $10^{-3}$  Hz. A better agreement was observed between ANNACAP and backcalculated results at frequencies less than  $10^{-3}$  Hz.



(a) Relaxation modulus



(b) Shift factor



(c) Dynamic modulus

**Figure 53: Comparison of measured and backcalculated  $E(t)$ ,  $a_T(T)$  and  $|E^*|$  at section 010101.**

The section property and interpolated temperature profile for LTPP section 340802 is shown in Figure 54. The section was first evaluated to assess presence of any time delay. For this the  $E(t)$  obtained from  $D(t)$  and the unbound modulus values obtained from elastic backcalculation (Table 16) were used to calculate deflections. The forward calculated deflection curves were then shifted assuming first non-zero value as the initial starting point. Assuming that the  $E(t)$  obtained from  $D(t)$  and the elastic backcalculated modulus values approximately represent the AC and the unbound layer properties, the peaks of the measured and the calculated curves are expected to reach at the same time. The measured and calculated deflection histories are shown in Figure 55. The curves were found to reach peak at the same time and hence the

section was chosen for further backcalculation analysis. Further it also indicates that the  $E(t)$  obtained from  $D(t)$  approximates the viscoelastic properties of the AC layer. Relaxation modulus, time-temperature shift factor and dynamic modulus curves for section 340802 are compared in Figure 56, respectively.

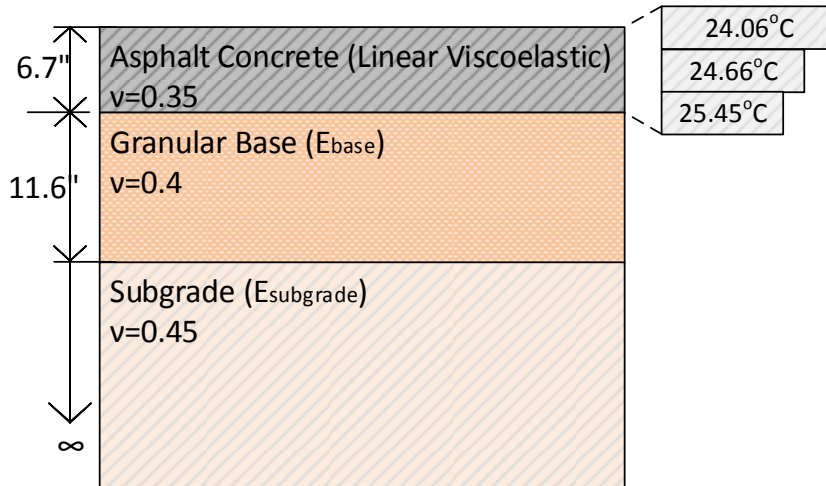


**Figure 54: LTPP section 340802 cross section and temperature profile in AC layer**

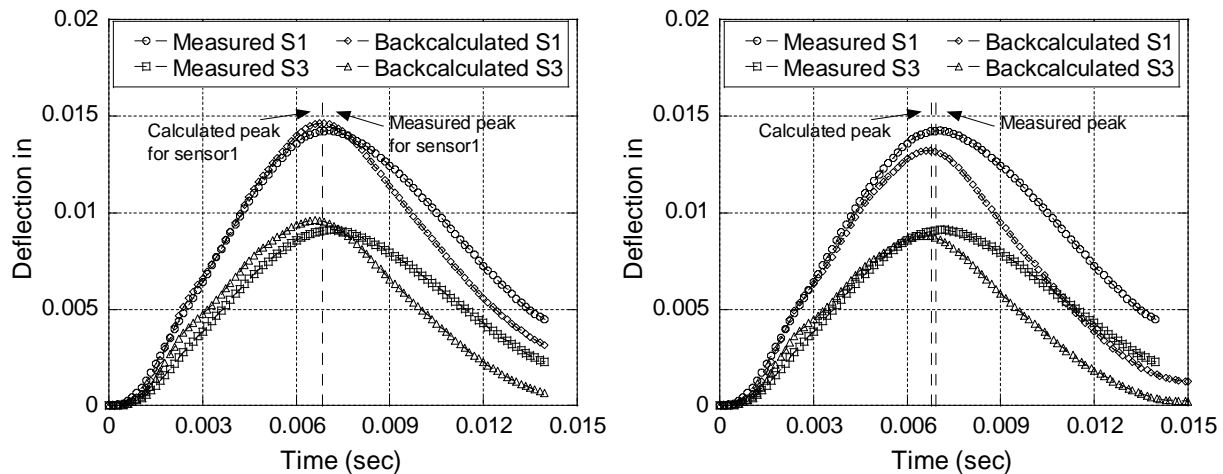
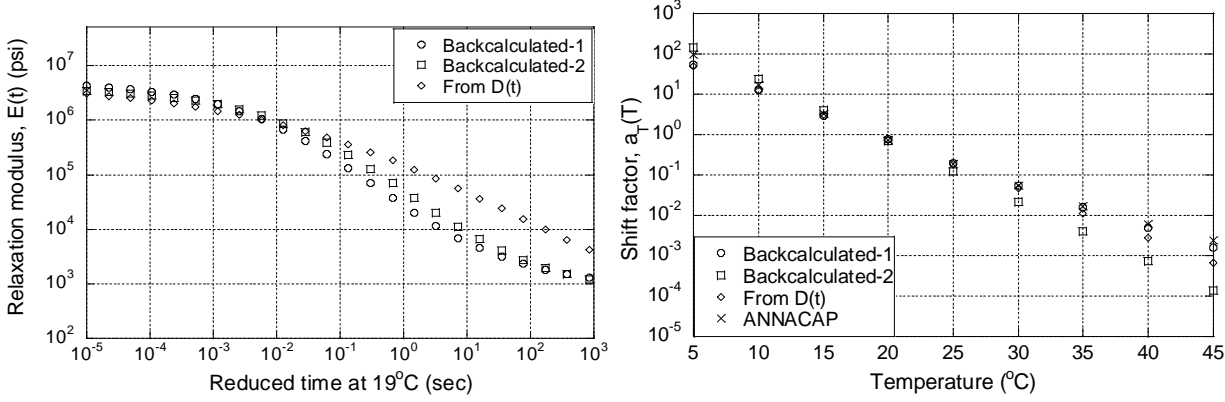


**Figure 55: Comparison of measured and forward calculated deflection histories for section 340802 (a) Viscoelastic backcalculation (b) Forward calculated using  $E(t)$  obtained from LTPP measured  $D(t)$  and elastic backcalculated modulus values.**

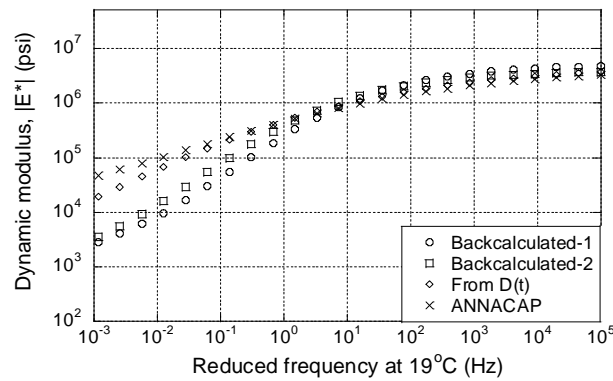
Although, time-temperature shift factor functions showed a good match over the entire temperature range, the backcalculated relaxation modulus and dynamic modulus curves showed

significant deviation at higher reduced time and lower frequencies. Better agreement was found at time less than  $10^{-2}$  seconds and frequencies greater than  $10^0$  Hz.



(a) Relaxation modulus

(b) Shift factor



(c) Dynamic modulus

**Figure 56: Comparison of measured and backcalculated  $E(t)$ ,  $a_T(T)$  and  $|E^*|$  at section 340802.**

The section property and interpolated temperature profile for LTPP section 460804 is shown in Figure 57. The section was first evaluated to assess presence of any time delay. For this the  $E(t)$  obtained from  $D(t)$  and the unbound modulus values obtained from elastic backcalculation (Table 16) were used to calculate deflections. The forward calculated deflection curves were then shifted assuming first non-zero value as the initial starting point. Assuming that the  $E(t)$  obtained from  $D(t)$  and the elastic backcalculated modulus values approximately

represent the unbound layer properties, the peaks of the shifted curves are expected to reach at the same time. The displaced measured and calculated deflection histories are shown in Figure 58. The curves were found to reach peak at the same time and hence the section was chosen for further backcalculation analysis. Further it also indicates that the  $E(t)$  obtained from  $D(t)$  approximates the viscoelastic properties of the AC layer. Relaxation modulus, time-temperature shift factor and dynamic modulus curves for section 460804 are compared in Figure 59a, b and c respectively. The predicted  $a_T(T)$  curve showed good agreement with ANNACAP at temperatures less than  $25^\circ\text{C}$ . However at temperatures greater than  $25^\circ\text{C}$  significant deviation was observed in shift factor which was also reflected in the relaxation modulus and dynamic modulus curves at time greater than  $10^0$  seconds and less than  $10^1$  Hz.

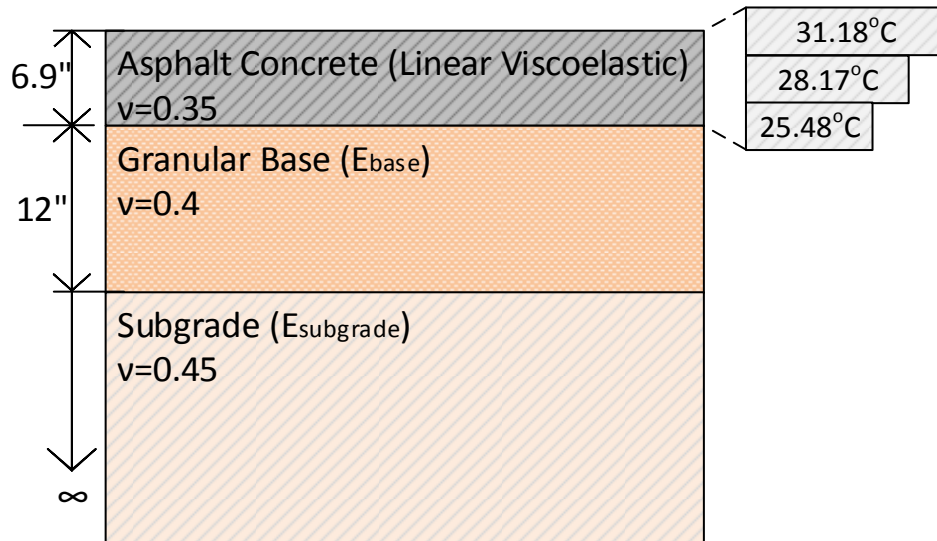


**Figure 57: LTPP section 460804 cross section and temperature profile in AC layer**

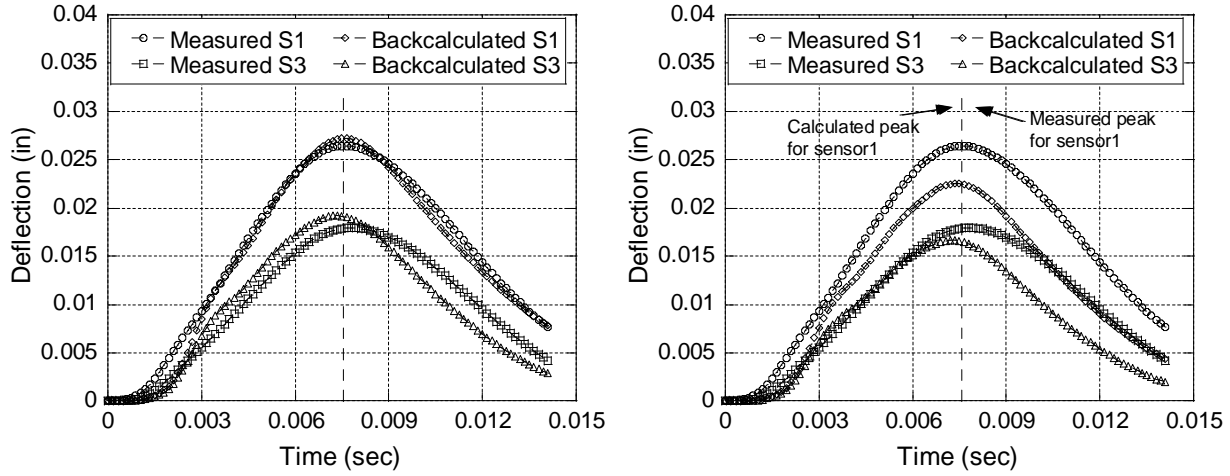
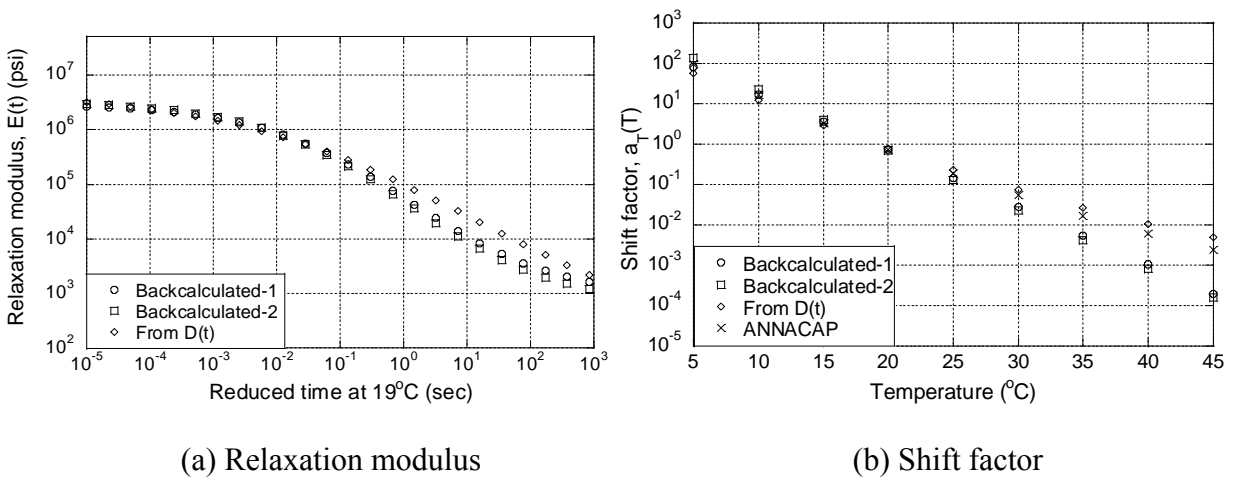
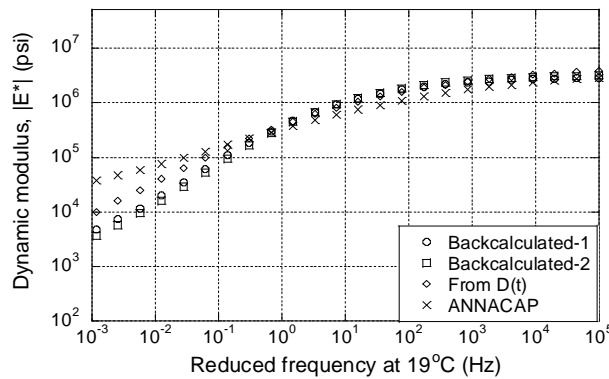


**Figure 58: Comparison of measured and forward calculated deflection histories for section 460804 (a) Viscoelastic backcalculation (b) Forward calculated using  $E(t)$  obtained from LTPP measured  $D(t)$  and elastic backcalculated modulus values.**



(a) Relaxation modulus

(b) Shift factor



(c) Dynamic modulus

**Figure 59: Comparison of measured and backcalculated  $E(t)$ ,  $a_T(T)$  and  $|E^*|$  at section 460804.**



### ***4.3.3 Backcalculation of Linear Viscoelastic Pavement Properties using Two-Stage Method***

In the previous backcalculation process, viscoelastic and unbound properties were calculated at the same step; however in this section a two stage linear viscoelastic backcalculation scheme is presented. The first stage was to perform linear elastic backcalculation of unbound material properties, which was followed by linear viscoelastic backcalculation (using BACKLAVA/BACKLAVAP) of AC layer viscoelastic properties ( $E(t)$  sigmoid coefficients:  $c_1$ ,  $c_2$ ,  $c_3$  and  $c_4$  and shift factor  $a_T(T)$  coefficients  $a_1$  and  $a_2$ ). Details of stage 1 and stage 2 steps are presented in the following sections.

Stage-1, Elastic backcalculation for Unbound Layer Properties: It is important to verify that the elastic backcalculation (Stage-1) gives unbound granular modulus values close to the actual values. If this is verified, the backcalculated  $E_{\text{unbound}}$  values can be fixed in viscoelastic backcalculation (Stage-2) and only the 6 unknowns of AC layer can be backcalculated. Known and unknown variables in the first and second stages of backcalculation are listed in Table 18. In the first stage, elastic backcalculation was performed assuming the AC layer as linear elastic. In the second stage, viscoelastic backcalculation was performed keeping the unbound granular layer modulus values obtained in the first stage fixed.

In order to perform the verification, first, various synthetic deflection time histories were obtained by running LAVA on the structure shown in Table 19 at various temperature profiles (also shown in Table 19). These synthetic deflections were used in “Stage 1 – Elastic Backcalculation”, which computed  $E_{\text{unbound}}$  values. Then these backcalculated  $E_{\text{unbound}}$  values were compared to the original  $E_{\text{unbound}}$  values used in the original layered viscoelastic forward computation.

**Table 18: Variables in two stage linear viscoelastic backcalculation analysis**

<b>Stage 1: Elastic backcalculation</b>	
<b>Known parameters</b>	<b>Unknown (backcalculated) parameters</b>
Thickness & Poisson’s ratio of each layer	$E_{ac}$ , elastic modulus of AC layer
FWD parameters (contact radius, pressure, locations of the sensors, etc.)	$E_{unbound (i)}$ , unbound layer moduli, $i=1 \dots N_L$ , $N_L$ = number of unbound layers.
<b>Stage 2: Viscoelastic backcalculation</b>	
<b>Known parameters</b>	<b>Unknown (backcalculated) parameters</b>
Thickness & Poisson’s ratio of each layer and FWD parameters	$E(t)$ sigmoid coefficients: $c_1, c_2, c_3$ and $c_4$
$E_{unbound (i)}$ , unbound layer moduli backcalculated in stage 1	Shift factor $a_T(T)$ coefficients $a_1$ and $a_2$

**Table 19: Pavement properties in two stage linear viscoelastic backcalculation analysis**

<b>Property</b>	
Thickness (AC followed by granular layers)	6, 20, inf (in)
Poisson ratio {layer 1,2,3...}	0.35, 0.3, 0.45
$E_{unbound}$ {layer 2,3...}	25560, 11450 (psi)
$E(t)$ sigmoid coefficient {layer 1}	0.841, 3.54, 0.86, -0.515
$a_T(T)$ shift factor polynomial coefficients {layer 1}	4.42E-04, -1.32E-01
Total number of sensors	8
Sensor spacing from the center of load (inches)	0, 8, 12, 18, 24, 36, 48, 60
AC layer temperature profile {T1-T2}: {10-0}, {15-10}, {20-10}, {20-15}, {25-20}, {30-20}, {30-25}, {35-30}, {15-10-5}, {20-15-10}, {25-20-15}, {30-25-20}, {35-30-25}, {40-35-30}	

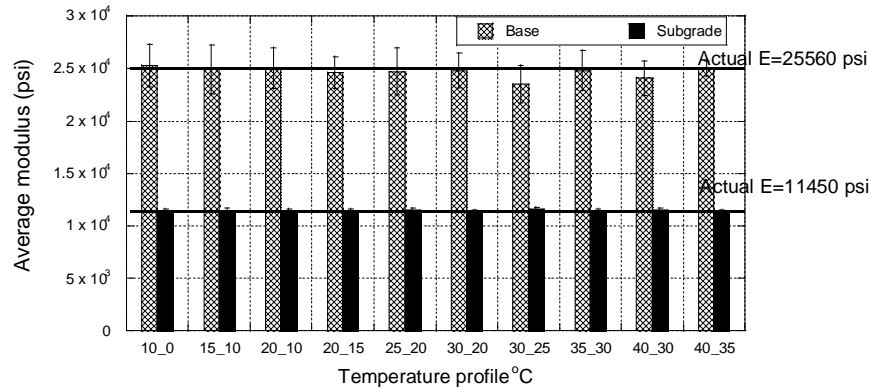


**Figure 60: Elastic backcalculation of two-step temperature profile FWD data, assuming AC as a single layer in two stage backcalculation**

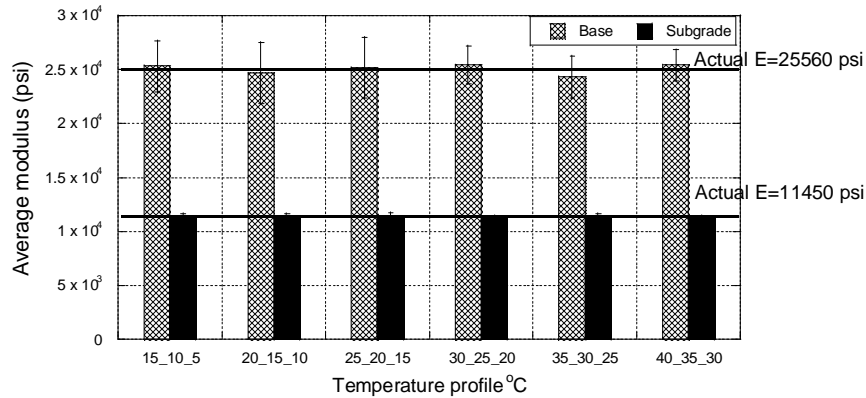


**Figure 61: Elastic backcalculation of three-step temperature profile FWD data, assuming AC as a single layer in two stage backcalculation**

The analysis results shown in Figure 60 and Figure 61 were based on elastic backcalculations that assumes a single AC layer. However, in the LAVA forward computations, because of different temperatures with depth, multiple layers of AC (2 layers for Figure 60 and 3 layers for Figure 61 analysis) were used. In order to investigate if selection of number of AC layers on the elastic backcalculation, the computations were repeated assuming the AC layer to be consisting of 2 or 3 independent elastic layers. Average backcalculated base and subgrade modulus values for two-step and three-step temperature profiles are shown in Figure 62 and Figure 63, respectively. Comparing Figure 60 to Figure 62 and Figure 61 to Figure 63, it can be seen that, assuming single or multiple AC layers didn't significantly affect backcalculation of base and subgrade elastic modulus. From these analyses (Figure 60 through Figure 63), it can be concluded that, it is possible to first perform elastic backcalculation (Stage-1) for the unbound layer properties and fix these in Stage-2.

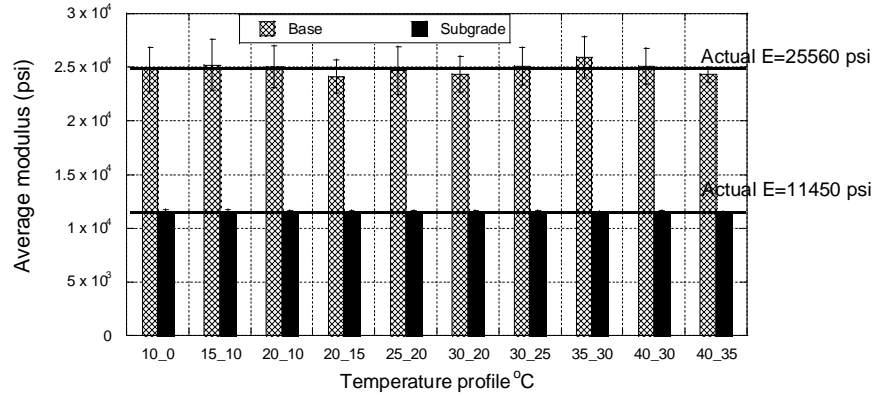


**Figure 62: Elastic backcalculation of two-step temperature profile FWD data, assuming two AC sublayers in two stage backcalculation**

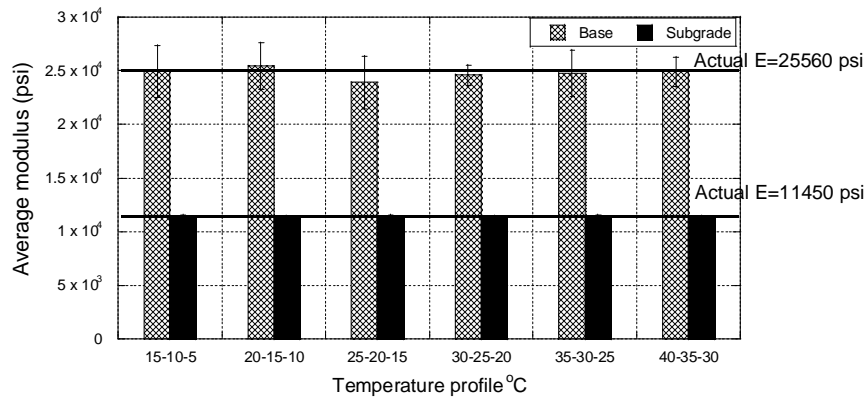


**Figure 63: Elastic backcalculation of three-step temperature profile FWD data, assuming three AC sublayers in two stage backcalculation**

Stage-2, Viscoelastic Backcalculation for  $E(t)$  of AC Layer: After fixing the unbound layer modulus values, the AC layer properties ( $E(t)$  sigmoid coefficients:  $c_1$ ,  $c_2$ ,  $c_3$  and  $c_4$  and shift factor  $a_T(T)$  coefficients  $a_1$  and  $a_2$ ) are backcalculated using viscoelastic backcalculation algorithm (BACKLAVA). It should be noted that for viscoelastic backcalculation, as done earlier, set of FWD test data at different temperature can be used for backcalculation. This is due to the fact that even though the temperatures are different, the characteristic properties of AC layer ( $E(t)$  or  $|E^*|$  master curves) remains the same. In this stage, viscoelastic backcalculation was performed on a set of temperature profiles keeping the actual unbound modulus values constant.

Average error (over reduced times from  $10^{-8}$  to  $10^8$  seconds) in  $E(t)$  master curve, obtained from set of two two-step and two three-step temperature profiles are shown in Figure 64 and Figure 65 respectively. It can be observed from Figure 64 that, for all the cases of presented 2-step temperature profile sets, average error in backcalculated  $E(t)$  is below 10-12% except for FWD test at {30-20}&{40-30}. It can be observed from Figure 65 that, for all the cases of presented for 3-step temperature profile sets, average error in backcalculated  $E(t)$  is below 5.5% except for FWD test at {30-25-20}&{25-20-15}. These results indicate that the 2-stage algorithm works well in backcalculating the  $E(t)$  of AC layer. From Figure 64 and Figure 65,  $E(t)$  errors obtained in 2-stage backcalculation are less when compared to single stage backcalculation (Figure 49). However, it should be noted that results presented in Figure 64 and Figure 65 are from backcalculation using a set of two FWD test data each obtained at different temperature profile, whereas results in Figure 49 are from backcalculation using single FWD data. But, the result does indicate that backcalculation using a set of FWD test data each obtained at different temperature profile may improve the accuracy.

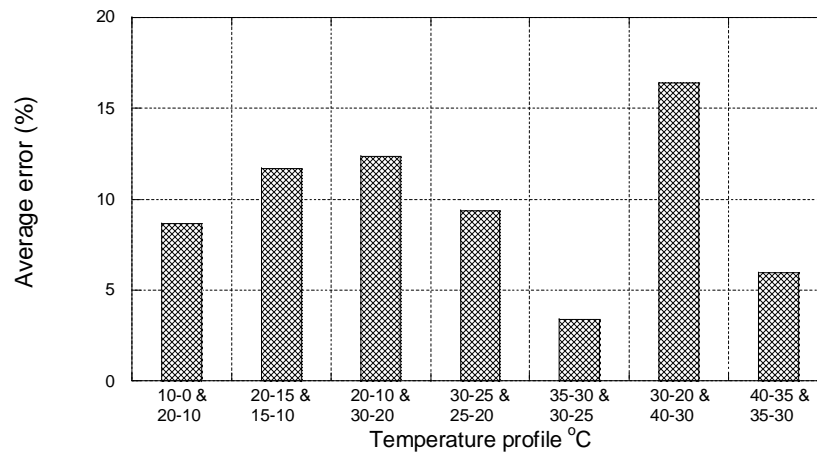


**Figure 64: Error in backcalculated  $E(t)$  curve from two-step temperature profile.**

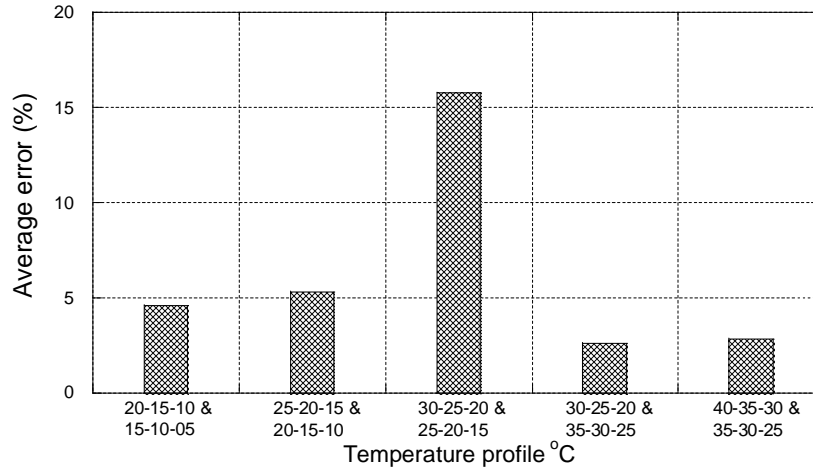


**Figure 65: Error in backcalculated  $E(t)$  curve from three-step temperature profile.**

#### 4.4 Layered Viscoelastic-Nonlinear Backcalculation (BACKLAVAN) Algorithm

##### 4.4.1 Introduction

In the previous section, analyses were performed assuming the unbound layers to be linear elastic. Due to the linear elastic assumption the forward engine in the backcalculation algorithms were computationally efficient. Because of inherent iterative nature of the viscoelastic-nonlinear forward solution (i.e., LAVAN), it can take very long time to backcalculate all the parameters (i.e.,  $c_1, c_2, c_3, c_4, a_1, a_2$  of the AC and  $k_1, k_2, k_3$  of the unbound layer) if all the parameters are varied simultaneously during the backcalculation. Furthermore, like many other complex engineering applications involving multi-variable optimization, backcalculation of pavement properties can also involve multiple local minima solutions. It is well known that even linear elastic backcalculation (considering all the pavement layers to be linear elastic) of pavement possess multiple local solutions, and hence, a unique solution using traditional optimization methods is difficult to obtain.

In this study, optimization tool GA along with a simplex method was utilized together. The GA-based optimization ensures that the solution approaches to a global minima, provided that proper GA parameters are used. GA can iteratively sweep search the entire search domain

(made by the variables), moving towards the global solution by systematically eliminating the local optimal solutions. The main advantage of GA algorithm is that it can avoid local minima and find the global solution; however it can be a relatively slow method. The main advantage of the simplex method is its speed; however, simplex method is influenced by the seed values and susceptible to reaching to a local minimum. A combination of GA and simplex may be a good alternative to reach an accurate solution.

In order to improve the computational efficiency of the backcalculation algorithm, three basic stages are proposed. These three stages optimize the use of GA and simplex methods to improve the speed and accuracy.

Stage-1: Nonlinear elastic backcalculation: The first stage involves nonlinear elastic backcalculation of the unbound granular layer properties (i.e.,  $k_1, k_2, k_3$ ). At this stage, the AC layer is assumed to be elastic and the unbound layers are assumed to be nonlinear. Due to the linear elastic assumption (instead of linear viscoelastic) of AC layer, a quick approximation of unbound layer properties is obtained. It is noted that this step ignores the effects of stress redistribution because of the viscoelasticity of AC layer, thus induces error in backcalculated  $k_1, k_2$  and  $k_3$ . However, this error may not significantly affect the backcalculated  $|E^*|$  master curve (if the ultimate goal is to obtain the  $|E^*|$ ), as illustrated in later parts of the chapter.

Formulation of the optimization model used in the first stage of genetic algorithm is as follows:

$$\xi_1^{GA} = \sum_{k=1}^m \sum_{i,o=1}^n \frac{|(d_i^k)_{max} - (d_o^k)_{max}|}{(d_i^k)_{max}} \quad (60)$$

where  $\xi_1^{GA}$  is the error to be minimized,  $m$  is the number of FWD sensors,  $(d_i^k)_{max}$  is the peak input deflection information obtained from field at sensor  $k$ ,  $(d_o^k)_{max}$  is the peak output (predicted) response at sensor  $k$ ,  $n$  is the total number of drops. In this stage, the following bounds were imposed for each of the unknowns:  $E_{AC}^l \leq E_{AC} \leq E_{AC}^u$ ,  $k_1^l \leq k_1 \leq k_1^u$ ,  $k_2^l \leq k_2 \leq k_2^u$ ,  $k_3^l \leq k_3 \leq k_3^u$ ,  $E_s^l \leq E_s \leq E_s^u$ , where  $E_{AC}$  is elastic AC modulus,  $k_1, k_2, k_3$  are constants shown in Equation 9,  $E_s$  is subgrade modulus, and the superscripts  $l$  and  $u$  represent lower and upper limits. For backcalculation of these six variables, population size of 200 and 15 numbers of generations were used. The default MATLAB values were used for the rest of the GA parameters.

Stage-2, Viscoelastic - nonlinear backcalculation with fixed unbound layer properties: In the second stage, the backcalculated unbound properties (i.e.,  $k_1, k_2, k_3$ ) are fixed, and the layered viscoelastic-nonlinear (LAVAN) forward model is used to backcalculate the linear viscoelastic properties of AC layer (i.e.,  $c_1, c_2, c_3, c_4, a_1, a_2$ ). Fixing the unbound layer properties in the viscoelastic-nonlinear response calculation significantly reduces the computational effort required in the backcalculation algorithm. Formulation of the optimization model used in the second stage of genetic algorithm based inverse analysis is

$$\xi_2^{GA} = \sum_{k=1}^m \sum_{i,o=1}^n \frac{|(d_i^k) - (d_o^k)|}{d_{max}^k} \quad (61)$$

where,  $m$  is the total number of sensors,  $d_i^k$  is the input deflection information obtained from field at sensor  $k$ ,  $d_o^k$  is the output deflection obtained from forward analysis at sensor  $k$ ,  $n$  is the total number of deflection data points recorded by a sensor. In this stage, the following bounds were imposed for each of the unknowns:



$$c_1^l \leq c_1 \leq c_1^u,$$

$$x^l \leq x \leq x^u \quad (x = c_1 + c_2),$$

$$c_3^l \leq c_3 \leq c_3^u, \quad c_4^l \leq c_4 \leq c_4^u,$$

$$a_1^l \leq a_1 \leq a_1^u, \quad a_2^l \leq a_2 \leq a_2^u$$

The superscripts  $l$  and  $u$  represent lower and upper limits and  $c_i$  are the sigmoid coefficients and  $a_i$  are the shift factor polynomial coefficients for the AC layer (see Equations (23) and (25)). The genetic algorithm (GA) results were obtained for population size of 100 and 15 number of generations.



Stage-3, Viscoelastic - nonlinear backcalculation, all parameters varied: In stage three, all the viscoelastic parameters (i.e.,  $c_1, c_2, c_3, c_4, a_1, a_2$ ) of the AC layer as well as the unbound parameters ( $k_1, k_2, k_3$ ) of the unbound layer are treated as unknowns. In this stage, a simplex method is employed. For this purpose, MATLAB's "*fminsearch*" algorithm, which is an unconstrained nonlinear optimization tool, is used (Lagarias 1998). It is well known that solutions obtained using such traditional methods depend on the seed value used in the optimization (Chatti et al., 2014). However, using "*fminsearch*" in the third stage offers three benefits:

- 1) The seed values obtained in stage-1 and stage-2 are generally very close to the actual values;

- 2) As GA in stage-2 has already moved toward the global optimal solution, the third stage improves the precision of the solution, which cannot be achieved using the GA alone, due to the inherent randomness and discreteness involved in the technique;
- 3) It reduces the number of iterations needed in the computationally expensive GA-based stage-2.

A detailed discussion on various hybrid optimization schemes and benefits can be found in Grosan and Abraham (2007) and El-Mihoub et al. (2006). It is worth noting that, in this study, the two-stage optimization may be sufficient, and the stage-3 slightly improves the results. Details of known and unknown properties used during all the stages are shown in Table 20.

**Table 20: Pavement properties and test inputs in staged nonlinear viscoelastic backcalculation.**

Property	Stage-1: Nonlinear elastic	Stage-2: Nonlinear Viscoelastic	Stage-3: Nonlinear Viscoelastic
Thickness (cm)	Known (AC), Known (BASE), inf (SUBGRADE)	Known (AC), Known (BASE), inf (SUBGRADE)	Known (AC), Known (BASE), inf (SUBGRADE)
Poisson ratio	Known (AC), Known (BASE), Known (SUBGRADE)	Known (AC), Known (BASE), Known (SUBGRADE)	Known (AC), Known (BASE), Known (SUBGRADE)
$E_{base}$ (MPa)	Unknowns ( $k_1, k_2, k_3$ ) 	Obtained from Stage-1	Unknowns ( $k_1, k_2, k_3$ )
$E_{subgrade}$ (MPa)	Unknown 	Obtained from Stage-1	Unknowns
$E(t)_{AC}$ (MPa)	Unknown ( $E(t) = \text{Constant}$ )	Unknown (sigmoid coefficient)	Unknown (sigmoid coefficient)
Backcalculation algorithm used	Genetic Algorithm	Genetic Algorithm	Simplex Algorithm
<b>Test Inputs</b>			
Surface loading (kPa)	Known peak stress	Known load history	Known load history
Surface deflection ( $\mu\text{m}$ )	Known peak deflection	Known deflection history	Known deflection history

#### 4.4.2 Verification of the Nonlinear Backcalculation Procedure

The BACKLAVAN algorithm was verified using synthetic deflection histories for two HMA mixes, namely, Control and CRTB (for mix properties refer to Table 22). The synthetic FWD test data (using 35milisecond haversine load) were generated at five test temperatures (10°C, 20°C, 30°C, 40°C and 50°C) for the pavement section shown in Table 22. Stresses at distance  $r=0$  were used in calculating unbound base modulus value for both forward calculation and backcalculation. An FWD test is generally composed of four independent test drops, where each drop corresponds to a different stress level. Typical ranges of stress levels in each drop are shown in Table 21. In this study, four FWD drops at peak stress levels of 379, 552, 689 and 950 kPa were simulated to generate synthetic FWD deflection-time history using LAVAN algorithm. In stage-1 of the BACKLAVAN algorithm, peak stress and deflection values during all the test drops are used as input in nonlinear elastic backcalculation. The AC layer modulus and unbound layer properties ( $k_1, k_2, k_3$ ) backcalculated from synthetic deflection at different temperatures are shown in Figure 66 and Figure 67, respectively. As expected, for both Control and CRTB mixes the backcalculated elastic AC modulus values dropped with increase in temperature. It is noted that the nonlinear elastic backcalculation was performed using an in-house nonlinear elastic backcalculation program developed based on the same iterative procedure used in LAVAN.

**Table 21: Typical FWD test load levels**

Load Level	Allowable range (for 11.81" diameter plate), psi	Used surface load, psi
Drop 1	49 - 60	55
Drop 2	74 - 96	80
Drop 3	99 - 120	110
Drop 4	132 - 161	137.8

**Table 22: Pavement geometric and material properties in two stage nonlinear viscoelastic backcalculation.**

Property	Value used
Thickness (cm)	15 (AC), 25 (Base), (Subgrade)
Poisson ratio ( $\nu$ )	0.35 (AC), 0.4 (Base), 0.4 (Subgrade)
Density ( $\text{kg/m}^3$ )	2082 (AC), 2082 (Base), 2082 (Subgrade)
Nonlinear $E_{\text{base}}$ (MPa)	$K_0=0.6, k_1=25, k_2=0.5, k_3=-0.5$
$E_{\text{subgrade}}$ (MPa)	68.95
AC: $E(t)$ sigmoid coefficient ( $c_i$ ) (MPa)	Control: 1.598, 2.937, -0.272, -0.562 CRTB: 0.895, 3.411, 0.634, -0.428
Shift factor coefficients ( $a_i$ )	Control: 5.74E-04, -1.55E-01 CRTB: 4.42E-04, -1.32E-01
(35 msec) Haversine peak stress (kPa)	Peak stress = 950

As shown, the backcalculated results are close to the actual values but they are generally under predicted by the algorithm.

In stage-2, the backcalculated unbound layer properties from stage-1 were used as known fixed values, and the viscoelastic layer properties of the AC layer were obtained. The forward algorithm used in stage-2 backcalculation and stage-3 backcalculation are same (LAVAN) except that, in stage-2 the nonlinear properties are fixed and not varied whereas in stage-3 all the AC as well as unbound layer properties are varied.

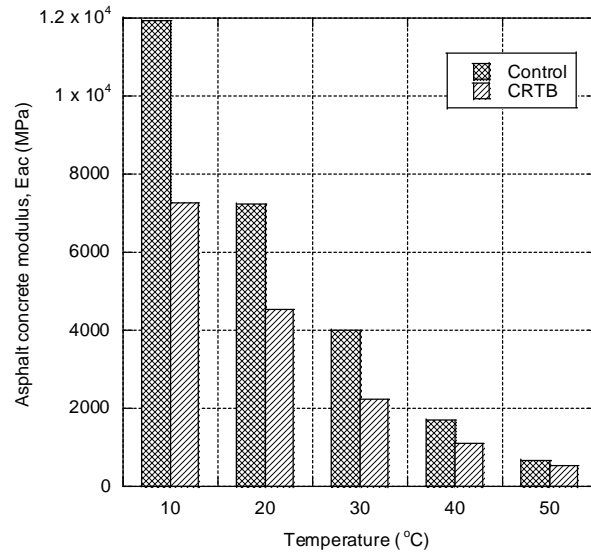


**Figure 66: Nonlinear elastic backcalculated AC modulus (in stage-1) for Control and CRTB Mixes, using FWD data at different test temperatures.**

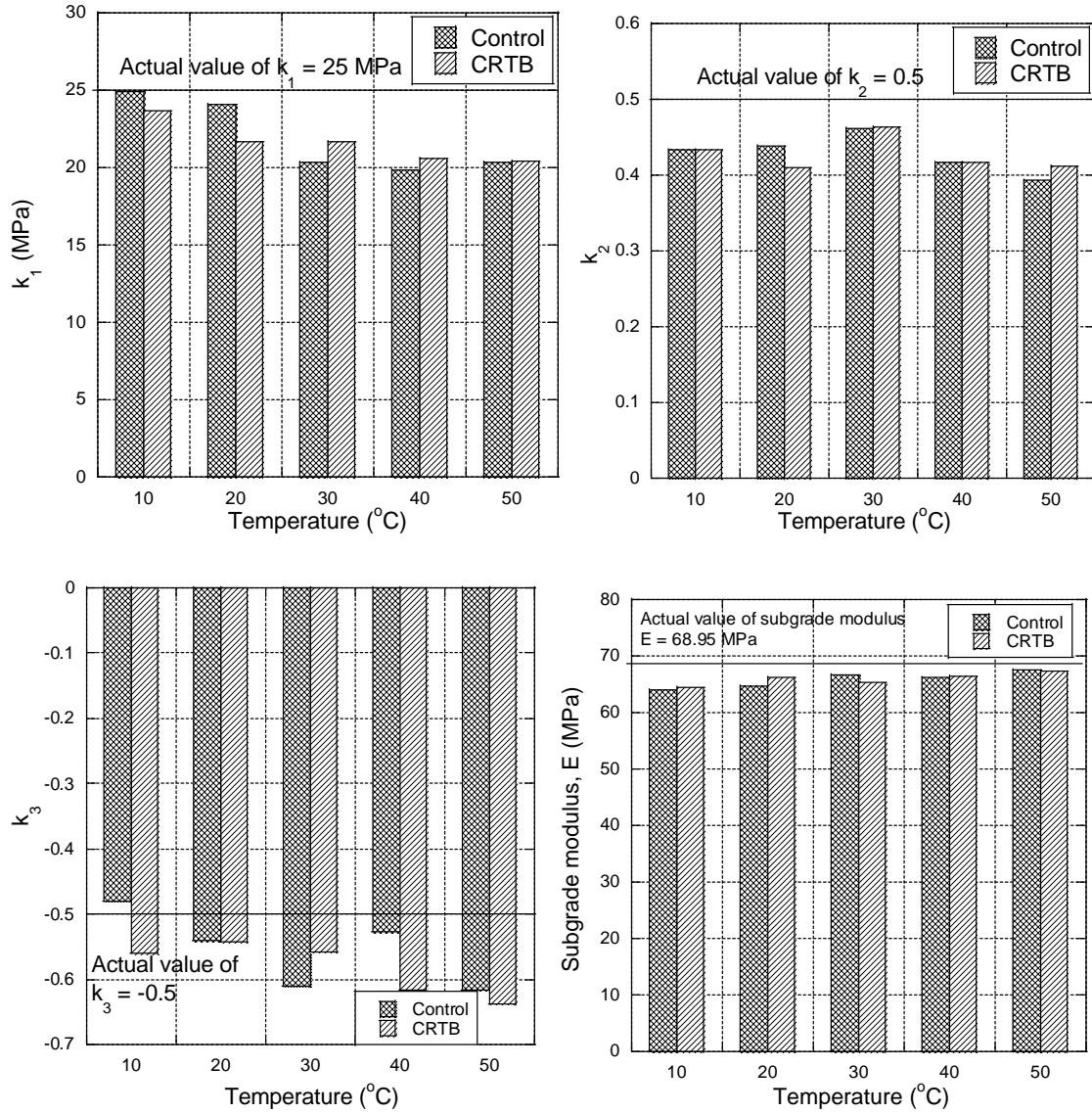
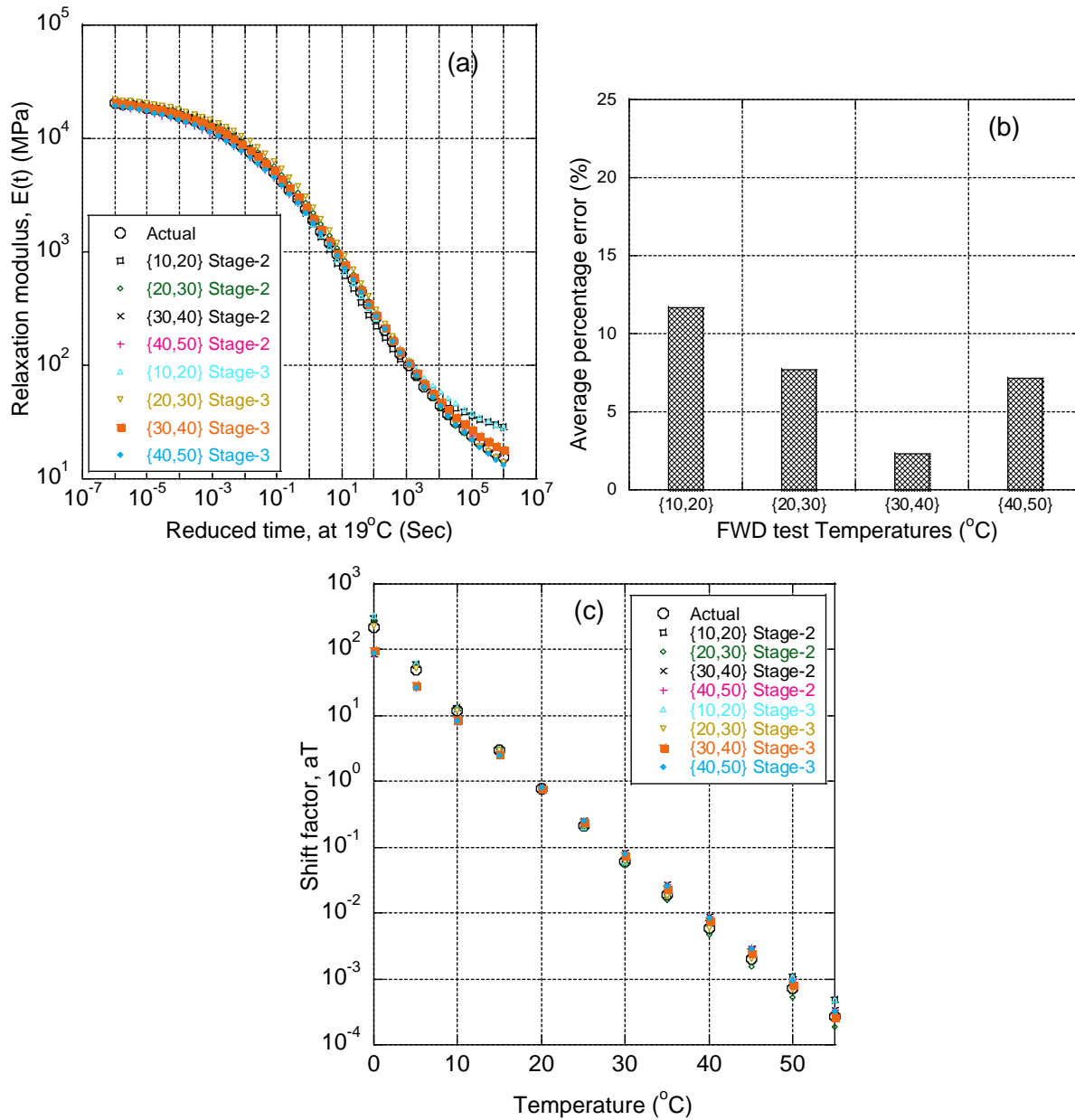


**Figure 67: Nonlinear elastic backcalculated unbound layer properties (in stage-1) for Control and CRTB Mixes, using FWD data at different test temperature.**

It should be noted that the relaxation modulus of linear viscoelastic AC layer is a function of time, therefore in nonlinear viscoelastic backcalculation, the error function is defined as the normalized percentage error along the entire deflection history. Although, the entire deflection history (~35-60msec) is used in the inverse analysis, it may not be sufficient to predict the entire relaxation modulus curve.

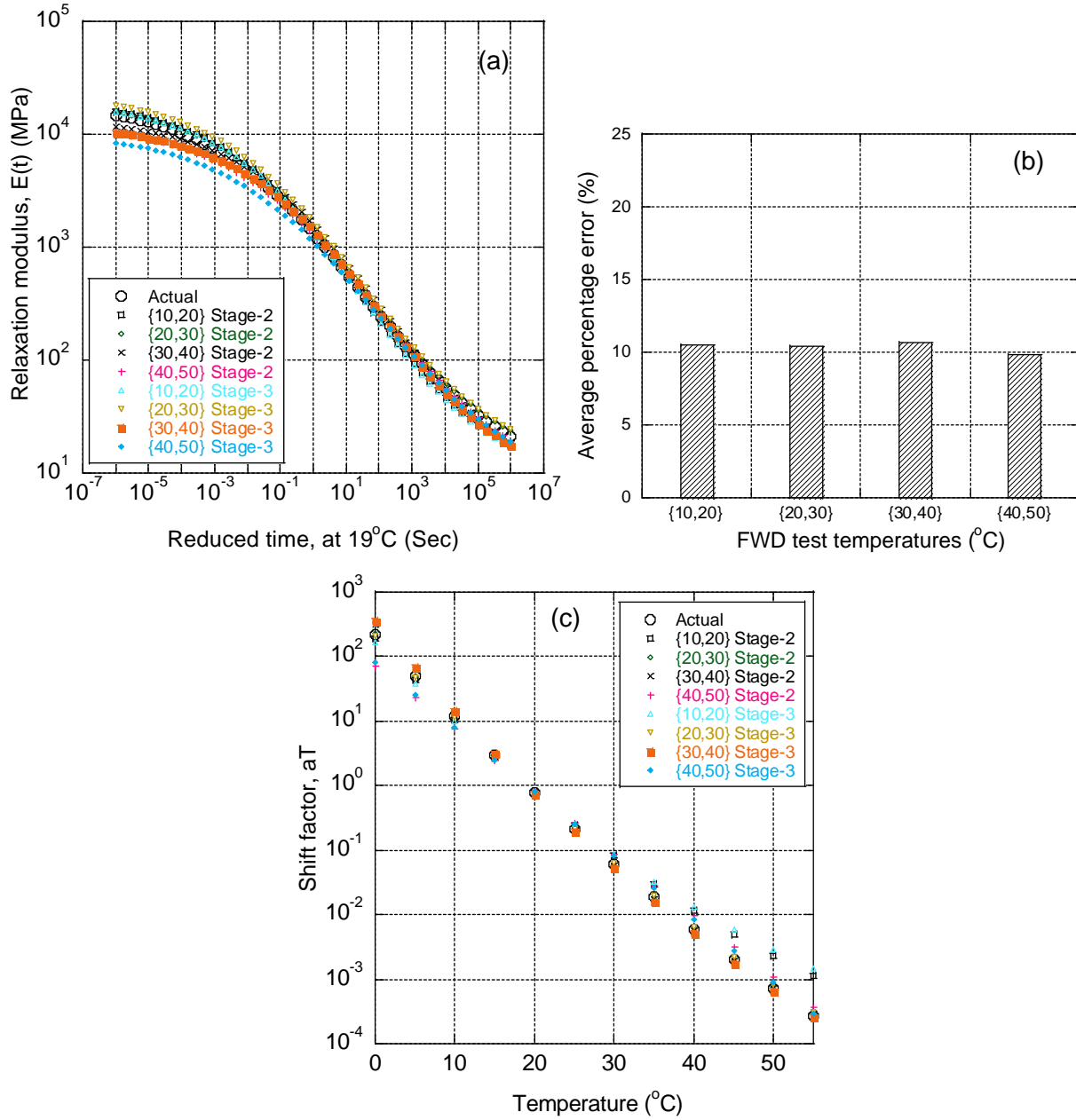
In order to obtain both the sigmoid coefficients (Equation (25)) and the shift factor coefficients (Equation (23)), FWD deflection histories obtained at (at least) two AC temperatures need to be used simultaneously during the backcalculation. In order to see the effect of AC temperature on backcalculated  $E(t)$ , the backcalculation was conducted at the following temperature pairs: a) 10°C & 20°C, b) 20°C & 30°C, c) 30°C & 40°C, and d) 40°C & 50°C. The average of backcalculated unbound layer properties obtained in stage-1 at each independent temperature were used in stage-2.

Figure 68 and Figure 69 show the backcalculation results for Control and CRTB mixtures, respectively. Figure 68 shows that the backcalculated  $E(t)$  master curve for Control mix was quite good for most of the FWD test temperature pairs. At the temperature pair of 10°C & 20°C, the backcalculated  $E(t)$  deviated from the actual  $E(t)$  after reduced time of about  $10^4$ sec, which is somewhat expected since the entire  $E(t)$  curve is not used during forward analyses at these temperatures. Figure 69 shows that the backcalculated  $E(t)$  master curve for CRTB mix was also quite good for most of the FWD test temperature pairs. In this mix, it was observed that the some deviation occurred at low reduced times ( $<10^4$ sec) when FWD test temperature pairs of 30°C & 40°C and 40°C & 50°C are used in the backcalculation. This deviation was attributed to coarse discretization of reduced time evaluated in the convolution integral (Equation 8) at these high temperatures. Theoretically, the results can be improved by increasing the number of time steps in the convolution integral given in Equation 8, at the expense of increasing the computational time. Accuracy of the backcalculation was evaluated based on average error in backcalculated  $E(t)$  master curve using Equation (57) over reduce time of  $t(1) = 10^{-6}$ sec to  $t(n) = 10^6$  sec. Figure 68a and Figure 69a shows average error ( $\xi_{AC}^{avg}$ ) calculated for the Control and CRTB mixtures, respectively.



**Figure 68: (a) Comparison of backcalculated and actual  $E(t)$  master curves (b) average percentage error,  $\zeta_{AC}^{avg}$  for the Control mixture and (c) time-temperature shift factor.**





**Figure 69: (a) Comparison of backcalculated and actual  $E(t)$  master curves (b) average percentage error,  $\xi_{AC}^{avg}$  for the CRTB mixture and (c) time-temperature shift factor.**

#### ***4.4.3 Validation of BACKLAVAN using Field FWD Data***

The backcalculation algorithm BACKLAVAN was validated using field FWD data obtained at the LTPP section 0101 from state 01 (Alabama). This section was selected since FWD tests were conducted in years 2004 and 2005, and the temperature of the AC layer in 2005 FWD test was about 23°C more than the AC layer temperature during the FWD test run in 2004. This helps in obtaining the shift factor coefficients of the AC layer. In addition, the section was not modified (i.e., there was no re-construction or rehabilitation) between the two tests.

In LTPP database, viscoelastic properties of the AC layer of the section 0101 were available from two different sources. The first source was the creep compliance ( $D(t)$ ) curve of the AC layer, which was measured using the cores from the field. The second source of viscoelastic properties in LTPP database is the ANNACAP predictive model developed under FHWA long term pavement program research (Kim et al. 2011).

In stage-1 of BACKLAVAN algorithm, peak stress and deflection values during all the test drops shown in Table 23 were used. As shown in Table 24, the separately backcalculated unbound base properties ( $k_1, k_2, k_3$ ) from 2004 and 2005 FWD data were found to be very close. As expected, the backcalculated elastic AC modulus values dropped with increase in temperature. However, the effect of the temperature on the unbound layer was not significant.

The nonlinear unbound layer properties obtained in stage-1 were used in stage-2, which uses the viscoelastic-nonlinear forward algorithm LAVAN during backcalculation of the  $E(t)$  of the AC layer. It should be noted that viscoelastic backcalculation requires the entire time history for backcalculation. In the FWD test run in 2004, entire deflection history was available only for drop 1, hence the backcalculation was performed only using drop 1.

**Table 23: FWD test data from LTPP section 01-0101 for years 2004-2005.**

Test date	Drop Level	Peak stress(kPa)	Deflection (in $\mu\text{m}$ ) at radial distance r cm						
			r=0	r=20.3	r=30.5	r=45.7	r=91.4	r=121.9	
23-Feb-04	1	373.0	127.0	108.0	94.0	75.9	62.0	39.9	27.9
	2	575.7	206.0	176.0	154.9	125.0	103.1	65.0	46.0
	3	781.2	295.9	254.0	224.0	181.1	149.1	96.0	66.0
	4	1025.3	410.0	353.1	309.1	252.0	208.0	133.1	91.9
28-Apr-05	1	359.9	226.1	164.1	128.0	89.9	63.0	37.1	23.9
	2	553.0	355.1	265.9	215.9	148.1	105.9	61.0	43.9
	3	766.7	513.1	395.0	327.9	226.1	162.1	95.0	70.1
	4	959.1	661.9	515.1	430.0	300.0	213.1	122.9	88.9

**Table 24: Nonlinear elastic backcalculation results for section 0101.**

FWD test year =		2004	2005	Average
Avg. AC temperature =		11.9°C	35.2°C	N/A
Properties	AC modulus (MPa)	6491.59	1567.50	N/A
	$k_1$ (dimensionless)	1223.79	1086.80	1155.29
	$k_2$ (dimensionless)	0.156	0.165	0.161
	$k_3$ (dimensionless)	-0.594	-0.577	-0.586
	$E_{\text{subgrade}}$ (MPa)	205.68	179.93	192.81

Comparison between predicted and measured deflection history for both the 2004 and 2005 FWD testing are shown in Figure 70. Although the two drops had very close peak loading stress (Table 23), the peak deflection in 2005 FWD test was 76% higher. Further the test temperature effect was also clearly visible in the deflection creeping between the two tests. Therefore, as expected the backcalculated deflection history for FWD test at higher temperature (i.e., in 2005 test) showed a better match compared to 2004.

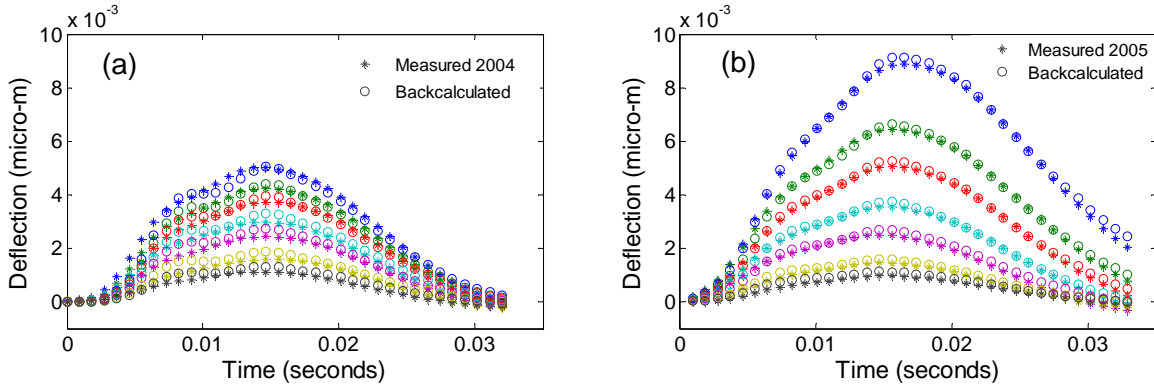


**Figure 70: Backcalculated and measured FWD deflection time histories for LTPP section 0101: (a) test run in 2004 and (b) test run in 2005.**

Figure 71 shows two relaxation modulus master curves “stage-2 run 1” and “stage-2 run 2” obtained from two independent backcalculation trials in stage-2. Both the stage-2 run 1” and “stage-2 run 2” results were obtained using the same population size and number of generations. The only difference between the two runs was in the initial values chosen for the generation of the first population to start the backcalculation. From the Figure 71, it can be seen that both the results almost overlap, illustrating a good convergence. It should be noted that  $E(t)$  from ANACAP was not available for comparison. ANACAP cannot predict phase angle and hence cannot be used to obtain  $E(t)$  from  $|E^*|$ . The dynamic modulus and phase angle master curves were calculated from the relaxation master curve at 19°C reference temperature via prony series-based interconversion procedure given by Park and Schapery (1999). As shown in Table 25, similar to the relaxation curves, the dynamic results obtained by two independent backcalculation attempts were identical. As shown in Figure 71b, the time-temperature shift factor curve computed using ANNACAP was found to be higher as compared to both the backcalculated and measured curves. It can be seen from the Figure 71b that the backcalculated time-temperature shift factor curves matched well with the measured for temperature less than 30°C. Further, it can be seen from Table 25 that that the dynamic modulus curves estimated using ANNACAP model, especially at higher frequencies, agrees well with the dynamic

modulus curves obtained through measured as well as the backcalculated results. However, ANNACAP predicted higher values at reduced frequencies less than  $10^{-2}$  Hz.

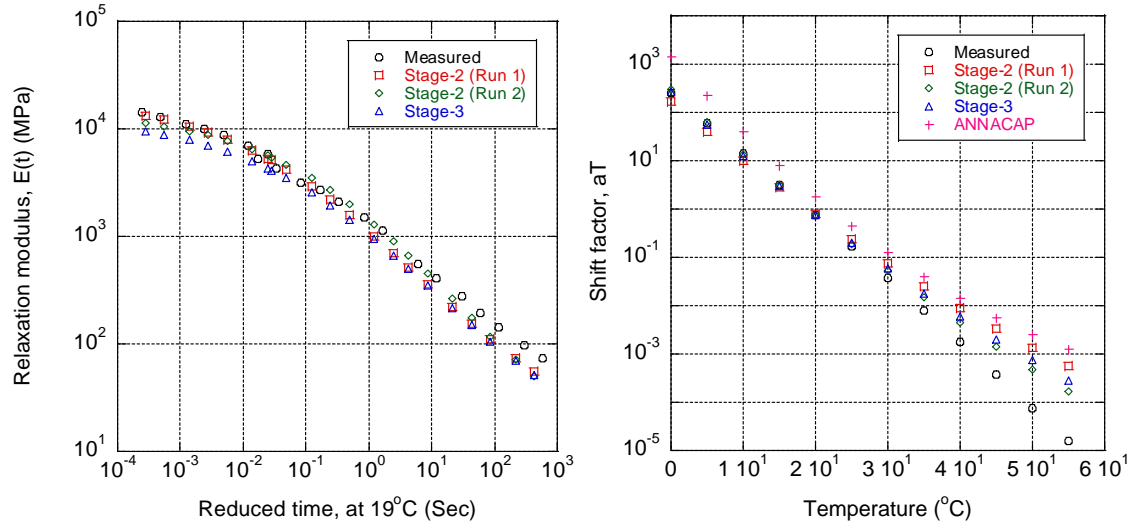


**Figure 71: Nonlinear viscoelastic backcalculation of section 0101 (a) Relaxation modulus (b) Shift factor at 19oC.**

**Table 25: Comparison of viscoelastic nonlinear viscoelastic backcalculated results obtained at different stages.**

T (C)	f (Hz)	E*  (MPa)					Phase angle (Degrees)			
		Measured	Stage 2 (GA) Run 1	Stage 2 (GA) Run 2	Stage 3 (fminsearch)	ANNACAP	Measured	Stage 2 (GA) Run 1	Stage 2 (GA) Run 2	Stage 3 (fminsearch)
-10	10	21268	18259	14230	13482	24920	4.5	3.7	1.6	3.9
-10	1	18698	16435	13502	11926	21804	6.4	5.9	2.8	3.8
-10	0.1	15220	13548	12119	10282	18045	10.9	10.2	5.8	8.5
10	10	13120	11513	10492	8680	12149	13.8	13.8	9.4	11.2
10	1	8498	7558	7718	6039	7556	21.3	21.8	16.3	18.7
10	0.1	4468	3717	4582	3323	4208	30.1	32.3	26.2	28.3
21	10	6713	6474	6501	5049	5786	24.8	24.4	19.8	22.0
21	1	3223	3155	3531	2620	2993	33.6	34.2	30.2	31.4
21	0.1	1206	1125	1379	1006	1353	40.9	42.9	41.4	40.5
37	10	1098	1785	1750	1370	1728	41.3	39.7	39.0	38.1
37	1	357	594	550	468	758	43.3	45.5	47.5	44.2
37	0.1	120	177	156	136	346	39.3	44.7	49.7	43.4
54	10	87	373	250	250	625	36.7	46.1	49.7	47.4
54	1	39	114	68	82	285	27.0	42.4	46.4	40.9
54	0.1	22	42	23	29	150	16.3	32.1	35.9	29.2

The nonlinear unbound layer properties obtained in stage-1 and linear viscoelastic properties obtained in stage-2 were used in stage-3 as seed values in MATLAB function “*fminsearch*”. It should be noted that similar to stage-2, stage-3 also involves viscoelastic nonlinear backcalculation, and so requires entire time history for backcalculation. The stage-3 results are labeled as “*fminsearch*” in Figure 71 and Table 25. As shown in the Table 25, the backcalculated relaxation modulus, shift factor, dynamic modulus and phase angle does not change much, as compare to the stage-2 results. Since the unbound layer properties were also considered as unknown variables in stage-3, new set of values for  $k_1, k_2, k_3$  and  $E_s$  were obtained. A marginal increase of 2.5%, 0.11%, 1.5% and 14.0% in  $k_1, k_2, k_3$  and  $E_s$  were observed. This agrees with the results obtain in synthetic data analysis, where although the backcalculated results obtained from stage-2 were close to the actual values, they were in general under predicted by the algorithm.

#### **4.5 Chapter Summary**

A summary of the work presented in chapter 4 is as follows:

- Genetic Algorithm based backcalculation procedures (BACKLAVA, BACKLAVAP and BACKLAVAN) were developed, which are capable of backcalculating relaxation and dynamic modulus master curves as well as time-temperature shift factor coefficients of AC pavements, and nonlinear  $k_1, k_2,$  and  $k_3$ .
- For backcalculation using multiple FWD (BACKLAVA), the simulated FWD model shows that, accuracy of backcalculation depends on the set of temperatures at which FWD test have been conducted. The present study suggests that FWD data collected at a

set of temperatures, between 20-40°C would be useful in estimating  $E(t)$  or  $|E^*|$  master curve.

- In a sensitivity analysis, it is shown that the influence of unbound layer properties increases with incorporation of data from further sensors and with increase in test temperature. But using only further sensors is not recommended.
- For backcalculation using single FWD at a known temperature profile (BACKLAVAP), the analyses indicated that, the accuracy of  $E(t)$  backcalculation is the highest if FWD is run at a temperature profile between 30°C and 20°C, with preferably  $\pm 5^\circ\text{C}$  or more.
- For backcalculation using temperature profile (BACKLAVAP), it is recommended to use data from two or more FWD tests ran at different temperature profiles.

## CHAPTER 5

### EVOLUTION OF DYNAMIC MODULUS OVER TIME

#### 5.1 Introduction

Chemical and physical changes in HMA, due to construction and in-service use may significantly affect its mechanical properties. It is well known that one of the significant changes encountered by asphalt pavements is age hardening. Several studies have shown that factors such as mean annual air temperature, moisture, binder type, volumetrics of mixture and pavement structure can significantly influence aging of HMA (Houston et al., 2005; Dickson, 1980; Jung, 2006; Raghavendra et al., 2006; Mirza and Witczak, 1995).

Aging may lead to higher stiffness and embrittlement in HMA. Embrittlement of HMA adversely affects its healing potential which leads to an increased rate of cracking. Similarly, higher stiffness may reduce the fatigue life ( $N_f$  at constant strain level) of the pavement. This is also illustrated by the Asphalt Institute fatigue formulation, where the fatigue life is inversely related to the stiffness of asphalt (Asphalt Institute (1999)).

$$N_f = 18.4 \times (4.32 \times 10^{-3} \times \varepsilon_t^{-3.29} \times E^{-0.854}) \quad (62)$$

where,  $\varepsilon_t$  is horizontal tensile strain at the bottom of asphalt layer and  $E$  is elastic modulus of asphalt mix.

Traditionally, in field aging is determined using core samples obtained from the field. Field coring is resource intensive (time consuming and cumbersome) and the limited amount of samples yields insufficient information. In the present study, a simple method based on typical



FWD backcalculation is proposed to quantify hardening of an in-service pavement. In the next section popular methods to simulate field aging and their limitations are discussed, which is followed by the FWD based proposed procedure to quantify age hardening.

## 5.2 Aging Models

Aging in field is mainly attributed to physical and chemical changes in asphalt binder. These changes are mainly caused by oxidation and loss of volatile oils from the asphalt binder (Houston et al., 2005). Aging in asphalt mixtures is typically investigated using two approaches: (1) interpolating the aging potential of asphalt mixtures based on aging potential of asphalt binders (2) interpolating the aging potential of asphalt mixtures based on laboratory aging under different aging conditions. Two popularly used aging models under the above categories are the Global Aging System (GAS) model and AASHTO R30 (AASHTO R30, 2008). Both the methods, however, fail to account for the effects of in situ field conditions on age hardening such as compaction, air voids, moisture, temperature fluctuations and influence of aggregates.

### 5.2.1 GAS Model

The GAS predictive equation used in Mechanistic Pavement Design Guide (NCHRP 1-37A) is based on the work by Mirza and Witzak (Mirza and Witzak, 1995). The model predicts field aged viscosity of binder with time and depth using the following equation

$$\log \log \eta_{aged} = \frac{\log \log \eta_{t=0} + At}{1+Bt} \quad (63)$$

where,

$$A = -0.004166 + 1.41213C + C \times \log(MAAT) + D \times \log \log \eta_{t=0}$$

$$B = 0.197725 + 0.068384 \log C$$

$$C = 10^{274.4946 - 193.381 \log(T_R) + 33.9366 \log(T_R)^2}$$

$$D = -14.5521 + 10.47662 \log(T_R) - 1.88161 \log(T_R)^2$$

$\eta_{aged}$  = aged viscosity (centipoise)

$\eta_{t=0}$  = viscosity at mix/laydown (centipoise)

$MAAT$  = mean annual air temperature ( $^{\circ}F$ )

$T_R$  = temperature in Rankine ( $^{\circ}R = ^{\circ}F + 459.7$ )

$$\eta_{aged,z} = \frac{\eta_{aged}(4+H) - A\eta_{t=0}(1-4z)}{4(1+Hz)} \quad (64)$$

$$H = 23.82e^{(-0.0308 MAAT)} \quad (65)$$

Equation (64) represents in situ viscosity at a depth of 0.25 inches, which is used in Equation 52 to predict viscosity at other depths. The predicted age hardening of the binder (in situ viscosity in Equation (65)) is then used to estimate the aged  $|E^*|$  of HMA as follows:

$$\log |E^*| = -1.249937 + 0.029232P_{200} - 0.001767(P_{200})^2 - 0.002841P_4 - 0.058097V_a - 0.802208 \frac{v_{b_{eff}}}{(v_{b_{eff}} + V_a)} + \frac{3.871977 - 0.0021P_4 + 0.003958P_{38} - 0.000017(P_{38})^2 + 0.005470P_{34}}{(1 + e^{(-0.603313 - 0.31335 \log(f) - 0.393532 \log(\eta))})} \quad (66)$$

where,

$|E^*|$  = Dynamic modulus, in  $10^5$  psi

$\eta$  = Aged bitumen viscosity in  $10^6$  poise

$f$  = Loading frequency in Hz

$V_a$  = % air void in HMA

$Vb_{eff}$  = % effective binder content (by volume)

$P_{34}$  = Cumulative % retained on the  $\frac{3}{4}$  inch sieve (by total aggregate weight)

$P_4$  = Cumulative % retained on the No. 4 sieve (by total aggregate weight)

$P_{200}$  = Cumulative % passing the No. 200 sieve (by total aggregate weight)

The GAS model predicts an exponential decrease in hardening with most of the changes in the viscosity in the top 25 mm. Farrar et al. (2006) conducted verification of the GAS model using field cores collected four years after construction and found that, the GAS method under predicts hardening in field, particularly in top 13 mm of pavement. Furthermore due to the limited data, the existing GAS method incorporated in MEPDG ignores the influence of air voids in field hardening predictions.

### ***5.2.2 Mixture Conditioning of HMA: AASHTO R30***

The AASHTO R30 standard was developed under SHRP studies to simulate field oxidative age hardening in HMA (Houston et al., 2005). To simulate long term aging, the compacted samples are required to be prepared from short term aged samples as specified in the standard (AASHTO R30). The test aims to simulate field aging of five to seven years. The standard requires conditioning of the compacted test specimen for 5 days in a forced-draft oven at 85°C. In an NCHRP study to verify the field applicability of the AASHTO R30 standard, Houston et al. (2005) compared dynamic moduli of field and laboratory aged samples. They concluded that the existing AASHTO standard is not sufficient to simulate field aging. It was pointed out that the existing laboratory method ignores the effect of volumetric properties, field

temperature (MAAT) and other environmental conditions which limits the applicability of the method.

Both the GAS and AASHTO methods in their current form possess serious limitations in estimating in field age hardening of HMA. Hence more research on in field age hardening of HMA is needed to:

1. Generate field data in developing/calibrating aging models/tests.
2. Estimate loss in pavement life due to hardening (Roque et al., 2010 and Jung, 2006).

### **5.3 Effect of Aging on Viscoelastic Properties of HMA**

As previously discussed, viscoelastic behavior of HMA requires determining both the time/frequency and time-temperature functions. Each parameter in the sigmoid function and the time-temperature shift factor polynomial function influence their shape (property). It is expected that, with time, the HMA will get stiffer and less temperature dependent. In an NCHRP study Roque et al. (2010) showed the effect of aging on parameters in the dynamic modulus and time-temperature shift factor. The study was performed on a single mixture aged for three separate durations in lab. The laboratory aging time was related to field aging time using a lab to field aging relationship proposed in SHRP (Bell et al., 1994). The effect of aging was shown as the ratio of aged values to unaged values. They concluded that the viscoelastic behavior in HMA diminishes with aging. To further illustrate this point, the physical meaning of each parameter and the hypothesized effect of hardening on these parameters is shown in Figure 72 to Figure 77. CRTB mix was used as the base mixture in the illustrations. The dynamic modulus and the shift factor polynomial coefficient of the mix are ( $c_1=0.807$ ,  $c_2=3.519$ ,  $c_3=1.066$ ,  $c_4=0.407$ ) and ( $a_1=4.42E-04$ ,  $a_2=-1.32E-01$ ) respectively.

### 5.3.1 Effect of Variation of $c_1$

The  $|E^*|$  plots in Figure 72 show the effect of coefficient  $c_1$  on the sigmoid. Three trial mixes with constant  $c_1$ ,  $c_3$ ,  $c_4$  coefficients and varying the  $c_2$  coefficient were generated. Trial 1 is the figure refers to CRTB mix which was used as the base mix in the illustration. It can be seen from the figure that, an increase or decrease in the coefficient  $c_1$  shifts the entire curve up or down without significantly changing the shape of the function. Further, it should be noted that the coefficient represents the long term modulus of a mixture. Since HMA hardens with aging, it is expected that the coefficient should increase with time.

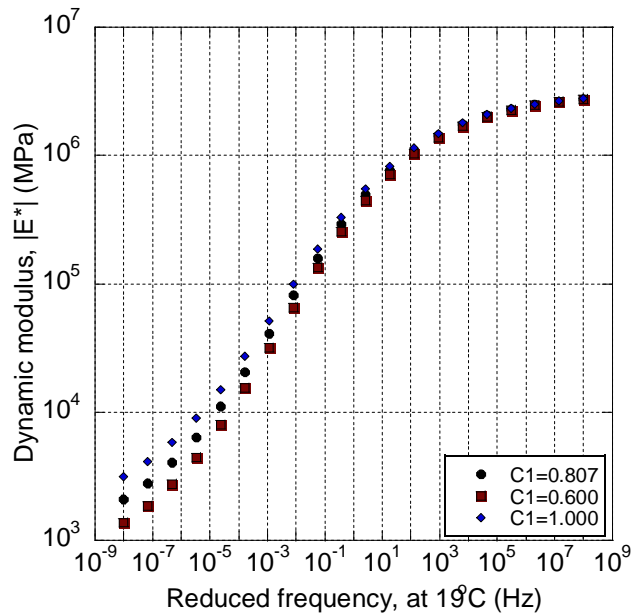


**Figure 72: Effect of variation in  $c_1$  on  $|E^*|$  master curve**

### 5.3.2 Effect of Variation of $c_2$

The  $|E^*|$  plots in Figure 73 show the effect of coefficient  $c_2$  on the sigmoid. Three trial mixes with constant  $c_1$ ,  $c_3$ ,  $c_4$  coefficients and varying the  $c_2$  coefficient were generated. Trial 1 is the figure refers to CRTB mix which was used as the base mix in the illustration. It can be seen from the figure that, an increase or decrease in the coefficient shifts the instantaneous modulus of

the mix up or down. It should be noted that in the present study instead of  $c_2$ ,  $c'_2$  (defined as sum of  $c_1$  and  $c_2$ , refer to Equation 47) has been used in the analysis. This is because  $c'_2$  is much easier to physically interpretate (the coefficient represents long term modulus of a mixture) and use in backcalculation. Since the HMA hardens with aging it is expected that the coefficient should increase with time.

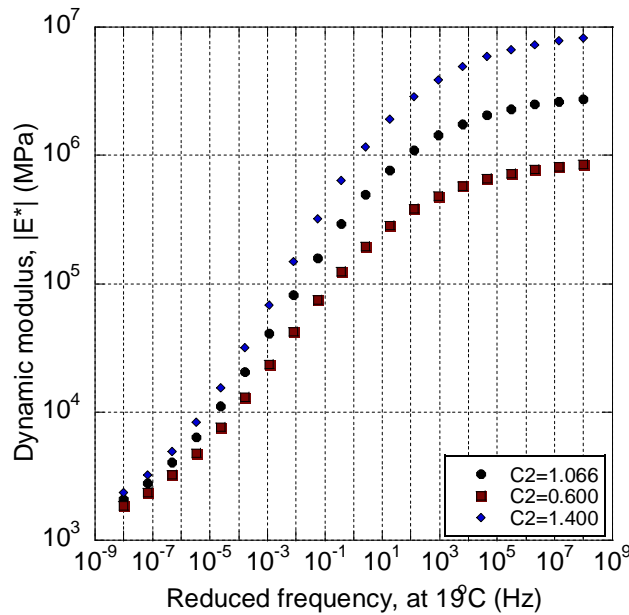


**Figure 73: Effect of variation in  $c_2$  on  $|E^*|$  master curve**

### 5.3.2 Effect of Variation of $c_3$

The  $|E^*|$  plots in Figure 74 show the effect of coefficient  $c_3$  on the sigmoid. Three trial mixes with constant  $c_1$ ,  $c_2$ ,  $c_4$  coefficients and varying the  $c_3$  coefficient were generated. It can be seen from the figure that, an increase or decrease in the coefficient shifts the entire curve to the left or to the right without changing the shape of the function. Since HMA hardens with aging it is expected that the coefficient should increase with time.

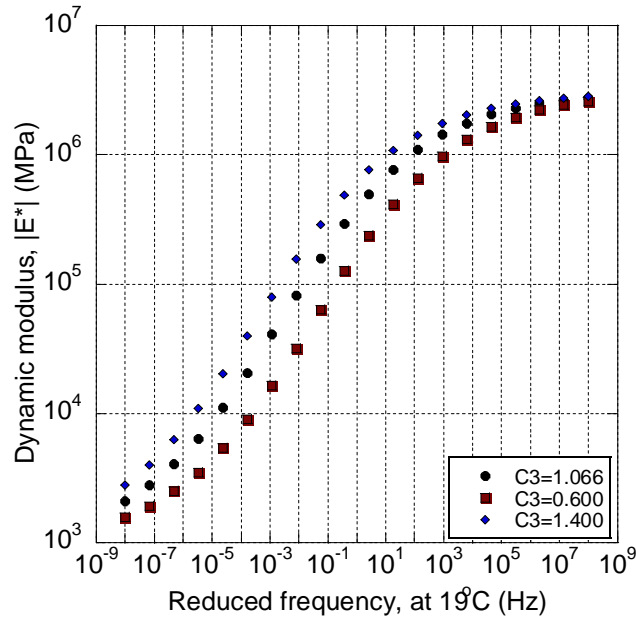


**Figure 74: Effect of variation in  $c_3$  on  $|E^*|$  master curve**

### 5.3.2 Effect of Variation of $c_4$

The  $|E^*|$  plots in Figure 75 show the effect of coefficient  $c_4$  on the sigmoid. Three trial mixes with constant  $c_1$ ,  $c_2$ ,  $c_3$  coefficients and varying the  $c_4$  coefficient were generated. It can be seen from the figure that, change in the coefficient  $c_4$  increases or decreases the slope of the entire curve. Since HMA hardens with aging, it is expected that the coefficient would decrease with time.

### 5.3.2 Effect of Variation of $a_1$

The time-temperature shift factor plots in Figure 76 show the effect of coefficient  $a_1$  on the polynomial function. Three trial mixes with constant  $a_2$  coefficients and varying the  $a_1$  coefficient were generated. It can be seen from the figure that a change in the coefficient  $a_1$  increases or decreases the slope of the entire curve. Since HMA hardens with aging, it is expected to get less temperature dependent; the coefficient should increase with time.

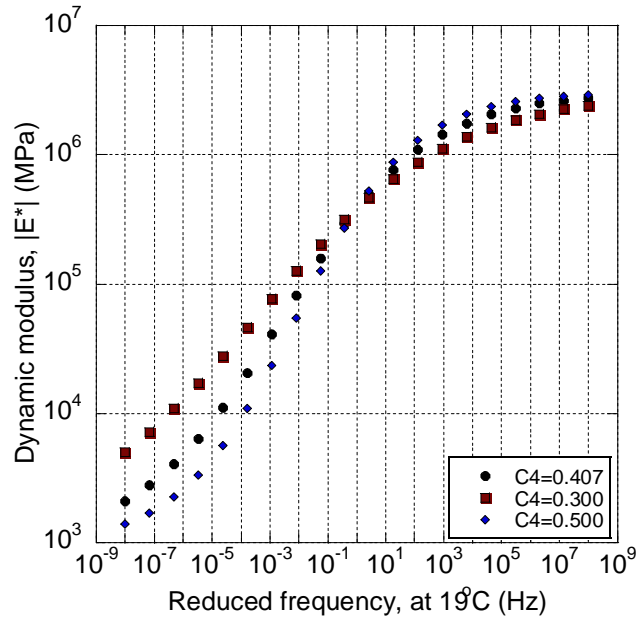


**Figure 75: Effect of variation in  $c_4$  on  $|E^*|$  master curve**

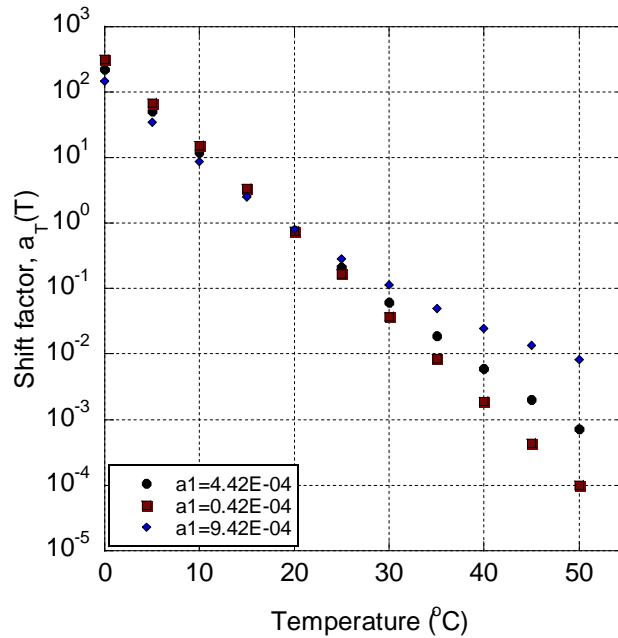


**Figure 76: Effect of variation in  $a_1$  on  $a_T(T)$  master curve**

### 5.3.2 Effect of Variation of $a_2$

The time-temperature shift factor plots in Figure 77 show the effect of coefficient  $a_2$  on the polynomial function. Three trial mixes with constant  $a_2$  coefficients and varying the  $a_2$  coefficient were generated. It can be seen from the figure that a change in the coefficient  $a_2$



increases or decreases the slope of the entire curve. Since HMA hardens with aging, it is expected to get less temperature dependent; the coefficient should increase with time.

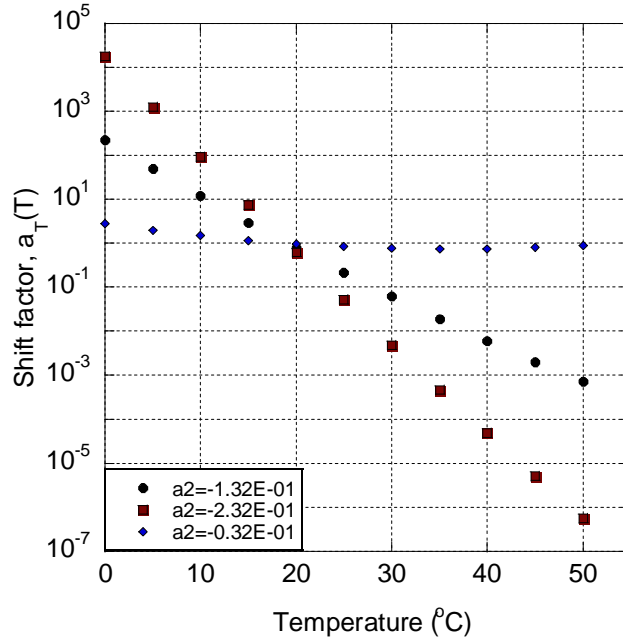


**Figure 77: Effect of variation in  $a_2$  on  $a_T(T)$  master curve**

### 5.4 Proposed Solution

In this study a new methodology is suggested that allows investigation of in-service age hardening in pavement using data obtained from commonly used FWD Test.

*Steps in proposed solution:*

- (1) Collect FWD deflection data and HMA layer temperature profile over the analysis period.
- (2) Backcalculate  $E(t)$  and shift factor for each FWD test using BACKLAVAP.
- (3) Convert  $E(t)$  to  $|E^*|$ .
- (4) Calculate normalized  $|E^*|$  and shift factor coefficients to quantify aging with time.

It is well known that, with time, apart from aging, HMA may undergo other various physical changes such as densification and damage. It should be noted that the above procedure ignores these factors and lumps everything as age hardening. To recognize when damage could become dominant in the analysis, backcalculation results are plotted along with fatigue distress data. Furthermore, a method proposed by MEPDG to analyze damage of an in-service pavement was used for comparison.

For rehabilitation design in MEPDG the determination of the HMA layer dynamic modulus follows a modified procedure to account for damage incurred in the HMA layer during the life of the existing pavement. The procedure therefore determines a “field damaged” dynamic modulus master curve as follows:

***For Level 1 analysis, the MEPDG calls for the following procedure:***

1. Conduct FWD tests on the pavement to be rehabilitated; calculate the mean backcalculated HMA modulus,  $E_i$ .
2. Determine mix volumetric parameters and asphalt viscosity parameters from cores. Determine binder viscosity-temperature properties through extraction/recovery.
3. Develop an undamaged dynamic modulus master curve using the data from step 2 and the modified Witczak equation. Calculate  $|E^*|$  for the same temperature recorded in the field at the frequency equivalent to the FWD load pulse.
4. Estimate damage,  $d_i = 1 - E_i/|E^*|$ , with  $E_i$  obtained from step 1 and  $|E^*|$  obtained from step 3.

5. Calculate  $c_2^d = (1-d_i)c_2$ ; where  $c_2$  is a function of mix gradation parameters and represents a parameter in the sigmoidal curve definition of  $|E^*|$  expressed as sigmoid function.
6. Determine field damaged dynamic modulus master curve using  $c_2^d$  instead of  $c_2$  in the modified Witczak equation.

The above MEPDG method has the following limitation:

1. Inappropriate conversion of time to frequency in step 3. Many time-frequency relationships have been proposed by various researches. The two most popular conversions are as follows.

$$f = \frac{1}{t} \quad (67)$$

$$f = \frac{1}{2\pi t} \quad (68)$$

Equation (67) and Equation (68) would work best for harmonic/sinusoidal pulses (Al-Qadi et al., 2008). For computing a frequency equivalent to the loading pulse Seo et al. (2012) suggested using Equation (67) where  $t$  was assumed to be loading pulse. Al-Qadi et al. 2008 suggested using Equation (67) where  $t$  was assumed to be the compressive stress pulse duration developed by the surface loading in the AC layer. However, such a conversion does not apply to FWD pulse loading.

2. Inappropriate calculation of damage. In MEPDG damage in the HMA is defined through reduction in dynamic modulus value at computed equivalent frequency. As discussed in the previous paragraph, the computed equivalent frequency does not represent the actual loading frequency and hence the calculated reduction in dynamic modulus would result in

misleading stiffness of the HMA. Further, it was observed that the MEPDG method may not show any damage up until damage in existing pavement is dominant over the age hardening effect.

Due to the above limitations the MEPDG method was used only as a reference for comparison.

#### ***5.4.1 Results and Discussion of Age Hardening in LTPP Test Section***

FWD test data over 5-12 years from three different LTPP sections were used to study in-field age hardening. The genetic algorithm based viscoelastic backcalculation model BACKLAVAP was used to backcalculate both dynamic modulus as well as the time-temperature shift factors from the FWD test data. The investigation in this chapter focused on quantifying the effect of aging on dynamic modulus and time-temperature properties of HMA. The LTPP sections and pavement properties selected in the analysis were the same as listed in Table 13 and Table 14. Backcalculated  $|E^*|$  and  $a_T(T)$  for the sections are shown in Figure 78 to Figure 80.

Dynamic modulus and time-temperature shift factor curves for section 010101 were backcalculated for 3 FWD tests conducted in year 1993, 1996 and 2000. Fatigue cracking for the section was observed prior to FWD testing in 2000. Hence it is expected to experience hardening in year 1996 followed by damage in 2000. As shown in Figure 78 this was observed at higher frequencies, however, at lower frequencies no trend in the results was found.

Dynamic modulus and time-temperature shift factor curves for section 340802 were backcalculated for 2 FWD tests conducted in year 1993 and 1998. The backcalculation dynamic modulus and shift factor from both the results (Figure 79) gave similar results indicating no change in AC properties.

Dynamic modulus and time-temperature shift factor curves for section 460802 were backcalculated for 5 FWD tests conducted in year 1993, 1995, 1999, 2004 and 2011. Fatigue cracking for the section was observed prior to FWD testing in 2007. Hence it is expected to experience hardening in year 1995 followed by 1999 and 2004.

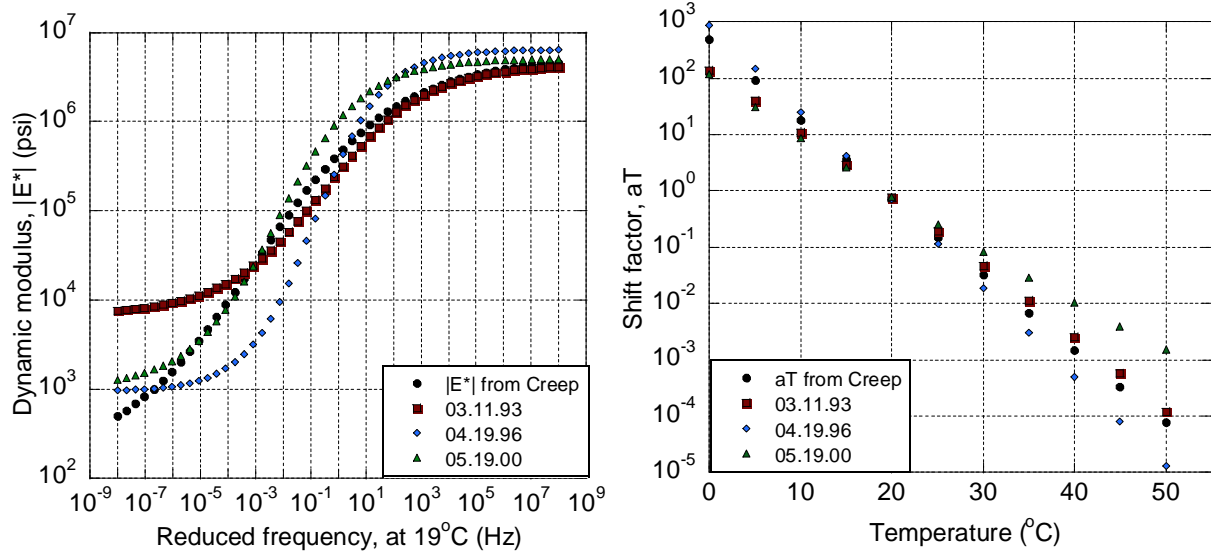


Figure 78: Backcalculated  $|E^*|$  and  $a_T(T)$  at section 01-0101 for year 1993, 1996 and 2000.

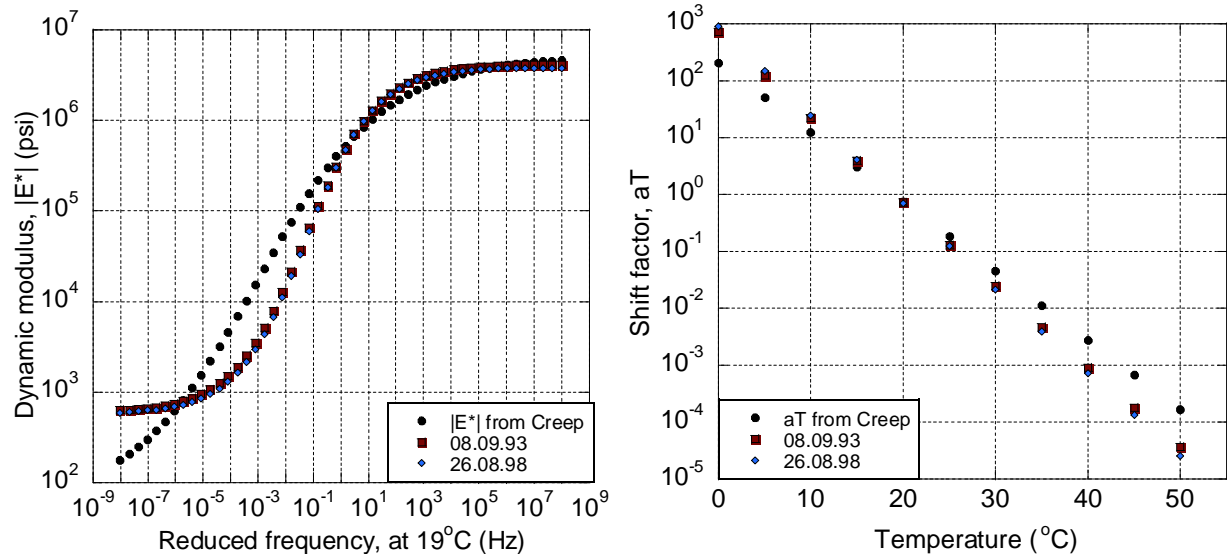
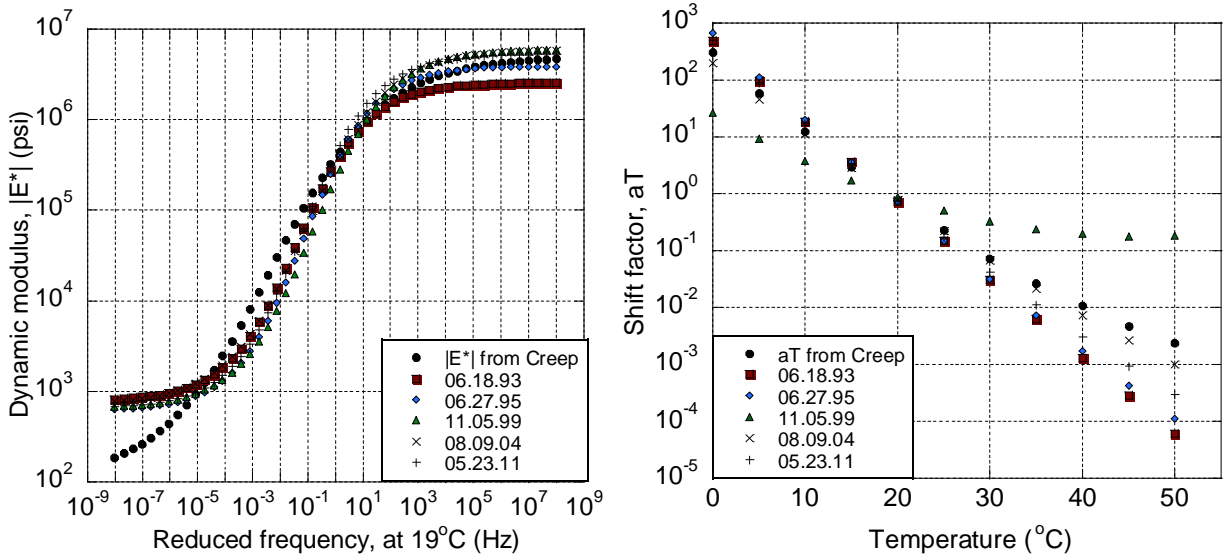


Figure 79: Backcalculated  $|E^*|$  and  $a_T(T)$  at section 34-0802 for year 1993 and 1998.



**Figure 80: Backcalculated  $|E^*|$  and  $a_T(T)$  at section 46-0802 for year 1993, 1995, 1999, 2004 and 2011.**

As discussed earlier, MEPDG suggests calculating change in dynamic modulus in an in-service pavement using modular ratio, where the ratio is defined as

$$\text{Modular Ratio} = \frac{E_i}{|E^*|} \quad (58)$$

where,  $E_i$  is backcalculated AC modulus value (obtained from elastic backcalculation) and  $|E^*|$  is original dynamic modulus value for the same temperature recorded in the field at frequency equivalent to the FWD load pulse. MEPDG suggest using volumetric and binder rheological properties in predicting original dynamic modulus using Witczak model (Equation 58). However, the LTPP database does not provide all the necessary inputs to the model and hence the dynamic modulus obtained from creep compliance data was used. Further, for temperature correction, the shift factor obtained from the creep data was used.

In field, pavement is subjected to different temperature, vehicle speed and loading. Hence, the viscoelastic response in HMA is a resultant of both time and temperature. In

literature, moving load in field is typically assumed to correspond to 10Hz. Hence the dynamic modulus value at 10 Hz is assumed to be critical in fatigue cracking. For comparison the Modular Ratio was plotted along with dynamic modulus at 10 Hz. Measured field fatigue cracking, backcalculated  $|E^*|$  at 10 Hz at temperature 10°C, 20°C and 30°C and Modular Ratio for the sections are shown in Figure 81 to Figure 83.

In general it was observed that, before the initiation of fatigue cracking, both the modular ratio and backcalculated dynamic modulus (at 10 Hz) shows hardening trend, with exception in section 46-0804. As oppose to the age hardening trend in section 46-0804 a drop in modulus value was observed in 1999. It should be noted that Modular Ratio was calculated based on 44 independent FWD test performed at 10 different locations in each test section, whereas, viscoelastic backcalculation was performed only at a single station using a single FWD.

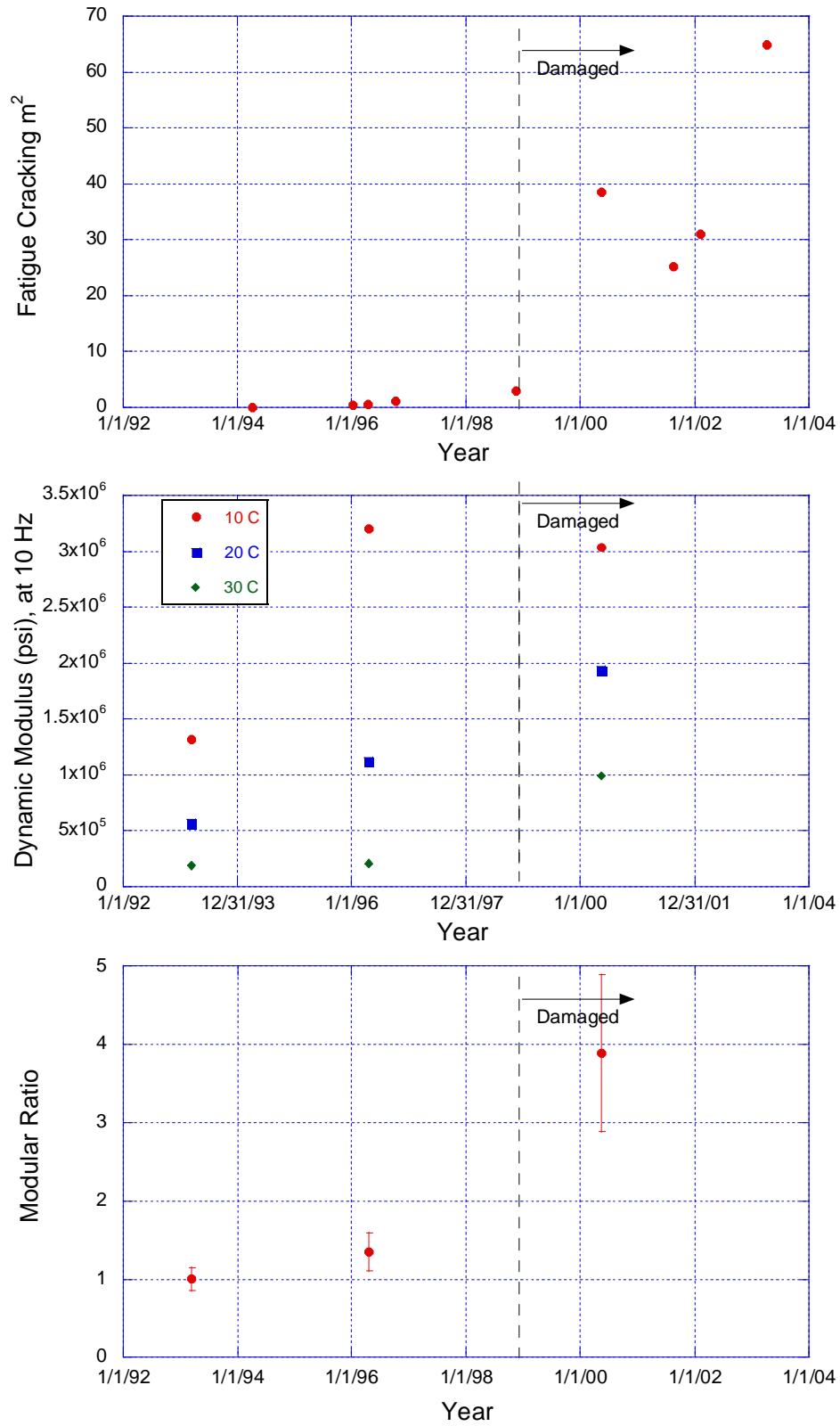


**Figure 81: Comparison of static and viscoelastic backcalculation ( $|E^*|$  at 10 Hz) for section 01-0101**



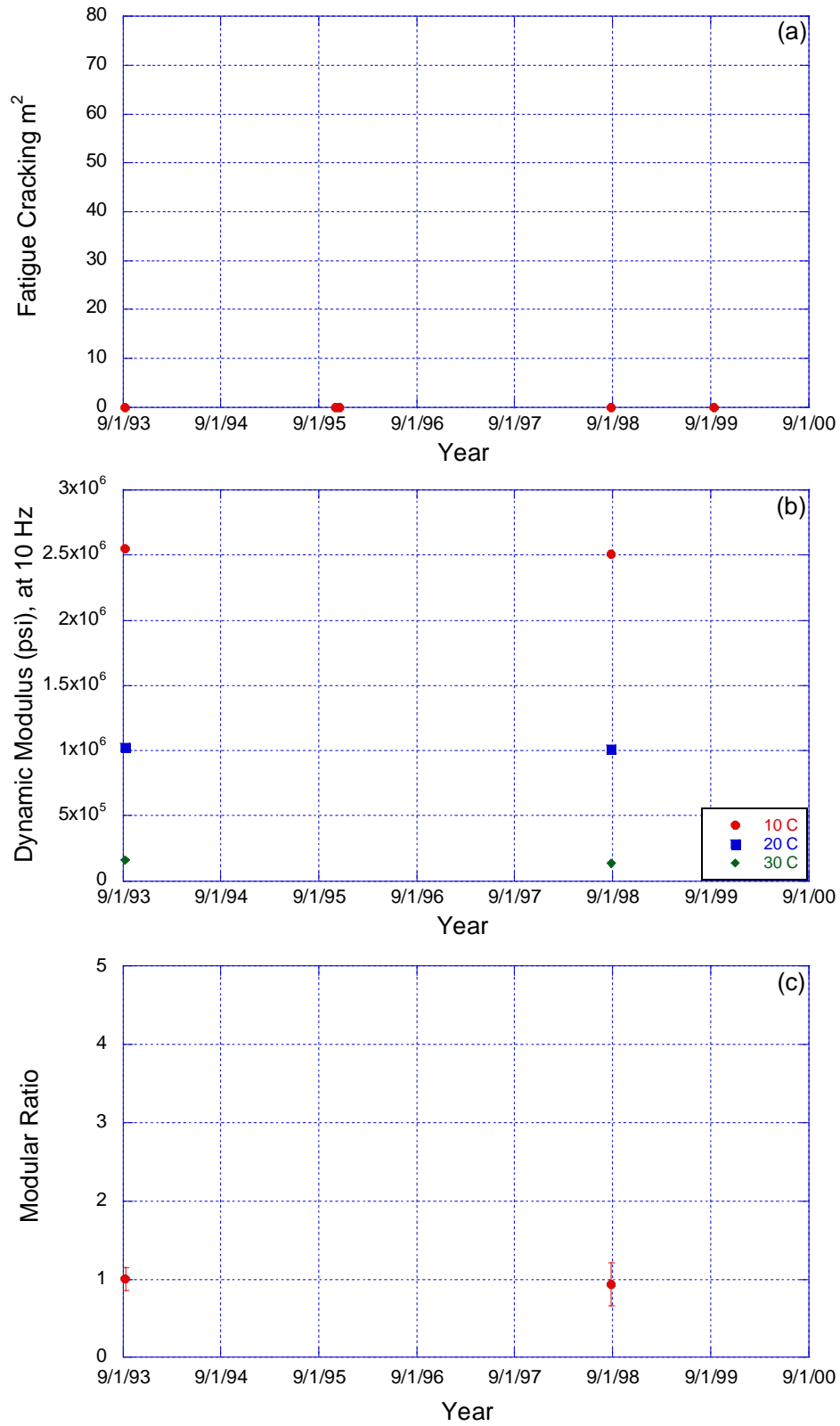


**Figure 82: Comparison of static and viscoelastic backcalculation ( $|E^*|$  at 10 Hz) for section 34-0802**

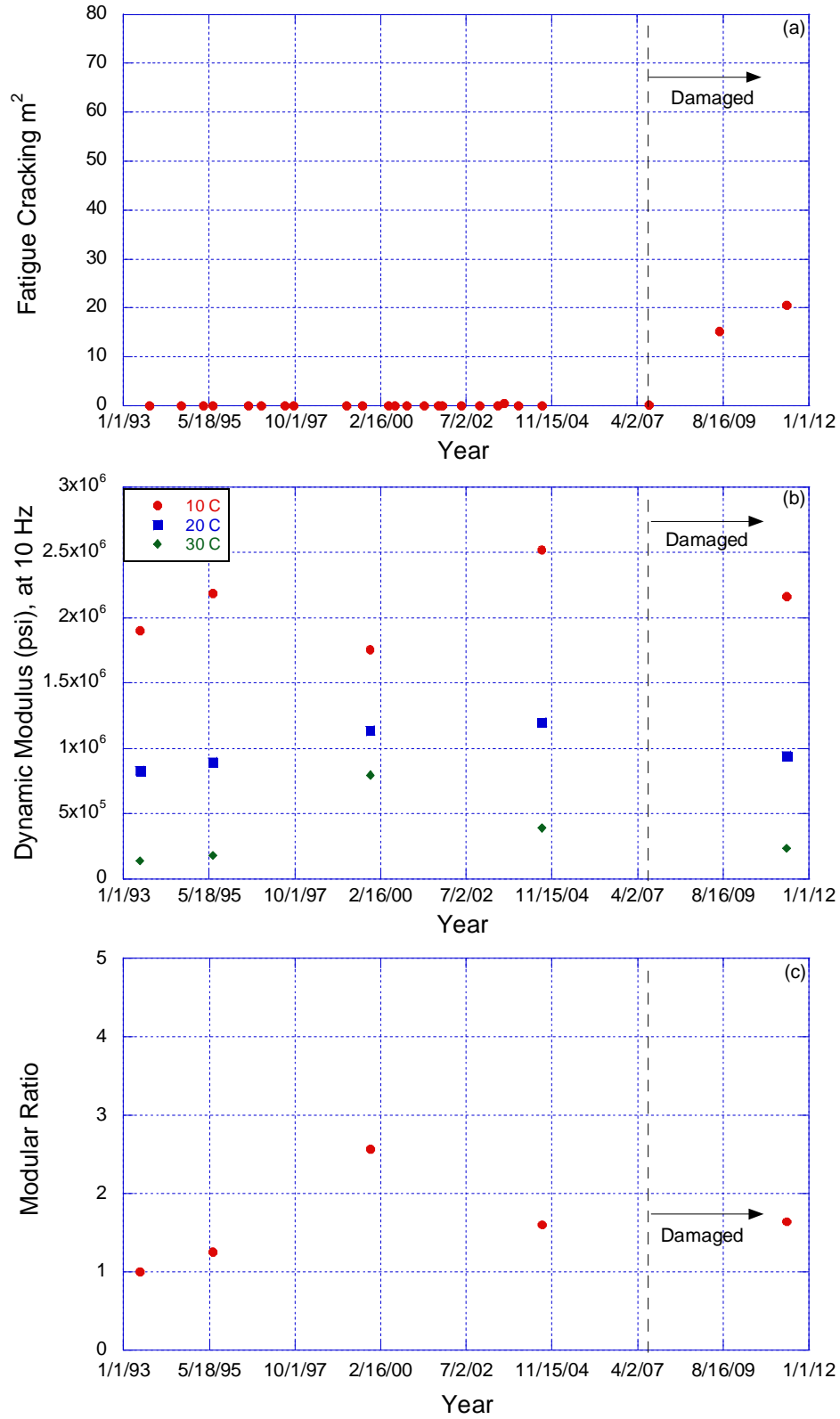


**Figure 83: Comparison of static and viscoelastic backcalculation ( $|E^*|$  at 10 Hz) for section 46-0802**

Next, the normalized dynamic modulus and shift factor coefficients were plotted over time. It was observed that none of section gave the expected age hardening trend in coefficient  $c_1$ . It should be noted that the backcalculation algorithm, due to the data limitations is not sensitive to capture modulus value at very low frequencies. Coefficient  $c_1$  physically represents the long term modulus value of mixture, and may not be captured with accuracy using the existing backcalculation procedure. In two out of three sections the hardening trend in  $c_2$  and  $c_3$  was captured by the backcalculation and one section demonstrated hardening effect in coefficient  $c_4$ . Summary of the aging prediction performance in each LTPP section is presented in Table 26.

**Table 26: Backcalculation performance in predicting aging of LTPP section.**

Station	C1	C'2	C3	C4	a1	a2
01-0101	X	✓	✓	✓	X	X
34-0802	X	X	✓	✓	✓	X
46-0804	X	✓	X	X	✓	✓

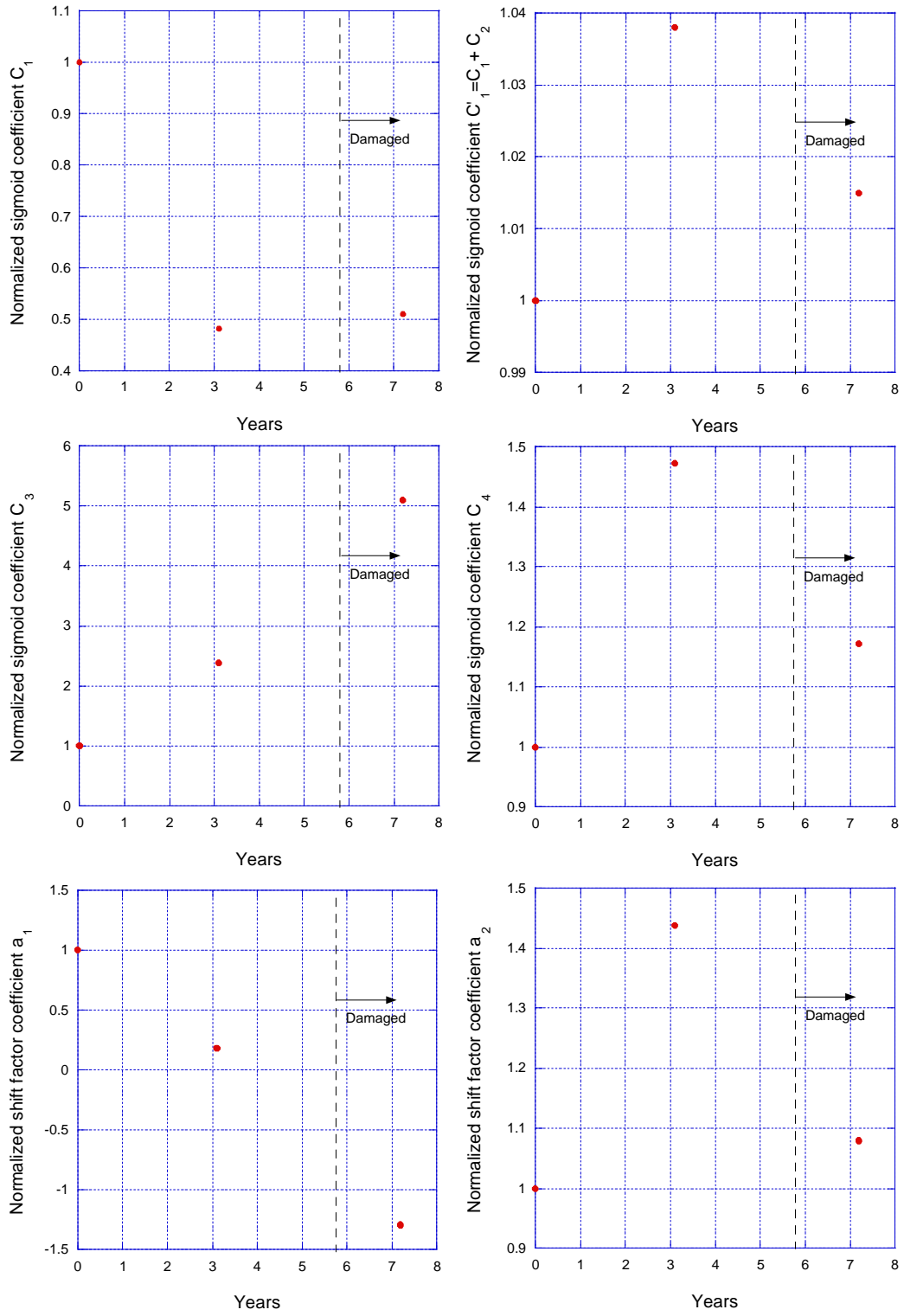


**Figure 84: Normalized  $|E^*|$  and  $a_T(T)$  coefficients with ageing time for section 01-0101**

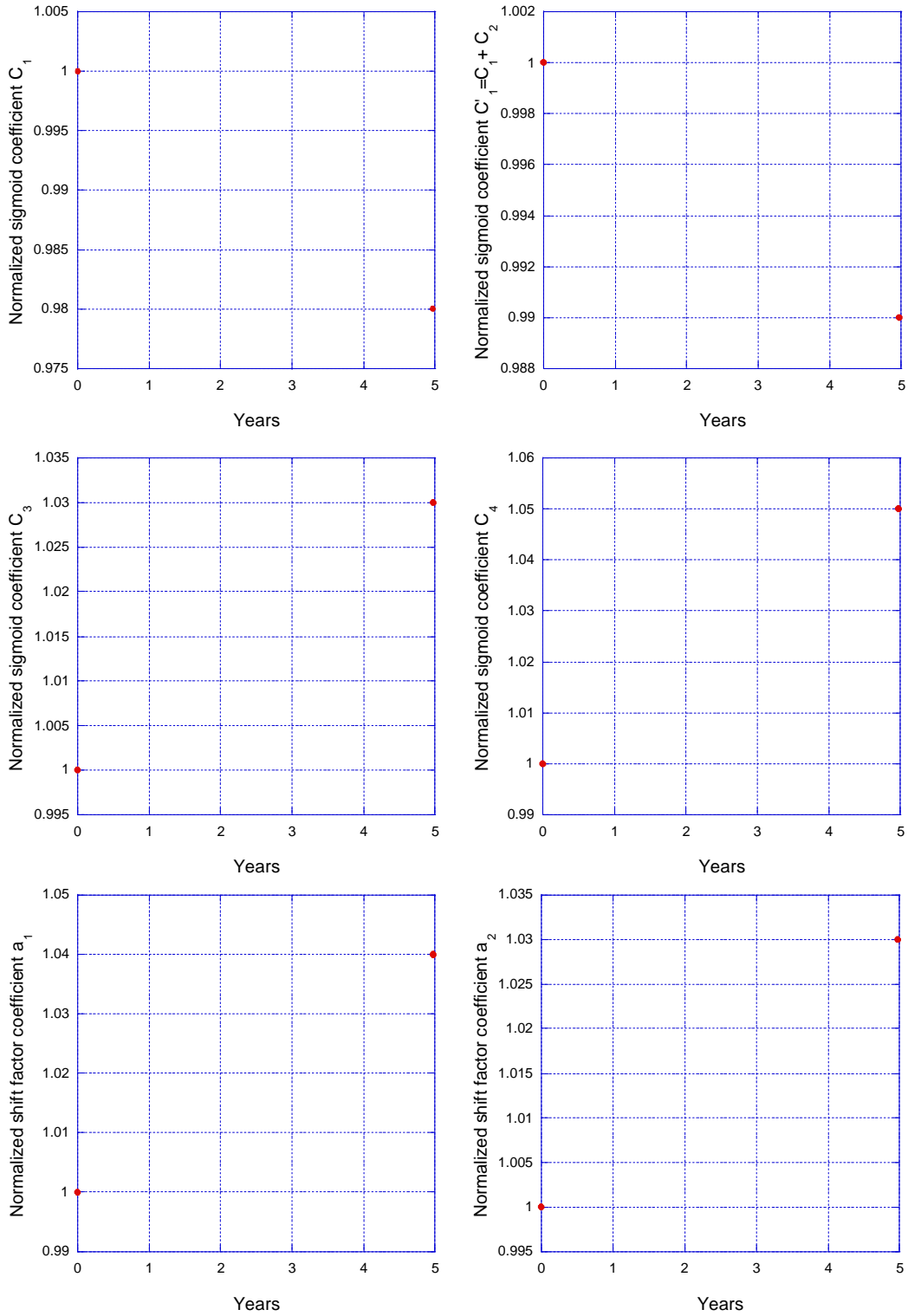


**Figure 85: Normalized  $|E^*|$  and  $a_T(T)$  coefficients with aging time for section 34-0802**

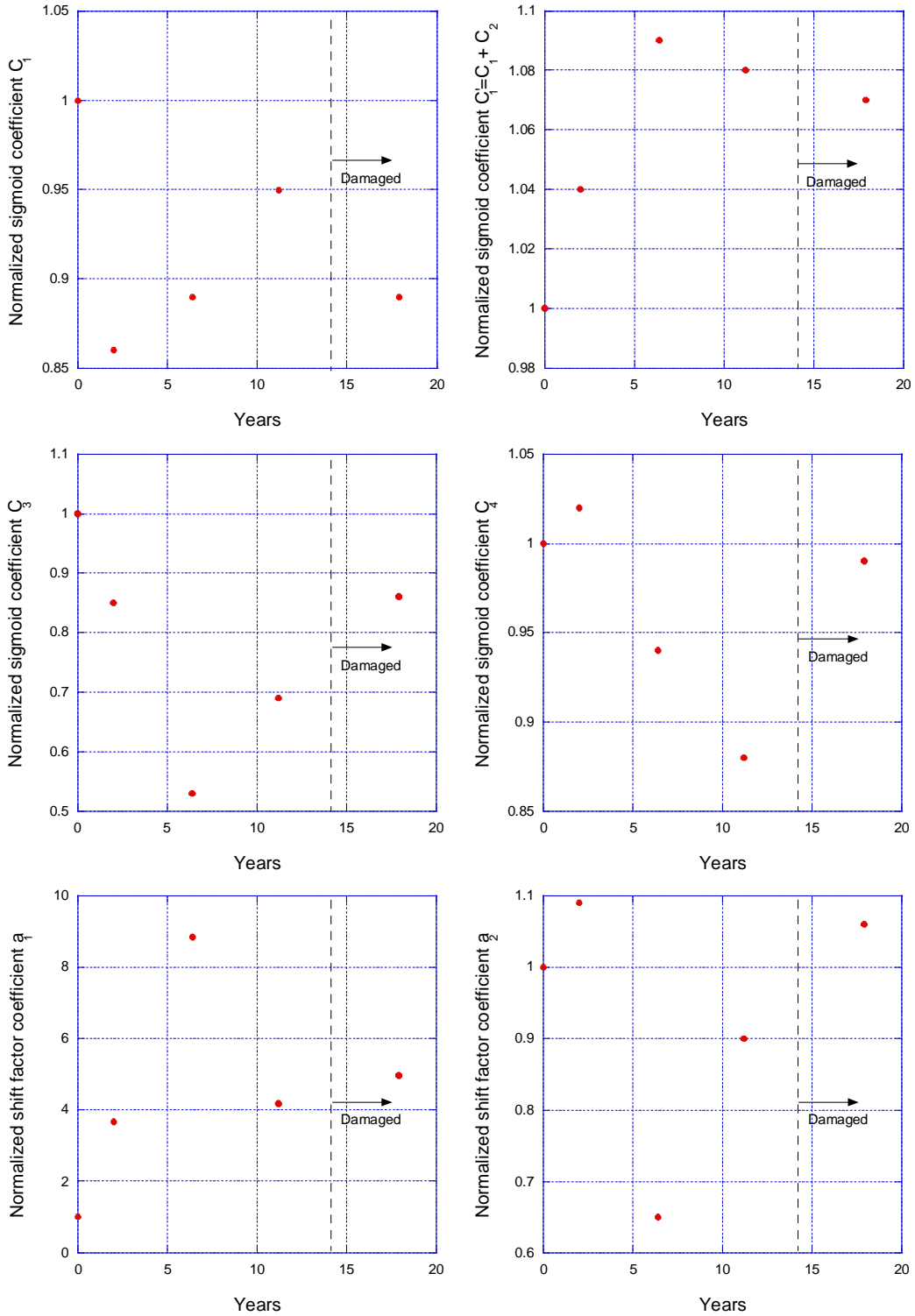


Figure 86: Normalized  $|E^*|$  and  $a_T(T)$  coefficients with aging time for section 46-0802

## 5.5 Summary

FWD data over 5-12 years were backcalculated using the backcalculation procedure (BACKLAVAP) developed in Chapter 4. The coefficients of the backcalculated dynamic modulus and time-temperature shift factor functions were normalized with respect to the backcalculated results from the first year and plotted with time. The following observations were made:

- Preliminary investigation indicated that the proposed method was able to show the as expected age stiffening effect for 8 coefficients out of total 18 backcalculated coefficients (4 sigmoidal coefficients and 2 time-temperature shift factor coefficients for each LTPP section) (refer Table 26).
- The MEPDG based modular ratio method was able to predict the age hardening trend in the pavement.

## CHAPTER 6

### SENSITIVITY ANALYSIS FOR LAYER THICKNESS

#### 6.1 Introduction

It is well known that pavement response and performance is sensitive to layer thickness. Therefore thickness is considered to be one of the most important factors both in design and quality control. Elevation measurement is one of the quickest methods in pavement thickness control during construction. The method possesses a main disadvantage: with construction of new layers the underlying layers undergo compaction. Changes in the underlying layer thicknesses are reflected in the thickness of subsequent layers, producing thinner lower layers and thicker upper layers compared to the design thicknesses.

In a study to analyze variability in LTPP pavement layer thickness, Selezneva et al. (2002) found that elevation measured thickness values were statistically different from core measured values. Important observations made in the study were:

- For 84 percent of layers, thickness variation within a section follows a normal distribution.
- For the same layer and material type, the mean constructed layer thickness tends to be above the design value for thinner layers and below the design values for thicker pavements.
- AC surface and binder layers show the highest number of sections with significant deviation from the design thickness.



Layer thickness variability has prompted many states to conduct inventory analysis using ground penetration radar (GPR) based non-destructive test method of pavement thickness evaluation (Noureldin et al., 2005; Uddin, 2006; Marc, 2007; Gucunski et al., 2008; Nazef, 2011). Occasionally, the FWD vehicles are also fitted with GPR to collect pavement surface thickness along with the FWD measurements. However, thickness measurement using GPR has the following issues:

1. GPR estimated HMA thickness may deviate from core thickness (in situ) by approximately 8%-10% (or  $\pm 1$  in), which could be even higher compared to actual design thickness. Furthermore GPR requires calibration using field cores to reach this accuracy.
2. The results are influenced by various other factors such as dielectric properties, moisture, and thickness of the constituent layer material. As an example, two layers with similar dielectric properties may not be separately recognized.
3. Typically GPR is used only for surface layer thickness evaluation; accuracy of GPR diminishes significantly with depth of the structure. As an example, occasionally interface between the unbound layers or surface and the unbound layer is not identifiable.

Because of the inevitable variability in pavement thickness it should be considered as a variable in FWD analysis. But considering layer thickness as a variable would increase the number of unknowns and reduce time efficiency of the analysis. Hence in most of the backcalculation studies, thickness is typically assumed to be a known (constant) parameter. This has generated interest in researchers in estimating error in backcalculation due to variation in pavement layer thickness. Irwin et al. (1989) studied the effect of random variation in layer thickness on elastic backcalculation. Backcalculation program, MODCMP2, was used to

backcalculate elastic modulus of pavement structure composed of 3 inches AC, 6 inches base, and 12 inches subbase layer course. They reported +37% to -21% error in AC modulus and +19% to -21% errors in base modulus. In another independent study, Rwebangira et al. (1987) studied the effect of variation in AC and base thickness on backcalculation. Backcalculation program BISDEF was used to backcalculate elastic modulus of a pavement structure composed of 2.5 inches of AC and 14.5 inches of base layer. They reported 60% error in AC and base modulus for a 1 inch change in AC layer thickness and 18% error in base modulus for 2 inch change in base layer thickness. Both the studies concluded that variation in AC thickness is most reflected in backcalculation of AC modulus, followed by base and subgrade. Both the studies reported insignificant error in subgrade modulus backcalculation. In a SHRP study, Briggs et al. (1992) evaluated the effect of AC and base layer thickness variation in GPS sites on backcalculation. They reported error up to 100% in AC layer modulus and 80 percent in the base layer modulus.

Given the focus of the dissertation is to backcalculate  $E(t)$ , in the present study, effect of variation in AC and base thickness on viscoelastic backcalculation is studied. Three cases were considered:

1. Case-1: Effect of variation in AC thickness (keeping the base thickness constant) on backcalculation of AC relaxation modulus, base modulus, and subgrade modulus. In case-1 the AC layer thickness was varied based on equation:

$$Actual AC_{TH} = Design AC_{TH} + (Design AC_{TH}) \times (\% variation) \quad (69)$$

$$Actual Base_{TH} = Design Base_{TH} \quad (70)$$

where, *Actual AC<sub>TH</sub>* and *Actual Base<sub>TH</sub>* are as constructed AC and base thicknesses, *Design AC<sub>TH</sub>* and *Design Base<sub>TH</sub>* are design AC and base thicknesses, % *variation* is error in *Actual AC<sub>TH</sub>* compared to the *Design AC<sub>TH</sub>*.

2. Case-2: Effect of variation in base thickness (keeping the AC thickness constant) on backcalculation of AC relaxation modulus, base modulus, and subgrade modulus. In case-2 the base layer thickness was varied based on equation:

$$Actual\ Base_{TH} = Design\ Base_{TH} + (Design\ Base_{TH}) \times (\% \ variation) \quad (71)$$

$$Actual\ AC_{TH} = Design\ AC_{TH} \quad (72)$$

3. Case-3: Effect of variation in AC and base thickness (keeping the sum of the AC and base layer constant) on backcalculation of AC relaxation modulus, base modulus, and subgrade modulus.

$$Actual\ AC_{TH} = Design\ AC_{TH} + (Design\ AC_{TH}) \times (\% \ variation) \quad (73)$$

$$Actual\ Base_{TH} = (Design\ AC_{TH} + Design\ Base_{TH}) - Actual\ AC_{TH} \quad (74)$$

The three cases were analyzed for two hypothetical pavement structures. The difference between the two structures was in the AC layer thickness: (i) 6 inch AC layer and (ii) 12 inch AC layer. All the analysis was performed on five different FHWA field HMA mixes as shown in Figure 87. Backcalculation was performed using the procedure BACKLAVAP developed in Chapter 4. To keep all the cases comparable same temperature profile of 30-25-20°C was assumed in the AC layer for all cases.

Steps followed in the sensitivity analysis are as followed:

Step-1: Use forward calculation algorithm LAVAP to calculate deflection histories considering actual (as built) pavement structure (i.e. using the thicknesses obtained from Equation (69) for case-1, Equation (71) for case-2 and Equation (73) for case-3).

Step-2: Use BACKLAVAP to backcalculate layer properties ( $E(t)$ , base and subgrade elastic modulus) assuming pavement layer thicknesses to be equal to the design thickness.

Step-3: Convert  $E(t)$  to  $|E^*|$ ; and calculate error in backcalculated  $|E^*|$  and base and subgrade elastic modulus.

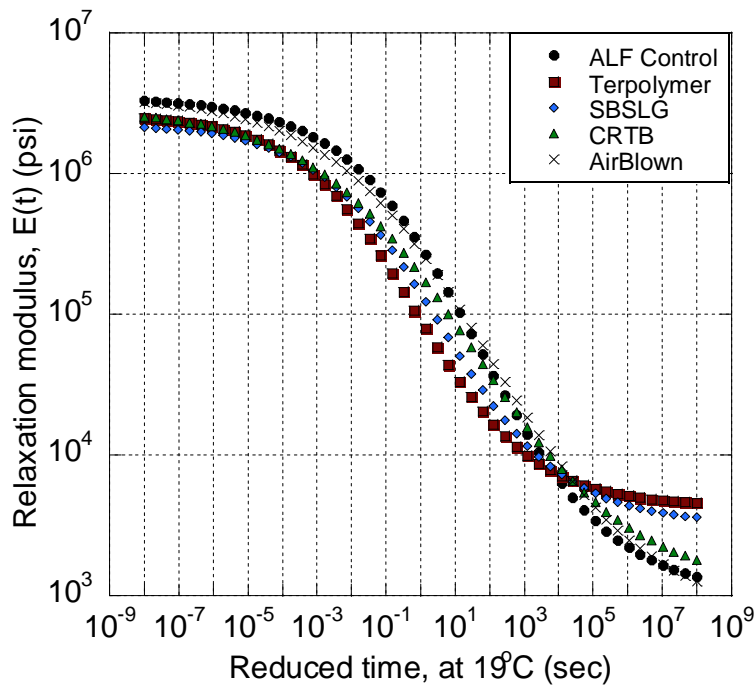


**Figure 87: Relaxation modulus master curves for the sensitivity analysis**

### 6.2 Sensitivity Analysis for Layer Thickness: 6 Inches AC Layer

The pavement properties used in the study are given in Table 27.  $E(t)$ , base modulus, and subgrade modulus were backcalculated assuming -10%, -20%, 0%, +10%, +20%, and 30% error

in pavement layer thicknesses. Results for the three case studies are presented in the following sections. The backcalculated  $E(t)$  master curves for all the mixes are presented in Appendix A.

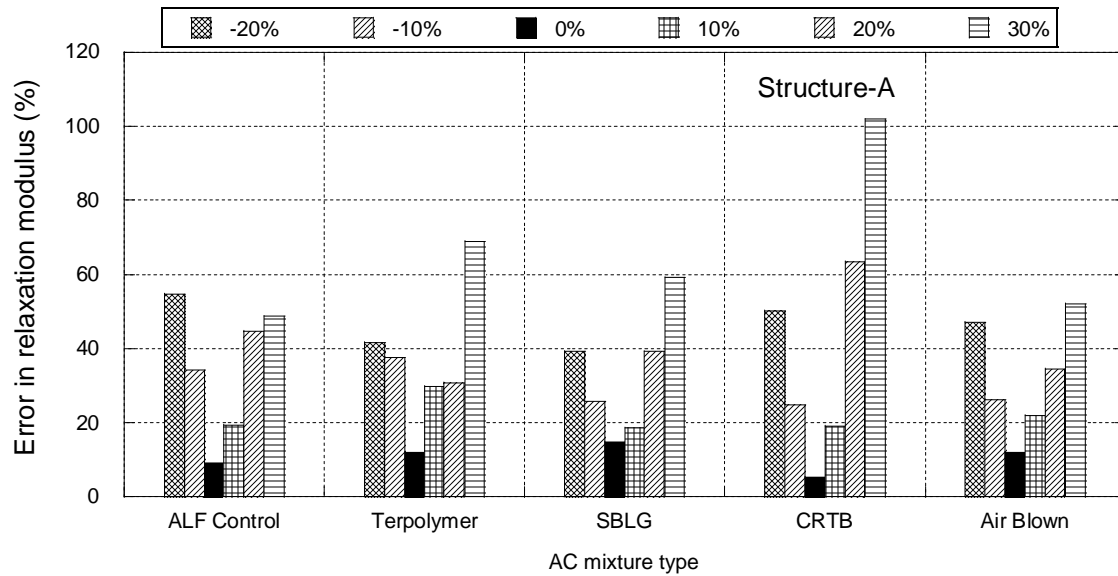
**Table 27: Pavement properties in sensitivity analysis**

Property	Structure-A	Structure-B
Design thickness	6, 12 (in)	12, 12 (in)
Poisson ratio {layer 1,2,3}	0.35, 0.4, 0.45	
$E_{unbound}$ {layer 2,3}	35000, 20000 (psi)	
E(t) sigmoid coefficients {layer 1}	5 AC mixtures: Control, Terpolymer, SBS-LG, CRTB, Air blown	
$a_T(T)$ shift factor polynomial coefficients {layer 1}		
Sensor spacing from the center of load	0, 8, 12,18,24, 36,48, 60 (in)	

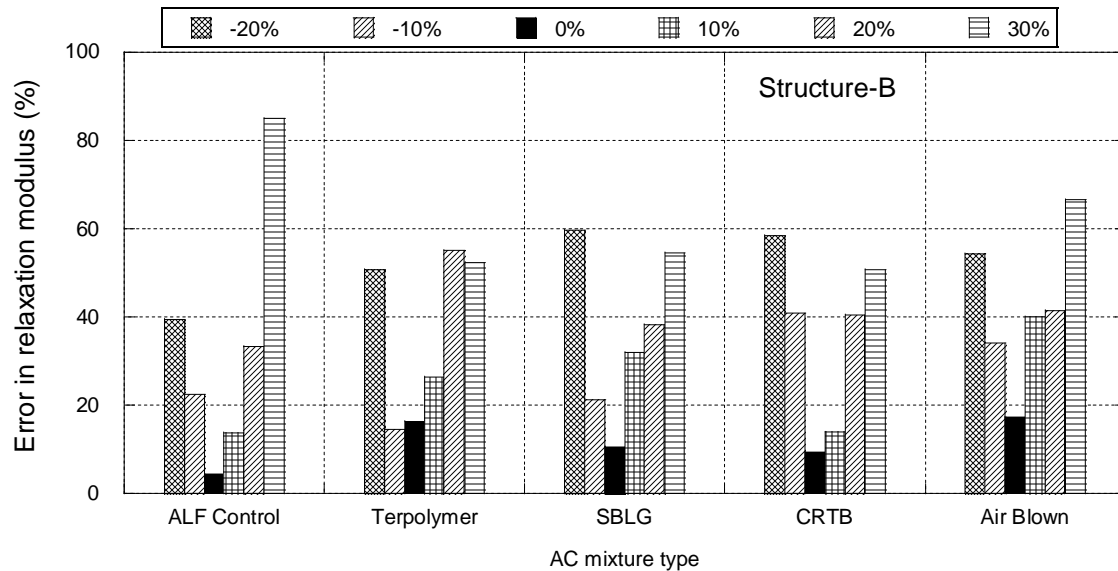
### 6.2.1 Sensitivity Analysis for AC Layer Thickness

Figure 88 and Figure 89 show error in backcalculated relaxation modulus for -10%, -20%, 0%, +10%, +20%, and +30% variation in 6 inches AC layer and 12 inches AC layer thicknesses. Error in the relaxation modulus was calculated using Equation (56). It should be noted that error corresponding to 0% thickness variation in AC layer corresponds to the case when no variation in thickness was considered, and hence represents the inherent error in the backcaulation procedure itself. It can be seen from both the figures that except for CRTB structure-B, error in the backcalculated relaxation modulus increased with increased error in AC layer thickness. Comparison of backcalculated dynamic moduli for all five HMA mixtures, for structures-A and structure-B are shown in Figure 90 and Figure 91. For comparison the backcalculated values were normalized with actual modulus values, defined as modular ratio in the figures. It can be seen from the figure that the dynamic modulus is overestimated with positive variation in AC layer thickness, were as the relaxation modulus is underestimated with negative variation in AC layer thickness. This trend was observed for the dynamic modulus at frequencies  $10^{+8}$ ,  $10^{+6}$ ,  $10^{+4}$  and  $10^0$  Hz. There was no trend observed at  $10^{-4}$  Hz and beyond.

The modular ratio for the five mixes at -20% and +30% error for frequencies greater than  $10^0$  Hz in structure-A ranged from 0.40-0.65 and 1.25-2.18 respectively. The modular ratio for the five mixes at -20% and +30% error for frequencies greater than  $10^0$  Hz in structure-B ranged from 0.35-0.65 and 0.92-2.34 respectively.



**Figure 88: Error in backcalculated relaxation modulus from variation in 6 inch AC thickness.**



**Figure 89: Error in backcalculated relaxation modulus from variation in 12 inch AC thickness.**

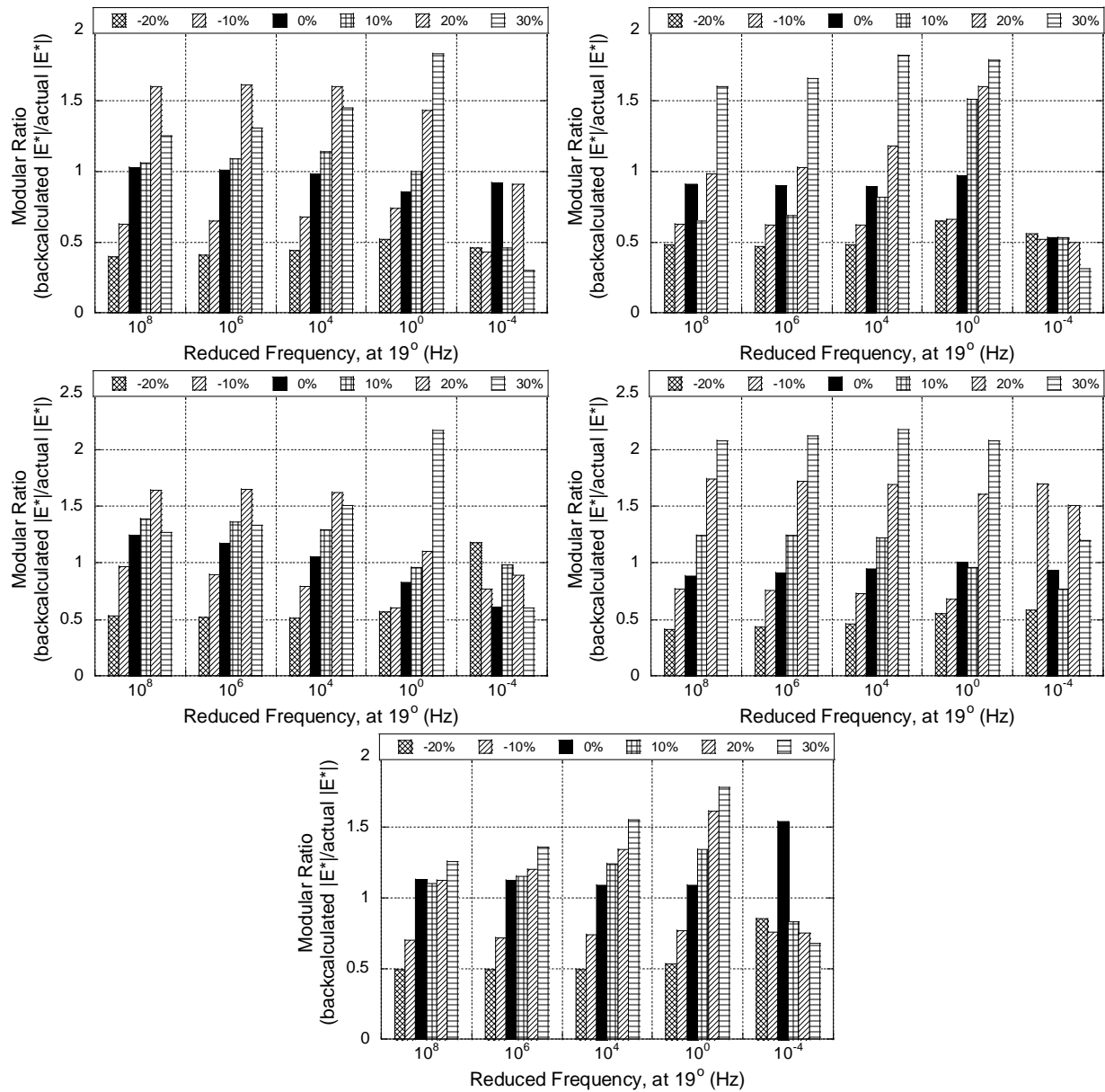


**Figure 90: Backcalculated relaxation modulus in 6 inch AC structure: Case-1 sensitivity analysis.**

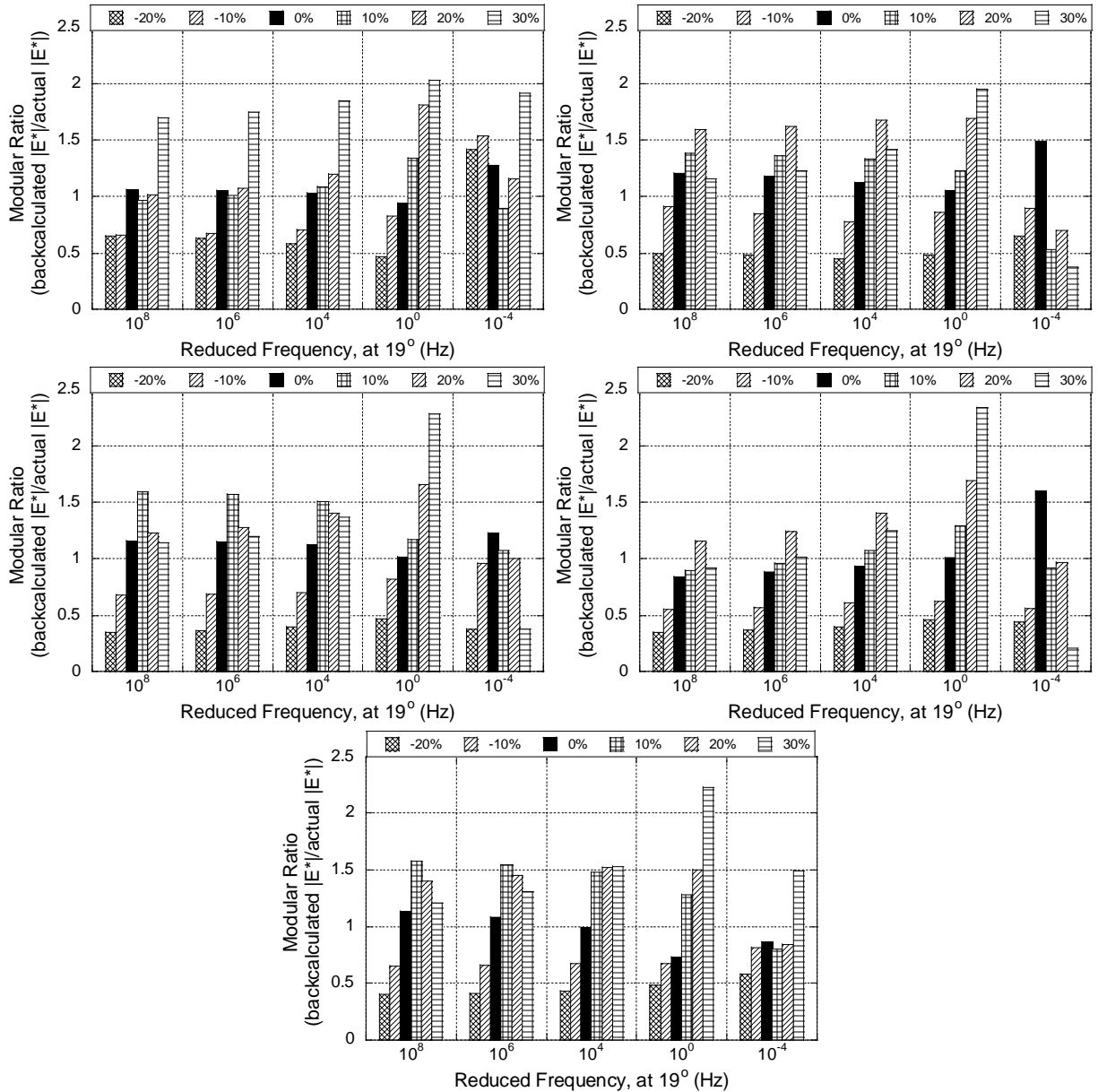


**Figure 91: Backcalculated relaxation modulus in 12 inch AC structure: Case-1 sensitivity analysis.**

### 6.2.2 Sensitivity Analysis for Base Layer Thickness

Figure 92 and Figure 93 show error in backcalculated relaxation modulus for -10%, -20%, 0%, +10%, +20%, and +30% error in base layer thickness for 6 inch AC layer and 12 inch AC layer thickness structures respectively. It should be noted that error corresponding to 0% variation in base thickness corresponds to the case when no variation in thickness was



considered, and hence represents the inherent error in the backcalculation procedure itself. It can be seen from both the figures that error in the backcalculated relaxation modulus was not significantly influenced with error in base layer thickness (compared to case-1). Comparison of backcalculated dynamic moduli for all five HMA mixtures, for structures-A (Figure 94) and structure-B (Figure 95) showed no trend with variation in base thickness.

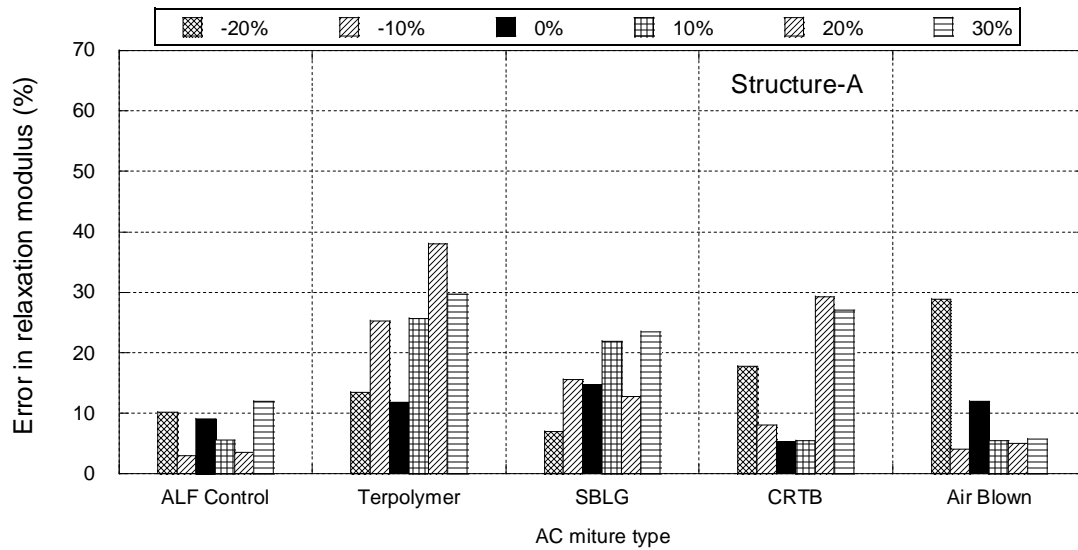


**Figure 92: Error in backcalculated relaxation modulus from variation in base thickness for 6 inch AC structure.**

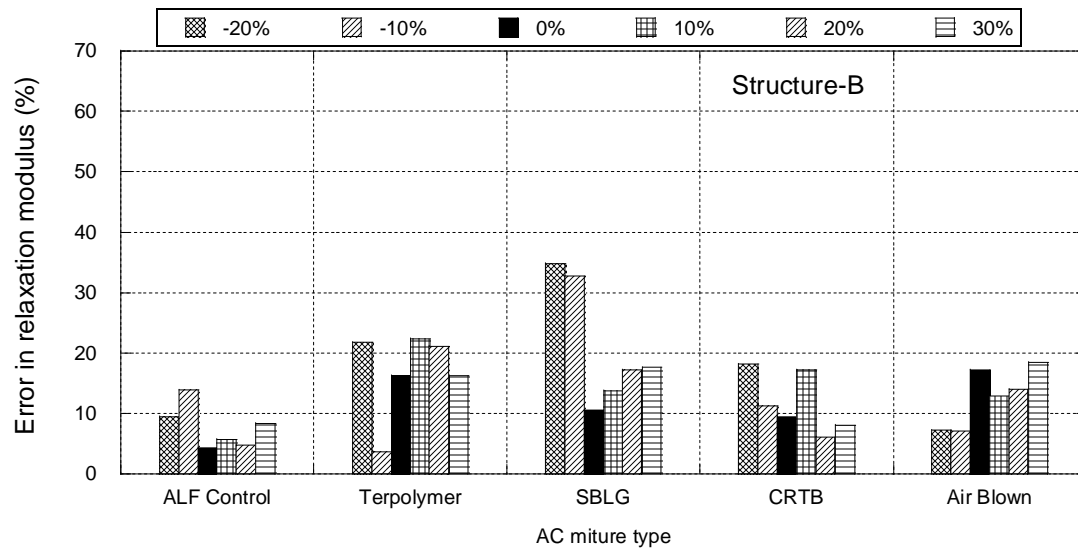


**Figure 93: Error in backcalculated relaxation modulus from variation in base thickness for 12 inch AC structure.**

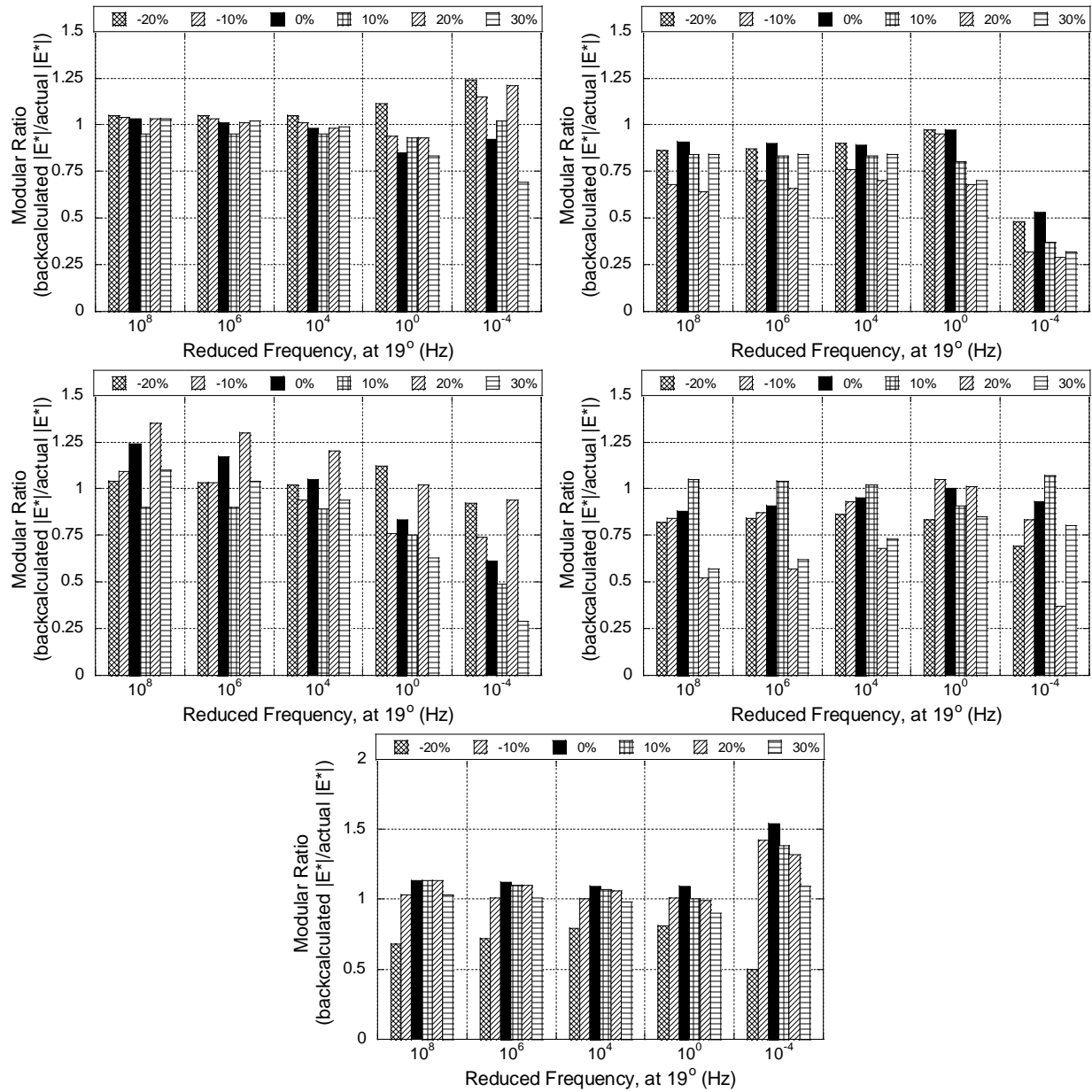


**Figure 94: Backcalculated relaxation modulus in 6 inch AC structure, case-2 sensitivity analysis.**

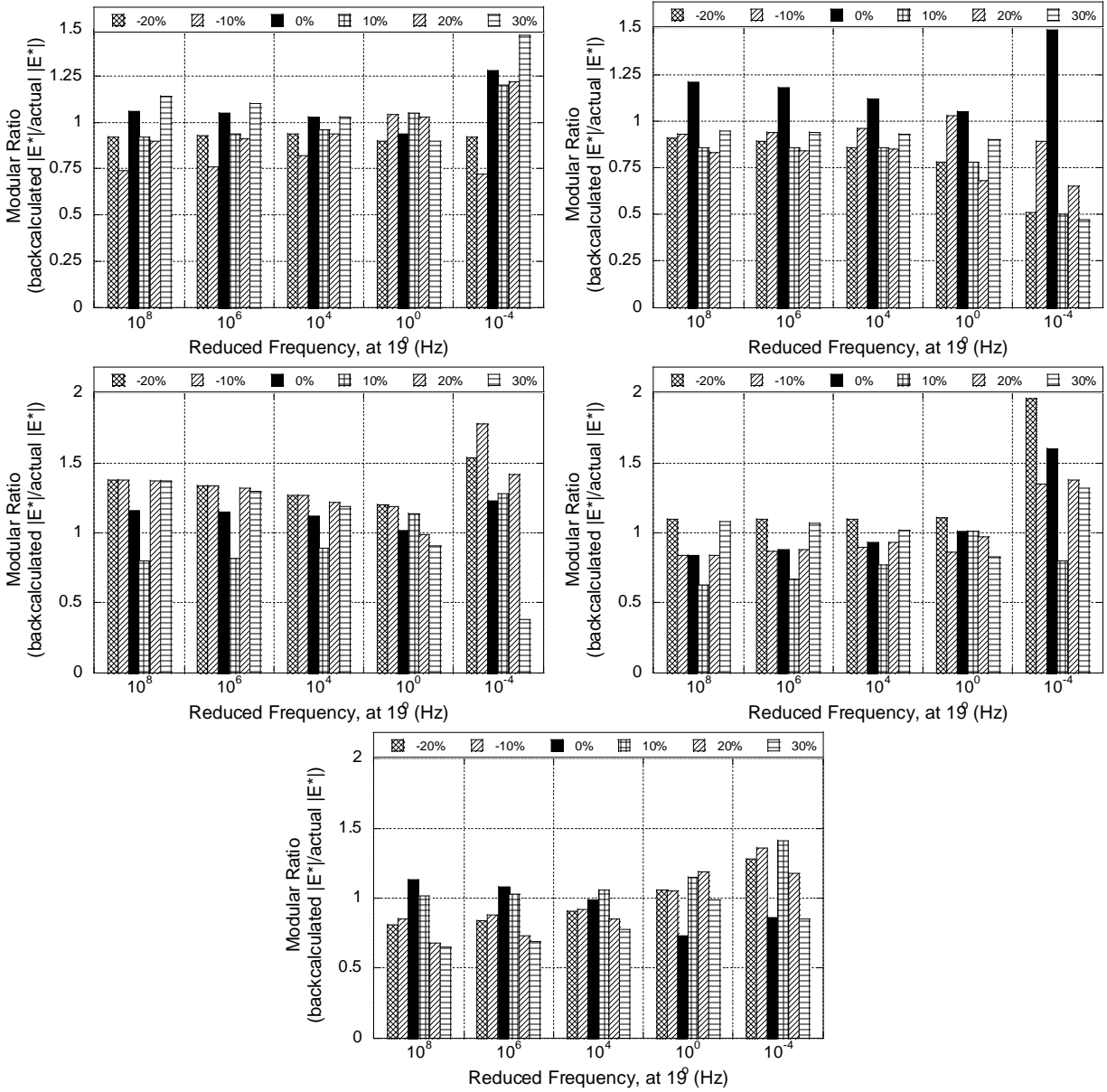
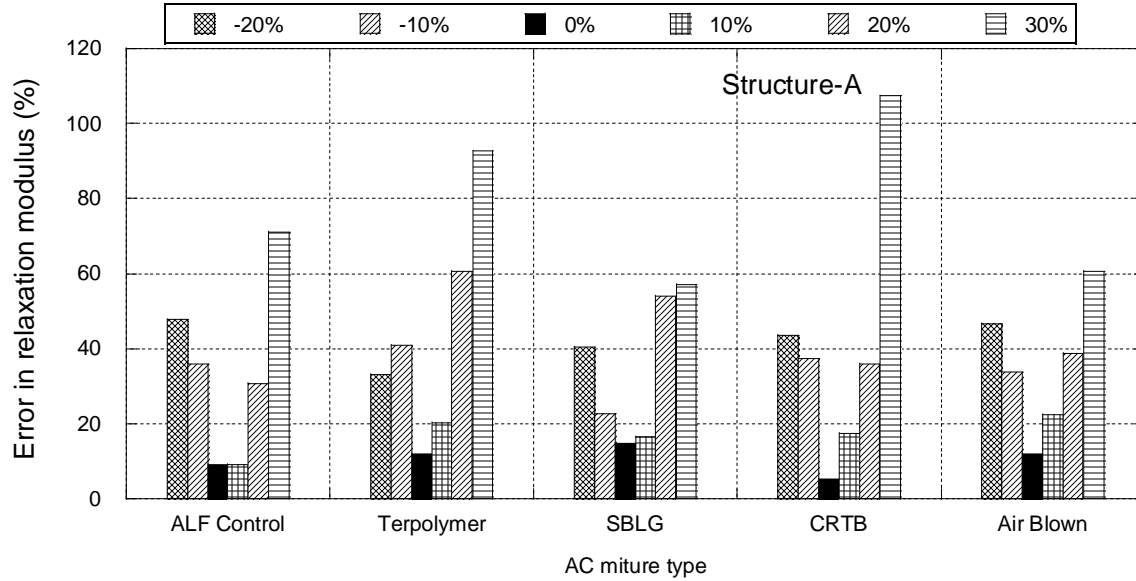


**Figure 95: Backcalculated relaxation modulus in 12 inch AC structure, case-2 sensitivity analysis.**

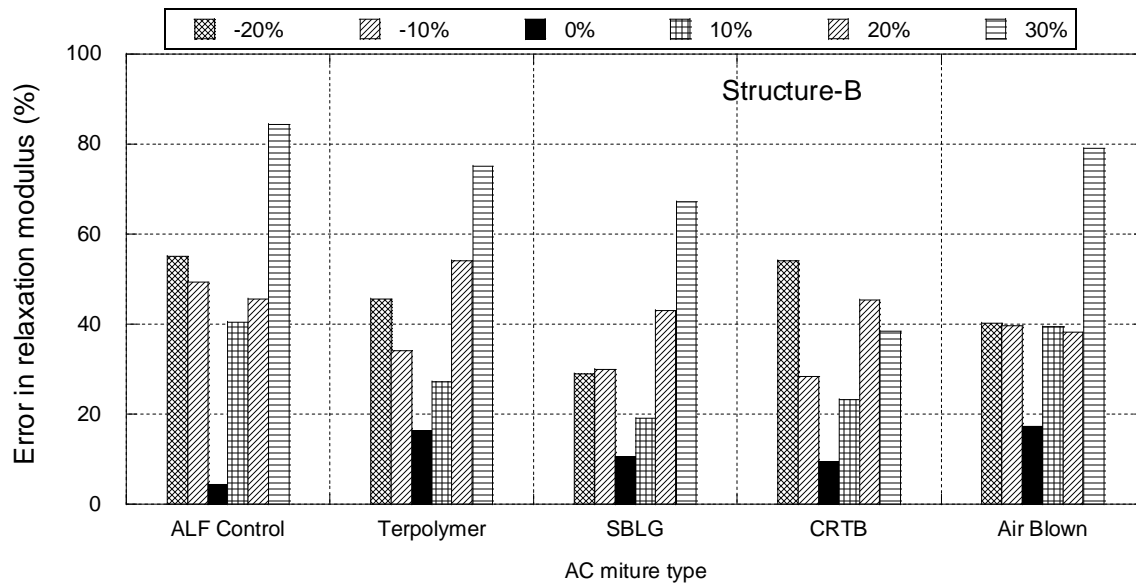
### **6.2.3 Sensitivity Analysis for Total Pavement Thickness**

Figure 96 and Figure 97 show error in backcalculated relaxation modulus for -10%, -20%, 0%, +10%, +20%, and +30% error in 6 inch and 12 inch AC layer thickness in case-3 sensitivity analysis. It can be seen from both figures that similar to case-1, error in the backcalculated relaxation modulus increased with increased variation in AC layer thickness. Comparison of backcalculated dynamic moduli for all five HMA mixtures, for structures-A and structure-B are shown in Figure 98 and Figure 99. Similar to case-1, the dynamic modulus is overestimated with positive variation in AC layer thickness, were as the relaxation modulus is underestimated with negative variation in AC layer thickness. Again this trend was observed for the dynamic modulus at frequencies  $10^{+8}$ ,  $10^{+6}$ ,  $10^{+4}$ , and  $10^0$  Hz and there was no trend observed at  $10^{-4}$  Hz and beyond.

The modular ratio for the five mixes at -20% and +30% error for frequencies greater than  $10^0$  Hz in structure-A ranged from 0.42-0.78 and 1.35-2.44 respectively. The modular ratio for the five mixes at -20% and +30% error for frequencies greater than  $10^0$  Hz in structure-B ranged from 0.31-0.93 and 0.92-2.29 respectively.



**Figure 96: Error in backcalculated relaxation modulus in 6 inch AC structure, case-3 sensitivity analysis.**



**Figure 97: Error in backcalculated relaxation modulus in 12 inch AC structure, case-3 sensitivity analysis.**

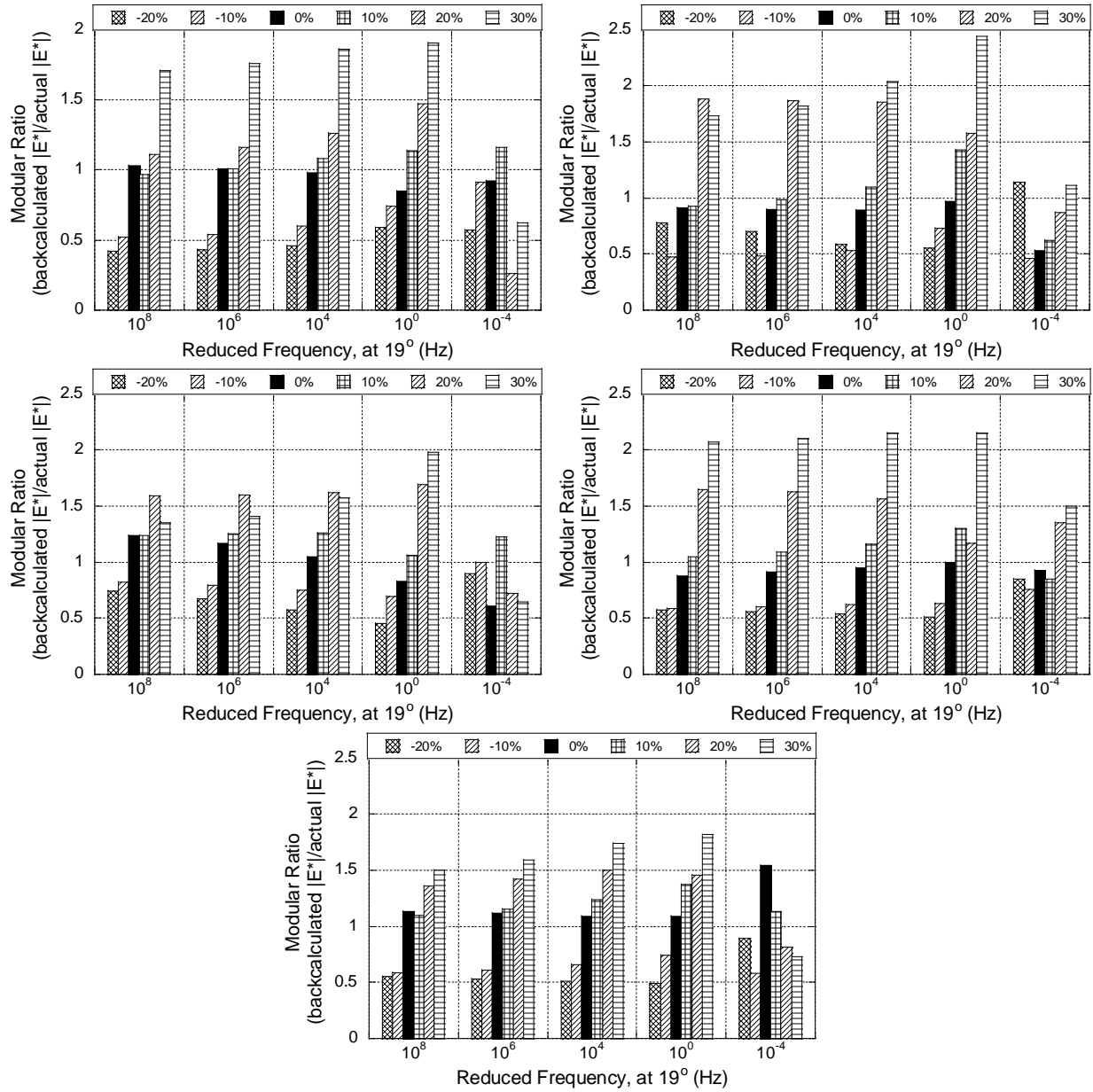


**Figure 98: Backcalculated relaxation modulus in 6 inch AC structure, case-3 sensitivity analysis.**

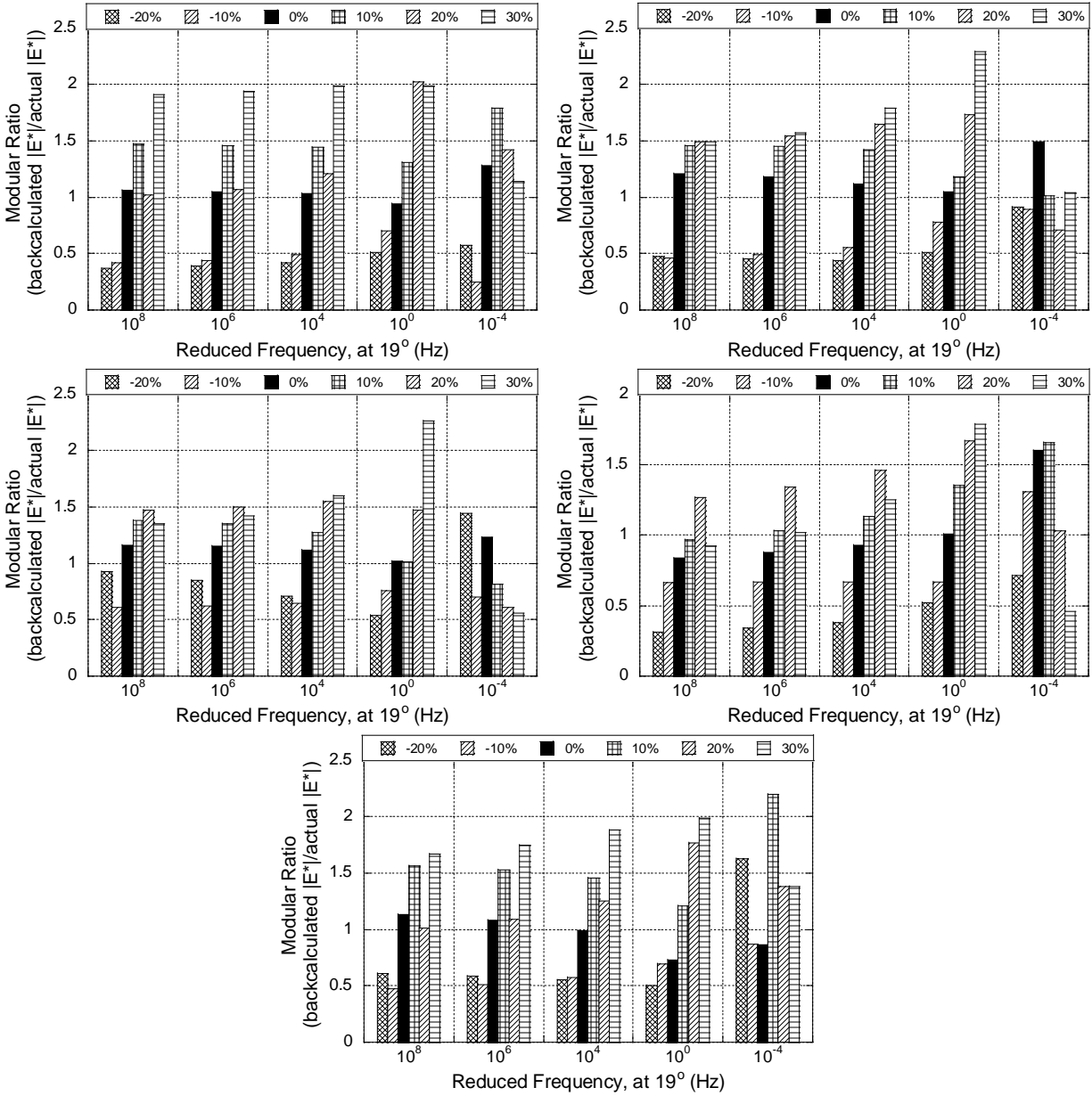


**Figure 99: Backcalculated relaxation modulus in 12 inch AC structure, case-3 sensitivity analysis.**

### 6.2.4 Summary and Discussion

Average error in backcalculated AC relaxation modulus for 6 inch and 12 inch AC structures are shown in Table 28 and Table 29 respectively. The observations in the study are similar to the observations made by Irwin et al. (1989) for elastic backcalculation. It was observed that AC layer relaxation modulus was most sensitive to variation in AC layer thickness.

As shown in Table 28 and Table 29 variation in AC thickness in case-3 was found to be more critical compared to variation in AC thickness in Case-1. This is due to the fact that, in case-3, change in AC layer thickness is compensated by thickness in base layer, keeping the overall structural thickness constant, which further underestimates AC modulus with positive variation in AC thickness and further overestimates AC modulus with negative variation in AC thickness.

**Table 28: Error in backcalculated relaxation modulus in structure-A**

%change in thickness	Error in Case-1		Error in Case-2		Error in Case-3	
	Average	Stdev	Average	Stdev	Average	Stdev
-20%	40.1	13.8	15.5	8.4	42.4	5.9
-10%	26.4	11.5	11.2	9.3	34.2	6.9
0%	10.6	3.6	10.6	3.6	10.6	3.6
10%	19.0	8.8	12.8	10.1	17.2	5.0
20%	35.7	6.4	17.8	15.3	44.0	12.7
30%	51.2	15.5	19.6	10.3	77.8	21.7

**Table 29: Error in backcalculated relaxation modulus in structure-B**

%change in thickness	Error in Case-1		Error in Case-2		Error in Case-3	
	Average	Stdev	Average	Stdev	Average	Stdev
-20%	41.5	15.5	18.3	11.0	44.8	10.8
-10%	21.7	10.7	13.7	11.3	36.2	8.6
0%	11.9	5.8	11.9	5.8	11.9	5.8
10%	24.2	8.3	14.4	6.0	29.9	9.6
20%	38.7	21.4	12.7	7.0	45.3	5.7
30%	62.8	39.8	13.8	5.1	68.8	18.1

Average error in backcalculated base modulus for 6 in and 12 in AC structure is shown in Table 30 and Table 31 respectively. It was observed that base modulus was over predicted for negative variation in thickness in all the three cases and under predicted for positive variation. Error in subgrade modulus was insignificant with variation in thickness in all the three cases. The maximum error in subgrade modulus was found to be 3%.



**Table 30: Error in backcalculated base modulus in structure-A**

%change in thickness	Error in Case-1		Error in Case-2		Error in Case-3	
	Average	Stdev	Average	Stdev	Average	Stdev
-20%	9.3	5.2	15.2	3.9	2.8	7.6
-10%	5.4	4.6	8.2	3.9	2.1	5.8
0%	3.1	5.4	3.1	5.4	3.1	5.4
10%	-11.3	10.1	-6.0	9.3	-7.3	5.8
20%	-20.6	11.3	-11.9	1.8	-14.0	13.7
30%	-32.8	9.4	-19.4	5.8	-16.7	8.2

**Table 31: Error in backcalculated base modulus in structure-B**

%change in thickness	Error in Case-1		Error in Case-2		Error in Case-3	
	Average	Stdev	Average	Stdev	Average	Stdev
-20%	20.9	3.2	13.6	9.1	21.0	1.8
-10%	21.7	3.0	7.4	6.3	16.3	3.4
0%	-4.4	15.0	-4.4	15.0	-4.4	15.0
10%	-25.3	11.1	-2.6	7.7	-19.4	7.6
20%	-37.8	2.9	-11.9	6.7	-28.9	11.6
30%	-34.2	11.9	-10.5	3.8	-32.7	12.3

## CHAPTER 7

### SUMMARY AND CONCLUSION

In an effort towards obtaining in-situ  $|E^*|$  of AC layer and linear and non-linear properties of base/subgrade, several time domain algorithms were developed. The models developed can consider temperature in AC layer as both constant (LAVA) as well as varying with depth (LAVAP). The developed model LAVAN also assumes the AC layer as a linear viscoelastic material; however, it can consider the nonlinear (stress-dependent) elastic moduli of the unbound layers. The models have been validated using Finite Element Method (FEM) based solutions.

LAVA was used to develop a genetic algorithm-based backcalculation algorithm (BACKLAVA) that is capable of backcalculating relaxation (and complex) modulus master curves as well as time-temperature shift factor coefficients of AC pavements. The algorithm uses multiple FWD drop time history data and AC layer temperature during each test. Simulated (theoretical) data showed an excellent match between the backcalculated and actual values of relaxation moduli. The algorithm was subsequently modified to incorporate FWDs at known temperature profile in the AC layer and have been referred to as BACKLAVAP, which uses a single FWD drop time history data and variation of temperature with depth of AC layer. In order to further validate the algorithm FWD test data from LTPP sections were utilized. To evaluate the backcalculation performance, laboratory creep compliance data available in the LTPP database and the  $|E^*|$  data from ANN-based software ANNACAP were compared.

The LAVAN was used to develop a genetic algorithm-based three stage backcalculation methodology (called BACKLAVAN). The study showed that FWDs run at two different

temperatures can be sufficient to compute  $|E^*|$  master curve of asphalt pavements as well as nonlinear properties of unbound layers. The BACKLAVAN algorithm was further validated using two FWD test runs at an LTPP test section. The backcalculated viscoelastic properties were compared with measured values converted from laboratory creep tests and the ANN-based software ANNACAP.

In order to be able to backcalculate the entire  $|E^*|$  master curve of the asphalt layer, accurate measurement of deflection time history from FWD is crucial. Measurement errors in the time history of the deflections may lead to significant errors. The current versions of the algorithms developed in this study are not able to consider the dynamics, i.e., the effects of wave propagation. In pavements where the bedrock is close to the surface and/or there is a shallow groundwater table, the FWD test deflection time history may exhibit significant wave propagation effects. In such cases the current version of the algorithms should not be used.

*Following conclusions can be drawn regarding the FWD data collection:*

1. Accurate measurement of FWD deflection data is crucial. As a minimum, highly accurate deflection time history at least until the end of the load pulse duration is needed for  $E(t)/|E^*|$  master curve backcalculation. The longer the duration of the deflection time history, the better.
2. The temperature of the AC layer needs to be collected during the FWD testing. Preferably temperatures at every 2" depth of AC layer should be collected.

3. Either a single FWD run on an AC with large temperature gradient or multiple FWD runs at different temperatures can be sufficient to compute  $E(t)/|E^*|$  master curve of asphalt pavements.
4. For backcalculation using multiple FWD test data, tests should be conducted at least two different temperatures, preferably  $10^{\circ}\text{C}$  or more apart. FWD data collected at a set of temperatures between  $20^{\circ}\text{C}$  and  $40^{\circ}\text{C}$  should maximize the accuracy of backcalculated  $E(t)/|E^*|$  master curve with less than 10% error.
5. For backcalculation using single FWD test data at a known AC temperature profile, FWD testing should be conducted under a temperature variation of preferably  $\pm 5^{\circ}\text{C}$  or more.
6. Study on the effect of FWD sensor data on backcalculation indicates that, the influence of the unbound layer properties increases with incorporation of data from sensors further from the load and with an increase in test temperature. Further it could be concluded that all sensors in the standard FWD configuration are needed for accurate backcalculation of viscoelastic AC layer and unbound layers.

*Following conclusions can be made for the backcalculation procedure:*

1. Viscoelastic properties of the AC layer can be obtained using a two-stage scheme. The first stage being an elastic backcalculation to determine unbound layer properties, which is followed by viscoelastic backcalculation of  $E(t)$  of the AC layer, while keeping the unbound layer properties fixed.

2. In the case of presence of considerable dynamic effects in FWD data (e.g. shallow bedrock), the algorithms (BACKLAVA/ BACKLAVAP and BACKLAVAN) should not be used.
3. For the genetic algorithm-based backcalculation procedures, following population and generation sizes are recommended:
  - (i) BACKLAVA model, using a set of FWD tests run at different (but constant) asphalt layer temperatures: population size = 70 and generations = 15.
  - (ii) BACKLAVAP model, using a single FWD test with known AC temperature profile: population size = 300 and generation 15.
  - (iii) BACKLAVAN (nonlinear) model, using FWD tests run at different (but constant) asphalt layer temperatures: population size = 100 and generations = 15.

*Following conclusions can be drawn from field backcalculation study:*

1. For in-service pavement, AC relaxation modulus ages with time, which is reflected as stiffening of the dynamic modulus at high frequencies. However, this was not observed at lower frequencies.
2. Very limited data was available for analyzing the proposed procedure. More research is needed for a comprehensive conclusion.

*Following conclusions can be drawn from the sensitivity analysis:*

1. Backcalculated AC layer relaxation modulus is most influenced by variation in AC layer thickness.

2. Backcalculated relaxation modulus is not significantly influenced with error in base layer thickness.
3. Subgrade modulus is least affected by variation in AC or base thickness. The maximum error in subgrade modulus was found to be 3%.

## **APPENDIX**

## APPENDIX

### *Sensitivity Analysis for AC Layer Thickness*

Backcalculated relaxation moduli for all the five HMA mixtures, for the structure-A and structure-B are shown in Figure 100 and Figure 101.

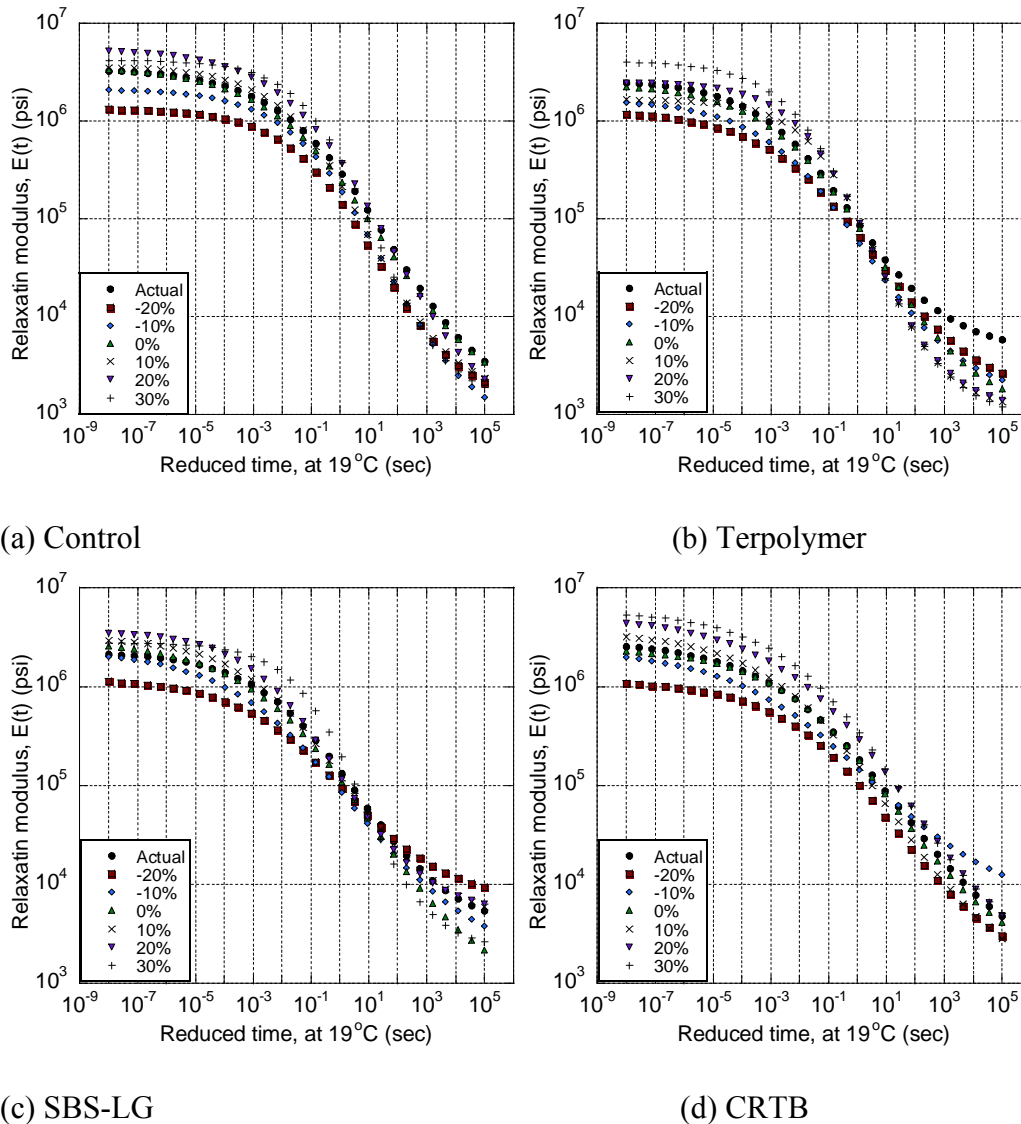
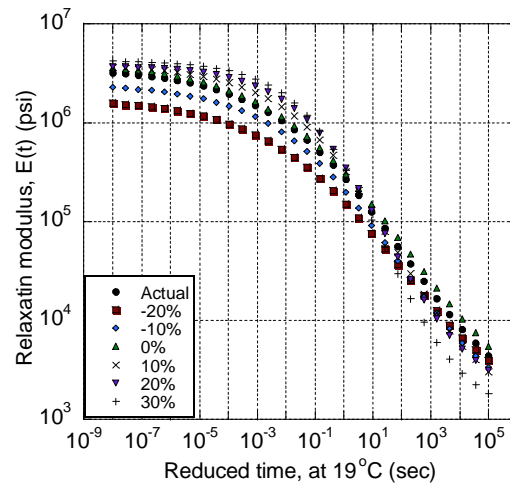


**Figure 100: Backcalculated relaxation modulus for structure-A: Case-1 sensitivity analysis.**



Figure 100 (cont'd)



(e) Air blown

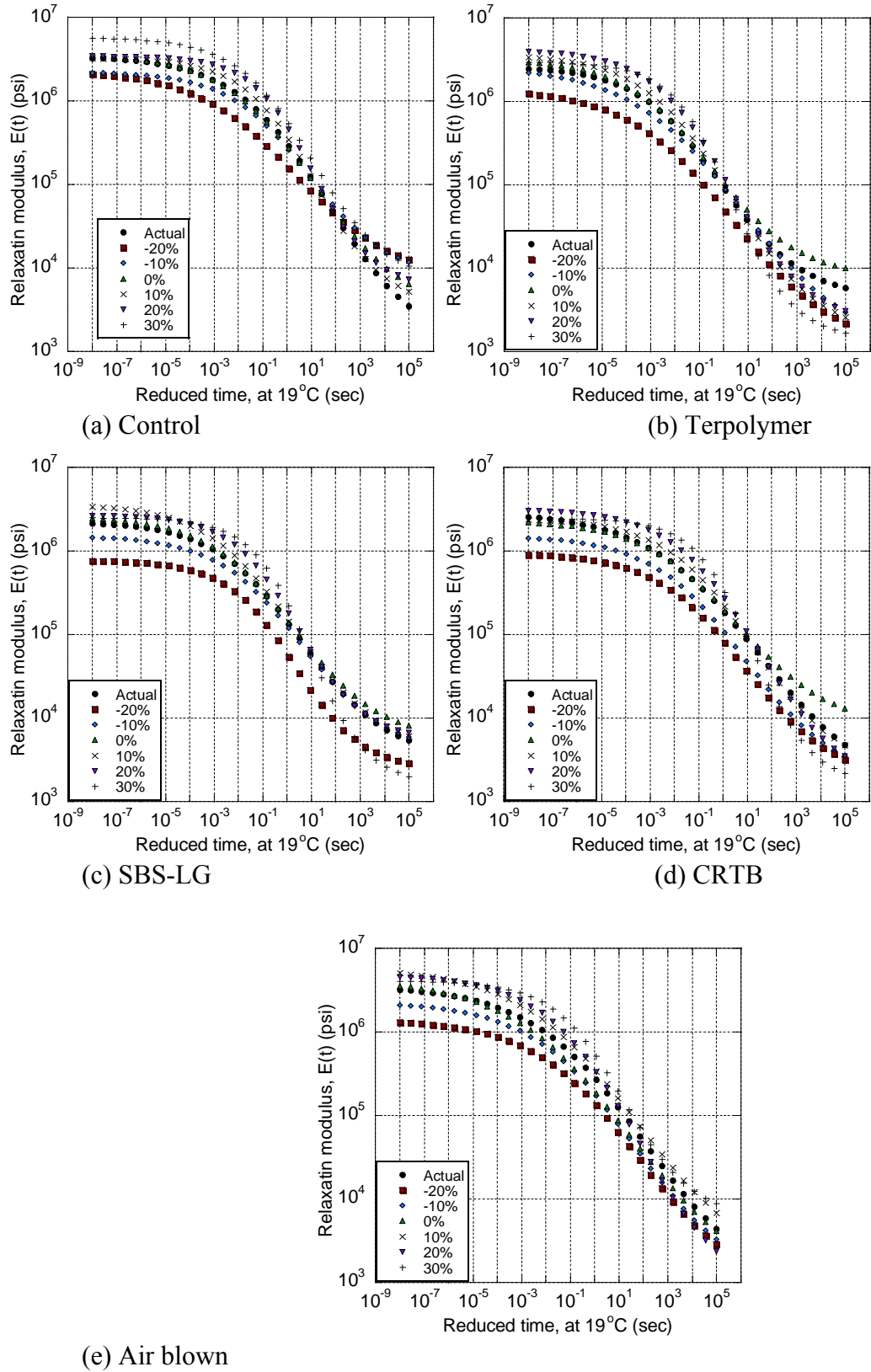
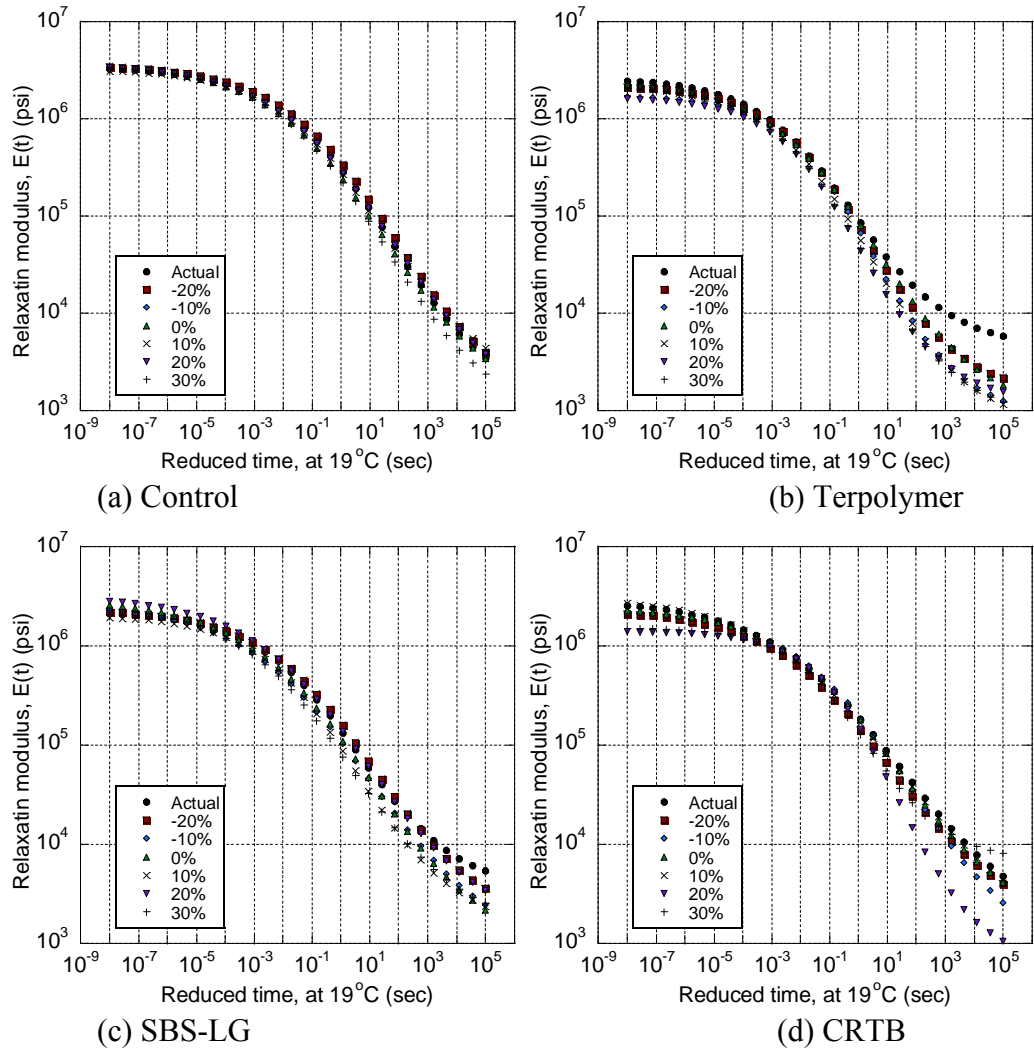


Figure 101: Backcalculated relaxation modulus for structure-B: Case-1 sensitivity analysis.

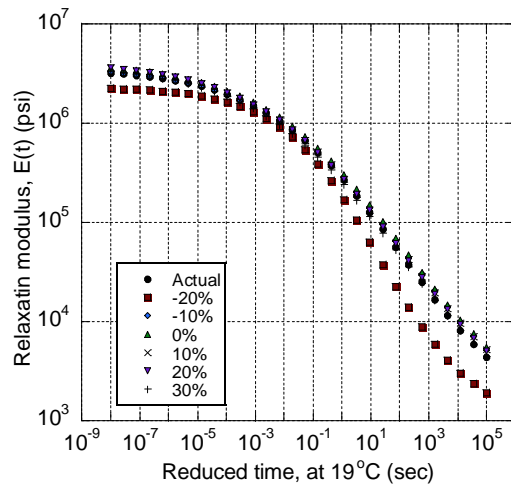
*Sensitivity analysis for Base layer thickness*

Backcalculated relaxation moduli for all the five HMA mixtures, for the structure-A and structure-B are shown in Figure 102 and Figure 103.

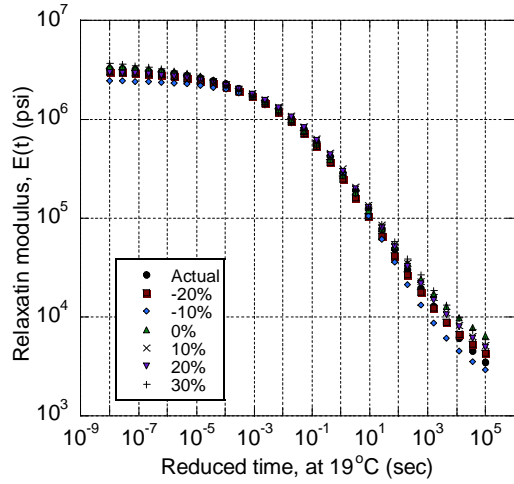


**Figure 102: Backcalculated relaxation modulus for structure-A: case-2 sensitivity analysis.**

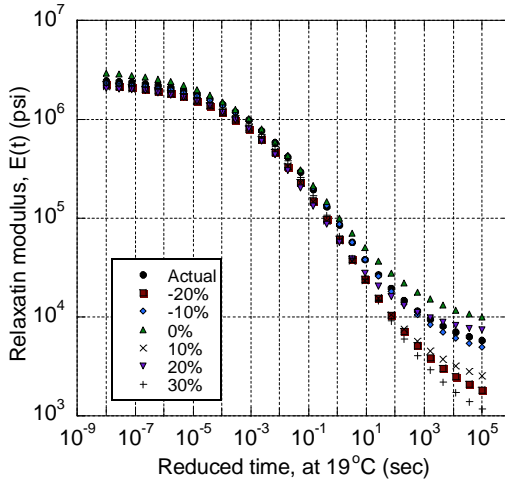
Figure 102 (cont'd)



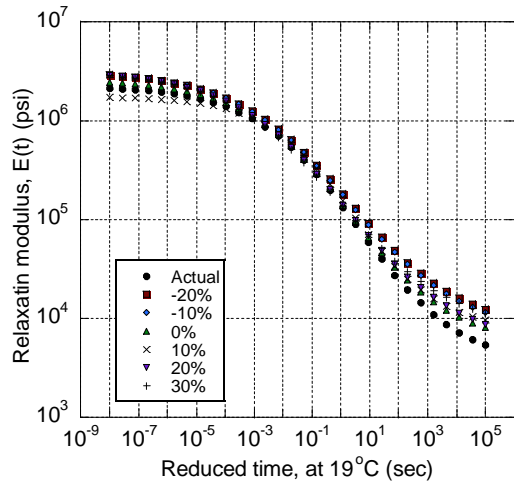
(e) Air blown



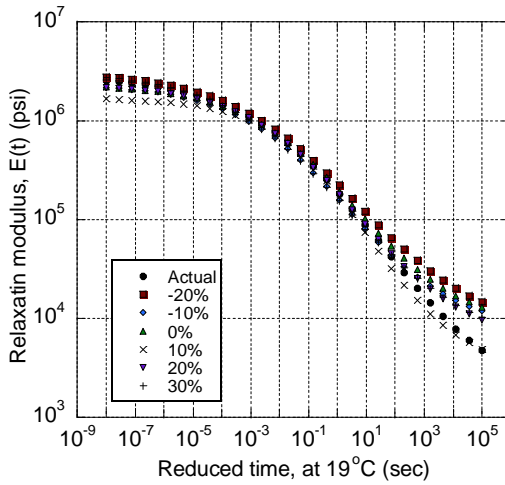
(a) Control



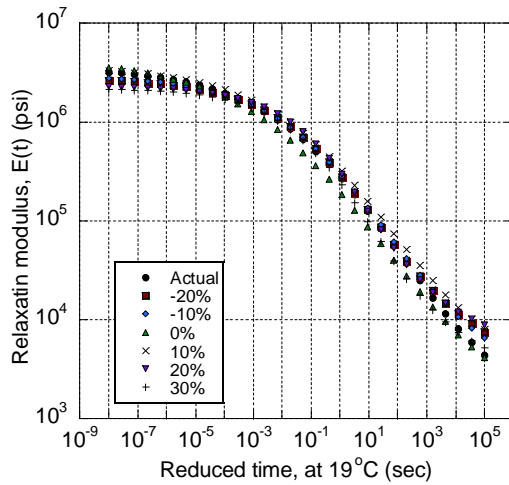
(b) Terpolymer



(c) SBS-LG



(d) CRTB



(e) Air blown

Figure 103: Backcalculated relaxation modulus for structure-B: case-2 sensitivity analysis.

*Sensitivity analysis for total layer thickness*

Backcalculated relaxation moduli for all the five HMA mixtures, for the structure-A and structure-B are shown in Figure 104 and Figure 105.

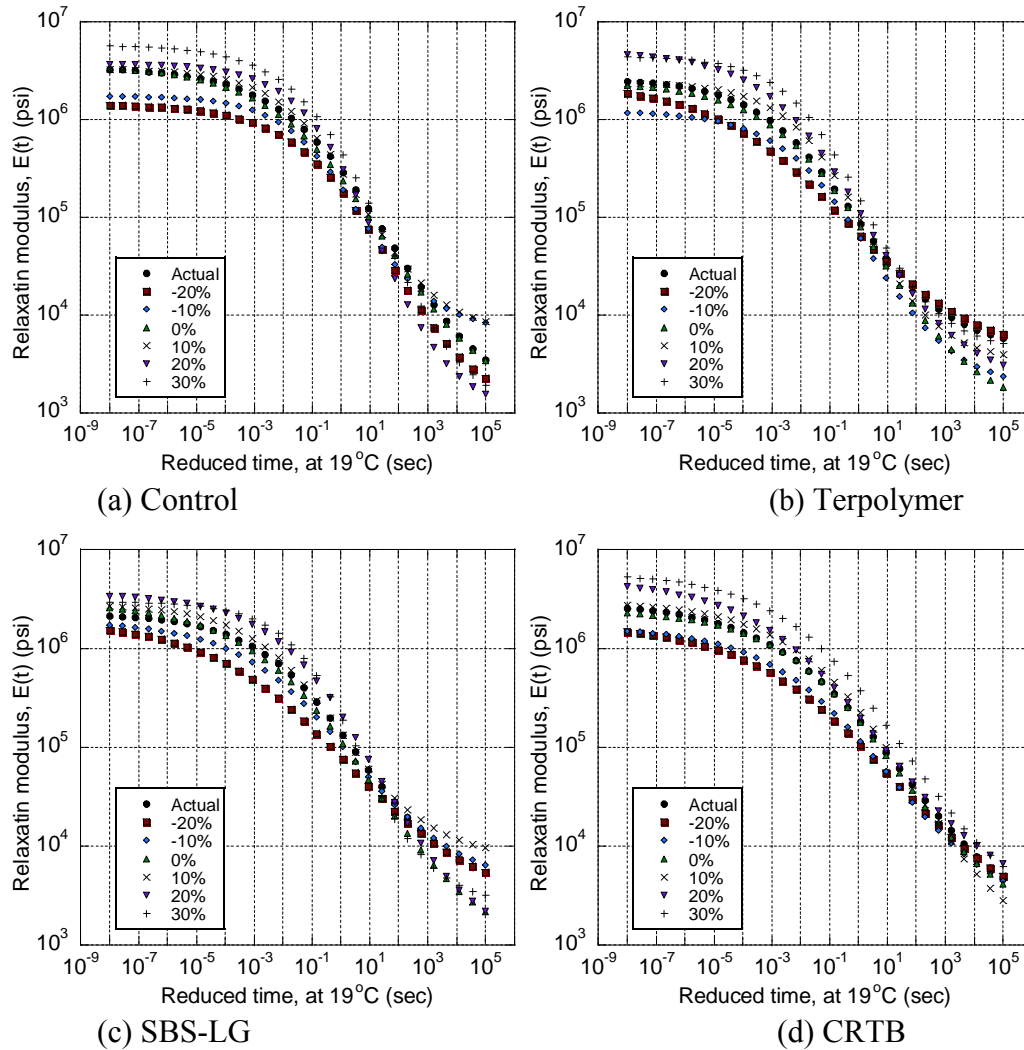
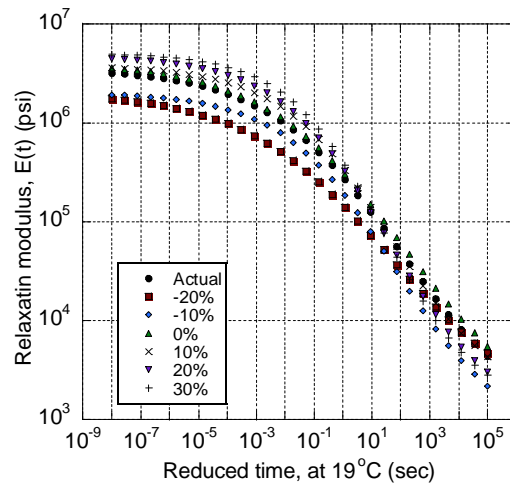
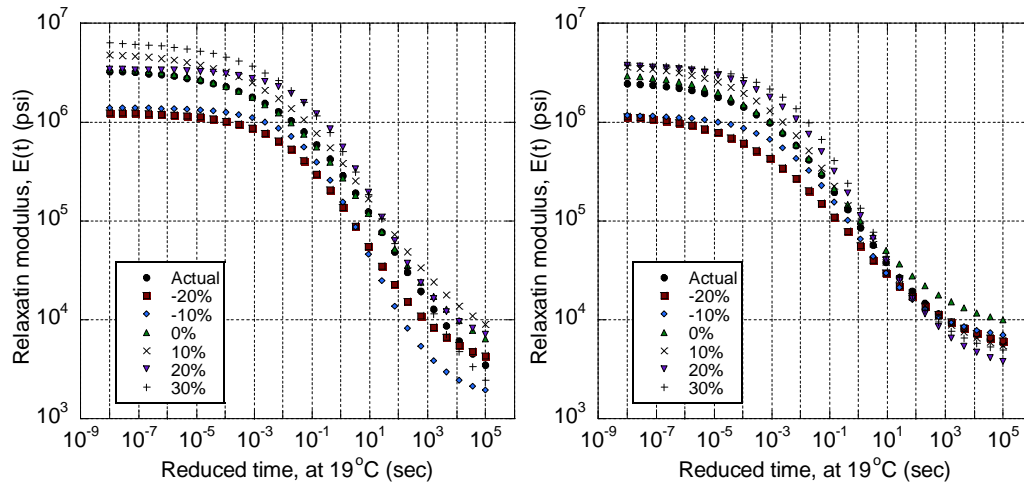


**Figure 104: Backcalculated relaxation modulus for structure-A, case-3 sensitivity analysis.**

Figure 104 (cont'd)

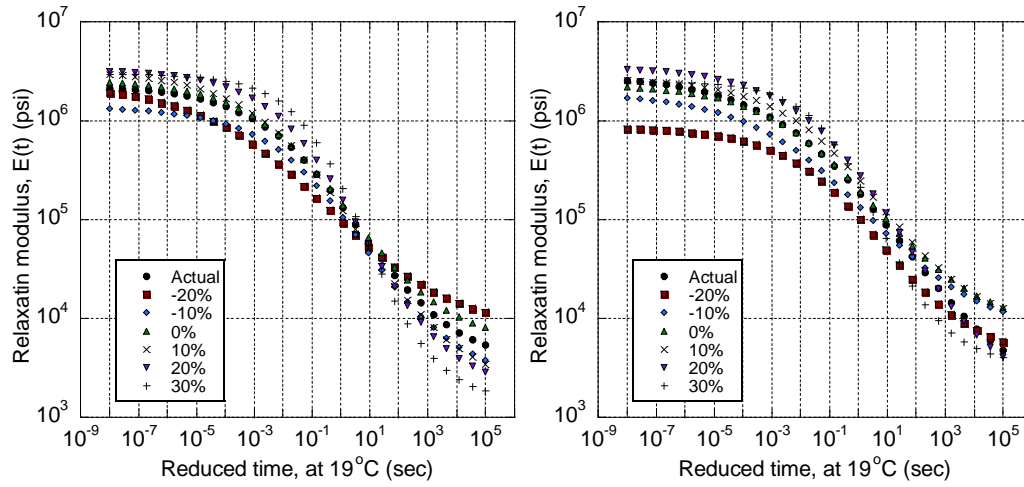


(e) Air blown



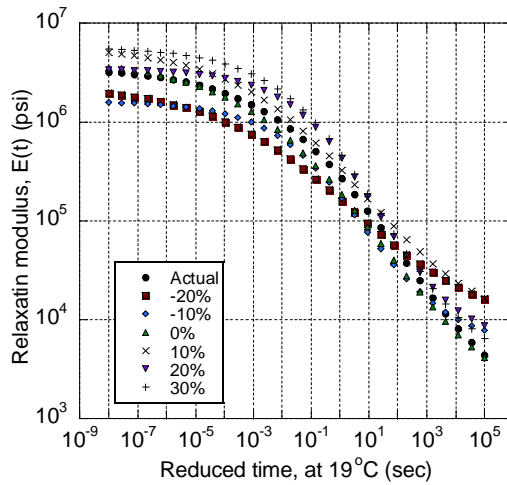
(a) Control

(b) Terpolymer



(c) SBS-LG

(d) CRTB



(e) Air blown

Figure 105: Backcalculated relaxation modulus for structure-B, case-3 sensitivity analysis.



## **BIBLIOGRAPHY**

## BIBLIOGRAPHY

- AASHTO (1993). "AASHTO Guide for Design of Pavement Structures." American Association of State and Highway Transportation Officials. Washington, D. C.
- AASHTO R30 – 02. (2008). "Standard Practice for Mixture Conditioning of Hot-Mix Asphalt (HMA)". Washington, D.C.
- ABAQUS. (2011). "Abaqus analysis user's Manual." version 6.11.
- Alkasawneh, W., Pan, E., Han, F., Zhu, R., and Green, R. (2007). "Effect of Temperature Variation on Pavement Response using 3D Multilayered Elastic Analysis." *International Journal of Pavement Engineering*, Vol. 8, No. 3, pp. 203-212.
- Al-Khoury, R., Kasbergen, C., Scarpus, A., and Blaauwendraad, J. (2001). "Spectral Element Technique for Efficient Parameter Identification of Layered Media. Part II: Inverse calculation." *Int. J. of Solids and Struct.*, Vol. 38, pp. 8753-8772.
- Al-Khoury, R., Scarpus, A., Kasbergen, C., and Blaauwendraad, J. (2002). "Spectral Element Technique for Efficient Parameter Identification of Layered Media. Part III: Viscoelastic Aspects." *Int. J. of Solids and Struct.*, Vol. 39, pp. 2189-2201.
- Alksawneh, W. (2007). "Backcalculation of Pavement Moduli Using Genetic Algorithms." PhD Thesis, The University of Akron.
- Al-Qadi, I., Wei, X., and Mostafa, E. (2008). "Frequency Determination from Vehicular Loading Time Pulse to Predict Appropriate Complex Modulus in MEPDG." *Journal of the Association of Asphalt Paving Technologists*, Vol.77, pp. 739-772.
- Anderson, M. (1989). "A Data Base Method for Backcalculation of Composite Pavement Layer Moduli." *Nondestructive Testing of Pavements and Backcalculation of Moduli*, ASTM STP 1026, A. J. Bush III and G. Y. Baladi, Eds., American Society for Testing and Materials, Philadelphia, pp. 201-216.
- Appea, A. K. (2003). "Validation of FWD Testing Results At The Virginia Smart Road: Theoretically and by Instrument Responses." PhD Thesis, Virginia Polytechnic Institute and State University.
- Asphalt Institute (AI). (1999). "Thickness design-Asphalt pavements for highways and streets." 9th Ed., Manual Series No.1, Lexington.
- Austroroads. (2004). "Pavement design." Australian Department of Transportation, Sydney, Australia.
- Bell, C. A., Wieder, A. J., and Fellin, M. J. (1994). "Laboratory Aging of Asphalt-Aggregate Mixtures: Field Validation." SHRP-A-390, Strategic Highway Research Program, National Research Council, Washington, D.C.

Bremermann, H. J. (1958). "The evolution of intelligence. The nervous system as a model of its environment." Technical report, no.1, contract no. 477(17), Dept. Mathematics, Univ. Washington, Seattle.

Briggs, R., Scullion, T., Maser, K. (1992). "Asphalt thickness variation on Texas Strategic Highway Research Program Sections and Effect on Backcalculation Moduli." Transportation Research Record 1377, National Research Council, Washington, D.C.

Burmister, D. M. (1943). "The theory of stress and displacements in layered systems and applications to the design of airport runways." Highway Research Board, Proc. Annual Meet., Vol. 23, pp. 126–144.

Burmister, D. M. (1945a). "The general theory of stress and displacements in layered soil systems. I." Journal of Applied Physics, Vol. 16(2), pp. 89–94.

Burmister, D. M. (1945b). "The general theory of stress and displacements in layered soil systems. II." Journal of Applied Physics, Vol. 16(3), pp. 126–127.

Burmister, D. M. (1945c). "The general theory of stress and displacements in layered soil systems. III." Journal of Applied Physics, Vol. 16(5), pp. 296–302.

Bush, A. J. (1985). "Computer Program BISDEF." US Army Corps of Engineer Waterways Experiment Station, Vicksburg, MS.

Chatti, K. (2004) "Use of Dynamic Analysis for Interpreting Pavement Response in Falling Weight Deflectometer Testing." Material Evaluation, Vol. 62, No. 7, pp. 764-774.

Chatti, K., Ji, Y., and Harichandran, R. S. (2006). "Dynamic Backcalculation of Pavement Layer Parameters Using Frequency and Time Domain Methods." Proc., 10<sup>th</sup> International Conference on Asphalt Pavements, Vol. 3, Canada, pp. 5-14.

Chatti, K., Kutay, E., Lajnef, N., Zaabar, I., Varma, S., and Lee, S. (2014). "Enhanced Analysis of Falling Weight Deflectometer Data for use with Mechanistic-Empirical Flexible Pavement Design and Analysis and Recommendations for Improvements to Falling Weight Deflectometer." FHWA Report, Federal Highway Administration, Washington, DC.

Chen, D., Bilyeu, J., Lin, H., and Murphy, M. (2000). "Temperature correction on falling weight deflectometer measurements." In Transportation Research Record: Journal of the Transportation Research Board, 1716, Transportation Research Board of the National Academies, pp. 30-39.

Chou, Y. J., and Lytton, R. L. (1991). "Accuracy and Consistency of Backcalculated Pavement Layer Moduli." Transportation Research Record 1022, TRB, National Research Council, Washington, D.C., pp. 1-7.

De Jong, D. L., Peutz, M. G. F., and Korswagen, A. R. (1979). "Computer program BISAR, layered systems under normal and tangential surface loads." Koninklijke-Shell Laboratorium, Amsterdam, Netherlands.

Dickson, E. J. (1980). "The hardening of Middle East Petroleum Asphalts in Pavement Surfacing." *Journal of the Association of Asphalt Paving Technologists*, Vol. 49, pp. 30-63.

El-Mihoub T., Hopgood A., Nolle, L., and Battersby A. (2006). "Hybrid genetic algorithms: A review." *Engineering Letters*, 13, pp. 124-137.

Farrar, M., Harnsberger, M., Thomas, K., and Wisler, W. (2006). "Evaluation of oxidation in asphalt pavement test sections after four years of service", *Proceedings of the international conference on perpetual pavement*, Columbus, Ohio.

Fogel L. J. (1962). "Autonomous automata." *Ind Res* 4:14-19.

Fogel L. J., Owens A. J., and Walsh M. J. (1966). "Artificial intelligence through simulated evolution." Wiley, New York.

Foinquinos, R., Roesset, J. M., and Stokoe, K. H. (1995). "Response of Pavement Systems to Dynamic Loads Imposed by Nondestructive Tests." *Transportation Research Record* 1504, pp. 57-67.

Fung, Y. C. (1996). "Biomechanics mechanical properties of living tissues." 2<sup>nd</sup> edition, Springer, New York.

Fwa, T. F., Tan C. Y., and Chan, W. T. (1997). "Backcalculation analysis of Pavement-Layer Moduli Using Genetic Algorithms." *Transportation Research Record*, 1570, pp. 134- 142.

Gibson, N., Qi, X., Shenoy, A., Al-Khateeb, G., Kutay, M. E., Andriescu, A., Stuart, K., Youtcheff, J., Harman, T. (2012). "Performance Testing for Superpave and Structural Validation." *Federal Highway Administration Publication*, FHWA-HRT-11-045.

Goldberg, D. E. (1989). "Genetic Algorithms in Search, Optimization, and Machine Learning." Addison-Wesley.

Gopalakrishnan, K., Thompson, M. R., and Manik, A. (2006). "Rapid Finite-Element Based Airport Pavement Moduli Solutions using Neural Networks." *International Journal of Computational Intelligence*. Vol. 3, No. 1. World Enformatika Society.

Grosan C., and Abraham A. "Hybrid evolutionary algorithms: Methodologies, Architectures, and Reviews." *Hybrid Evolutionary Algorithms Studies in Computational Intelligence*. Vol. 75, 2007, pp. 1-17.

Gucunski, N., Rascoe, C., and Maher, A. (2008). "New Jersey Department of Transportation" Report no 166-RU9309.

Harichandran, R. S., Baladi, G. Y., and Yeh, M. S. (1989). "MICH-PAVE user's manual, Final Report." FHWA-MI-RD-89-023, Department of Civil and Environmental Engineering, Michigan State University, East Lansing, MI.

Harichandran, S., Mahmood, T., Raab, R., and Baladi, G. (1993). "Modified Newton Algorithm for Backcalculation of Pavement Layer Properties." *Transportation Research Record*, 1384, pp. 15-22.

Hermansson, A. (2001). "Mathematical model for calculation of pavement temperatures comparison of calculated and measured temperatures." *Transportation Research Record: Journal of the Transportation Research Board*, 1764, pp. 180-188.

Hicks, R. G., and Monismith, C. L. (1971). "Factors influencing the resilient properties of granular materials." *Highway Research Record*, Vol. 345, pp. 15-31.

Hjelmstad, K. D., and Taciroglu, E. (2000). "Analysis and implementation of resilient modulus models for granular solids." *Journal of Engineering Mechanics*, Vol. 126 (8), pp. 821-830.

Holland, J. H. (1975). "Adaptation in natural and artificial systems." Ann Arbor: The University of Michigan Press.

Horak, E. (1987). "The Use of Surface Deflection Basin Measurements in the Mechanistic Analysis of Flexible Pavements." *Proceedings, Sixth International Conference on Structural Design of Asphalt Pavements, Volume I*. University of Michigan, Ann Arbor, MI.

Houston, W., Mirza, M., Zapata, C., and Raghavendra, S. (2005). "Environmental effects in pavement mix and structural design systems." NCHRP web-only document 113, NCHRP Project 9-23.

Huang, Y. H. (2004). "Pavement analysis and design." Second Edition, Prentice-Hall.

Indian Roads Congress (IRC). (2001). "Guidelines for the design of flexible pavements." IRC: 37-2001, 2nd Revision, New Delhi, India.

Irwin, H., Yang, W., and Stubstad, R. (1989). "Deflection reading accuracy and layer thickness accuracy in backcalculation of pavement layer moduli" *Nondestructive testing of pavements and backcalculation of pavement layer moduli*, American Society for Testing and Materials, ASTM STP 1026, Philadelphia, pp. 229-224.

Irwin, L. H. (1994). "Instruction Guide for Backcalculation and The Use of MODCOMP." CLRP Publication No. 94-10, Cornell Univ., Local Road Program, NY.

Jamrah, A., Kutay, M. E., and Ozturk, H. I. (2014) "Characterization of Asphalt Materials Common to Michigan in Support of the Implementation of the Mechanistic-Empirical Pavement Design Guide." *Proceedings of 93rd Annual Transportation Research Board Conference*, Washington, D.C., January 12-16.

Ji, Y. (2005). "Frequency and Time domain Backcalculation of Flexible Pavement Layer Parameters" Michigan State University, Department of Civil and Environmental Engineering, Ph.D. thesis.

- Jung, S. (2006). "The effects of asphalt binder oxidation on hot mix asphalt concrete mixture rheology and fatigue performance." Phd Thesis, Chemical Engineering, Texas A&M University.
- Khazanovich, L., and Roesler, J. (1997). "DIPLOBACK: neural-network-based backcalculation program for composite pavements." Transportation Research Board, 1570 pp. 143-150.
- Kim, M., Tutumluer, E., and Know, J. (2009). "Nonlinear pavement foundation modeling for three-dimensional finite-element analysis of flexible pavements." International Journal of Geomechanics, Vol 9(5), pp. 195-208.
- Kim, Y. R. (2009). "Modeling of Asphalt Concrete." 1<sup>st</sup> ed., McGraw Hill, ASCE press.
- Kim, Y. R., Underwood, B., Sakhaei, F., Jackson, N., and Puccinelli, J. (2011). "LTPP Computed Parameters: Dynamic Modulus." FHWA-HRT-10-035, U.S. Department of Transportation, McLean, VA 22101-2296.
- Kutay, M.E., Chatti, K. and Lei, L. (2011) "Backcalculation of Dynamic Modulus from FWD Deflection Data." Transportation Research Record: Journal of the Transportation Research Board, 2227, Vol. 3, pp. 87-96.
- Lagarias, J.C., Reeds, J. A., Wright, M. H., and Wright, P. E. (1998). "Convergence Properties of the Nelder-Mead Simplex Method in Low Dimensions." SIAM Journal of Optimization, Vol. 9 Number 1, pp. 112-147.
- Leaderman, H. (1943). "Elastic and Creep Properties of Filamentous Materials and other Higher Polymers." The Textile Foundation, Washington, DC.
- Lee, H. (2014). "Viscowave-a new solution for viscoelastic wave propagation of layered structures subjected to an impact load." International Journal of Pavement Engineering, Vol. 15, No. 6, pp. 542-557.
- Lei, L. (2011). "Backcalculation of Asphalt Concrete Complex Modulus Curve by Layered Viscoelastic Solution." PhD Dissertation, Michigan State University.
- Levenberg, E. (2008). "Validation of NCAT Structural Test Track Experiment using INDOT APT Facility." Final Report, North Central Superpave Center, Joint Transportation Research Program Project No. C-36-31R SPR-2813, Purdue University.
- Levenberg, E. (2013). "Inverse Analysis of Viscoelastic Pavement Properties using Data from Embedded Instrumentation." International Journal for Numerical and Analytical Methods in Geomechanics, Vol. 37, pp. 1016-1033.
- Losa, M. (2002). "The influence of Asphalt Pavement Layer Properties on Vibration Transmission." Int. J. of Pavements, Vol. 1, No.1, pp. 67-76.

Lukanen E., Stubstad, R., and Briggs, R. (2000). "Temperature predictions and adjustment factors for asphalt pavement." Publication No. FHWA-RD-98-085, Federal Highway Administration (FHWA), McLean, VA.

Marc, L. (2007). "Use of Ground Penetrating Radar to Evaluate Minnesota Roads." Minnesota Department of Transportation, Report No MN/RC-2007-01, Maplewood, MN.

Masad, E., Huang, C., Airey, G., and Muliana, A. (2008). "Nonlinear viscoelastic analysis of unaged and aged asphalt binders." *Construction and Building Materials*, Vol. 22, pp. 2170-2179.

Meier R.W., Rix G.J. (1994). *Backcalculation of Flexible Pavement Moduli Using Artificial Neural Networks*. Transportation Research Record 1448. Transportation Research Board. Washington, D.C.

Meier R.W., Rix G.J. (1995). *Backcalculation of Flexible Pavement Moduli From Dynamic Deflection Basins Using Artificial Neural Networks*. Transportation Research Record 1473. Transportation Research Board. Washington, D.C., 1995.

MEPDG (2004). "Guide for Mechanistic-Empirical Design of New and Rehabilitated Pavement Structures." National Cooperative Highway Research Program Transportation Research Board National Research Council.

Michelow, J. (1963). "Analysis of stress and displacements in an N-Layered elastic system under a load uniformly distributed on a circular area" Chevron Research Corporation, Richmond, California.

Mirza, M. W., and Witeczak. M.W. (1995). "Development of a Global Aging System for Short and Long Term Aging of Asphalt Cements." *Journal of the Association of the Asphalt Paving Technologists*, Vol. 64, pp. 393-424.

Monismith, C. L. (2004). "Evolution of Long-Lasting Asphalt Pavement Design Methodology: A Perspective. Distinguished Lecture, International Society for Asphalt Pavements." *International Symposium on Design and Construction of Long Lasting Asphalt Pavements*. Auburn University.

Nazef, A. (2011). "US 27/SR 25 Pavement Evaluation." State of Florida Department of Transportation, Research Report no. FL/DOT/SMO/11-542.

Nekouzadeh, A., and Genin, G. M. (2013). "Adaptive Quasi-Linear Viscoelastic Modeling." *Computational Modeling in Tissue Engineering. Studies in Mechanobiology, Tissue Engineering and Biomaterials*, Vol. 10, pp. 47-83.

Newcomb, D. E. (1986). "Development and Evaluation of Regression Methods to Interpret Dynamic Deflections." Ph.D. Dissertation. Department of Civil Engineering. University of Washington, Seattle, WA.

- Noureldin, S., Zhu, K., Harri, D. and Li, S. (2005). “Non-destructive estimation of pavement thickness, structural number and subgrade resilience along INDOT highways” Indiana Department of Transportation, Publication No.: FHWA/IN/JTRP-2004/35.
- Ooi, P. S., Archilla, A. A., and Sandefur, K. G. (2004). “Resilient modulus models for compacted cohesive soils.” *Transportation Research Record: Journal of The Transportation Research Board*, Vol. 1874, pp. 115-124.
- Park, S. W. and Schapery, R. A. (1999). “Methods of Interconversion between Linear Viscoelastic Material Functions. Part I – a Numerical Method Based on Prony Series.” *International Journal of Solids and Structures*, Vol. 36, pp. 1653-1675.
- Park, S. W., Park, H. M., and Hwang, J. J. (2009). “Application of Genetic Algorithm and Finite Element Method for Backcalculating Layer Moduli of Flexible Pavements.” *KSCE Journal of Civil Engineering*, Vol. 14(2), pp. 183-190.
- Park, D.Y, Buch, N. and Chatti, K. (2001). “Effective layer temperature prediction model and temperature correction via falling-weight deflectometer deflections.” In *Transportation Research Record: Journal of the Transportation Research Board*, 1764, pp. 97-111.
- Park, H. M., Kim, Y. R., and Park, S. (2002). “Temperature correction of multiload-level falling weight deflectometer deflections.” *Transportation Research Record: Journal of the Transportation Research Board*, 1806, pp. 3-8.
- Raad, L., and Figueroa, J. L. (1980). “Load response of transportation support systems.” *Transp. Engg. J.*, 106 (1), pp. 111–128.
- Raghavendra, S., Zapata, C., Mirza, M., Houston, W., and Witczak. M. (2006), “Verification of the Rate of AsphaltMix Aging Simulated by AASHTO PP2-99 Protocol.” In *TRB Meeting*, Washington DC.
- Rechenberg, I. (1965). “Cybernetic solution path of an experimental problem.” Royal Aircraft Establishment, Library translation NO. 1122, Farnborough, Hants., UK, August.
- Reddy, M. A., Reddy, K. S., and Pandey, B. B. (2004). “Selection of Genetic Algorithm Parameters for Backcalculation of Pavement Moduli.” *The International Journal of Pavement Engineering*, Vol. 5 (2), pp. 81-90.
- Roeset, J. M., Stokoe, K. H., and Seng, C. (1995). “Determination of Depth to Bedrock from Falling Weight Deflectometer Test Data.” *Transportation Research Record*, 1504, pp. 68-78.
- Rohde, G. T. and T. Scullion. (1990). “Modulus 4.0: Expansion and Validation of the Modulus Backcalculation System.” FHWA/TX-91/1123-3. Texas State Department of Highways & Public Transportation, Austin, TX.
- Roque, R., Zou, J., Kim, R., Baek, C., Thirunavukkarasu, S., Underwood, S. and Guddati, M. (2010). “Top-down cracking of hot-mix asphalt layers: models for initiation and propagation.” NCHRP web-only document 162, NCHRP Project 1-42A.



- Rwebangira, T., Hicks, R., and Truebe, M. (1987). "Sensitivity analysis of selected backcalculation procedures." Transportation Research Record 1117, National Research Council, Washington, D.C.
- Sangghaleh, A., Pan, E., Green, R., and Wang, R. (2014). "Backcalculation of pavement layer elastic modulus and thickness with measurement errors." International Journal of Pavement Engineering, Vol. 15 (6), pp. 521-531.
- Schapery, R. A. (1969). "On the characterization of nonlinear viscoelastic materials." Polymer Engineering and Science, Vol. 9, No 4.
- Schapery, R. A. (1965). "Method of Viscoelastic Stress Analysis using Elastic Solutions". Journal of the Franklin Institute, Vol. 279(4), pp. 268-289.
- Schapery, R. A. (1974). "Viscoelastic Behavior and Analysis of Composite Materials." Mechanics of Composite Materials, New York, Academic Press, Inc., pp. 85-168.
- Schiffman, R. L. (1962). "General Solution of Stresses and Displacements in Layered Elastic Systems." Proceedings of the International Conference on the Structural Design of Asphalt Pavement, University of Michigan, Ann Arbor, USA.
- Schmalzer, P. (2006). "LTPP Manual for Falling Weight Deflectometer Measurements, Version 4.1." FHWA-HRT-06-132, U.S. Department of Transportation, McLean, VA 22101-2296.
- Schwartz, C. W. (2002). "Effect of stress-dependent base layer on the superposition of flexible pavement solutions." International Journal of Geomechanics, 2(3), pp. 331–352.
- Seo, J., Kim, Y., Cho, J., and Jeong, S. (2012). "Estimation of in situ dynamic modulus by using MEPDG dynamic modulus and FWD data at different temperatures." International Journal of Pavement Engineering, Vol. 1, pp. 1-11.
- Selezneva O., Jiang, Y., and Mladenovic, G. (2002). "Evaluation and analysis of LTPP pavement layer thickness data." Publication no. FHWA-RD-03-041, McLean, Virginia.
- Shames, I. H., and Cozzarelli, F. A. (1997). "Elastic and Inelastic Stress Analysis", revised printing. Taylor and Francis.
- Shell. (1978). "Shell Pavement Design Manual-Asphalt Pavements and Overlay for Road Traffic." Shell International Petroleum Company Limited, London.
- Shook, J. F., Finn, F. N., Witczak, M. W., and Monismith, C. L. (1982). "Thickness Design of Asphalt Pavements-The Asphalt Institute Method." Proceeding of 5<sup>th</sup> International Conference on Structural Design of Asphalt Pavements, Vol. I, pp. 17-44.
- Taylor, A. J., and Timm, D. H. (2009). "Mechanistic characterization of resilient moduli for unbound pavement layer materials." NCAT Report 09-06.

Theyse, H. L., Beer, M., and Rust, F. C. (1996). "Overview of the South African mechanistic pavement design analysis method." Transportation Research Record 1539, Transportation Research Board, Washington, DC, pp. 6–17.

Tsai, B., Kannekanti, V., and Harvey, J.T. (2004). Application of Genetic Algorithm in Asphalt Pavement Design, Transportation Research Board, No. 1891, National Research Council, Washington, D.C., pp. 112-120.

Tutumluer, E. (1995). "Predicting behavior of flexible pavements with granular bases," Ph.D. dissertation, School of Civil and Environmental Engineering, Georgia Institute of Technology, Atlanta.

Ullidtz, P. (1988). "Pavement Analysis." Elsevier Science. New York, NY.

Uddin, W. (2006). "Ground penetrating radar study — Phase I technology review and evaluation" FHWA/MS-DOT-RD-06-182, Mississippi Department of Transportation.

Uzan, J. (1994). "Advance Backcalculation Techniques. Nondestructive Testing of Pavements and Backcalculation of Moduli (Second Volume)." ASTM STP 1198, American Society for Testing and Materials, Philadelphia.

Uzan, J. (1994). "Dynamic Linear Backcalculation of Pavement Material Parameters." J. of Transp. Eng., 120(1), pp. 109-126.

Uzan, J. (1985). "Characterization of granular material." Transportation Research Record 1022, Transportation Research Board, Washington, D.C. pp. 52–59.

Varma, S. , Kutay, M. E., and Chatti, K. (2013b). "Data Requirements from Falling Weight Deflectometer Tests for Accurate Backcalculation of Dynamic Modulus Master curve of Asphalt Pavements," Airfield & Highway Pavement Conference, Los Angeles, California, pp. 445-455.

Varma, S., Kutay, M. E. and Levenberg, E. (2013a). "A Viscoelastic Genetic Algorithm for Inverse Analysis of Asphalt Layer Properties from Falling Weight Deflections," Transportation Research Record: Journal of the Transportation Research Board, Vol. 4, pp. 38-46.

Wang, H., and Al-Qadi, I. L. (2013). "Importance of nonlinear anisotropic modeling of granular base for predicting maximum viscoelastic pavement responses under moving vehicular loading." Journal of Engineering Mechanics, Vol. 139, pp. 29-38.

Warren, H., and Dieckmann, W. L. (1963). "Numerical computation of stresses and strains in a multiple-layered asphalt pavement system," California Research Corporation, Richmond, California.

Witczak, M. W., and Uzan, J. (1988). "The universal airport pavement design system, Report I of IV: Granular material characterization." University of Maryland, College Park, Md.

Yan, A., and Von Quintus, H. L. (2002). "Study of laboratory resilient modulus test data and response characteristics." Final Report, Federal Highway Administration. Publication No. FHWA-RD-02-051.

Yong, Y., Yang, X., and Chen, C. (2010). "Modified Schapery's model for asphalt sand." *Journal of Engineering Mechanics*, Vol. 136(4), pp. 448-454.

Zaabar, I., Chatti, K., and Lajnef, N. (2014). "Backcalculation of asphalt concrete modulus master curve from field measured falling weight deflectometer data using a new time domain viscoelastic dynamic solution and hybrid optimization scheme." *Sustainability, Eco-efficiency and Construction in Transportation Infrastructure Asset Management*-Losa and Papagiannakis (Eds). Taylor & Francis, ISBN 978-1-138-00147-3.

Zhou, H. (2000). "Comparison of backcalculated and laboratory measured moduli on AC and granular base layer materials." *Nondestructive Testing of Pavements and Backcalculation of Moduli: Third Vol.*, ASTM STP 1375, S. D. Tayabji and E. O. Lukamen, Eds., American Society of Testing and Materials, West Conshohocken, PA.